Dublin City University
Ollscoil Chathair Bhaile Átha Cliath

Uniaxial Stress-strain Properties of Metallic Materials at High Strain Rates and at Higher Temperatures

By

Jian Sun B. Eng., M. Eng.

Supervisor: Professor M. S. J. Hashmi

This thesis is submitted to Dublin City University in fulfilment of the requirement for the award of Degree of

Doctor of Philosophy

School of Mechanical & Manufacturing Engineering
Dublin City University
January 1993

To My Wife

DECLARATION

I hereby certify that this material, which I now submit for assessment on the programme of study leading to the award of Doctor of Philosophy, is entirely my own work and has not been taken from the work of others save and to the extent that such work has been cited and acknowledged within the text of my work.

Signed: Jian Sun

Jian Sun

I. D. No: 89701194

Date: 11 January 1993

2.4.3 Numerical integration 39

2.5 Simulations of the Program 46

2.5.1 The constitutive equation 46

2.5.2 Initial data and input 47

2.5.3 Results and discussions 49

2.6 The Effect of Various Initial Parameters 56

2.6.1 Shock stress wavefront 56

2.6.2 The length of the specimen 62

2.6.3 The initial velocity of the projectile 68

2.6.4 The dimensions of the specimen 73

2.7 The Elastic-plastic Boundary Conditions at the Fixed End .. 79

Chapter 3 Experiments and Results 82

3.1 The Quasi-static Compression Tests 82

3.1.1 Tests under the ambient temperature 82

3.1.2 Tests at high temperatures 85

3.2 The Static Stress-Strain Equations 87

3.2.1 Commercially pure copper 89

3.2.2 Mild steel 92

3.3 Dynamic Impact Tests 96

3.3.1 Apparatus and principle 96

3.3.2 Modification of the test machine 102

3.3.3 Performance of impact tests under the ambient temperature 111

3.3.4 Experimental results 113

Chapter 4 Constitutive Equations 118

4.1 Introduction 118

4.2 The Constitutive Equation Review 119

4.3 General Physical Description of Mechanical Response 130

4.4 Adiabatic Shear Phenomena 132

4.4.1 Phenomenon mechanism 132

4.4.2 The temperature rise in a struck specimen 133
4.5 The Effect of Shock Loading ... 139
4.6 The Dynamic Constitutive Equations ... 141
4.6.1 Commercially pure copper ... 141
4.6.2 Mild steel ... 153
4.7 The Effect of Radial Expansion ... 160
4.8 Discussion of the Constitutive Relations ... 161

Chapter 5 Conclusions and Suggestions ... 167
5.1 Concluding Remarks ... 167
5.2 The Existing Problems and Further Suggestions ... 170

References ... 172

Appendix I. List of Figures ... A-1
Appendix II. Program of Conversion of Data ... A-8
Appendix III. Program for the Drawing of Curves ... A-9
Appendix IV. Program for Numerical Solution of Plastic Wave A-16

ACKNOWLEDGEMENTS

The author wishes to express his sincere thanks to Professor M. S. J. Hashmi for his elaborate supervision and valuable guidance during the period of this research.

He would like to take this opportunity to express his deep appreciation to Ms. Lesley Lawlor, Mr. Tommy Walsh, Mr. Ian Hooper, Mr. Liam Domican and all the others for their kind assistance and valuable support at various stages of this work.

Finally, thanks to his wife for her support and encouragement during the period of completion of his work.

January 1993

ABSTRACT

Uniaxial Stress-strain Properties of Metallic Materials at High Strain Rates and at Higher Temperatures

Jian Sun B. Eng., M. Eng.

A combined experimental and numerical technique for the determination of uniaxial stress-strain properties of metallic materials at high strain rates and temperatures of up to 440 °C is presented.

Experiments were carried out using an existing ballistic test machine. Small cylindrical specimens of commercially pure copper and mild steel were placed upon a rigid anvil and were impacted by a hardened tool steel projectile at temperatures of up to 440 °C. The initial velocity of the projectile up to 120 m/s was recorded by a laser velocity-measuring device, and the deformation of the impacted specimen was measured after each test. For the purpose of high temperature tests, a modification for the machine have been made and a movable anvil unit to reduce the loss of heat has been designed and used.

A mathematical model with a mixed boundary condition, to which the theory of propagation of longitudinal waves of plastic deformation is applied, has been established. Based on the model, a numerical method of the iterative procedure to determine dynamic properties of materials considering adiabatic shear effects at various temperatures has been utilized. The corresponding computer programs have also been written. The properties of wave-propagation in the impact process of the specimen have been analyzed. The factors affecting the deformation of the impacted specimen such as adiabatic shear phenomena, the effects of shock loading and the boundary conditions at the anvil end have been discussed, and the optimum parameters to determine the corresponding constitutive equations have been selected. Further, a method to examine and determine the validity of the constitutive equations of materials is recommended. The forms of constitutive equations at high strain rates up to 10^5 s^{-1} for metals (commercially pure copper and mild steel) at various temperatures up to 440 °C have been proposed and the parameters in these suggested equations have been determined by means of agreement of the experimental results and numerical calculations.

NOMENCLATURE

E Younge's moudulus.

T Temperature.

t Time.

v Velocity.

c_0 The velocity of wave propagation.

x Rectangular coordinates.

σ Stress.

τ Shear stress.

ε Strain.

$\dot{\varepsilon}$ Strain rate.

$\dot{\varepsilon}^e$ Elastic strain rate.

$\dot{\varepsilon}^p$ Plastic strain rate.

λ Strain rate sensitity.

ρ Density.

Chapter 1 Overview

The mechanical metals and alloys deformed plastically at high strain rates has extensively been studied during the last four decades. The subject is of interest both because a wide range of practical problems require a knowledge of the properties of materials subjected to dynamic straining and because it is now clear that rate effects are a key factor in differentiating and elucidating the micro-mechanisms of plastic flow. Progress in studying high-speed deformation has been in three main areas: advances in experimental methods, which have permitted the measurement of dynamic material response at both the macroscopic and microscopic levels; the widening of macroscopic plasticity theory to include wave-propagation and rate effects; and the development of dislocation theory to provide models of the rate-controlling deformation processes.

A large amount of research work in these fields has been done, especially, in the recent four decades. This chapter will briefly make a review on concerning topics.

1.1 Experimental Methods

1.1.1 Low rates of strain (10^{-4} to 10^{-1} s^{-1})

In this range, conventional screw-driven or hydraulic test machines may be used, together with pen recorders. If the total deformation is controlled, the specimen behaviour is governed partially by the compliance of the machine and in order to maintain, for example, an approximately constant strain rate it is necessary for this compliance to be low (hard machine). By the use of feed back control, the imposed deformation may be automatically varied in response to the output of a transducer measuring directly the specimen load or deformation. Closed-loop control also makes it possible to impose arbitrary stress or strain-time histories on the specimen during the test. The technique of sudden strain-rate changes during the test has been widely used to investigate rate effects in the "quasi-static" range (10^{-4} -10^{-2} s^{-1}).

1.1.2 Medium rates of strain (10^{-1} to 10^{2} s^{-1})

At these rates, it becomes necessary to use an energy storage system to supply energy to the specimen during the test, since the instantaneous power required becomes inconveniently high. The first energy-storing machines employed the kinetic energy of a moving mass (pendulum, drop-weight or rotating flywheel) [1,2]. In general, with this method large transient oscillations are generated by the impact at the beginning of the test, so that yield-point and low-strain behaviour cannot be accurately recorded. To overcome this disadvantage machines have been developed by the use of a special cam to connect a rotating flywheel to the specimen [3-6] or driven by the potential energy in a compressed gas or liquid [7,8]. By controlling the fluid flow rate, relatively rigid machines were also developed [9-11].

For adequate measurement of loads and deformations at a strain rate of 10^{2} s^{-1}, a frequency response of the order of 10 *khz* is needed, so that oscilloscope recording is almost invariably used.

1.1.3 High rates of strain (10^{2}-10^{4} s^{-1})

At these rates, vibration or wave effects in the test machine or load-measuring device normally become too large to be neglected, so that it becomes necessary to design the test apparatus in such a way that these effects can be taken into account and allowed for. Hopkinson [12] used compression waves in a long elastic bar as a means of estimating the transient pressures caused by explosions, and Kolsky [13] adapted this technique as a means of both loading and measuring the load and deformation of a disc-shape specimen. This method, usually known as the split Hopkinson-bar method, uses an apparatus in which the specimen is sandwiched between two long elastic bars, along one of which a pulse or step wave is propagated towards the specimen; this wave is partially transmitted through the specimen into the second or recording bar, and the amplitude of the transmitted wave is used as a measure of the specimen load. By recording the incident and reflected waves in the first bar as well, and using the elementary theory of wave propagation in an elastic bar, it is possible to deduce the particle velocities at the two boundaries of the specimen, and hence to determine its means strain rate. Since its introduction, the method has been used in various forms for dynamic compression[10,14-23]; tension [24-27]; simple shear [28-31] and torsion [32]. By this technique, valid test results are obtainable at strain rates approaching and even exceeding 10^4 s^{-1} if certain precautions are taken [33].

The use and limitations of the Hopkinson pressure bar have been examined by Davies [34] and the split Hopkinson-bar method has been discussed by several authors [13,18,19,23,27]. The use of longitudinal waves introduces a basic limitation, in that such waves show significant geometric dispersion for wavelengths which are not large compared with the bar diameter; thus very sharp-fronted pulses cannot be transmitted or measured by means of these waves. A further complication in the use of the split Hopkinson-bar method for compression tests arises from the radial expansion of the specimen during its deformation. This expansion affects the stress in the specimen in two ways: firstly by causing frictional shear stresses which act at the specimen-bar interfaces, and secondly by introducing inertial body forces within the specimen. The first of these effects can be minimized by lubrication of the specimen surfaces, but the second constitutes a limitation on the strain rates at which accurate results can be obtained. By an approximate analysis, it has been shown [23,35] that, because of radial inertia, in a test at constant strain rate the measured axial stress exceeds the true uniaxial flow stress by an amount which increases as the square of the strain rate. In two particular cases, it was found that the error amounted to 0.05% at a strain rate of 2.2×10^3 s^{-1} and 17.5% at a strain rate of 2.5×10^4 s^{-1}.

Similar problems arise in the use of the split Hopkinson-bar method for tension test, and in addition stress concentrations at the specimen-bar connections are inevitable. In both compression and tension tests, the strain distribution within the specimen becomes increasingly non-uniform as the strain increases, because of barrelling or necking of the specimen.

The effect of inertia on the load in high-velocity metal working have been considered by Hillier [36] and Lippmann [37]. They studied the axially symmetric and plane strain forging by rigid overlapping dies for a variety of frictional conditions. Hillier evaluated the effects of inertia at the start of a forging operation thereby demonstrating the effect of impact velocity alone, and disregarding the effect of die deceleration; this predominates towards the end of the process. Lippmann concluded that although lateral inertial effects may be neglected when using slow presses, they can become significant in conventional speed forging processes, and will predominate at high working velocities. Explicit solutions for the estimation of inertial effects in high-velocity plane strain and axisymmetric compression for a variety of frictional conditions excluding the effect of strain rates have been derived by Sturgess and Jones [38], which predicts that increased impact velocity increases inertial effects, but increased interface friction tends to suppress these effects.

Most of the difficulties and limitations experienced in the compression and tension versions of the split Hopkinson bar are eliminated by the use of the torsional version. A variation of the split Hopkinson bar that has been developed at several laboratories to achieve high rates of strain in torsion was first described by Duffy *et al* [39]. The primary advantages of the torsional mode of wave propagation are that it is non-dispersive and that three-dimensional or radial inertia effects are not present. The major problems in the torsional version of the split Hopkinson bar are the attachment of the specimen to the incident and transmitter bars and the generation of a high-amplitude, short rise-time torsional pulse without any axial disturbances. The specimen is generally thin walled tubular type and has been successfully attached through bonding with epoxy adhesives. The generation of the torsional wave has been achieved either through simultaneous explosive loading on diagonally opposite sides of a bar or by pre-torquing a bar and then suddenly releasing a clamp. Increasingly higher strain rates can be achieved by higher input torques or by using shorter gage-length specimens. Specimens of the order of 1 mm gage length have been employed to achieve strain rates in excess of 10^4 s^{-1} by several investigators. Nicholas and Lawson [40] demonstrated that data from extremely short specimens could be reliably reproduced with longer gage-length specimens. The torsional version of the Hopkinson bar was first used by Baker and Yew [32]. Alternate versions of the apparatus and its application are given by Campbell and Dowling [41] and Lewis and Campbell [42]. The apparatus has found extensive application in incremental strain-rate tests. Further development in this area has considerable potential because of the inherent advantages of torsional testing, including the absence of hydrostatic components of stress.

Two other completely different methods have also been used to investigate material behaviour at high rates of strain. Both of these avoid setting up significant stress waves in the specimen or straining apparatus. In the first method [43,44] the specimen is made in the form of a thin circular ring to which a radial motion is imparted by explosive or electro-magnetic means. If the impulse occurs in a very short time, after which the specimen moves freely, the circumferential stress is given directly by the radial deceleration of the ring. However, the accuracy obtainable in practice is severely limited because measurement of the deceleration involves double differentiation of an experimental displacement-time trace; in addition, the imposed radial force is likely to persist for at least an appreciable part of the test and its measurement presents great difficulties. One advantage of the test is the avoidance of stress concentrations in the specimen and this makes it potentially very suitable for investigating yield-point phenomena. Behaviour at high strains cannot be studied, since necking and fracture supervene as in a conventional tensile test. Maximum strain rates of about 2×10^3 s^{-1} have been achieved [45], but the rate falls rapidly during the test.

The second method is based on measuring the forces required to deform a material which passes continuously through the deformation zone, so that the system is in a steady state. This type of deformation occurs in many practical metal forming processes, *e.g.* rolling, extrusion and machining, so that in principle any of these could be used to determine the effect of strain rate on material behaviour. The method was first used in experiments on strip rolling [46] in which strain rates of up to 200 s^{-1} were obtained. Using orthogonal machining [47-49], strain rates of up to 2.8×10^4 s^{-1} were achieved. The advantage of using a steady-state process is that the applied forces are essentially constant and so can be easily measured. However, the strain and strain rate vary rapidly through the deformation zone so that it is necessary to measure accurately the flow of the material within this zone. The method suffers from the difficulty that the measured forces give average stress values only and hence a complete stress-strain curve cannot be derived from the measurements; in addition because of the large strains considerable temperature rises occur in the material, which must be estimated by independent means. In spite of these complications, it has proved possible to correlate the results obtained in machining tests with those obtained at lower rates using other methods.

1.1.4 Very high rates of strain (above 10^4 s^{-1})

There has been increased emphasis, especially in recent years, to achieve ever-increasing strain rates using the Hopkinson bar apparatus. Within the constraints and limitations of the physical apparatus and the assumptions, one of the most direct methods for achieving higher strain rates is through the use of smaller test specimens. Edington [50] was one of the first to achieve strain rates up to 10^4 s^{-1} by using 2 mm long by 12.5 mm diameter specimens that were fabricated using extremely accurate machining. Lindholm [51] achieved rates up to 10^5 s^{-1} on specimens of 1100-0 aluminium and copper by reducing specimen lengths to 4 mm. He was careful, however, to preserve a constant effects of specimen geometry on the resultant data. There are, however, practical limitations to the size of specimen that can be used, and the problems of neglect of radial inertia and shear are always a factor. These difficulties have led investigators to explore other methods of subjecting materials the high rates of strain such as in torsion or in shear.

The concept of original Hopkinson bar, which involves measurements at one end or at some position along the bar to deduce what is occurring at other end, has been applied in an attempt to achieve extremely high strain rates and very large strains in compression. Samanta [23] utilized a direct impact version of a Hopkinson bar by firing a projectile directly against the specimen, thus eliminating the input bar as such. This procedure allowed him to obtain very large compressive strains in aluminum and copper. Load was determined in the conventional manner from strain gauges on the output bar, while an optical method was employed to observe strain directly. Wulf and Richardson [52] reported measurements of strain rates up to 10^5 s^{-1} and true strains up to 2.0 using a hardened projectile impacting the specimen directly in place of the input bar. In their procedure, strain was measured directly using a coaxial capacitor. Their report describes this new circuit for measuring rapid changes of capacitance that is an improvement of a capacitance-type gauge for measuring strains in a Hopkinson bar set up described earlier by Wingrove [53]. Gorham [54] describes a modified Hopkinson bar system also using the direct impact of a striker bar against the test specimen. He used a high-speed camera with a novel optical system to achieve very high radial displacement resolution from which to calculate strain. In tests of 8 μs duration which subjected 1 mm diameter by 0.5 mm long tungsten-alloy specimens to strains of 30%, a strain rates of 4×10^4 s^{-1} was achieved. These high strain rates could generally not be achieved in a conventional split Hopkinson bar experiment because of limitations on the strength of the bars and because of the large forces necessary to deform very high strength materials.

Strain rates are so high that experimental results involving the observation of the transient wave propagation phenomena are also often used indirectly to determine the dynamic mechanical properties of materials. In experiments involving the properties of uniaxial stress waves in rods, the procedure applied is to assume that the material submits to a certain constitutive law and then through calculations based on the law to predict the propagation characteristics. The predicted results are then compared with the experiment results. Agreement between the two usually leads to the logical conclusion that the assumed constitutive law is an accurate description of the phenomenological behaviour of the material.

Experimental observations of plastic wave propagation phenomena have been used for determining constitutive law for dynamic study and high strain rate for number of metallic materials. Taylor [55] put forward an analytical method in conjunction with ballistics test results obtained experimentally by Whiffin [56]. Hawkyard *et al* [57] extended the work of Whiffin to estimate the mean dynamic flow stress of copper and mild steel at elevated temperatures. The experimental technique used by Whiffin and Hawkyard involved firing cylindrical projectiles against a rigid anvil.

By the technique of firing projectile on to the anvil, Hashmi [58] measured the impact velocity using a wire-breaking contact system and recorded the corresponding load-time history using a piezo-electric load cell positioned just behind the anvil insert. A finite difference numerical technique was used to establish the constitutive law of a mild steel from ballistic experimental results which gave rise to strain rates of up to 10^5 s^{-1} [59].

The experimental technique in which a cylindrical specimen placed on a flat rigid anvil was struck by a high speed projectile caused by means of compressed air was used by Haque and Hashmi [60]. In their experiments, a ballistic test rig was used to fire a hardened tool steel projectile onto a small cylindrical specimen placed upon a rigid anvil. Compressed air was used to propel the projectile and a high speed image converter camera was used to continuously record the deformation-time history of the specimen. These records were then used to obtain force-time, strain-time, stress-time and strain rate-time histories during the entire deformation process. From these results the stress-strain properties of structural steel at strain rates between 10^3-10^5 s^{-1} were then established. The friction, material inertia and temperature rise during the high speed deformation were considered.

There are two kinds of fundamental difficulties in applying an approach of this type. The first concerns the sensitivity of experimentally obtained propagation characteristics to variations in the constants of the form of the proposed constitutive relationship. The second is the lack of a unique solution even if the experimental results are predicted by the proposed constitutive law. There is nothing to say that some other constitutive law might not predict the same characteristics. These points have been illustrated through the calculated results by Ripperger and Watson [61] for the case of uniaxial stress waves in a bar subjected to a step input in stress at one end and by Percy [62] for waves of uniaxial strain.

1.2 Experimental Results

There is clear experimental evidence that most metals and alloys exhibit some increase in strength with increasing strain rate. The oldest experiments in dynamic plasticity seem to be those of J. Hopkinson [63] and B. Hopkinson [64], who studied the propagation of longitudinal waves in iron wires. They observed that the dynamic yield stress is approximately twice as high as the static yield stress. Brown and Vincent [65] reached a similar conclusion: for mild steel the yield point is considerably increased when the duration of the test is very short. Taylor and Quinney [66] used very rapid dynamic tests to show that the dynamic yield stress is much higher than the static one for mild steel; for copper it is only a little higher. Taylor [66] studied the dynamic properties of various materials, by means of experiments in which short cylindrical specimens were projected with great velocity against a rigid wall; he showed that for paraffin wax the ratio between the dynamic yield stress and the static one ranges from 1.3/1 to 2/1. For mild steel this ratio is higher than 2, but for duralumin it is lower. Davies [67] also determined the ratio of the dynamic yield stress to the static one for various types of steel. In this case the specimens were thick plates of the steel considered. A ball of very hard steel was either thrown or alternately only pressed against them. He reached he conclusion that for nickel-chrome steel the ratio is approximately 1, for armourplates 1.1, and for mild steel 2. Duwez and Clark [68] reached a similar conclusion by showing that under certain conditions the dynamic yield stress of annealed mild steel can be double or triple the static yield stress. The dynamic characteristics of some high polymers (nylon, neoprene, *etc.*) have been studied by Hillier and Kolsky [69]. These authors determined the velocity of propagation of sound and hence the dynamic value of Young's modulus for the respective materials. Kolsky [13] determined the dynamic stress-strain diagram for materials such as rubber, polyethylene, perspex, copper and lead. A modified Hopkinson pressure bar apparatus was used, and the specimens were in the form of circular disks of uniform thickness. It was found that for polythene, rubber and perspex the effective elastic modulus for the dynamic tests is very much higher than that observed statically, and that the whole dynamic stress-strain curve differs from the static one. An important delayed recovery phenomenon was discovered in the case of these materials; the strain continued to increase rapidly after the stress had passed its maximum value. However, these materials showed no permanent strain after the experiments. Their results have been further discussed theoretically [70,71], pointing out similar conclusions for various steels, *i.e.* the displacement upwards of the plastic portion of the stress-strain curve and the existence of a certain delay in dynamic yield phenomena. Similar results for polythene were obtained by Taylor and Volterraec [66].

By measuring the velocity of longitudinal waves travelling along a rod, Campbell [72] showed that in dynamic experiments mild steel behaves elastically up to stresses much higher than the static yield stress. De Costello [73] found that for rates of strain of about 10^4 to 10^5 s^{-1}, the ratio of dynamic to static yield strength is 2.9 for mild steel and 1.5 for Vibrac. To obtain an indication of the strain-rate sensitivity of various metals, Davis and Hunter [74] proposed a method for measuring dynamic hardness. They showed that for many metals the dynamic hardness is bigger than the static one. The use of dynamic indentation techniques for investigating the dynamic yield stress has been reported by many authors [75,76].

The same conclusions are valid for various photo-elastic materials used to study transient phenomena. Durelli and Riley [77] used an epoxy resin for this purpose, Feder *et al* [78] used plastics, Clark [79] as well as Goldsmith and Dabaghian [80] used Columbia Resin No. 39, Clark and Sanford [81] various photo-elastic materials, Perkins [82] photo-elastic rubber and gelatine, *etc.*

Many high-speed testing machines have been built in order to study the dynamic properties of various plastics [83-87]. These authors all showed that plastics are to a great extent rate dependent; the elastic constants are also rate dependent, and certainly the yield points. In addition, the relaxation phenomena are more important in high rate experiments than in low rate experiments. Thus for each rate of strain the plastics possess different mechanical properties [88]. Pilsworth and Hoge [89] have shown that nylon yarns and rubber strip subjected to longitudinal impact at up to 100 m/s are also rate dependent. By using high-speed photography Ivanov and Stepanov [90] determined the strength of two reinforced plastics and of two pure resins at temperatures ranging between -196°C and +150°C for impact velocities up to 1500 m/s. They concluded that the strength of plastics at elevated temperatures is more rate sensitive than at low temperatures; at -196°C the difference between static and dynamic properties was found to be insignificant.

The experiments made by Kolsky [13] with copper and lead showed that the dynamic elastic modulus does not differ sensibly from the static one, but that the whole dynamic stress-strain curve is higher than the static curve. Since the strain increases even after the stress has begun to fall, it follows that the dynamic constitutive equation for copper is time-dependent (dynamic relaxation). It should also be noted that the static stress-strain curve does not seem to be to a great extent rate dependent. The properties of lead were found to be similar to those of a viscous liquid: the stress was approximately proportional to the rate of straining. The dynamic yield stress in lead is found [91] to be far in excess of the static yield stress and sometimes even to exceed the static ultimate strength. A technique similar to that used by Kolsky was used by Davies and Hunter [18] who tested annealed copper, aluminium, zinc, magnesium and α-brass specimens. In all case, a rate effect which raised the stress level for any given strain by a factor varying form 1.0 to 3.0 was confirmed. Davies and Hunter have also tested certain polymers and have revealed the large stress relaxation shown by these materials at constant strain. It is certain that polymers are highly rate dependent. The Hopkinson pressure bar was also used by Lindholm [19] in order establish the dynamic properties of lead, aluminium and copper; results similar to those mentioned above were obtained, *i.e.* an increase in the rate of strain (averaged out over the entire specimen) increased the dynamic yield stress for all three of these metals. The influence of the rate of strain is generally large, not only on the dynamic stress-strain curve, but also on the static curve. Since the density of slip bands increases with increasing strain rate, the structure of a metal deformed to a given strain differs according to whether deformation occurred statically of dynamically. A certain decrease of the static yield stress seems to result due to previous dynamic loadings. Experiments have also been performed with epoxy resin and moulding plaster; both were found to be highly rate sensitive, including the initial elastic modulus which increases with the rate of strain. The same experimental method was also used by Chiddester and Malvern [92] who have confirmed the existence of a large rate influence for aluminium at various temperatures. The rate sensitivity seems to increase with temperature.

The difference between the dynamic and static properties of various metals was also studied by Ainbinders [93,94]. He too showed that for various steels, copper and zinc the dynamic yield stresses are higher than the static ones and that of all the mechanical parameters of a metal, yield stress is the one most sensitive to an increase in the rate of loading.

Campbell [95] performed dynamic tests on aluminium alloy specimens. In the plastic range investigated, the stress-strain curve during loading is found to be 15-20% higher than the quasi-static one. Dynamic tests on aluminium under compression impact have also been performed by Johnson *et al* [96]. They found that the dynamic stress-strain relation lies above the static stress-strain curve, but that it was necessary to use a family of dynamic stress-strain relations rather than any single one. These authors also discussed the stress relaxation phenomena and showed that the dynamic stress-strain relation describes the momentary behaviour of the material but not its permanent behaviour. After experiments with steel specimens, Campbell [97] again showed that the stress necessary to cause yield is about twice as great under the conditions of an impact test, than the stress required under normal static conditions. A certain "delayed yield" phenomenon was revealed, *i.e.* it was found that in a certain section the strain increases rapidly, remains constant for a short time, and then increases again before being reduced by the unloading wave coming from the free end. The delayed yield phenomenon was also demonstrated by Taylor [98] for mild steel, pure iron and carbon manganese. He repeatedly loaded these materials at an initial straining velocity of $V{=}4.5\ ft/s$ which fell to zero after the metal had plastically yielded for *T msec*. Repeated dynamic loadings of mild steel specimens have also been reported by Taylor [99]; once more the conclusion is that the dynamic yield stress increased with the rate of strain. Harris and White [100] showed that plastic straining under longitudinal impact causes a greater hardening in annealed mild steel than what an equal static strain does.

The influence of dynamic loading and temperature on the yield point for iron and steel was studied by Krafft *et al* [15]. They showed that the dynamic yield stresses are higher than the static ones, by an amount that varies with temperature. Lowering the temperature or increasing the strain rate affects the stress in a similar way: the yield stress increases. Maiden and Campbell [101], doing experiments with carbon steel, noticed that increasing the average strain rate to up to 600 s^{-1} or decreasing the temperature to -183°C had the same effect on the stress-strain curve. In the dynamic experiments the upper yield point was 2.5 times higher than the static one, while the lower yield strain was considerably increased. Similar results have been obtained by Koshelev and Uzhik [102] for specimens made of iron and by Uzhik and Voloshenko-Klimovitskii [103,104] for some types of steel and armco-iron. Their experiments generally showed an increase of the yield stress due to dynamic testing or to a decrease of the temperature; with some steels however, the yield stress seemed to decrease during dynamic testing. Voloshenko-Klimovitskii [105] continued these researches and showed that increasing the rate of loading and decreasing the temperature produce the same effect on the stress-strain curves, i.e. they are raised. If both phenomena intervene, the effects are assumed to be additive. The same phenomena were studied by Vitman *et al* [106-108]. The temperature and rate influences have also been studied by other authors [109-110].

The dynamic properties of mild steel have been studied by Campbell and Duby [16]. They showed that the dynamic yield stress can be 2.5 times bigger than the static one [109,111,112] and that after a previous dynamic straining the static stress-strain curve lies about 10% below the one obtained by reloading a specimen strained an equal amount statically. Thus, the static stress-stain curve seems to fall due to the rate influence of a previous dynamic experiment, while in steel the density of slip bands is greater after rapid straining than after slow straining. A similar result is reported by Riparbelli [113] and Smith [114]. Hawkyard and Freeman [115] found an increase of the dynamic yield stress with respect to the static one for carbon steel, aluminium and an aluminium alloy. Similarly Campbell and Harding [25] found that the yield stressed of refined iron and carbon steel increased considerably due to an increase of the rate of strain.

The dynamic properties of some types of steels were also studied by Voloshenko-Klimovitskii [116]. He showed that the dynamic stress-strain curves in tension are approximately of the same shape as the static ones; it is only the yield point that increases. For steels which possess a horizontal portion in the stress-strain curve, the elastic limit increases by approximately 42%, and for steels with no horizontal portion by 11% only. In another paper Voloshenko-Klimovitskii [117] studied for different types of steels the modification of the yield stresses of various steels resulting from an increase of the loading velocity. He showed that in dynamic experiments the yield limit, especially for armco-iron, is 2.5-3 times higher than the static yield point. It should however be noted that for other steels the yield point does not increase in dynamic test. Similar results were reported by Moldovan [118]. He showed that in dynamic experiments the strengths of copper, aluminium, lead and tin increase significantly.

Working with various steels and with lead, Chang and Chao [119] showed that the rate of strain has an important influence on the stress-strain curves at various temperatures, although the experiments were performed at fairly small rates of strain. These authors indicated various rate-dependent types of stress-strain relations, and confirm that aluminium is to a less extent rate dependent at the strain rates considered.

The dynamic properties of a certain aluminium alloy were studied by Konstantinov and Timofeev [120]. Such kind of alloy is also rate dependent, *i.e.* the dynamic yield stress is much bigger than the static one. These authors studied the influence of ageing on the static and dynamic yield stresses, and showed that the yield limit increased with time of ageing. They also discuss the behaviour of the metastable phase, when the dynamic yield stress can be below the static one.

Campbell and Dowling [41] performed a series of experiments using mild steel, copper, and aluminium prestressed in torsion. They noted that the propagation speed of a stress wave set up by a shear stress increment is essentially that of elastic waves for a range of values of pre-strain. They concluded that a rate-dependent constitutive law that predicts instantaneous plastic strain increments must be used to describe those materials. Nicholas and Campbell [121] performed incremental wave experiments on a high-strength aluminium alloy in torsion. For this material, which was found to be effectively insensitive to strain rate in constant-strain-rate torsional Hopkinson bar tests, a wave front travelling at the elastic shear-wave velocity was found in all cases, although this over-stress was sustained for a very short time period and its peak magnitude was only some 4% of the static flow stress. Klepaczko [122] performed incremental wave experiments in annealed aluminium, annealed copper, and deep drawn steel in tension when the specimens were pre-loaded at a constant strain rate. The precursor was again found to propagate at c_0 in apparent verification of a rate dependent theory. Klepaczko pointed out, however, that these types of experiments must be performed under constant-strain-rate pre-loading, since either constant-stress or constant-strain pre-loading will lead to creep or stress relaxation, respectively, for a material that is strain-rate dependent. He further emphasized both the improved accuracy in the use of incremental wave speed measurements over those in unstressed rods as well as the importance of strain-rate history in the material response.

The influence of pressure and temperature on the dynamic elastic moduli was studied by Hughes and Maurette [123]. It was showed that for armco-iron, pure aluminium and fused quartz the elastic moduli can be represented by linear functions of pressure and temperature. Concerning the elastic constants of a material, Jukov [124,125] has shown that even in static experiments on metals the plastic strain decreases the elastic constants. The increase of the elastic modulus in dynamic experiments was also reported by Hrazdil and Krejči [126,127] for low carbon steel and tool steel.

Klepaczko [128,129] has investigated strain-rate history effects in commercially pure aluminium (99.80%) tested in shear at rates of 1.6×10^{-5} and 0.624 s^{-1}. In these tests, specimens were strained at one rate, unloaded, and then strained at the other rate; the flow stresses were compared with those obtained at constant strain rate. These experiments showed that strain-rate history effects are significant when large changes in rate occur suddenly. During continued straining at the new rate, the flow stress tends towards that corresponding to a constant-rate test, though an appreciable difference is still evident even after the strain has doubled. For a reduction of rate the initial decrement of stress is about 30% less than that obtained from constant-rate tests. For an increase in rate the increment of stress is strongly strain-dependent, its initial value being very small. He discussed the interpretation of these results in terms of variations in dislocation density with strain-rate history.

Using the torsional version of the split Hopkinson's pressure bar, Tsao and Campbell [130] compared typical stress-strain curves for commercial-purity aluminium at shear strain rates from 600 to 2800 s^{-1} with the quasi-static response at $\sim2\times10^{-3}$ s^{-1}. Similar results for annealed titanium obtained by Eleiche and Campbell [131] on the same apparatus. In these tests only the specimens tested at the highest and the lowest rates were strained through failure. For both materials there is a significant increase in flow stress with strain rate. The greatest strain rate sensitivity, however, is usually found in materials of body-centred cubic structure.

A large amount of the available data has been reviewed by Lindholm and Bessey [132]; and Jiang and Chen [133]. The materials extensively tested include aluminium and several commercial aluminium alloys, lead, copper, iron and iron alloys, titanium alloys and beryllium. The data cover strain rates from 10^{-5} to about 10^3 s^{-1}, and for many fcc metals and alloys the logarithmic rate sensitivity $\lambda = \partial\sigma / \partial(\log \dot{\varepsilon}^p)$ is a constant over a considerable range of rates. However, the value of λ is found to increase with increasing strain.

Results of many researchers shows that at very high strain rates, of the order of 10^3 s^{-1} and above, the flow stress of many materials increases much more rapidly with strain rate. After studying the references listed in Table 1, Follansbee [33] concluded that the strain-rate sensitivity, evaluated at constant strain, is found to increase when the strain rate is raised above roughly 10^3 s^{-1}. When the maximum strain rate investigated is limited to 10^3 s^{-1}, such an increase is usually not observed.

1.3 Wave Propagation

As already noted, many metallic materials show only slight rate dependence of their mechanical behaviour at low and moderate strain rates. However, under impact conditions the behaviour is often, or perhaps always, essentially rate-dependent. Thus impact testing is a very important technique in the study of dynamic behaviour.

When a specimen is subjected to impact, inertial stresses must be taken into account, that is, wave propagation in the material must be allowed for in interpreting the results. The earliest theories of plastic-wave propagation in a rod [66,149-151] were based on a rate-independent quasi-static stress-strain relation $\sigma = f(\varepsilon)$. Combining this with the equations of motion and continuity gives the wave speed as

$$c = \sqrt{\frac{1}{\rho}\frac{df}{d\varepsilon}} \tag{1}$$

where ρ is the density of the material.

The wave speed thus decreases rapidly from the elastic value $(E/\rho)^{1/2}$ as the plastic strain increases. For a uni-directional wave it follows that

Table 1 *Previous investigations of high rate deformation of FCC metals.*

Reference	Maximum $\dot{\varepsilon}$ (10^3 s^{-1})	Material	Rate Sensitivity
Hauser et al[17]	15	pxtl Al	Increasing
Lindholm[19]	2	pxtl Al, Cu,Pb	Constant
Karnes and Ripperger [134]	4	pxtl Al	Increasing
Holt et al [135]	1	Al alloys:7075,6061	Constant
Ferguson et al [136]	10	sxtl Al	Increasing
Kumar et al [137]	26	sxtl Al	Increasing
Lindholm and Yeakley [27]	2.6	1100 Al	Increasing
Dharan and Hauser [138]	120	pxtl Al	Increasing
Green et al [139]	1	1060 Al, Pb	Increasing
Lindholm [51]	60	1100 Al	Constant
Chiem and Duffy [140]	5	pxtl Cu	Increasing
Ripperger [141]	5	OFHC Cu	Increasing
Kumar and Kumble [142]	2	pxtl Cu	Increasing
Edington [50]	10	sxtl Cu	Increasing
Dusek et al [143]	10	sxtl Cu	Increasing
Stelly and Dormeval [144]	20	sxtl Cu	Increasing
Shioiri et al [145]	2.5	OFHC Cu	Increasing
Follansbee et al [146]	30	OFE Cu	Increasing
Malatynski and Klepaczko [147]	2	pxtl Pb	Increasing
Mullerl [148]	10	pxtl Ni	Increasing

$$\sigma = \rho \int_0^{\varepsilon} c^2 d\varepsilon = \rho \int_0^{u} c du \qquad (2)$$

where u is the particle velocity.

Eq. (2) can be used to determine the function $f(\varepsilon)$ from experiments in which the speed of propagation is measured as a function of strain or particle velocity. This method has been used by Bell [152], Rakhmatulin [153], Malvern [154] and others. It may be noted that the method is applicable even when the dynamic behaviour of the material differs from the behaviour at low strain rates, provided that the former is effectively characterized by a single "dynamic" stress-strain relation. However, it has been shown in theoretical studies using different forms of constitutive relation [61] that the technique is unreliable as a method of determining the type of relation that governs the behaviour of the material.

The rate-independent theory has been applied to various problems including radial shear wave propagation in a cylinder or disc, spherical waves, and deformation of wires and membranes [153,155,156].

Eq. (1) predicts that if a small incremental stress is applied to a material while it is prestressed to a strain ε_0, the incremental wave will propagate at a speed $[f'(\varepsilon_0)/\rho]^{1/2}$. Experiments of this type have been carried out by several workers [157-160]; the results have shown that in fact the speed of the wave front is essentially that of elastic waves $(E/\rho)^{1/2}$. The use of the one-dimensional theory to treat the problem of incremental waves in rods has been criticized by Craggs [161], and an approximate analysis by De Vault [162] has shown that the neglect of radial inertia leads to an under-estimate of the wave speed. To avoid this complication, incremental shear-wave propagation in thin-walled cylinders has been investigated [41,163,164]. It was found that under this type of loading, in which the simple theory is exact, the wave front is propagated shear waves, for a variety of metals and alloys. It thus appears that the constitutive relation governing the dynamic behaviour is in principle rate-dependent, though as noted above it may be adequate in certain situations to use a rate-independent "dynamic" stress-strain relations as an approximation.

Another important technique in investigating rate effects in metals is the flat-plate impact test. In this test the material is subjected to a uniaxial strain and shock waves of very high intensity may be produced. Under these conditions it is found that an elastic precursor wave is generated, followed by as plastic shock wave whose speed depends on the impact velocity. At sufficiently high velocities this speed may reach or exceed the elastic wave speed, so that a single shock is propagated. It is found that the amplitude of the elastic precursor wave, if it exists, may be considerably greater than that corresponding to the "static" elastic limit. The amplitude decreases as the wave propagates and this attenuation has been related to the plastic strain rate [165,166].

It is clear from the results referred to above that in general plastic wave propagation requires the use of a rate-dependent constitutive relation for its proper description. In particular, a relation such as that proposed by Malvern [167], in which the plastic strain rate is a function of stress and strain, implies that an incremental wave propagates at the elastic wave speed, in accordance with experiment. A somewhat more general relation [156,168] is

$$\frac{\partial \varepsilon_p}{\partial t}=\Phi(\sigma,\varepsilon)\frac{\partial \sigma}{\partial t}+\Psi(\sigma,\varepsilon) \tag{3}$$

in which the function $\Phi(\sigma,\varepsilon)$ governs the instantaneous plastic flow and the function $\Psi(\sigma,\varepsilon)$ the non-instantaneous flow. Although there seems to be no theoretical basis for assuming that the instantaneous response of metallic materials is other than elastic, it is possible that in certain cases part of the inelastic deformation may occur sufficiently rapidly to be considered as instantaneous. According to Eq. (3), an incremental wave propagates at a speed $c_0(1+E\Phi)^{-1/2}$, where c_0 is the elastic wave speed. Experiments using thin-walled cylinders subjected to incremental torques have shown that for aluminium Φ is essentially zero while for copper it increases with plastic strain but is always small compared with the elastic compliance [41].

The subject of plastic waves has been treated extensively in the literature and reviewed from various points of view. Wave problems in the theory of plasticity are treated extensively in the book by Nowacki [169]. A general discussion of plastic waves is provided by Clifton [170]. The mathematical basis for plastic wave propagation is treated in detail by Cristescu [156]. Plastic waves are also reviewed by Craggs [171], while a survey of visco-elastic waves is provided by Hunter [172]. The earlier work in plastic waves is reviewed from a nonmathematical viewpoint by Hopkins [173]. A review of theoretical treatments and experimental methods in dynamic plasticity is presented by Campbell [174], and discussed in terms of the rated controlling mechanisms. Plastic wave theory, especially for uniaxial strain conditions, is reviewed by Herrmann, Chou and Hopkins [175] also treat high amplitude stress waves, primarily shock waves. A number of papers are to be found in the symposium proceedings of Kolsky and Prager [176].

1.4 Applications

1.4.1 Metal forming

Many metal-forming processes involve plastic deformation at medium or high rates of strain. In most such processes the material is subjected to a complex stress and strain history as it is deformed, and it is therefore difficult to determine precisely the strain rates involved. However, estimates of the orders of magnitude of these rates may be obtained by making reasonable assumptions concerning the kinematics of deformation. Atkins [177] has derived the following values for typical dimensions and speeds of working: sheet, rod or wire drawing, $1\text{-}10^3$ s^{-1}; cold rolling, $10^2\text{-}10^3$ s^{-1}; deep drawing, 1 s^{-1}. Theories of such processes, however, are usually based on a highly idealized constitutive relation, in which rate effects are ignored or taken into account simply by an empirical factor.

In metal-forming processes, the plastic strains reached are often very large, so that data obtained in simple tension or compression tests are inadequate because of the limited strains that can be achieved. One method of circumventing this difficulty is to test, at medium or high rate, specimens which have previously been cold-worked to a given strain. This method has been used by Karnes and Ripperger [134] for aluminium, and by Atkins and Porter [178] for mild steel.

The strain rates involved in machining have been estimated by Stevenson and Oxley [179]. By the measurement of grids inscribed on the work-piece, they were able to deduce the velocity gradients, *i,e,* strain rates, in the deformation zone; it was found that the mean shear strain rate in the zone was given by

$$\dot{\gamma}_m \sim V_s / d, \tag{4}$$

where V_s is the shear velocity and d is the depth of cut. For the typical values $V_s = 5\ m/s$ and $d = 0.55\ mm$, therefore, the value of $\dot{\gamma}_m$ is of the order of $10^4\ s^{-1}$. By measurement of the tool force it is possible to estimate the flow stress at large strains as a function of strain rate [48,49]. Results obtained in this way for mild steel agree well with extrapolation from values obtained at lower strains and strain rates. In particular, there is a rapid increase in the logarithmic rate sensitivity at high rates, which corresponds to that observed in shear tests using the split Hopkinson-bar technique.

Punching or blanking may also give rise to very high strain rates [180-183]. By measurement of the punch force and displacement it is possible to determine approximate shear stress-strain curves at rates of from 10^{-4} to 10^4 s^{-1} [31]. It is found that although the flow stress increases as the strain rate is increased, the energy absorbed in punching remains approximately constant; this is because the displacement to rupture decreases with increasing speed of deformation.

Many metal-working processes have in recent years been performed at high speed by use of stored energy rather than continuously supplied energy. The types of energy source used have included chemical (explosives), electrical, and mechanical or pneumatic, In some cases it is possible to form in this way objects which cannot easily be formed by conventional means. For example, very large domes can be formed by explosive forming in which the explosive is used to produce high pressures in water (standoff operation); in other applications such as welding or cladding, the explosive is in direct contact with the workpiece. In standoff operations the strain rates produced are typically of the order of 10^2 s^{-1}; in contact operations strain rates one or two orders of magnitude higher may be reached. The mechanical properties of materials formed by such operations may differ appreciably from those formed by conventional methods.

1.4.2 Structural mechanics

The advent of plastic design methods in structural engineering has led to the requirement that the post-yield behaviour of structural elements (beams, plates, *etc.*) should be known. In the case of structures which are subjected to impact loading, this means that the dynamic plastic behaviour must be determined. Cristescu [156] has considered the mechanics of wires and membranes under dynamic loading. The strength of steel beams in rapid plastic flexure has been measured [184,185] and the response of beams, frames and plates under impact loading has been studied [186-190]. These investigations have shown that in general it is necessary to allow for the strain rate in determining the dynamic plastic behaviour of structures. For mild-steel and aluminium-alloy beams in pure bending, an empirical relation due to Bodner and Symonds [187] has been found to be adequate at least as a first approximation:

$$k=C(M/M_0-1)^p \qquad (5)$$

In this equation, k is the curvature, M is the bending moment, M_0 is the "full-plastic" or "limit" moment, and C, p are constants for a given material; the equation therefore neglects work-hardening.

1.4.3 Crack propagation

The problem of crack propagation is one of the most important topics in applied mechanics, and also one the most intractable. The original paper of Griffith [191] is still the basis of many of the theoretical approaches to the problem. The subject of Fracture Mechanics, stemming from the ideas of Orowan and Irwin [192], has developed as a generalization of Griffith's energy method. Central to the subject is the concept of fracture toughness K_c, which is related to the energy absorbed by plastic deformation in extending the crack. The critical applied stress at which a crack of length a may propagate is given by

$$\sigma=\beta\frac{K_c}{\sqrt{a}} \tag{6}$$

where β is a numerical constant.

The quantity K_c is, however, not a material constant, but depends on various factors including specimen thickness, temperature and crack velocity. The problems involved in applying the fracture-toughness concept to rate-sensitive materials have been discussed in a review by Kenny and Campbell [193], where it was pointed out that progress depended on the development of an adequate description of the stress and strain distribution within the plastic zone at the crack tip, such a description incorporating strain-rate sensitivity effects. Kanninen *et al* [194] have made measurements of the speed of crack propagation in steel-foil specimens, and showed that strain rates exceeding 10^4 s^{-1} existed in the plastic zone. The research work of Klahn *et al* indicated that the speed of unstable crack propagation depends critically on the rate dependence of the flow properties of the material in the plastic zone in front of the crack tip and that the development of more detailed models of the mechanism of propagation requires further experimental data on this rate dependence.

1.5 Present work

Using an existing ballistic test machine, small cylindrical specimens of commercially pure copper and mild steel at various temperatures were impacted by a hardened tool steel projectile with very high speeds of up to 100 m/s. The initial velocity of the projectile is recorded by a laser velocity-measuring device and the deformation of the impacted specimen is measured. For the propose of high temperature tests, the improvements for the machine have been made and a movable anvil unit to reduce the loss of heat was designed and used.

A mathematical model with a mixed boundary condition, to which the theory of propagation of longitudinal waves of plastic deformation is applied, has been established. A numerical method of the indirect or iterative procedure to determine dynamic properties of materials at various temperatures based on the model has been utilized. The corresponding computer programs have also been written and used. The properties of wave-propagation in the impact process of the specimen have been analyzed, the factors affecting the deformation of the impacted specimen such as adiabatic shear phenomena, and the effects of shock loading and the boundary conditions at the anvil end have been discussed, and the optimum parameters have been selected. Further, a method to examine and determine the validity of the constitutive equations of materials is recommended. The forms of constitutive equations at high strain rates up to 10^5 s^{-1} for metals commercially pure copper and mild steel at various temperatures up to 400 °C have been proposed and the parameters in these suggested equations have been determined by means of agreement of the experimental results and numerical calculations. High strain rate properties established using the present technique have been compared with those found in the literature.

Chapter 2
Model Configurations and Numerical Solutions

2.1 Introduction

Generally, the theoretical analysis of an experimental system requires idealization of the system into a form that can be analyzed, formulation of governing equilibrium equations, and interpretation of the results. Therefore, it is necessary to establish a mechanical model of the experimental configuration which may be used to formulate corresponding mathematical equations, and it is also indispensable to develop a method which can be used to solve these governing equations. The solution obtained can be used both to examine the detail of mechanical properties with regard to the experimental system under the conditions of the model and to provide a means to further determine the constitutive equation of the material of the tested specimen.

In this chapter the mechanical model is first simplified based on the experimental system in which a small cylindrical specimen placed upon a hardened anvil is struck by a projectile with a high speed as shown in Fig. 1. Compressed air is used to propel the projectile and the dimensions of the impacted specimen before and after the test are measured. Secondly, the system equilibrium equations are derived and the elastic solution is given in which some basic concepts of the propagation of longitudinal wave are exhibited. Thirdly, the theory of propagation of longitudinal waves of plastic deformation is applied to the model, the quasi-linear elastic-plastic system equilibrium equations are established, along their characteristic lines, the program of the numerical solutions of the forward integration procedure is given. Finally the solutions of the equations subjected to the constitutive equation reported elsewhere under the typical parameters in the form of graphics are given and discussed.

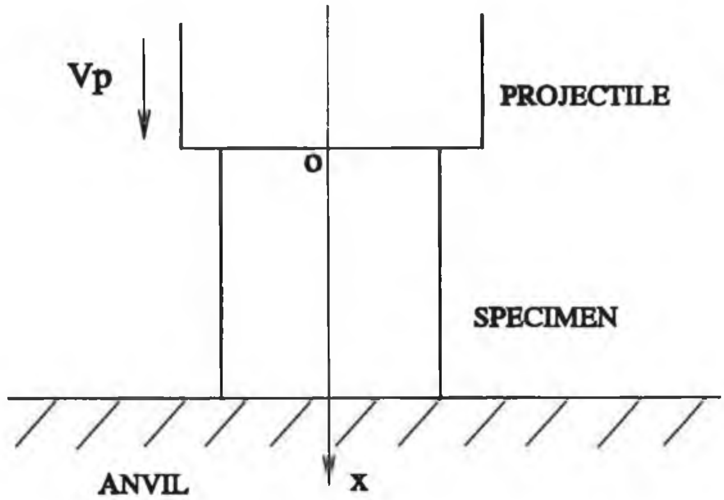

Fig. 1 *Arrangement of projectile, specimen and anvil.*

2.2 The Idealization of the System

(1) Compared with the impacted specimen, both the yield point and the elastic modulus of the projectile are considerably higher, so that, it can be considered as a rigid body in the process of the impact.

(2) The anvil is also considered as a rigid body for the same reasons as above, *i.e.* no deformation occurs in it in the process of the impact. Furthermore, because it is fixed at the frame of the testing machine, its mass is so great that the inertial acceleration of the surface between the anvil and the specimen can be negligible, which also means that the velocity at this surface remains zero.

(3) The stresses parallel to the central axis of the specimen are distributed uniformly over the cross section that is vertical to the axis.

(4) The friction between the projectile and the specimen is ignored.

2.3 The Elastic Theory of the Propagation of Waves

2.3.1 Longitudinal waves in a uniform bar

Considering an arbitrary cross section x of the model shown in Fig. 2 which has a increment dx, the element dx is regarded as in simple (tension) compression corresponding to the axial strain $\partial u/\partial x$, u being a function of x and t only. The other stress components are taken as negligible. Further considering the element originally between cross sections at x and $x+dx$, the equation of motion is

$$\frac{\partial(\sigma A)}{\partial x}dx=\rho A dx\frac{\partial^2 u}{\partial t^2} \tag{7}$$

where A is the area of the cross section of the specimen. When the variation of the area is ignored, we can obtain:

$$\frac{\partial\sigma}{\partial x}=\rho\frac{\partial^2 u}{\partial t^2} \tag{8}$$

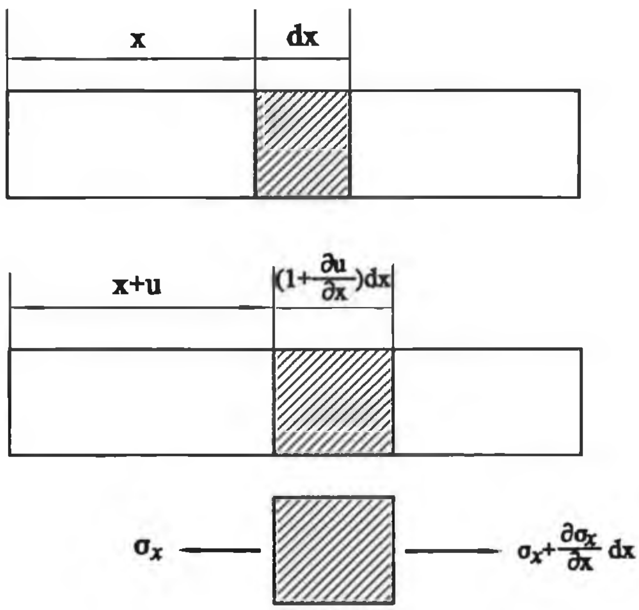

Fig. 2 *Diagram for governing equilibrium equation.*

Considering now the case when the stress applied to a specimen is below the dynamic elastic limit of the material (it is noted that both the stress and strain are conventional), the constitutive equation is

$$\sigma = E\frac{\partial u}{\partial x} \tag{9}$$

then, from Eq. (8)

$$\frac{\partial^2 u}{\partial x^2} = c^2\frac{\partial^2 u}{\partial t^2} \tag{10}$$

where

$$c = \sqrt{E/\rho} \tag{11}$$

It can be shown by substitution that any function $f(x\text{-}ct)$ is a solution of Eq. (10), any function $g(x+ct)$ is also a solution, and the general solution of Eq. (10) can be represented in the form

$$u = f(x-ct) + g(x+ct) \tag{12}$$

The general solution (12) represents two waves travelling along the x axis in two opposite directions with the velocity given by Eq. (11) dependent on the properties of the material. For stresses below the dynamic elastic limit of the material, this velocity of propagation depends on the density and the elastic constant.

When only the function f is retained in Eq.(12) (forward wave propagation), combined Eqs. (9) with (12) gives,

$$\sigma = -\rho c\frac{\partial u}{\partial t} = -\rho c v \tag{13}$$

whereas for g alone (backward wave propagation) one has

$$\sigma = \rho c\frac{\partial u}{\partial t} = \rho c v \tag{14}$$

where $v=\partial u/\partial t$ is the velocity of particles in the compressed zone of the specimen by the compressive forces. From Eqs. (11) and (14) one can get

$$\sigma = E\frac{v}{c} \tag{15}$$

or

$$\sigma = v\sqrt{E\rho} \tag{16}$$

The stress in the wave is thus determined by the ratio of the two velocities and by the modulus E of the material. If an absolutely rigid body, moving with a velocity strikes longitudinally the left-hand end of the specimen as shown Fig. 3, compressive stress on the surface of contact at the first instant is given by Eq. (16).

2.3.2 The elastic solution of the equations

Consider now the problem of a bar specimen with a fixed end struck by a moving mass at the other end (Fig. 3). Let M be the mass of the moving body per unit area of the cross section of the bar and v_0 the initial velocity of this body. Considering the body as absolutely rigid, the velocity of particles at the end of the bar at the instant of impact $(t=0)$ is v_0, and the initial compressive stress, from Eq. (16) is

$$\sigma_0 = v_0\sqrt{E\rho} \tag{17}$$

Owing to the resistance of the bar, the velocity of the moving body and hence the pressure on the bar will gradually decrease, and a compression wave is obtained with a decreasing compressive stress travelling along the length of the bar (Fig. 3b). The change in compression with the time can easily be found from the equation of motion of the body, it can be written as

$$M\frac{dv}{dt} + \sigma = 0 \tag{18}$$

or, substituting for v from Eq. (16),

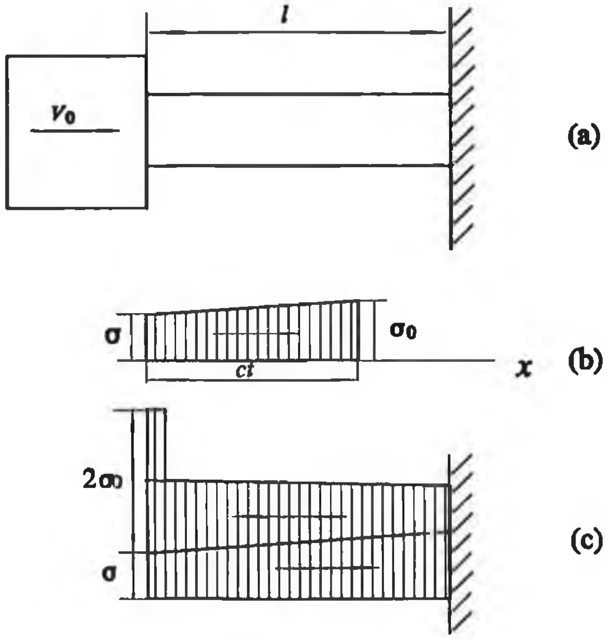

Fig. 3 *A bar with a fixed end struck by a moving mass at the other end.*

$$\frac{M}{\sqrt{E\rho}}\frac{d\sigma}{dt}+\sigma=0 \tag{19}$$

from which

$$\sigma=\sigma_0 e^{-t\sqrt{E\rho}/M} \tag{20}$$

This equation can be used so long as $t<2L/c$. When $t=2L/c$, the compressive wave with the front pressure σ_0 returns to the end of the bar that is in contact with the moving body. The velocity of the body cannot change suddenly, and hence the wave will be reflected from the fixed end and the compressive stress at the surface of contact suddenly increases by $2\sigma_0$, as is shown in Fig. 3c. Such a sudden increase of pressure occurs during impact at the end of every interval of time $T=2L/c$, and a separate expression for σ must be obtained for each one of these intervals. For the first interval, $0<t<T$, Eq. (20) is used. For the second interval, $T<t<2T$, the conditions represented by Fig. 3c applies, and the compressive stress σ is produced by two waves moving *away* from the struck end and one wave moving *toward* this end. Designating the total compressive stresses produced at the struck end by all waves moving away from this end $s_1(t)$, $s_2(t)$, $s_3(t)$,..., after the intervals of time T, $2T$, $3T$.... The waves coming back towards the struck end are merely the waves sent out during the preceding interval, delayed a time *T*, due to their travel across the bar and back. Hence the compression produced by these waves at the struck end is obtained by substituting *t-T*, for *t*, in the expression for the compression produced by waves sent out during the preceding interval. The general expression for the total compressive stress during any interval $nT < t < (n+1)T$ is therefore

$$\sigma = s_n(t) + s_{n-1}(t-T) \tag{21}$$

The velocity of particles at the struck end is obtained as the difference between the velocity due to the pressure $s_n(t)$ of the waves going away, and the velocity due to the pressure $s_{n-1}(t)$ of the waves going toward the end. Then, from Eq. (16),

$$v = \frac{1}{\sqrt{E\rho}}[s_n(t) - s_{n-1}(t-T)] \tag{22}$$

The relation between $s_n(t)$ and $s_{n-1}(t-T)$ can be obtained by using the equation of motion (18) of the striking body. Denoting by α the ratio of the mass of the bar to the mass of the striking body, and by L the length of the bar, one gets

$$\alpha = \frac{L\rho}{M}; \qquad \frac{\sqrt{E\rho}}{M} = \frac{cL\rho}{ML} = \frac{2\alpha}{T} \tag{23}$$

Comparing Eqs. (21), (22) and (23), and substituting Eq. (18), one has

$$\frac{d}{dt}[s_n(t) - s_{n-1}(t-T)] + \frac{2\alpha}{T}[s_n(t) + s_{n-1}(t-T)] = 0 \tag{24}$$

from which, s_n may be derived as

$$s_n = s_{n-1}(t-T) - \frac{4\alpha}{T} e^{-2\alpha t/T}\left[\int e^{2\alpha t/T} s_{n-1}(t-T)dt + C\right] \tag{25}$$

in which C is a constant of integration. This equation will now be used for deriving expressions for the consecutive values s_1, s_2... During the first interval $0<t<T$, the compressive stress is given by Eq. (20). During the interval, the velocity, strain and strain rate are respectively

$$\left.\begin{array}{l} v=v_0 e^{-t\alpha/M} \\ \varepsilon=\varepsilon_0 e^{-t\alpha/M} \\ \dot{\varepsilon}=-\dot{\varepsilon} e^{-t\alpha/T} \end{array}\right\} \tag{26}$$

where $\varepsilon=\sigma/E$ and $\dot{\varepsilon}=(\alpha\sigma_0)/(EM)$.

At the moment when the wave-front reaches the end of the specimen, the corresponding expressions at the arbitrary position x of the bar, are equal to those at $t=(T/2-x/c)$, which are formulated as

$$\left.\begin{array}{l} v=v_0 e^{-(1-x/L)\alpha} \\ \varepsilon=\varepsilon_0 e^{-(1-x/L)\alpha} \\ \dot{\varepsilon}=-\dot{\varepsilon}_0 e^{-(1-x/L)\alpha} \end{array}\right\} \tag{27}$$

It can be seen that all the variables at the struck end have linear relations between themselves, but decrease exponentially with regard to time. The variation of strain rate in the process of impact is dependent on the dimensions of the specimen, the ratio between the masses of the specimen and the projectile, and the initial velocity of impact.

2.4 The Elastic-Plastic Solution of the Equations

2.4.1 The equations and initial conditions

The plastic strain rate $\dot{\varepsilon}_p$ is a function of dynamic stress σ and strain ε

$$E\dot{\varepsilon}_p=g(\sigma,\varepsilon), \tag{28}$$

but elastic deformation is independent of strain rate and the elastic strain rate $\dot{\varepsilon}_e$ is related to the stress rate through Hooke's law

$$E\dot{\varepsilon}_e=\dot{\sigma}. \tag{29}$$

where E is the Young's modulus. Therefore, in order to study the problem of the propagation of longitudinal waves in a cylindrical specimen, a solution can be obtained from the following first order quasi-linear system containing three unknown functions σ, v and ε

$$\left.\begin{aligned} &E\frac{\partial\varepsilon}{\partial t}=\frac{\partial\sigma}{\partial t}+g(\sigma,\varepsilon),\\ &\frac{\partial v}{\partial t}=\frac{1}{\rho}\frac{\partial\sigma}{\partial x},\\ &\frac{\partial v}{\partial x}=\frac{\partial\varepsilon}{\partial t}. \end{aligned}\right\} \tag{30}$$

The first equation is the expression of constitutive relation proposed by Malvern [167], where ε denotes the total strain. The function $g(z)$ possesses the following properties

$$\begin{aligned} &g(z)>0 \quad \text{if } z>0,\\ &g(z)=0 \quad \text{if } z\leq 0. \end{aligned} \tag{31}$$

The second is the equation of motion Eq. (8), in which v is the particle velocity in the specimen, and ρ is the density of the material.

The third is the compatibility equation which is a consequence of the fact the $\varepsilon=\partial u/\partial x$ and $v=\partial u/\partial t$, where $u(x,t)$ is the displacement at time t of the cross section which is initially at distance x from the impact end of the specimen (see Fig. 1).

The initial height of the cylindrical specimen is h, so that the initial and boundary conditions can be formulated as follows:

(a) the initial condition is:

$$t=0,\quad 0\leq x\leq h:\quad \sigma=0,\quad \varepsilon=0,\quad v=0. \tag{32}$$

(b) the boundary condition at the fixed end $x=h$ is given by

$$x=h,\quad \begin{cases} T_1>t\geq 0: & v=0,\\ t\geq T_1: & \sigma=0. \end{cases} \tag{33}$$

where T_1 is the contact time of the specimen with the anvil, which can be determined during the calculation.

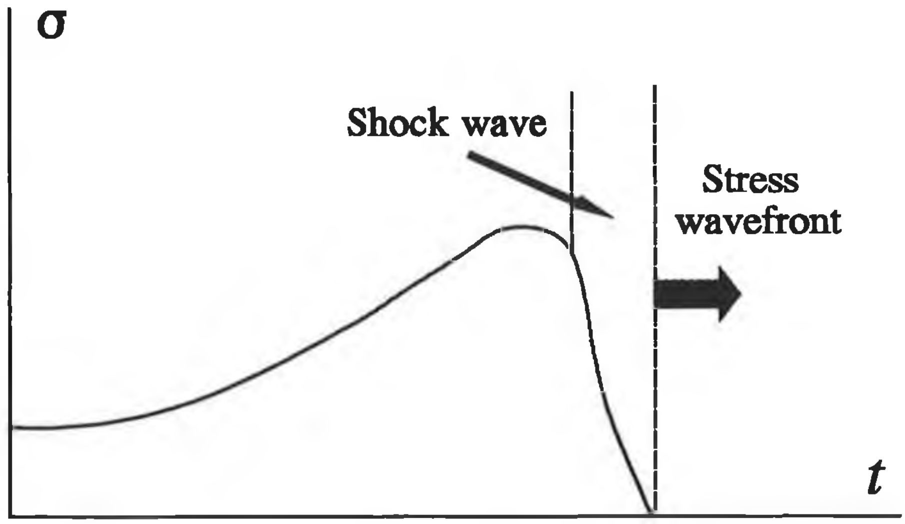

Fig. 4 *Idealized schematic view of a shock pulse travelling through a solid material.*

(c) At the impacted end, although the load is suddenly applied to the specimen, in reality this stress wave-front may not be abrupt, and is therefore not planar in the form of a planar interface. It might therefore be illustrated in the context of time and stress as shown in the schematic of Fig. 4. In the figure, the shock front is shown as a region where the material is subjected to increasing stress up to the peak shock pressure.

For materials with an upper yield point, high strain rate tests show a relatively greater strain rate sensitivity at yield stress than at other flow stress. This has been suggested to take place due to dislocation inertia or "Cottrel Rotation". However, in the present study, it has been shown that due to shock wave a large over-stress develops during the initial stages of deformation. The question arises that the so called dislocation inertia effect is due to shock wave or a combination of shock wave and "Cottrel Rotation". In the absence of any experimental stress-time results it was not possible to fully investigate this aspect.

Considering the effect of shock waves, the conditions on the moving end that is acted on by the projectile is a mixed boundary condition. The final forms of which are expressed by following equation

$$x=0, \quad \begin{cases} v=\dfrac{v_0}{T_0}t & 0\le t\le T_0, \\ M\dfrac{\partial v}{\partial t}+\sigma=0 & t>T_0. \end{cases} \tag{34}$$

where v_0 is the velocity of the projectile at $t=0$, M is the mass of the projectile per unit area of the cross-section of the specimen and σ is the compressive pressure between the projectile and the specimen. In order to simplify the calculation, in the first condition of Eq. (34) the sudden impact has been handled by a fast, but smooth variation of the impact within T_0 which is the time during which the shock wave-front increases up to the peak stress. The second condition in Eq. (34) is a so-called mixed boundary condition used in the following calculation.

2.4.2 *Method of characteristics*

A powerful mathematical tool for the solution to many problems in wave propagation is the method of characteristics. The method can be applied to systems of equations in the space and time variables x and t to determine the values of the dependent variables such as σ, v and ε numerically. The method is applicable to equations of the form

$$a_{ij}\frac{\partial u_j}{\partial x}+b_{ij}\frac{\partial u_j}{\partial t}=R_i \tag{35}$$

where repeated subscripts indicate summation. These are a set of quasi-linear equations, that is linear in the first derivatives, in the variables u_j, where the coefficients a_{ij}, b_{ij} and R_i may be functions of u_j, x, and t.

Eqs. (30), which describe a problem of waves propagating in a long rod governed by the rate dependent theory of plastic wave propagation, may be written as the following linear combination multiplied by α_1, α_2 and α_3, respectively, in terms of the stress σ, strain ε and particle velocity v, as

$$\alpha_2\frac{\partial v}{\partial t}+\alpha_3\frac{\partial v}{\partial x}-\alpha_1\frac{\partial \sigma}{\partial t}-\frac{\alpha_2}{\rho}\frac{\partial \sigma}{\partial x}+(\alpha_1 E-\alpha_3)\frac{\partial \varepsilon}{\partial t}=\alpha_1 g(\sigma,\varepsilon) \tag{36}$$

Note that the differential of a function $f(x,t)$ in the x-t plane is

$$df=\frac{\partial f}{\partial x}dx+\frac{\partial f}{\partial t}dt \tag{37}$$

Therefore, Eq. (36) may also be rewritten as

$$\frac{\alpha_2}{\alpha_1}(\frac{\partial v}{\partial t}dt+\frac{\alpha_3}{\alpha_2}\frac{\partial v}{\partial x}dt)-(\frac{\partial \sigma}{\partial t}dt+\frac{\alpha_2}{\rho\alpha_1}\frac{\partial \sigma}{\partial x}dt)+(E-\frac{\alpha_3}{\alpha_1})\frac{\partial \varepsilon}{\partial t}dt=g(\sigma,\varepsilon)dt \tag{38}$$

In order to find such a direction along which Eq. (36) can be written as a form of an entire differential, the following three relations are required,

$$\frac{\alpha_3}{\alpha_2}dt=dx, \qquad \frac{\alpha_2}{\rho\alpha_1}dt=dx \quad \text{and} \quad E-\frac{\alpha_3}{\alpha_1}=0, \tag{39}$$

from which one can obtain

$$\frac{dx}{dt}=\sqrt{\frac{E}{\rho}}=c \tag{40}$$

and

$$\frac{dx}{dt}=-\sqrt{\frac{E}{\rho}}=-c. \tag{41}$$

Along the Eqs.(40) and (41) the differential relations from (38) are respectively

$$d\sigma-\rho c dv=-g(\sigma,\varepsilon)dt \tag{42}$$

and

$$d\sigma+\rho c dv=-g(\sigma,\varepsilon)dt. \tag{43}$$

where

$$c=\sqrt{\frac{E}{\rho}}=Const. \tag{44}$$

It can be found that when $\alpha_2=\alpha_3=0$, or $dx=0$, Eq. (38) can also be written as a form of entire differential, *i.e.* along

$$dx=0, \tag{45}$$

$$Ed\varepsilon=d\sigma+g(\sigma,\varepsilon)dt. \tag{46}$$

The fact that the characteristic directions are fixed straight lines in the x-t or characteristic plane (Fig. 6), can greatly simplify the numerical integration. The solution is obtained by a numerical forward integration procedure using the initial conditions Eq. (32) along x-axis and the boundary conditions Eqs.(33) and (34) that are prescribed along the t-axis. The region as shown in Fig. 6, ahead of the leading elastic wave front $x=ct$, is at rest for assumed zero initial conditions.

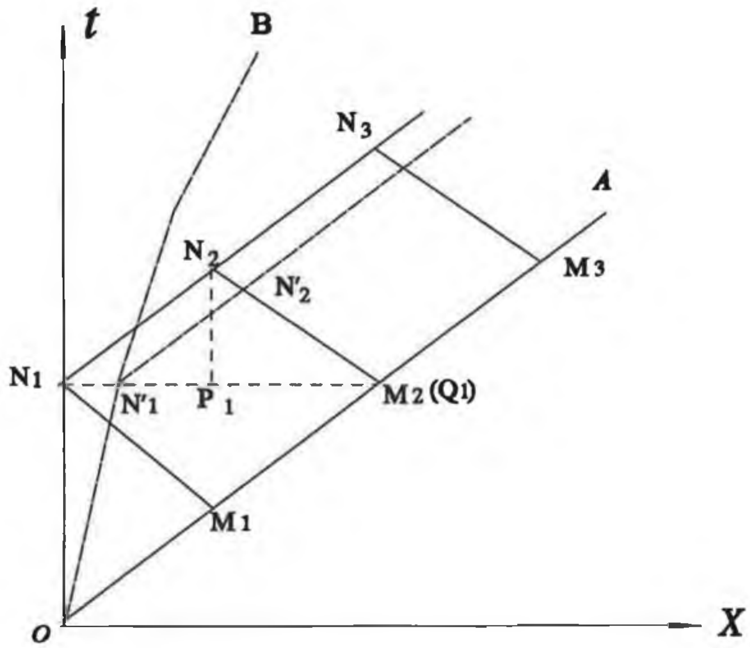

Fig. 5 *Characteristic field for floating boundaries.*

2.4.3 *Numerical integration*

Considering the case as shown in Fig. 5, the region under and including line *OA* is at rest for assumed zero initial conditions. This line is divided into a number (*NELEM*) of small segments OM_1, M_1M_2, etc., whose lengths are chosen to be equal. The length and the time interval corresponding to a segment are $DLETH = h / NELEM$ and $DTIME=DLETH / c$ respectively where c is the velocity of the propagating wave and is given by Eq. (11). In the condition of the interval of the initial shock stress wave *TLIMIT*>0, the stress, strain and velocity along the line *OA* are set as zero, else, they are set as the peak value, *i.e.* the effect of the shock stress wave is ignored. The corresponding program is shown as Subroutine *INITIAL*.

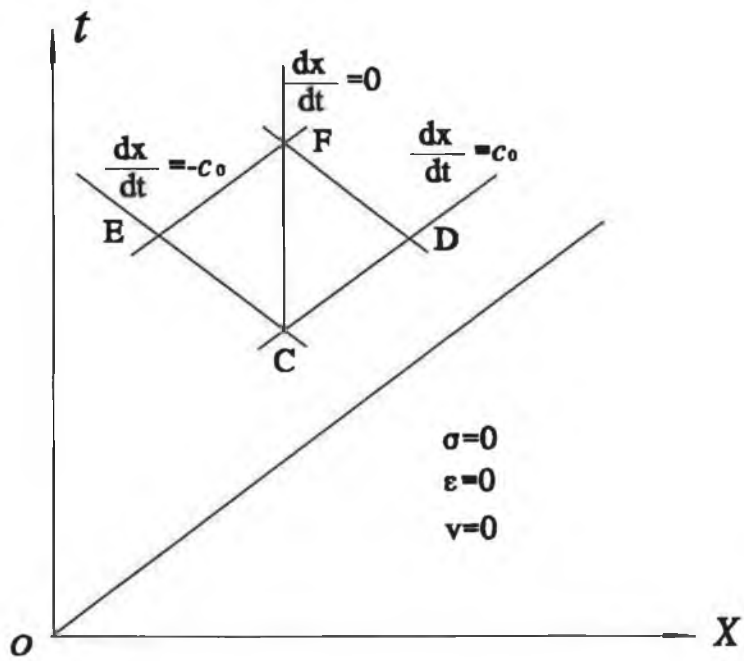

Fig. 6 *Characteristic line showing leading wave front and interior mesh points.*

```
      SUBROUTINE INITIAL(DVECO,DTIME)
C*********************************************************************
C                        ***  THE INITIAL CONDITIONS ***
C*********************************************************************
      COMMON NELEM,NCONT(0:500),PLETH,PMODL,PPEXP,PCOFB,PYILD,PBROK,
     . TLIMIT,SWITCH,PDESY,PVELO,XLETH(0:50000),TIME(0:50000),
     . STRAN(0:50000),STRES(0:50000),VELOY(0:50000),DEFOM(0:50000)
      IF (TLIMIT .NE. 0.) THEN
```

```
      DO 100 J=0,NELEM
      STRES(J)=0.
      STRAN(J)=0.
      VELOY(J)=0.
      TIME(J)=J*DTIME
      XLETH(J)=DVEC0*TIME(J)
      DEFOM(J)=0.
100   CONTINUE
      ELSE
      DO 200 J=0,NELEM
      VELOY(J)=PVELO
      STRES(J)=-PVELO*SQRT(PMODL*PDESY)
      STRAN(J)=STRES(J)/PMODL
      TIME(J)=J*DTIME
      XLETH(J)=DVEC0*TIME(J)
200   CONTINUE
      END IF
      RETURN
      END
```

From the point M_1 (Fig. 5) the characteristic line of negative slope (41) is

$$x-x_{M_1}=-c(t-t_{M_1}) \tag{47}$$

From Eq. (47) the position of point N_1 on Ot axis is obtained as

$$x_{N_1}=0,\quad t_{N_1}=\frac{x_{M_1}}{c}+t_{M_1} \tag{48}$$

The boundary condition Eq. (34), written in the forms

$$x=0,\quad \begin{cases} v_{N_1}=\dfrac{v_0}{T_0}t_{N_1} & 0\le t\le T_0, \\[2ex] M\dfrac{v_{N_1}-v_0}{t_{N_1}-t_0}+\sigma_0=0 & t>T_0. \end{cases} \tag{49}$$

is integrated along ON_1. Therefore, the velocity at N_1 can be obtained as follows

$$\begin{aligned} v_{N_1}&=\frac{v_0}{T_0}t_{N_1} && 0\le t\le T_0, \\ v_{N_1}&=v_0-\frac{\sigma_0}{M}(t_{N_1}-t_0) && t>T_0. \end{aligned} \tag{50}$$

Then, the differential relation (43), written in the form

$$\sigma-\sigma_{M_1}=-\rho c(v-v_{M_1})-g(\sigma_{M_1},\varepsilon_{M_1})(t-t_{M_1}) \tag{51}$$

is integrated along M_1N_1. From Eq. (51) σ_{N1} is determined. Then Eq. (46) is transformed into a finite difference equation

$$E(\varepsilon-\varepsilon_0)=(\sigma-\sigma_0)+g(\sigma_0,\varepsilon_0)(t-t_0) \tag{52}$$

and is integrated. This yields ε_{N1}. Thus, at the point N_1 the values of all the functions required are now known.

In order to obtain a closer approximation of these functions, the calculation can be repeated again. For this purpose velocity v_{N1} in Eq. (50) and the function $g(\sigma,\varepsilon)$ in Eq. (51) are calculated using the values $(\sigma_0+\sigma_{N1})/2$ and $(\varepsilon_0+\varepsilon_{N1})/2$ for σ and ε, while that in Eq. (52) using $(\sigma_{M1}+\sigma_{N1})/2$ and $(\varepsilon_{M1}+_{N1})/2$ for σ and ε. Here σ_{N1} and ε_{N1} represent the first approximations of the respective functions. In this way, v_{N1}, σ_{N1} and ε_{N1} are obtained more exactly.

The subroutine to evaluate the unknown variables σ, ε and v on the boundary of the moving end is as follows:

```
      SUBROUTINE BOUND1(DPMAS,DLOC0,I)
C*********************************************************************
C     ***  CALCULATING THE BOUNDARY VALUES AT THE MOVING END   ***
C*********************************************************************
      COMMON NELEM,NCONT(0:500),PLETH,PMODL,PPEXP,PCOFB,PYILD,PBROK,
     . TLIMIT,SWITCH,PDESY,PVELO,XLETH(0:50000),TIME(0:50000),
     . STRAN(0:50000),STRES(0:50000),VELOY(0:50000),DEFOM(0:50000)
      TIME(NCONT(I))=TIME(NCONT(I-1)+1)-(XLETH(NCONT(I-1))
     . -XLETH(NCONT(I-1)+1))/DLOC0*PDESY
      IF (((TIME(NCONT(I))+TIME(NCONT(I-1)))/2) .LE. TLIMIT) THEN
      VELOY(NCONT(I))=PVELO*TIME(NCONT(I))/TLIMIT
      ELSE
      VELOY(NCONT(I))=VELOY(NCONT(I-1))+(TIME(NCONT(I))
     . -TIME(NCONT(I-1)))/DPMAS*STRES(NCONT(I-1))
      END IF
      STRES(NCONT(I))=STRES(NCONT(I-1)+1)-DLOC0*(VELOY(NCONT(I))
     . -VELOY(NCONT(I-1)+1))-(TIME(NCONT(I))-TIME(NCONT(I-1)+1))
     .   *FUNSTA(STRES(NCONT(I-1)+1),STRAN(NCONT(I-1)+1))
      STRAN(NCONT(I))=STRAN(NCONT(I-1))+(STRES(NCONT(I))
     . -STRES(NCONT(I-1))+(TIME(NCONT(I))-TIME(NCONT(I-1)))
     . *FUNSTA(STRES(NCONT(I-1)),STRAN(NCONT(I-1))))/PMODL
      ATRES1=(STRES(NCONT(I-1)+1)+STRES(NCONT(I)))/2.
```

```
      ATRAN1=(STRAN(NCONT(I-1)+1)+STRAN(NCONT(I)))/2.
      ATRES2=(STRES(NCONT(I-1))+STRES(NCONT(I)))/2.
      ATRAN2=(STRAN(NCONT(I-1))+STRAN(NCONT(I)))/2.
      IF (((TIME(NCONT(I))+TIME(NCONT(I-1)))/2) .GT. TLIMIT) THEN
      VELOY(NCONT(I))=VELOY(NCONT(I-1))+(TIME(NCONT(I))
     . -TIME(NCONT(I-1)))/DPMAS*ATRES2
      END IF
      STRES(NCONT(I))=STRES(NCONT(I-1)+1)-DLOC0*(VELOY(NCONT(I))
     . -VELOY(NCONT(I-1)+1))-(TIME(NCONT(I))
     . -TIME(NCONT(I-1)+1))*FUNSTA(ATRES1,ATRAN1)
      STRAN(NCONT(I))=STRAN(NCONT(I-1))+(STRES(NCONT(I))
     . -STRES(NCONT(I-1))+(TIME(NCONT(I))-TIME(NCONT(I-1)))
     . *FUNSTA(ATRES2,ATRAN2))/PMODL
100   RETURN
      END
```

To obtain the values of the unknown functions at an interior point, the procedure used is as follows. Considering the point N_2 (Fig. 5), its position will be found at the intersection of two characteristic lines Eqs. (40) and (41)

$$x-x_{N_1}=c(t-t_{N_1}),\qquad x-x_{M_2}=-c(t-t_{M_2}). \tag{53}$$

Then from the relation in Eqs. (42) and (43) written in the form

$$\sigma-\sigma_{N_1}=\rho c(v-v_{N_1})-g(\sigma_{N_1},\varepsilon_{N_1})(t-t_{N_1})$$
$$\sigma-\sigma_{M_2}=-\rho c(v-v_{M_2})-g(\sigma_{M_2},\varepsilon_{M_2})(t-t_{M_2}) \tag{54}$$

σ_{N2} and v_{N2} can be obtained. The algorithm necessary to obtain ε_{N2} is more complicated. The segment N_1M_2 can be drawn whose intersection with the straight line $x=$ *const.*, passing through N_2 gives the coordinates of P_1. Then, by interpolating linearly between N_1 and M_2, the values of σ_{P1} and ε_{P1} are obtained at this point

$$(x_{M_2}-x_{N_1})\sigma_{P_1}=(x_{P_1}-x_{N_1})\sigma_{M_2}+(x_{M_2}-x_{P_1})\sigma_{N_1} \tag{55}$$

and

$$(x_{M_2}-x_{N_1})\varepsilon_{P_1}=(x_{P_1}-x_{N_1})\varepsilon_{M_2}+(x_{M_2}-x_{P_1})\varepsilon_{N_1}. \tag{56}$$

Now, from Eq. (46) written in the form

$$E(\varepsilon-\varepsilon_{P_1})=\sigma-\sigma_{P_1}+g(\sigma_{P_1},\varepsilon_{P_1})(t-t_{P_1}) \tag{57}$$

one may proceed for obtaining ε_{N2} since σ_{N2} and t_{N2} are already known. For a second approximation the procedure is similar to that given above.

The mathematical model is a mixed boundary value problem, that is to say, the curve *OB* shown in Fig. 5 is a floating boundary, which can be obtained step by step at the same time as the solution is procured. This curve represents the motion of the projectile which strikes the specimen.

After the solution at each interior point has be completed, the coordinate of its adjoining point will be treated considering the floating boundary. In order to determine the position of N_1 within the time t_{N1}, a horizontal line of $t=t_{N1}$. is drawn from point N_1 to intersect the segment of the line *OA*. This gives the point Q_1 (which may not coincide with M_2), and then by interpolation between M_1 and M_2, ε_{Q1} is also obtained. Hence, the deformation between N_1 and Q_1, i.e. the displacement at the point N_1, is approximately given by

$$\Delta h_{N_1}=\frac{\varepsilon_{N_1}+\varepsilon_{Q_1}}{2}(x_{Q_1}-x_{N_1}) \tag{58}$$

Thus, the coordinate of the floating boundary at the point N'_1 is obtained.

The subroutine to determine the unknown functions in the inner points of integration framework and the coordinate of the floating boundary is as follows:

```
      SUBROUTINE INNER(DVEC0,DLOC0,I,J)
C**********************************************************************
C                ***  THE SOLUTION OF THE INNER FIELD  ***
C**********************************************************************
      COMMON NELEM,NCONT(0:500),PLETH,PMODL,PPEXP,PCOFB,PYILD,PBROK,
     . TLIMIT,SWITCH,PDESY,PVELO,XLETH(0:50000),TIME(0:50000),
     . STRAN(0:50000),STRES(0:50000),VELOY(0:50000),DEFOM(0:50000)
      XLETH(NCONT(I)+J)=((TIME(NCONT(I-1)+J+1)-TIME(NCONT(I)+
     . J-1))*DVEC0+XLETH(NCONT(I-1)+J+1)+XLETH(NCONT(I)+J-1))/2.
      TIME(NCONT(I)+J)=(TIME(NCONT(I-1)+J+1)+TIME(NCONT(I)+J-1)+
     . (XLETH(NCONT(I-1)+J+1)-XLETH(NCONT(I)+J-1))/DVEC0)/2.
      STRES(NCONT(I)+J)=((VELOY(NCONT(I-1)+J+1)-VELOY(NCONT(I)
     . +J-1))*DLOC0+STRES(NCONT(I-1)+J+1)+STRES(NCONT(I)+J-1)
     . -(TIME(NCONT(I)+J)-TIME(NCONT(I-1)+J+1))*FUNSTA(STRES(
```

```
.  NCONT(I-1)+J+1),STRAN(NCONT(I-1)+J+1))-(TIME(NCONT(I)+J)
.  -TIME(NCONT(I)+J-1))*FUNSTA(STRES(NCONT(I)+J-1),
.  STRAN(NCONT(I)+J-1)))/2.
   STRESP=((XLETH(NCONT(I)+J)-XLETH(NCONT(I)+J-1))
.  *STRES(NCONT(I-1)+J+1)+(XLETH(NCONT(I-1)+J+1)
.  -XLETH(NCONT(I)+J))*STRES(NCONT(I)+J-1))
.  /(XLETH(NCONT(I-1)+J+1)-XLETH(NCONT(I)+J-1))
   STRANP=((XLETH(NCONT(I)+J)-XLETH(NCONT(I)+J-1))
.  *STRAN(NCONT(I-1)+J+1)+(XLETH(NCONT(I-1)+J+1)
.  -XLETH(NCONT(I)+J))*STRAN(NCONT(I)+J-1)
.  )/(XLETH(NCONT(I-1)+J+1)-XLETH(NCONT(I)+J-1))
   TIMEP=((XLETH(NCONT(I)+J)-XLETH(NCONT(I)+J-1))
.  *TIME(NCONT(I-1)+J+1)+(XLETH(NCONT(I-1)+J+1)-XLETH(NCONT(I)
.  +J))*TIME(NCONT(I)+J-1))
.  /(XLETH(NCONT(I-1)+J+1)-XLETH(NCONT(I)+J-1))
   STRAN(NCONT(I)+J)=STRANP+(STRES(NCONT(I)+J)-STRESP+(TIME(
.  NCONT(I)+J)-TIMEP)*FUNSTA(STRESP,STRANP))/PMODL
   ATRES1=(STRES(NCONT(I-1)+J+1)+STRES(NCONT(I)+J))/2.
   ATRAN1=(STRAN(NCONT(I-1)+J+1)+STRAN(NCONT(I)+J))/2.
   ATRES2=(STRESP+STRES(NCONT(I)+J))/2.
   ATRAN2=(STRANP+STRAN(NCONT(I)+J))/2.
   ATRES3=(STRES(NCONT(I)+J-1)+STRES(NCONT(I)+J))/2.
   ATRAN3=(STRAN(NCONT(I)+J-1)+STRAN(NCONT(I)+J))/2.
   STRES(NCONT(I)+J)=((VELOY(NCONT(I-1)+J+1)-VELOY(NCONT(I)+J-1))
.  *DLOC0+STRES(NCONT(I-1)+J+1)+STRES(NCONT(I)+J-1)-(TIME(NCONT(I)
.  +J)-TIME(NCONT(I-1)+J+1))*FUNSTA(ATRES1,ATRAN1)-(TIME(NCONT(I)
.  +J)-TIME(NCONT(I)+J-1))*FUNSTA(ATRES3,ATRAN3))/2.
   VELOY(NCONT(I)+J)=(VELOY(NCONT(I-1)+J+1)+VELOY(NCONT(I)
.  +J-1))/2.+(STRES(NCONT(I-1)+J+1)-STRES(NCONT(I)+J-1)
.  +(TIME(NCONT(I)+J)-TIME(NCONT(I-1)+J+1))*
.  FUNSTA(ATRES1,ATRAN1)-(TIME(NCONT(I)+J)
.  -TIME(NCONT(I)+J-1))*FUNSTA(ATRES3,ATRAN3))/2./DLOC0
   STRAN(NCONT(I)+J)=STRANP+(STRES(NCONT(I)+J)-STRESP+
.  (TIME(NCONT(I)+J)-TIMEP)*FUNSTA(ATRES2,ATRAN2))/PMODL
   DXLETH=(STRAN(NCONT(I)+J-1)+STRAN(NCONT(I-1)+J+1))/2.
.  *(XLETH(NCONT(I-1)+J+1)-XLETH(NCONT(I)+J-1))
   DEFOM(NCONT(I)+J-1)=DEFOM(NCONT(I-1)+J+1)+DXLETH
   RETURN
   END
```

Since the velocity is a constant ($v=0$) at the fixed end, the procedure is similar to that at the moving end, and is also simpler. As shown in Fig. 7, since the unknown variables at points M_k and N_k have been obtained, for the point N_{k+1}, its position will be found at intersection of two characteristic lines (40) and (45), approximated by the straight lines

$$x-x_{N_k}=c(t-t_{N_k}),\quad x=h. \tag{59}$$

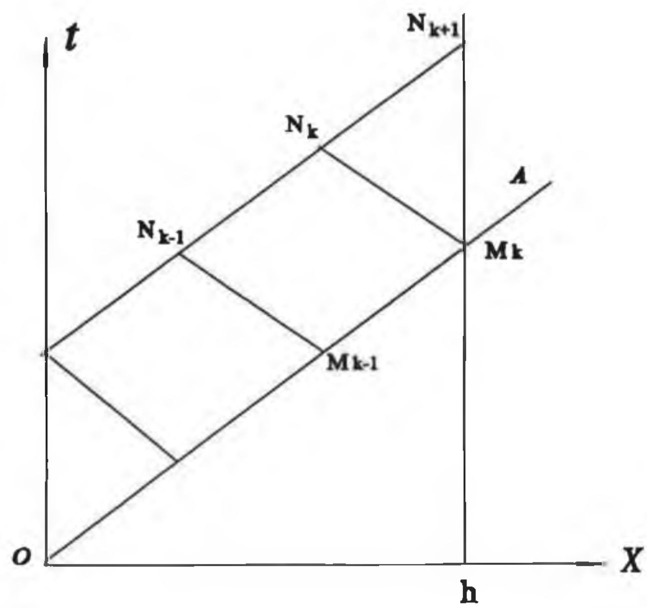

Fig. 7 *Characteristic field for fixed boundary.*

Then the differential relation from Eq. (42) written in the form

$$\sigma-\sigma_{N_k}=\rho c(v-v_{N_k})-g(\sigma_{N_k},\varepsilon_{N_k})(t-t_{N_k}) \tag{60}$$

is integrated along N_kN_{k+1} and σ_{k+1} is obtained.

Finally, the relation (46) is transformed into a finite difference equation

$$E(\varepsilon-\varepsilon_{M_k})=\sigma-\sigma_{M_k}+g(\sigma_{M_k},\varepsilon_{M_k})(t-t_{M_k}) \tag{61}$$

and is integrated to obtain ε_{k+1}.

In the same manner as before, a second approximation is also made. The subroutine to determine the unknown functions on the fixed boundary is as follows:

```
      SUBROUTINE BOUND2(NUMBR,DVECO,DLOCO,I)
C*********************************************************************
C       *** CALCULATING THE BOUNDARY VALUES AT THE MOVING END ***
C*********************************************************************
      COMMON NELEM,NCONT(0:500),PLETH,PMODL,PPEXP,PCOFB,PYILD,PBROK,
     . TLIMIT,SWITCH,PDESY,PVELO,XLETH(0:50000),TIME(0:50000),
     . STRAN(0:50000),STRES(0:50000),VELOY(0:50000),DEFOM(0:50000)
      XLETH(NCONT(I)+NELEM)=PLETH
```

```
      VELOY(NCONT(I)+NELEM)=0.
      TIME(NCONT(I)+NELEM)=TIME(NCONT(I)+NELEM-1)
     . +(XLETH(NCONT(I-1)+NELEM)-XLETH(NCONT(I)+NELEM-1))/DVEC0
      STRES(NCONT(I)+NELEM)=STRES(NCONT(I)+NELEM-1)+DLOC0*
     . (VELOY(NCONT(I)+NELEM)-VELOY(NCONT(I)+NELEM-1))
     . -(TIME(NCONT(I)+NELEM)-TIME(NCONT(I)+NELEM-1))
     . *FUNSTA(STRES(NCONT(I)+NELEM-1),STRAN(NCONT(I)+NELEM-1))
      STRAN(NCONT(I)+NELEM)=STRAN(NCONT(I-1)+NELEM)+(STRES(NCONT(I)
     . +NELEM)-STRES(NCONT(I-1)+NELEM)+(TIME(NCONT(I)+NELEM)
     . -TIME(NCONT(I-1)+NELEM))*FUNSTA(STRES(NCONT(I-1)+NELEM),
     . STRAN(NCONT(I-1)+NELEM)))/PMODL
      ATRES1=(STRES(NCONT(I)+NELEM-1)+STRES(NCONT(I)+NELEM))/2.
      ATRAN1=(STRAN(NCONT(I)+NELEM-1)+STRAN(NCONT(I)+NELEM))/2.
      ATRES2=(STRES(NCONT(I-1)+NELEM)+STRES(NCONT(I)+NELEM))/2.
      ATRAN2=(STRAN(NCONT(I-1)+NELEM)+STRAN(NCONT(I)+NELEM))/2.
      STRES(NCONT(I)+NELEM)=STRES(NCONT(I)+NELEM-1)+DLOC0
     . *(VELOY(NCONT(I)+NELEM)-VELOY(NCONT(I)+NELEM-1))
     . -(TIME(NCONT(I)+NELEM)-TIME(NCONT(I)+NELEM-1))
     . *FUNSTA(ATRES1,ATRAN1)
      STRAN(NCONT(I)+NELEM)=STRAN(NCONT(I-1)+NELEM)+(STRES(NCONT(I)
     . +NELEM)-STRES(NCONT(I-1)+NELEM)+(TIME(NCONT(I)+NELEM)
     . -TIME(NCONT(I-1)+NELEM))*FUNSTA(ATRES2,ATRAN2))/PMODL
      DXLETH=(STRAN(NCONT(I)+NELEM-1)+STRAN(NCONT(I)-2))/2.
     . *(XLETH(NCONT(I)-2)-XLETH(NCONT(I)+NELEM-1))
      DEFOM(NCONT(I)+NELEM-1)=DEFOM(NCONT(I)-2)+DXLETH
      DEFOM(NCONT(I)+NELEM)=0.
 100  RETURN
      END
```

2.5 Simulations of the Program

2.5.1 The constitutive equation

In order to check this method and easily compare with experimental results, in the numerical example the experimental data obtained by [33] for pure copper is used. Based on these experimental results, the quasi-static stress-strain curve is obtained as follows

$$f_0(\varepsilon)=255.1\times\log(34.1315\varepsilon+1) \quad (MPa) \tag{62}$$

and the dynamic constitutive equation as shown in Fig. 8 is

$$\begin{aligned} &\sigma=f_0(\varepsilon)+(0.64+43.1\varepsilon)(\log\dot{\varepsilon}_p+4) \ (MPa) && \dot{\varepsilon}_p\le 10^3 s^{-1} \\ &\sigma=f_0(\varepsilon)+(4.48+301.7\varepsilon)+2.9331\times(10^{-3}\dot{\varepsilon}_p-1) \ (MPa) && \dot{\varepsilon}_p>10^3 s^{-1} \end{aligned} \tag{63}$$

from which the function $g(\sigma,\varepsilon)$ in Eqs. (30) can be obtained.

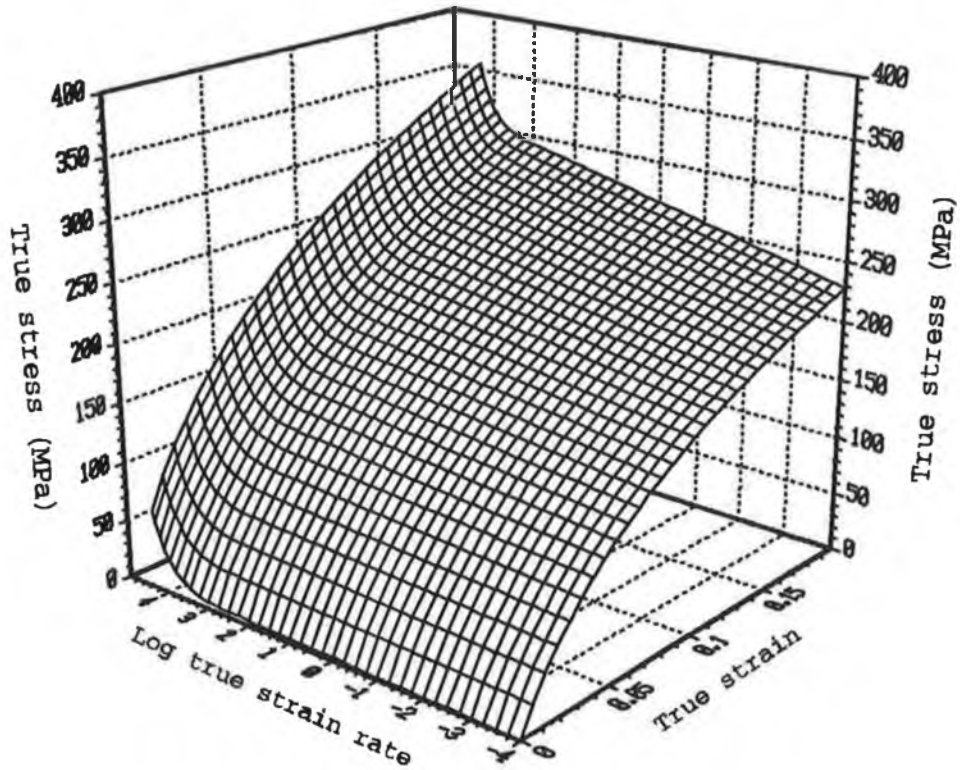

Fig. 8 *The regressed stress, strain and plastic strain-rate surface for copper at the room temperature based on data in [33].*

It has been noted that although the impact test can be considered as an adiabatic process, in the current analysis of the chosen commercially pure copper specimen and the velocity of the projectile, the effect of temperature can be neglected according to ref. [33] which estimated that the temperature rise and flow stress decrease for adiabatic deformation of this material deformed to a strain of 0.2 at the strain rate of 6×10^3 s^{-1} are 12 K and 2 MPa respectively (Details will be discussed later).

2.5.2 Initial data and input

The initial velocity of the projectile v_0=*40 (m/s)*, and the mass of the projectile *M=0.1 (kg)*. In the ballistic tests, the typical dimensions of the specimen are diameter *d=5 (mm)* and height *h=5 (mm)*. In order to demonstrate more clearly the mechanical properties in the process of the impact in graphical form, the dimensions of the specimen is chosen as *h=10 (mm)* and *d=5 (mm)*.

The loading time of shock stress T_0 is very short. Therefore, in the current calculation T_0=5 (μs). Under the condition of room temperature, the parameters and the symbols in the program are as follows:

The number of elements *NELEM=160,*
The length of the specimen *PLETH=10 (mm),*
The diameter of the specimen *PDAMT=5 (mm),*
The density of the specimen material *PDESY*=8.96×10^3 (kg/m^3),
The elastic modulus of the specimen material *PMODL=110 (GPa),*
The yield stress *PYILD=55 (MPa),*
The mass of the projectile *PPMAS= 10 (g),*
The initial velocity of the projectile *VELOY=40 (m/s),*
The acting time of shock stress *TLIMIT*=5 (μs).

NMUBR, JSTEP, NTP in Subroutine *DINPUT* are the controlling parameters in the process of the calculation of the output of results. *SWITCH* is a switch variable which controls the choice of constitutive equations.

```
      SUBROUTINE DINPUT (PDAMT,PPMAS,NUMX,NUMT,NTP)
C**********************************************************************
C          ***  INITIAL INPUT AND CALCULATION OF PARAMETERS   ***
C**********************************************************************
      COMMON NELEM,PLETH,PMODL,PHEAT,PCOFB,PYILD,PBROK,TLIMIT,SWITCH,
     . PDESY,PVELO,TEMP0,XLETH(0:20000),TIME(0:20000),STRAN(0:20000),
     . STRES(0:20000),VELOY(0:20000),DEFOM(0:20000),ERATE(0:20000),
     . TEMPR(0:20000)
      OPEN (5,FILE='TOND.DAT',STATUS='OLD')
      OPEN (10,FILE='TOND.RES',STATUS='NEW')
      READ (5,*) NELEM,NUMX,NUMT,NTP
      WRITE(10,301) NELEM,NUMX,NUMT,NTP
  301 FORMAT (/'NELEM =',I4/
     . 'THE PARAMETER OF STEP LENGTH OF x AXIS=',I4/
     . 'THE PARAMETER OF STEP LENGTH OF t AXIS =',I4/
     . 'THE NUMBER OF TIME PERIOD =',I4)
      READ (5,*) SWITCH,PDAMT,PLETH,PMODL,PYILD,PBROK,TLIMIT,PHEAT,
     . PCOFB,PDESY,TEMP0
      READ(5,*) PVELO,PPMAS
      TLIMIT=-PVELO/TLIMIT
      WRITE (10,303)
      WRITE (10,305) PDAMT,PLETH,PMODL,PYILD,PBROK,TLIMIT,PHEAT,
     .PCOFB,PDESY,TEMP0
  304 format(3f12.2)
  303 FORMAT(/5X,'INITIAL AND PROPERTY PARAMETERS'/)
  305 FORMAT('THE INITIAL DIAMETER= ',F12.4,'(m)'/
```

```
     .'THE INITIAL LENGTH  L=     ',F14.4,'(m)'/
     .'THE YOUNG'S MODULUS E=     ',E14.4,'(N/m²)'/
     .'STATIC YIELD STRESS σ0=    ',E14.4,'(N/m²)'/
     .'STATIC BREAKING STRESS σ1= ',E14.4,'(N/m²)'/
     .'TIME CONSTANT OF SHOCK τ=',E14.4,'(Sec)'/
     .'SPECIFIC HEAT p =',E14.4/
     .'CONVERT COEFFICIENT b=',E14.4/
     .'DENSITY OF SPECIMEN =',E14.4,'(Kg/m³)'/
     .'INITIAL TEMPERATURE =',E14.4,'°C'/)
      WRITE(10,311)PVELO,PPMAS
  311 FORMAT('INITIAL VELOCITY OF PROJECTILE=',F12.4,'(m/s)'/
     .'THE MASS OF PROJECTILE        =',F12.4,'(Kg)')
      CLOSE(5)
      RETURN
      END
```

2.5.3 Results and discussions

The computations have been performed on Dec Vax mainframe, the specimen is divided into 200 elements along x axial direction, *i.e.* Δx*=0.05 (mm),* Δt*= 0.014 (μs)*. The results in graphical forms are shown in Figs. 9 to 17.

The initial shock stress makes the stress at $x=0$ raised rapidly as shown in Fig. 9. After reaching its peak value, it begins to fall rapidly. Meanwhile, the stress wave-front moves towards the fixed end at the velocity c. When it reaches the fixed end, the reflected stress wave is produced, the stress at the end is doubled. Then it moves backwards to the opposite direction. At an arbitrary point the local resultant compressive stress is obtained by addition, but the resultant velocity of particles is obtained by subtraction.

From Figs. 9 to 11, it is evident that the over-stresses tend to fall, but the reflected stress waves coming from the fixed end keep on resisting their decrease and weakening the velocities of the particles (see Fig. 12). The rate of unloading $|\partial\sigma/\partial t|$ continuously slows down as the over-stress is reduced and approaches to zero at $t\approx 13$ *(μs)*. In this period, the over-stress plays a decisive part. Subsequently, the effect of the reflected stress becomes significant and withstands large scale decline of the stress. A loading phenomenon occurs because of the strong work-hardening of the material. This dynamic stalemate situation lasts until the velocity of the particle is reduced to zero. Afterwards, the dynamic over-stress dominates the variation of stress

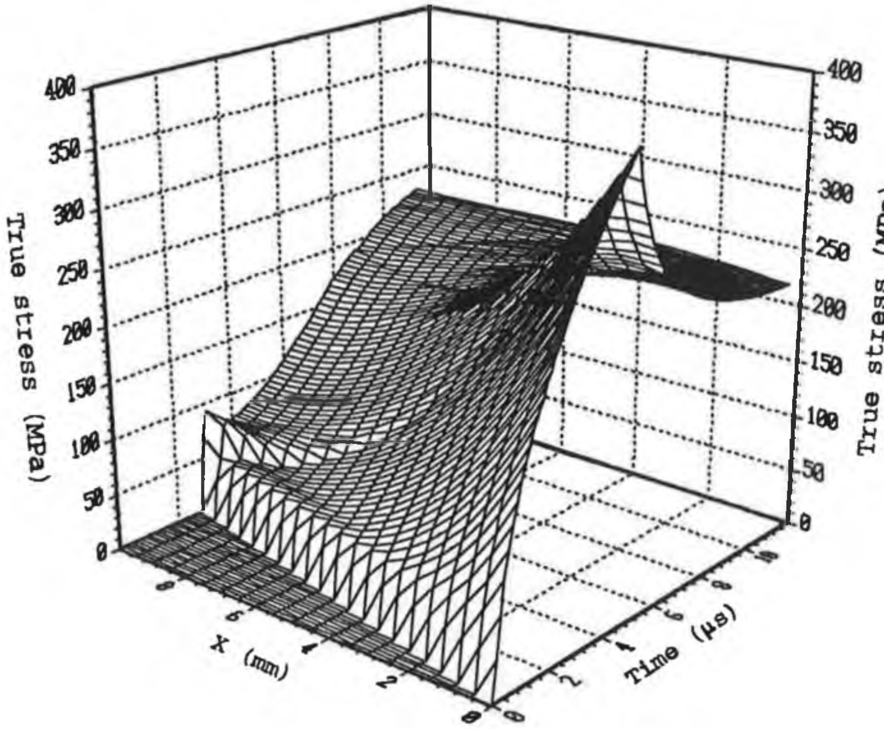

Fig. 9 *The initial variations of stress with respect to the time and positions.*

and makes it decrease rapidly. Finally, when it touches the static stress curve, the unloading occurs according to Hooke's law.

From Fig. 10, it can also be seen that the effect of shock stress wave at a distant position from the impact end is weakened explicitly. At $x=4$ *(mm)*, after a small shock, the stress begins to increase and at $t \approx 10$ *(µs)* it exceeds the stress at $x=0$. This status is kept until it is finally unloaded. The effect of shock stress wave on the section at $x=8$ *(mm)* has virtually disappeared but the reflective stress can be clearly seen.

The variation of velocity of the particles in the specimen is shown in Fig. 12. The velocity at $x=0$ varies submitting to Eq. (34) and that at $x=h$ keeps zero. At $t \approx 73$ *(µs)* the velocities of particles within the specimen falls to zero. Afterwards, because there exist compressive stresses in it, the specimen still keeps contacting with the anvil and the particles begin to move towards the opposite direction. At $t=T_0 \approx 86$ *(µs)*, the stresses within the specimen fall to zero. Then, the specimen is disengaged from the anvil.

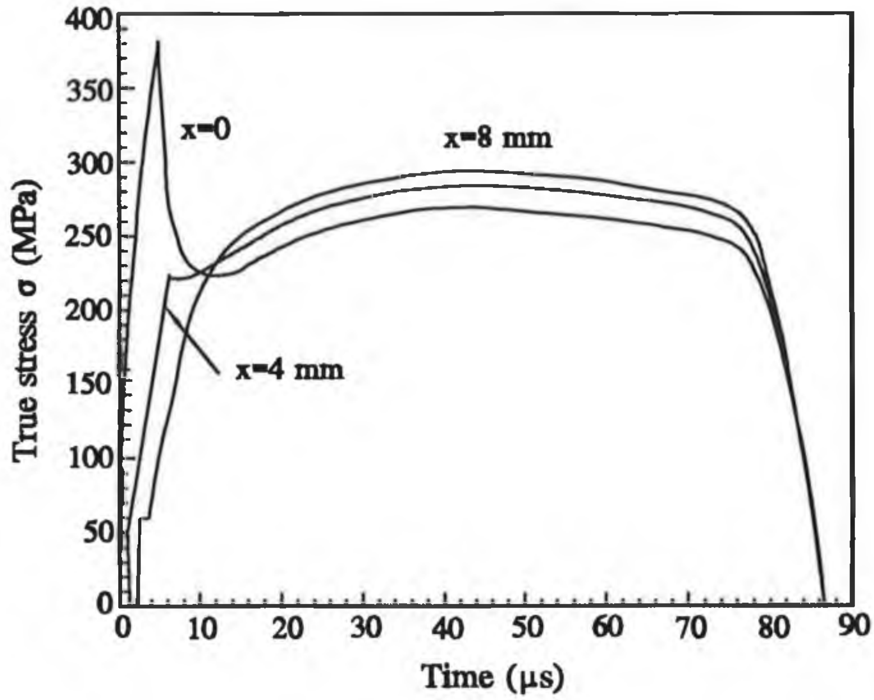

Fig. 10 *The process of the variation of stress at fixed cross sections of the specimen.*

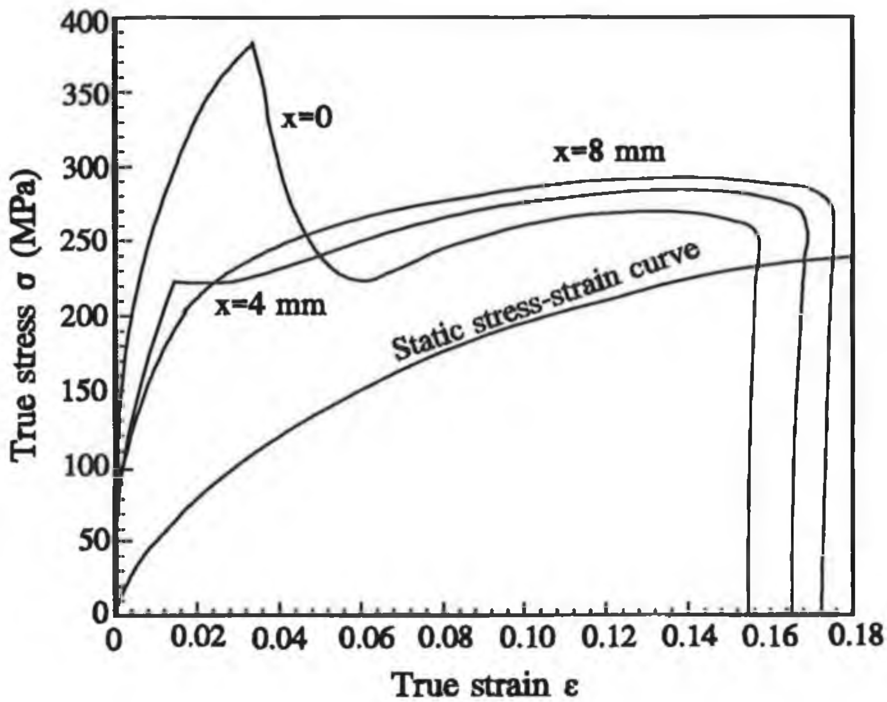

Fig. 11 *Dynamic stress-strain at fixed cross sections of the specimen.*

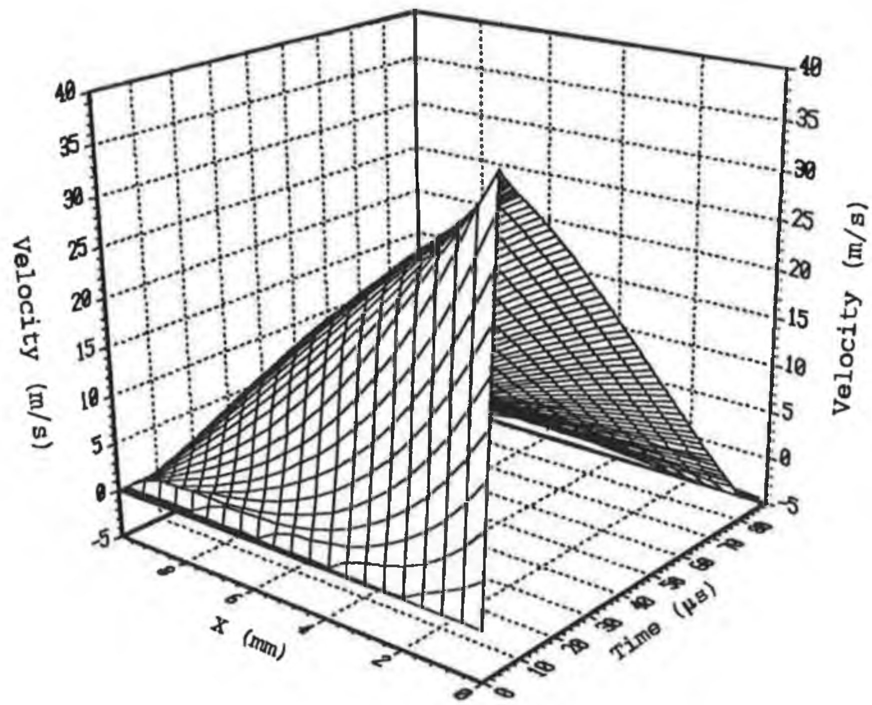

Fig. 12 *Variations of velocity with respect to the time and positions within the specimen.*

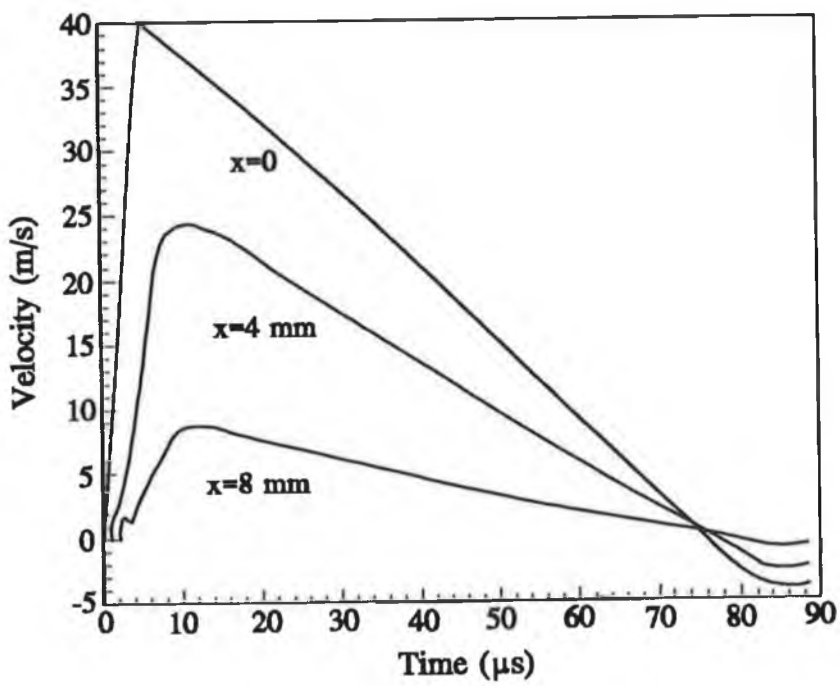

Fig. 13 *Variation of particle velocity at the fixed cross-sections.*

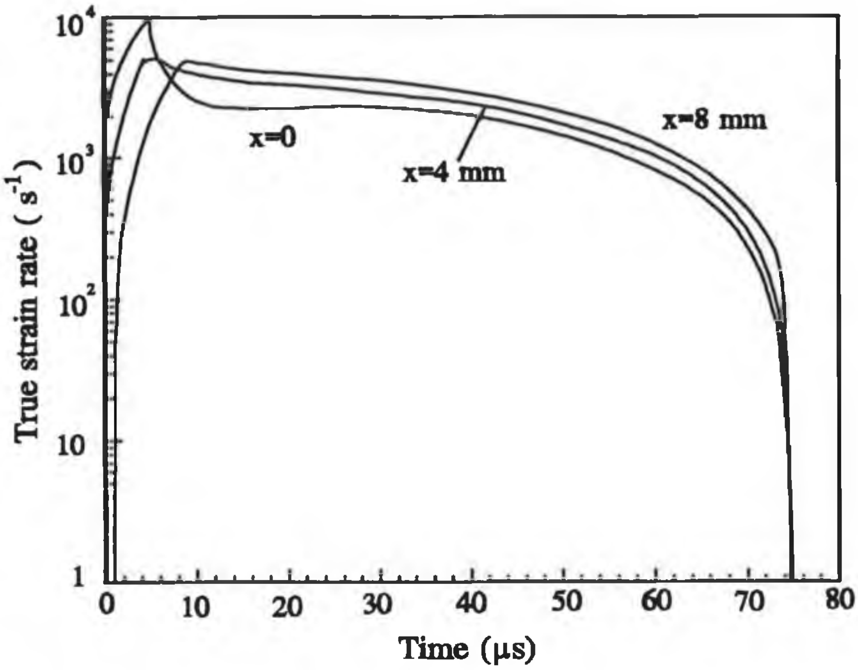

Fig. 14 *Variation of true strain rate at fixed cross sections of the specimen.*

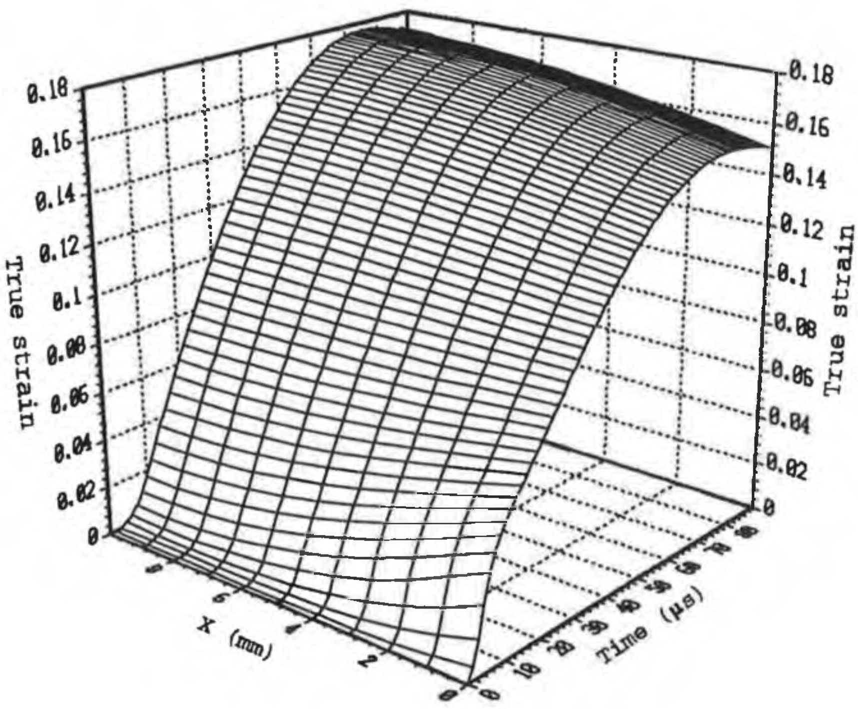

Fig. 15 *Variation of strain with respect to the time and positions within the specimen.*

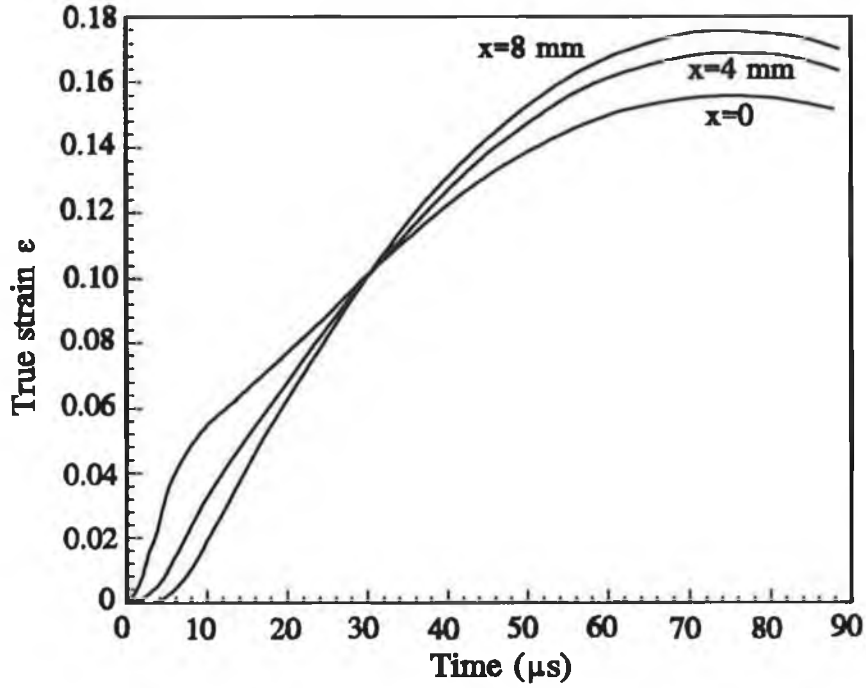

Fig. 16 *Variation of strain at the fixed cross-sections.*

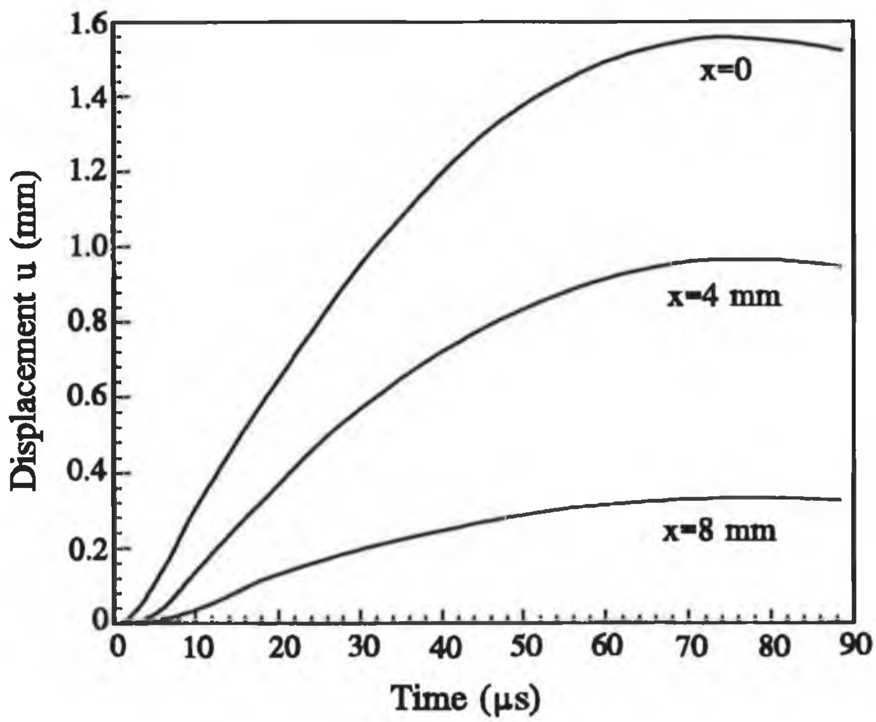

Fig. 17 *Variation of displacement at fixed cross sections of the specimen.*

It may be seen from Fig. 14 that except for the effect of shock stress at the beginning, the strain rate is kept at a steady level of $10^3\ s^{-1}$ during most of the time. On this level, it has been declining slowly until a large scale unloading begins at $t \approx 73$ *(μs)* when the velocities of particles tend to zero. When the over-stresses disappear at $t \approx 75$ *(μs)*, *i.e.* the function $g(z)$ in Eq. (31) tends to zero, the strain rate falls to zero.

The results in Fig. 15 show that in the initial stage the increment of strain at the moving end is faster than that at the fixed end. However, after about 5 *(μs)* the rate of increment of strain near the fixed end becomes greater than that near the moving end due to the effect of reflective stresses. In the final stage, the elastic strain recovery occurs due to the unloading.

The variation of displacement at different locations of the specimen is shown in Fig. 17, which can be used for the examination of the deformation of the specimen and also for the comparison with experimental observations to determine the new constitutive equations.

Cristescu [195] gave his numerical solutions for aluminium under different constitutive equations. In his solutions, the boundary conditions at the impact end is a constant velocity. Under the same constant velocity boundary condition Nicholas [196] also made calculations for other materials. In their results, the maximum stress and strain appear near the impact end during the entire process of impact, the duration of impact is longer than that in the present model. In ref. [156], due to constant-velocity applied at the impact end, the unloading seemed not to appear. Therefore, a so called *relaxation boundary* was recommended. The dynamic stress-relaxation does not coincide with what is generally called the *quasi-static* stress-strain curve. The suggested concept of *relaxation boundary* made the calculations more complicated.

In the present model, due to the gradual decrease of the velocity at the impact end, the stress, strain and strain rate at this end decline from the maximum values at the beginning to the final minimum value. The expected unloading begins at $t \approx 73$ (μs) when the particle velocities fall to zero. Then, the strain rates rapidly decrease. At $t \approx 75$ (μs), the dynamic stresses falls on static stress-strain curve and the strain rates are equal to zero. Finally, the elastic unloading lasts until the stresses within the specimen are removed at $t \approx 86$ (μs).

The current method provides a means of analyzing the process of deformation of the impacted specimen and the effect of the transient wave propagation on it in the ballistic test. It can also be used for the comparison of theoretical results under a proposed constitutive equation with the corresponding experimental observations to examine the validity of the suggested equation or to determine a new equation.

2.6 The Effect of Various Initial Parameters

In order to examine the effects of the various factors on the impact process, calculations have been made varying the initial parameters such as the shock duration, T_0, the striking velocity of the projectile, v_0, the length of the specimen, L, and the dimension of the specimen, $D \times L$.

2.6.1 Shock stress wavefront

For the variation of the shock duration T_0, the numerical solutions have been obtained graphically as shown in Figs. 18 to 23. The temperature rise in the impact process has also been estimated. The parameters in the calculation are as follows:

The mass of projectile *PPMAS=0.01 (kg)*,
The number of elements in the calculation *NELEM=160*,
The length of the specimen *PLETH=5 (mm)*,
The diameter of the specimen *PDAMT=5 (mm)*,
The density of the specimen material *PDESY*$=8.96 \times 10^3$ (kg/m^3),
The elastic modulus of the specimen material *PMODL=110 (GPa)*,
The yield stress of the specimen *PYILD=55 (MPa)*,
The initial velocity of the projectile *VELOY=40* (m/s),

The ambient temperature *TEMPER=20 °C.*
The specific heat C_p*=383 J/kg·K,*
The convert coefficient α*=0.92;*

The initial shock stress causes the stress at $x=0$ to rise rapidly as shown in Figs. 18 and 19. It can be seen that the acceleration of the particles of the specimen at $x=0$ increases with the reduction of the shock duration T_0 (Fig. 20), which results in the swift rise of the peak stress (Fig. 21). After reaching its peak value, the dynamic stress with a shorter T_0 falls more rapidly, but the dynamic stress with a longer T_0 keeps on a higher level until the end of the impact process. As well as the strain (Fig. 22), the final deformation of the specimen (Fig. 24), *i.e.* the displacement of the specimen at $x=0$, increases with the reduction of the shock duration T_0. Its effect on strain rates is most apparent, at $T_0=2.5\ \mu s$, the strain rate can reach up to 1.35×10^4 s^{-1}, but at $T_0=8\ \mu s$, the strain rate can only attain up to 9×10^3 s^{-1}.

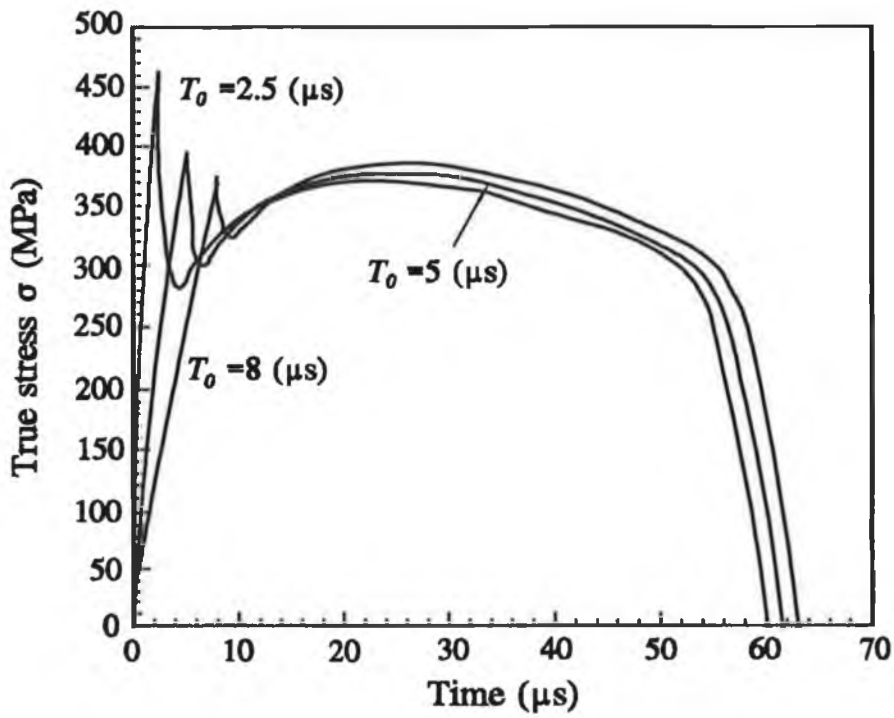

Fig. 18 *Variation of the stress with the time at x=0 at various* T_0.

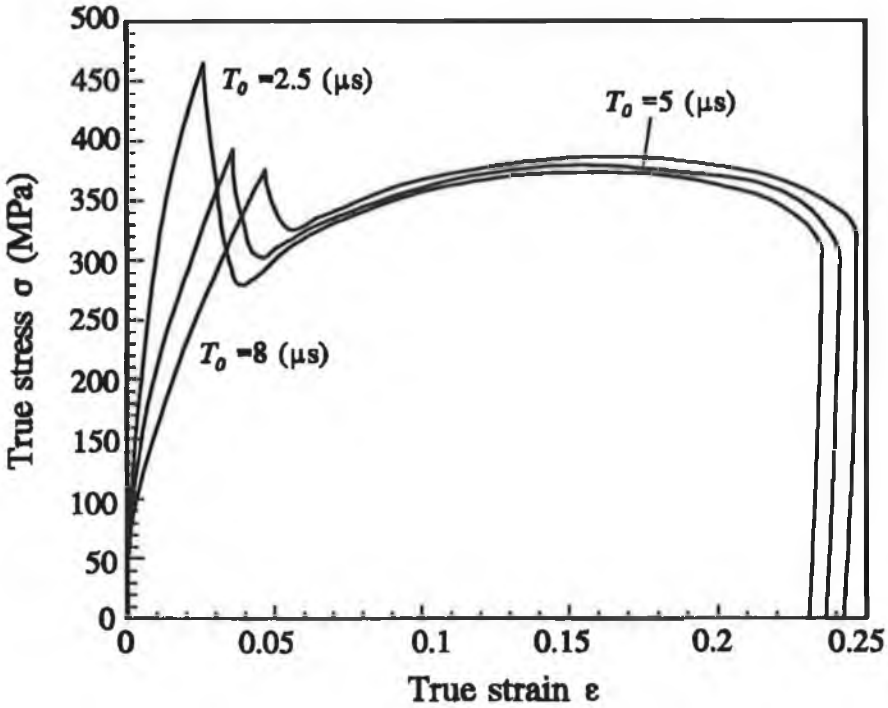

Fig. 19 *Variation of the stress with the strain at x=0 at various T_0.*

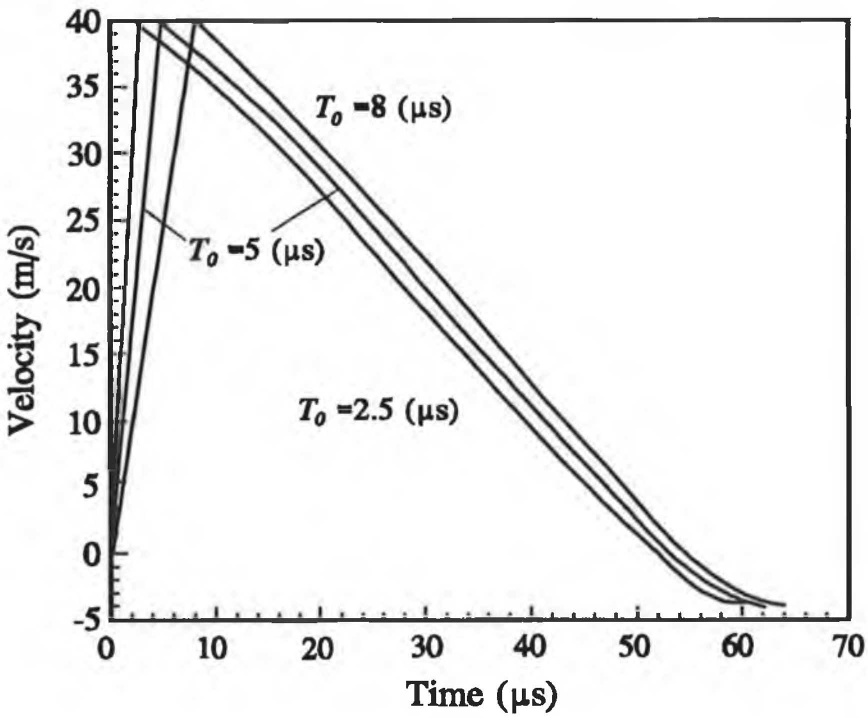

Fig. 20 *Variation of the velocity with the time at x=0 at various T_0.*

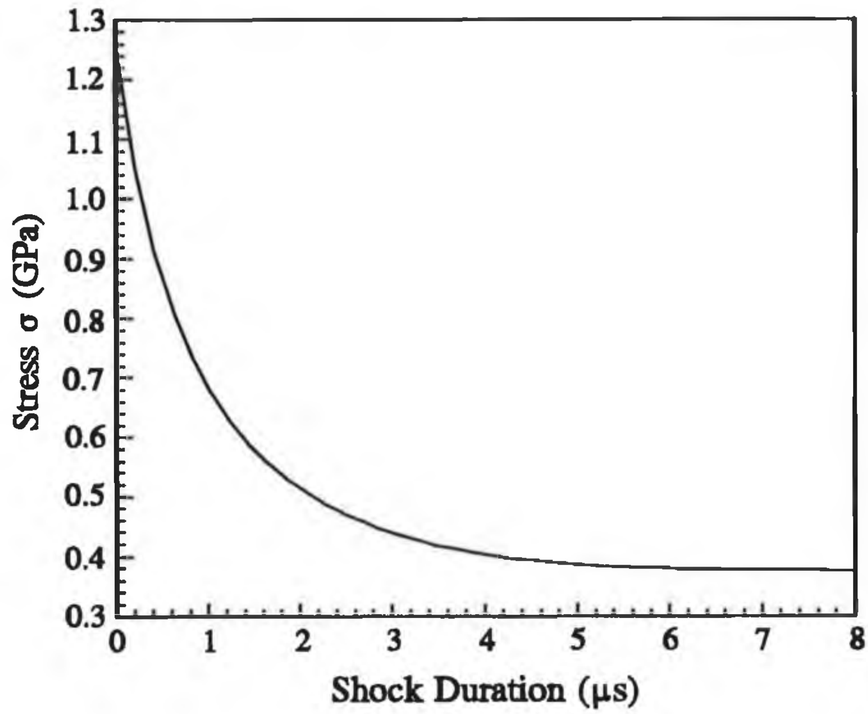

Fig. 21 *Variation of the peak stress with T_0 at $x=0$.*

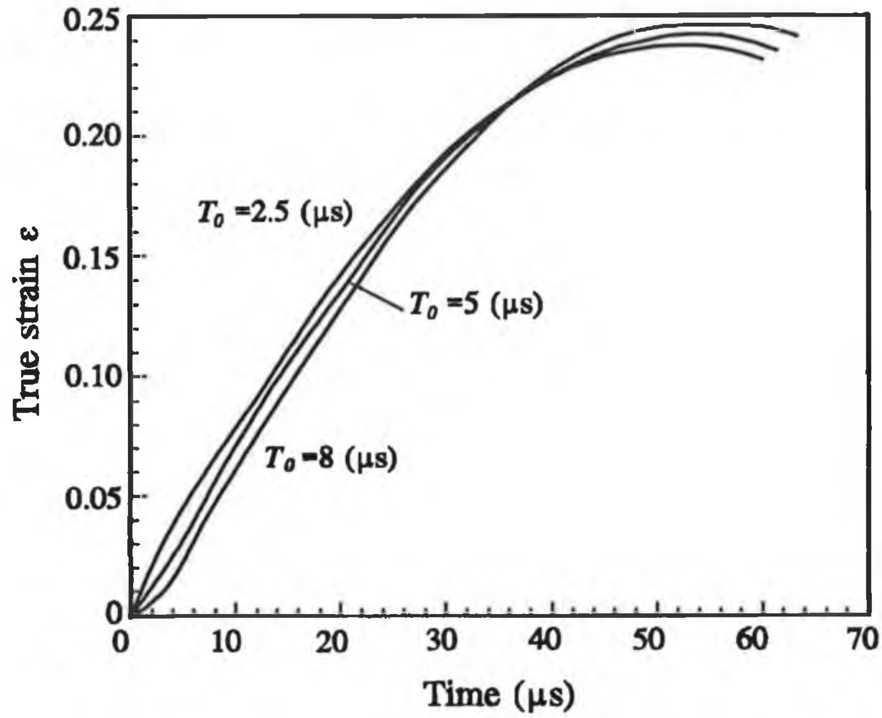

Fig. 22 *Variation of the strain with the time at $x=0$ at various T_0.*

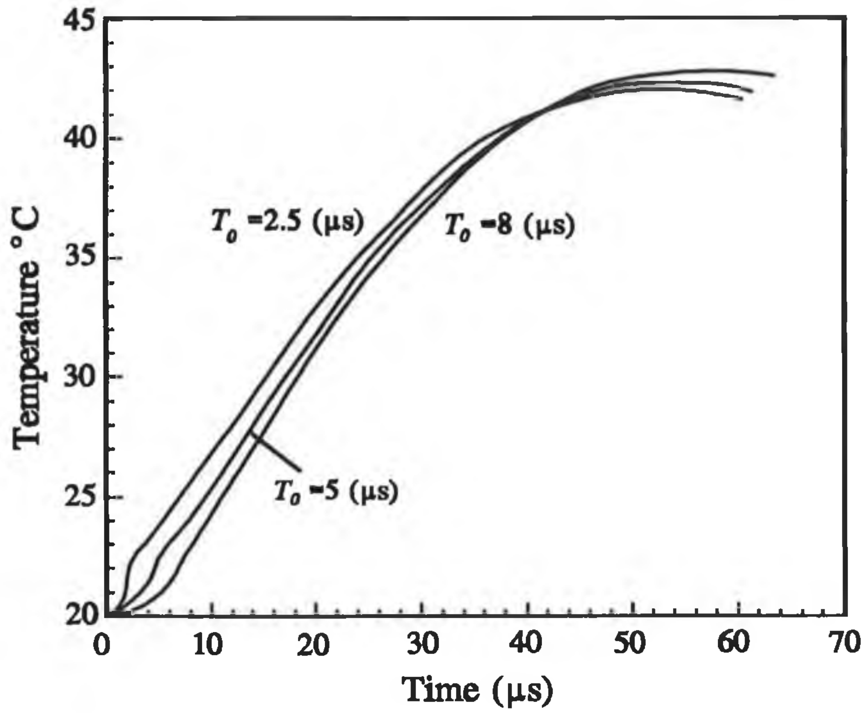

Fig. 23 *Variation of the temperature with the time at x=0 at various T_0.*

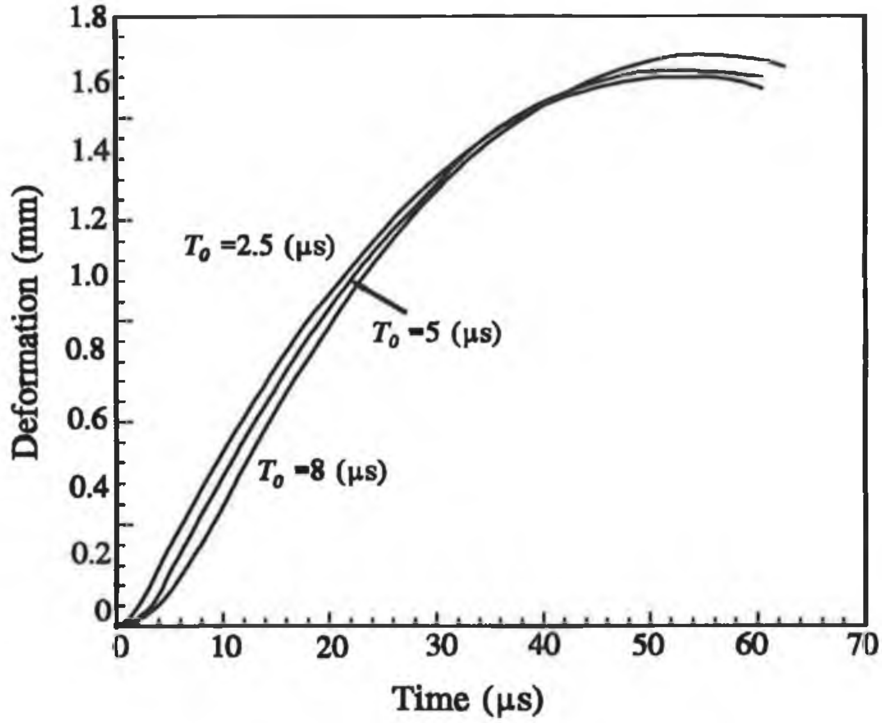

Fig. 24 *Variation of the deformation with the time at x=0 at various T_0.*

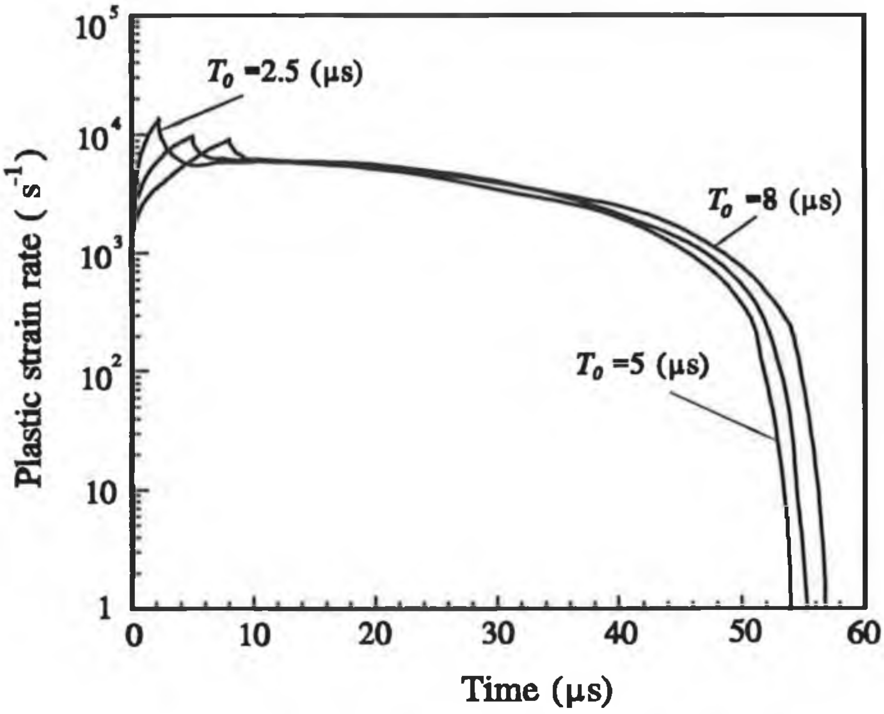

Fig. 25 *Variation of the plastic strain rate with times at x=0 at various T_0.*

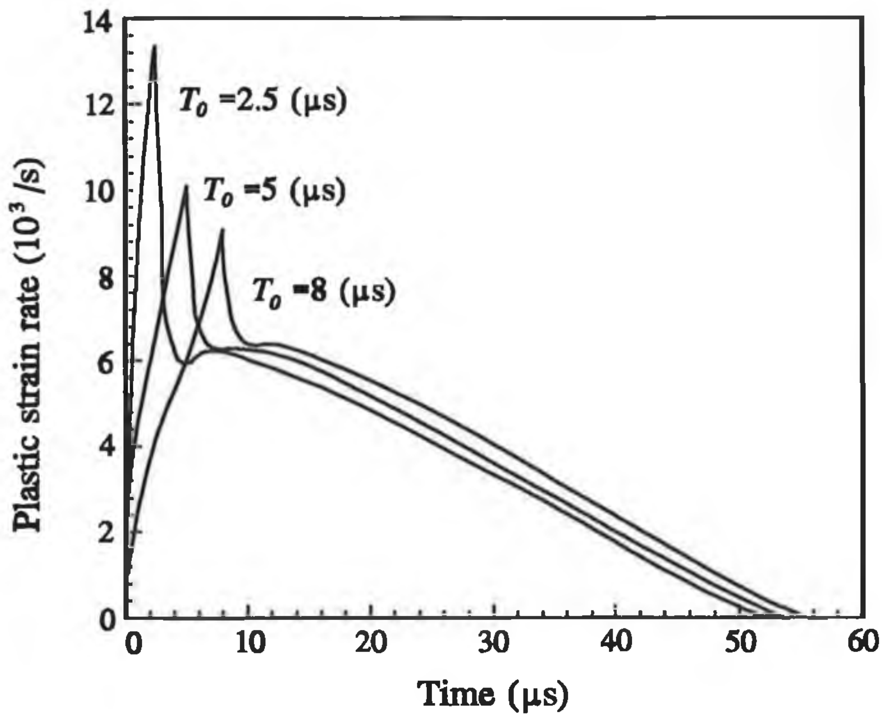

Fig. 26 *Variation of the plastic strain rate with times at x=0 around the peak at various T_0.*

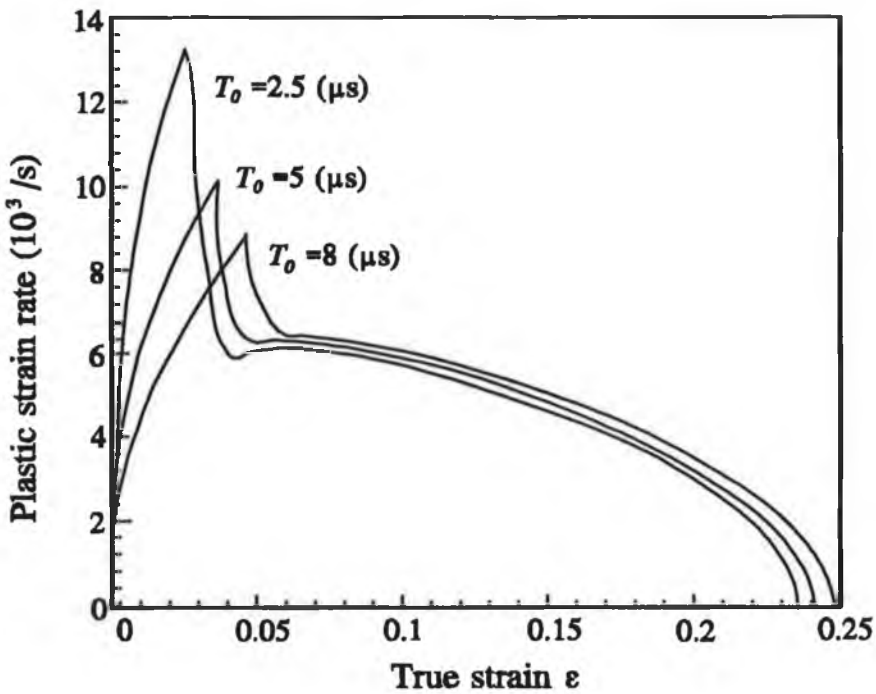

Fig. 27 *Variation of the plastic strain rate with the strain at x=0 around the peak at various T_0.*

2.6.2 The length of the specimen

In the condition of the variation of the length of the specimen, the numerical solutions have been obtained as Figs. 28 to 36 graphically. The parameters in the calculation are as follows:

The mass of projectile *PPMAS=0.01 (kg)*,
The acting time of shock stress *TLIMIT=5 (μs)*,
The number of elements in the calculation *NELEM=160,*
The diameter of the specimen *PDAMT=5 (mm)*,
The density of the specimen material *PDESY*=8.96×10^3 *(kg / m^3)*,
The elastic modulus of the specimen material *PMODL=110 (GPa)*,
The yield stress of the specimen *PYILD=55 (MPa)*,
The initial velocity of the projectile *VELOY=40 (m / s)*,
The ambient temperature *TEMPER=20 °C.*
The specific heat C_p=*383 J / kg·K,*
The convert coefficient α=*0.92;*

The shorter initial length for a specimen allows the struck bar to reach the higher stress and strain rate levels and it also cuts down the impact time. From the point of view of energy, a shorter specimen makes the energy release of the projectile more concentrated, which can be verified by the results from Figs. 28 to 33. In this case, both the dynamic stress and the strain are apparently higher for the shorter specimen (Fig. 30). Further, due to the reduction of the time taken by the impact process (Fig. 31), the average strain rates with regard to both time and strain for the shorter specimen are higher than these for the longer one (Fig. 31 to 33). The deformation for a longer specimen is greater(Fig. 34). Naturally, owing to the larger strain and the higher strain rate, the rise of temperature in a shorter specimen is obviously higher than that in the longer ones(Fig. 36). Therefore, to achieve high strain rates for a struck specimen, a short specimen is recommended to be used, but this usually causes a larger error for the uniaxial stress assumption because of the large deformation of the specimen impacted by a high speed projectile.

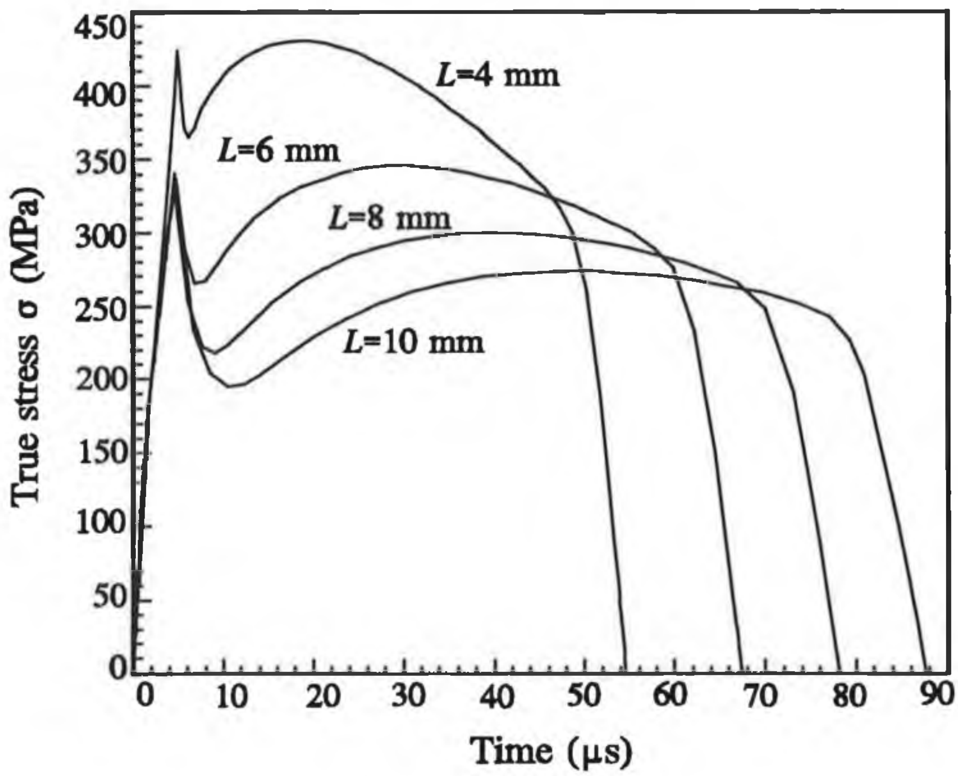

Fig. 28 *Variation of stresses with times at x=0 at various initial lengths of specimens.*

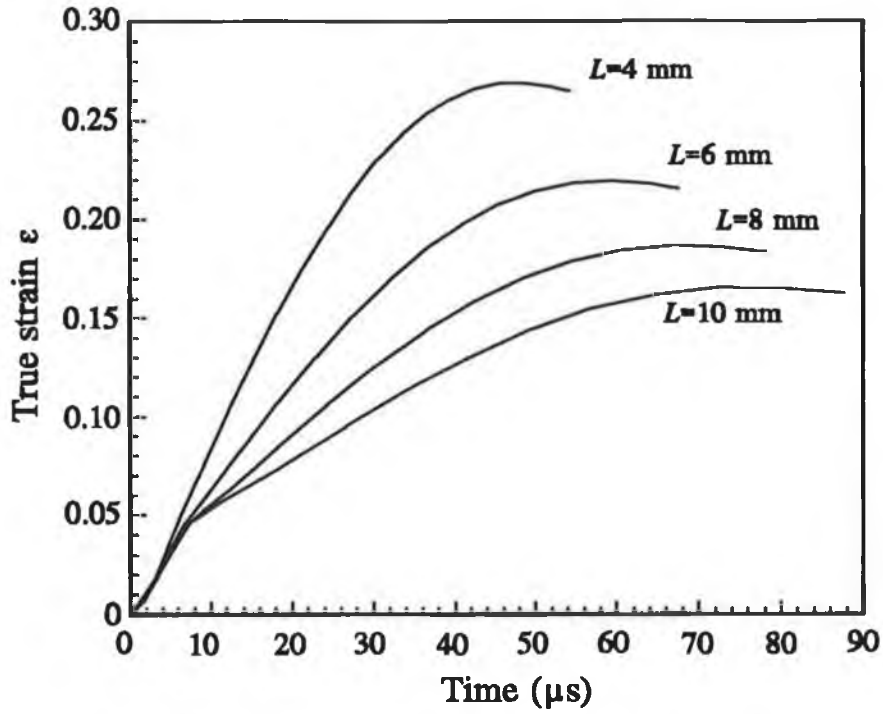

Fig. 29 *Variation of strains with times at x=0 at various initial lengths of specimens.*

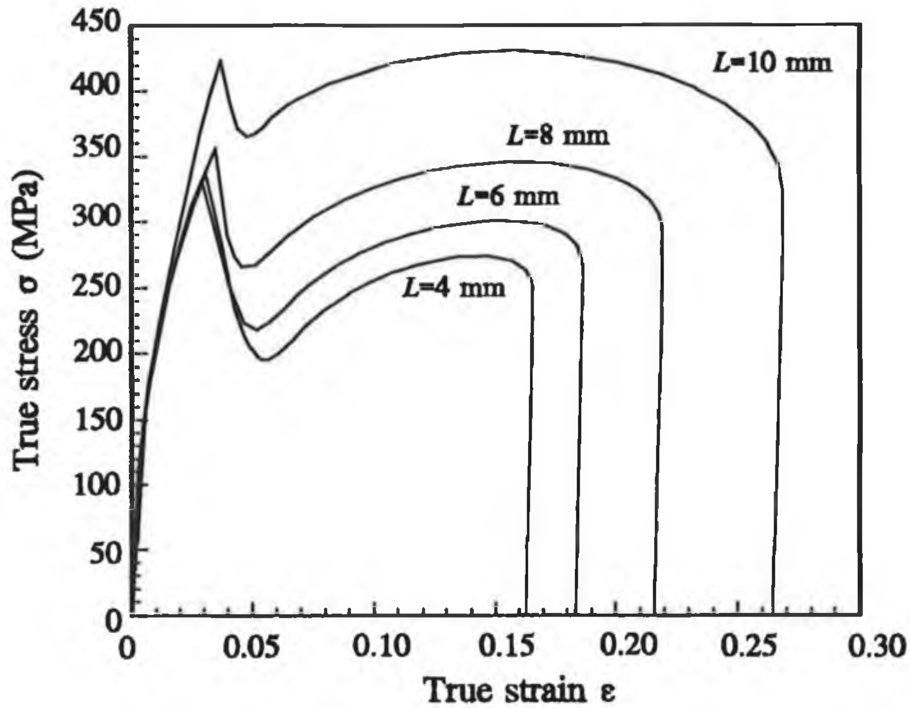

Fig. 30 *Variation of stresses with strains at x=0 at various initial lengths of specimens.*

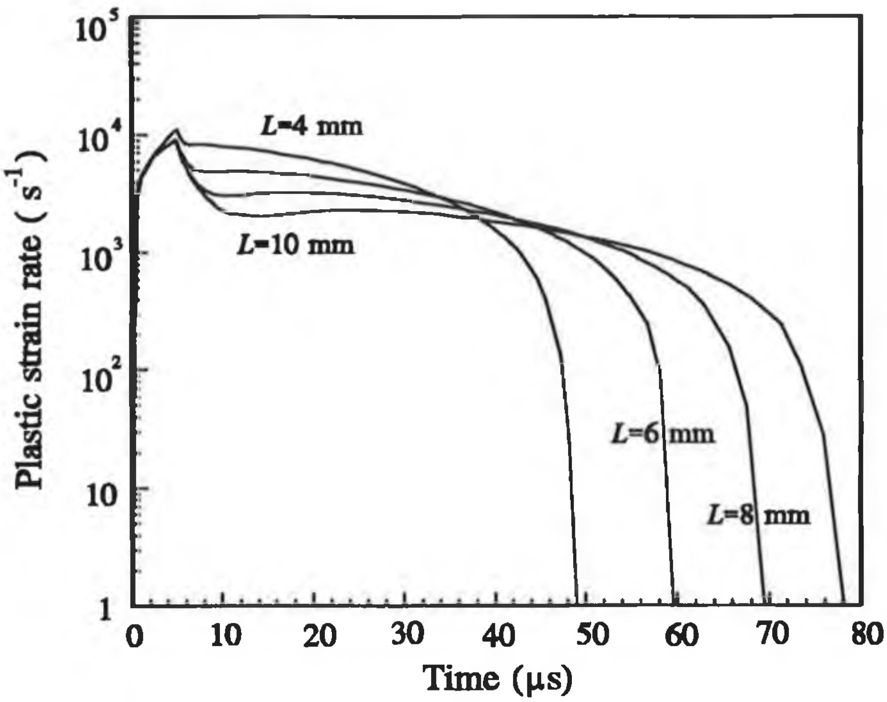

Fig. 31 *Variation of plastic strain rates with times at x=0 at various initial lengths of specimens.*

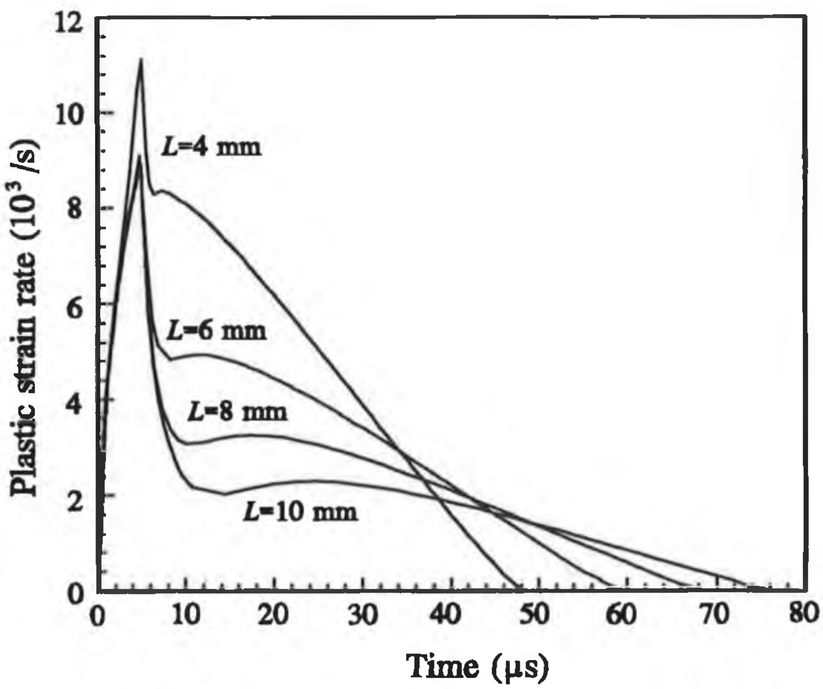

Fig. 32 *Variation of plastic strain rates with times at x=0 around the peak at various initial lengths of specimens.*

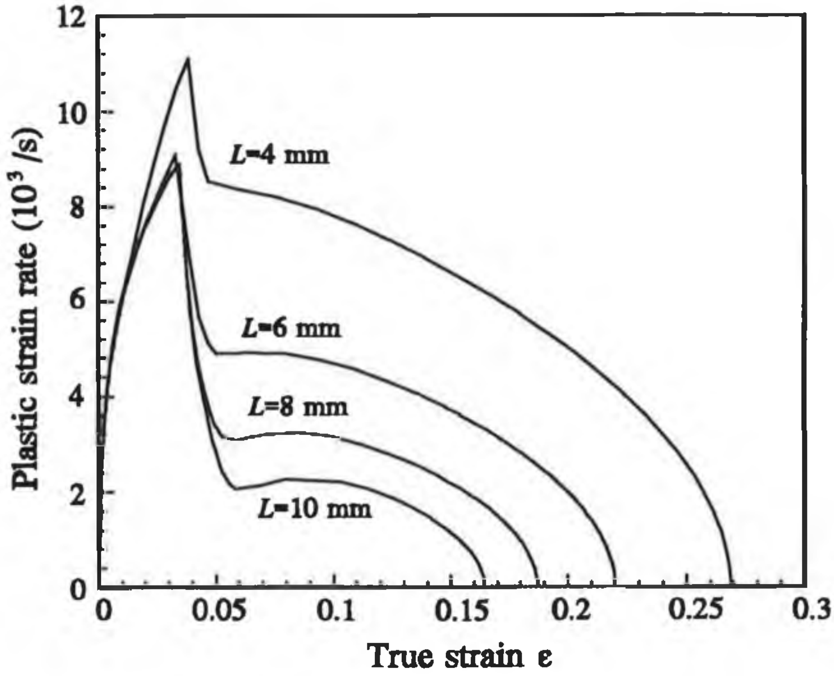

Fig. 33 *Variation of plastic strain rates with strains at x=0 at various initial lengths of specimens.*

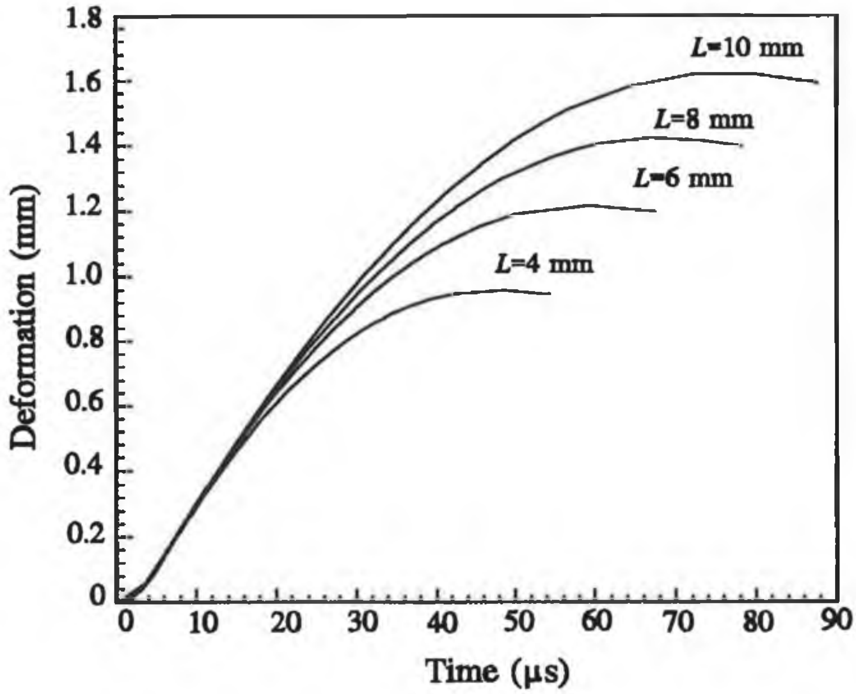

Fig. 34 *Variation of deformation with times at x=0 at various initial lengths of specimens.*

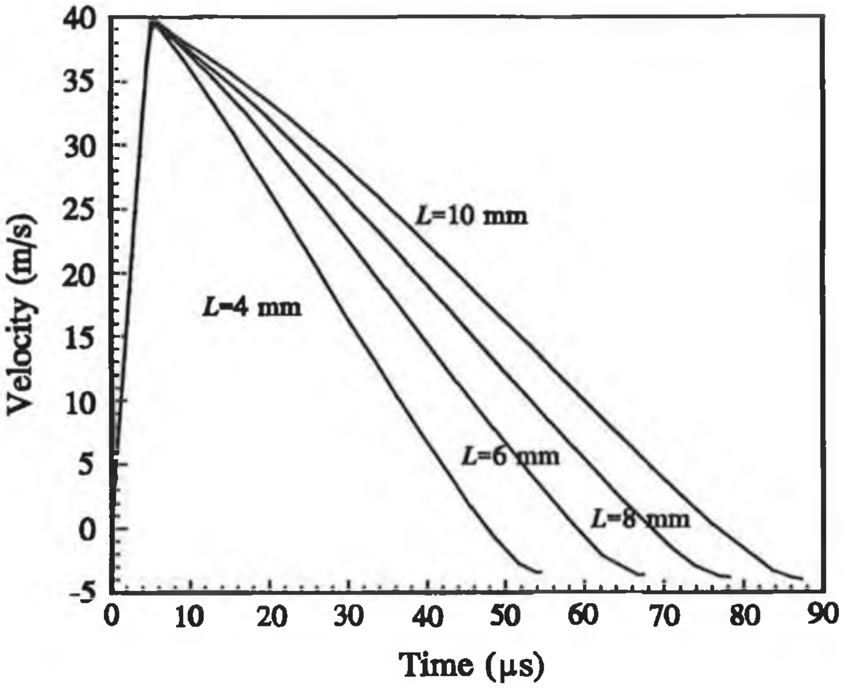

Fig. 35 *Variation of velocities with times at x=0 at various initial lengths of specimens.*

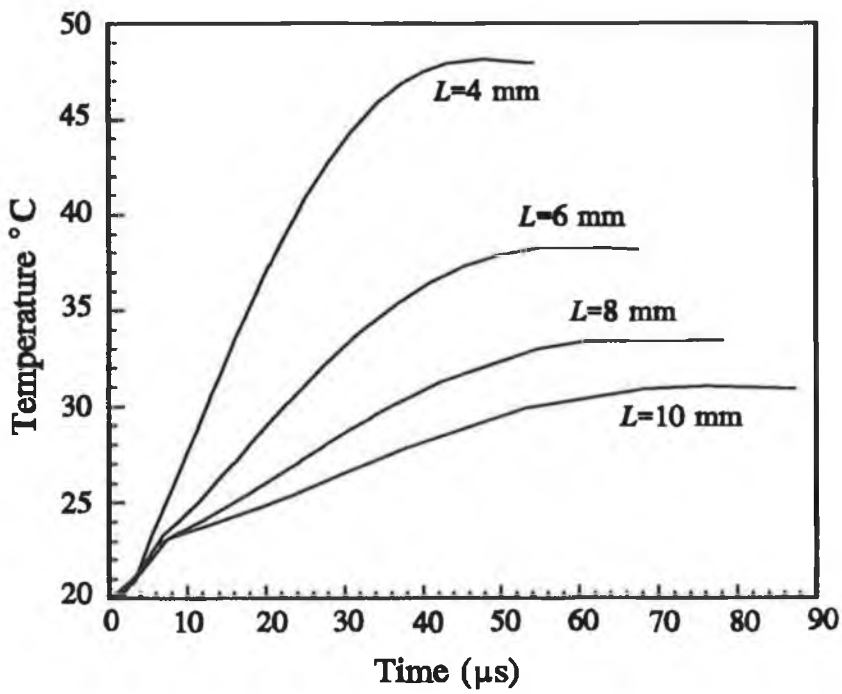

Fig. 36 *Variation of the temperature with the strain at x=0 at various initial lengths of specimens.*

2.6.3 The initial velocity of the projectile

In the condition of the variation of the initial velocity of the projectile, the numerical solutions have been obtained graphically as shown in Figs. 37 to 45. The parameters applied in the calculation are as follows:

The mass of projectile *PPMAS=0.01 (kg)*,
The acting time of shock stress *TLIMIT=5 (μs)*,
The number of elements in the calculation *NELEM=160,*
The diameter of the specimen *PDAMT=5 (mm)*,
The length of the specimen *PLETH=5 (mm)*,
The density of the specimen material $PDESY=8.96\times10^3\ (kg/m^3)$,
The elastic modulus of the specimen material *PMODL=110 (GPa)*,
The yield stress of the specimen *PYILD=55 (MPa)*,
The initial velocity of the projectile $VELOY=40\ (m/s)$,
The ambient temperature *TEMPER=20 °C.*
The specific heat $C_p=383\ J/kg{\cdot}K$,
The convert coefficient $\alpha=0.92$;

Calculations have been made for the variation of the initial velocity of the projectile. The results show that the strain rates of impacted materials almost increase proportionally with the increase of the initial velocity of the projectile.

As are shown in Figs. 37 to 39, the stress and strain obviously increase with the striking speed of the projectile. The difference of the period taken by the impact process is not very apparent, which may be because the fact that the velocities of the particles decrease more rapidly (Fig. 40). The final deformation of the specimen rises proportionally (Fig. 41). The increase of the strain rate is significant (Figs. 42 to 44), and the softening effect of temperature must be considered (Fig. 45). To increase the initial striking speed of the projectile will become a main step to obtain high strain rates of tested materials. However, this method may be restricted by test conditions, and the effect of multi-directional stresses may also become distinct.

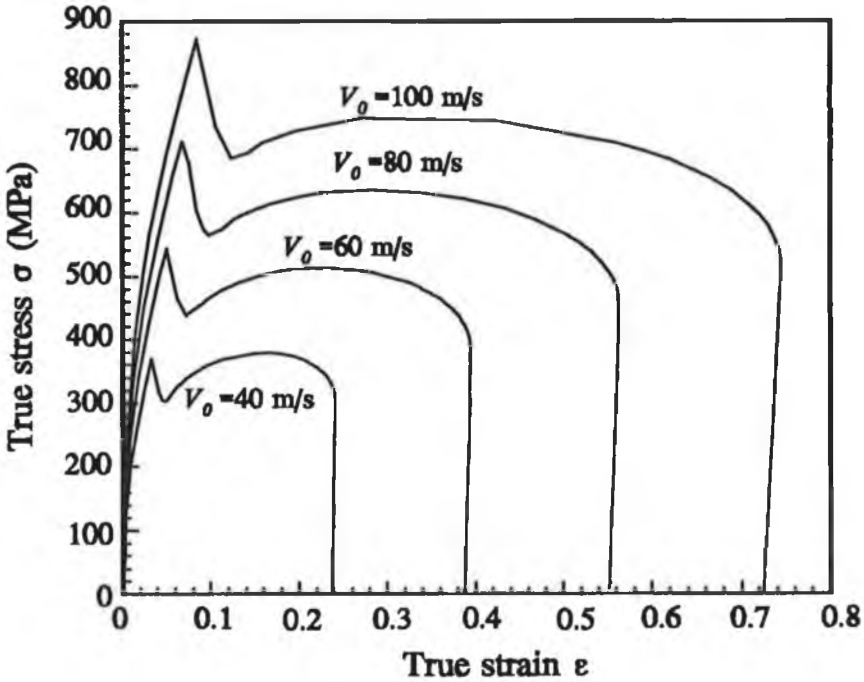

Fig. 39 *Variation of stresses with strains at x=0 at various initial velocities of the projectile.*

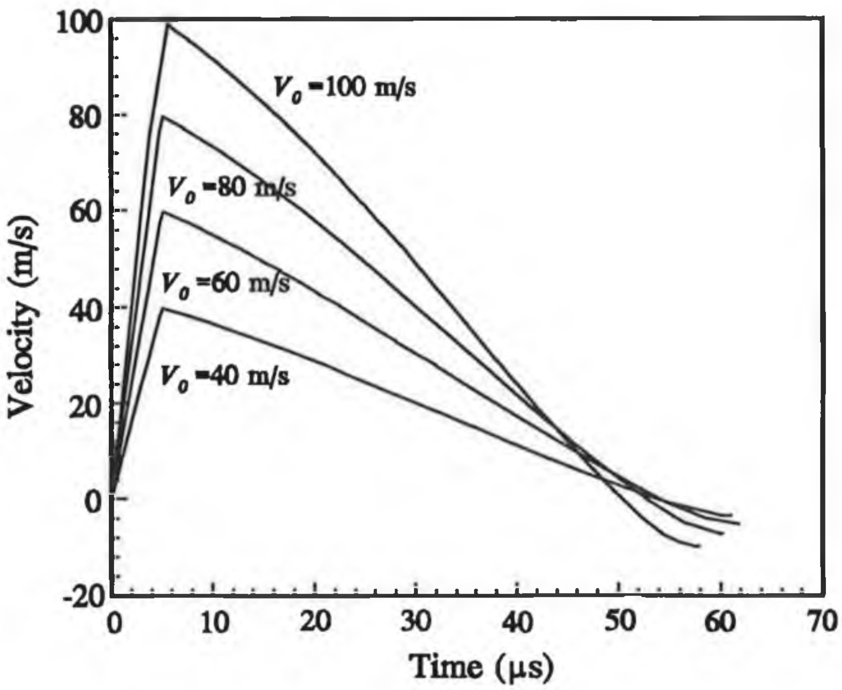

Fig. 40 *Variation of velocities with times at x=0 at various initial velocities of the projectile.*

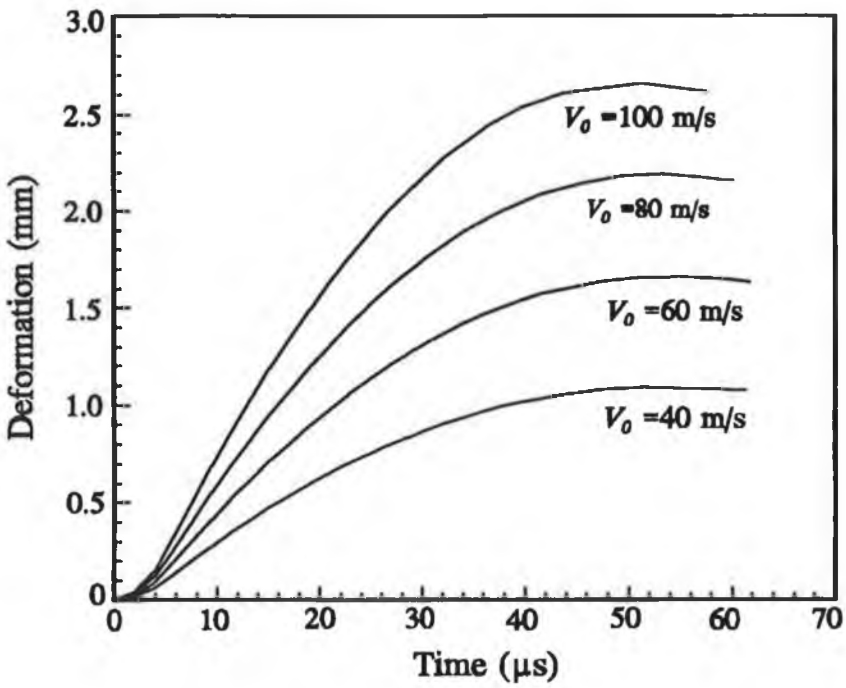

Fig. 41 *Variation of deformation with times at x=0 at various initial velocities of the projectile.*

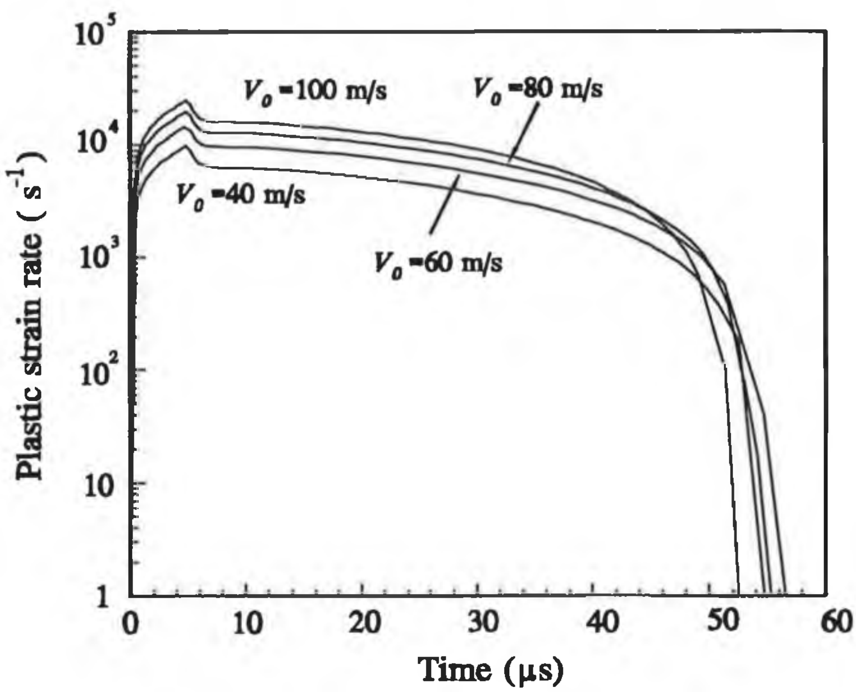

Fig. 42 *Variation of plastic strain rates with times at x=0 at various initial velocities of the projectile.*

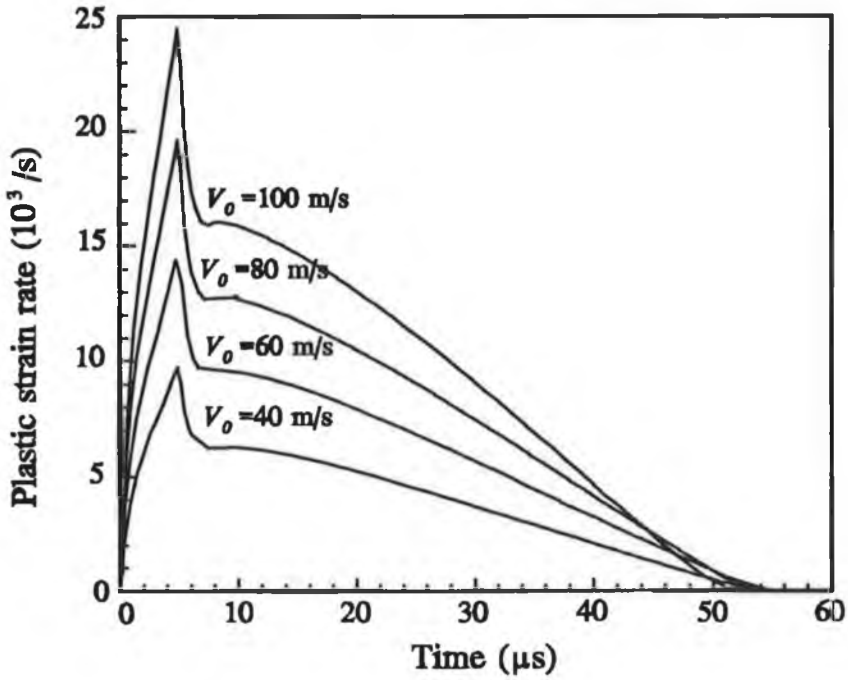

Fig. 43 *Variation of plastic strain rates with times at x=0 around the peak at various initial velocities of the projectile.*

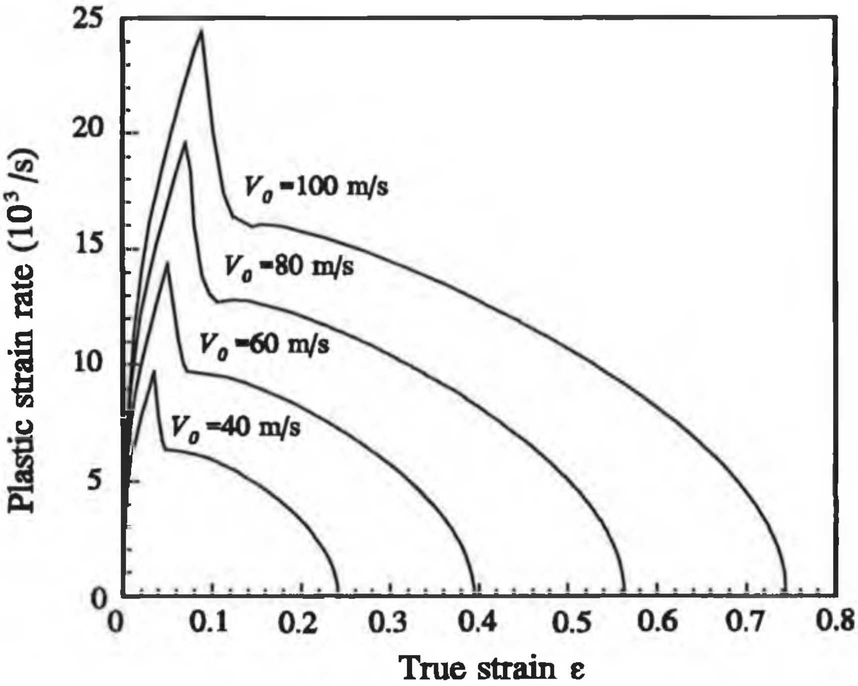

Fig. 44 *Variation of plastic strain rates with strains at x=0 at various initial velocities of the projectile.*

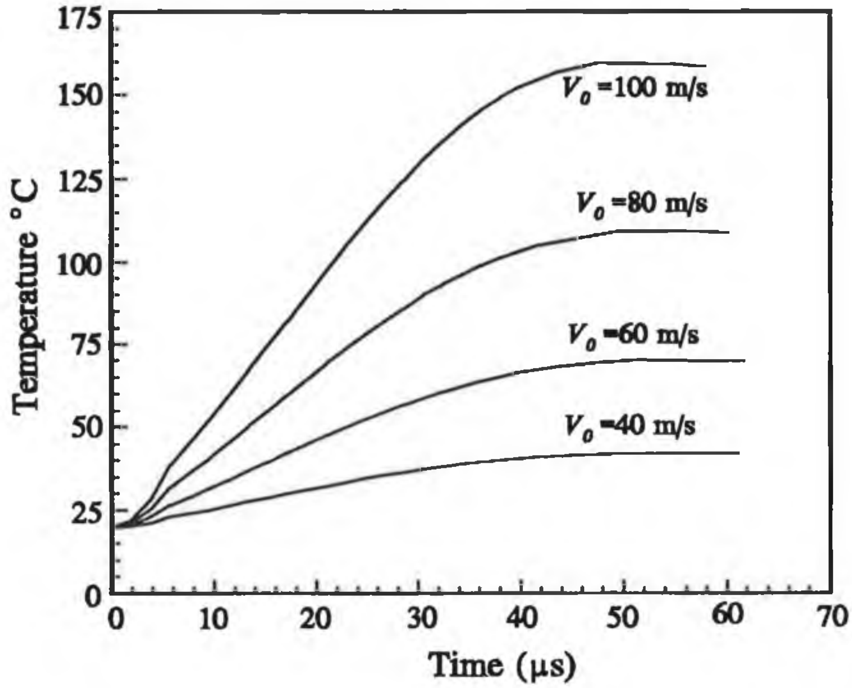

Fig. 45 *Variation of temperatures with strains at x=0 at various initial velocities of the projectile.*

2.6.4 The dimensions of the specimen

In the condition of the variation of the dimensions of the specimen *(D×L)*, the numerical solutions have been obtained graphically and are shown in Figs. 46 to 54. The parameters in the calculation are as follows:

The mass of projectile *PPMAS=0.01 (kg),*
The acting time of shock stress *TLIMIT=5 (μs),*
The number of elements in the calculation *NELEM=160,*
The density of the specimen material *PDESY*=8.96×10^3 (kg/m^3),
The elastic modulus of the specimen material *PMODL=110 (GPa),*
The yield stress of the specimen *PYILD=55 (MPa),*
The initial velocity of the projectile *VELOY=40 (m/s),*
The ambient temperature *TEMPER=20 °C.*
The specific heat C_p=*383 J/kg·K,*
The convert coefficient α=*0.92;*

Another acceptable approach to attain high strain rates of tested materials is to employ a small dimensional specimen. In the condition of the identical initial striking velocity, a small size specimen can propagate higher strain rates.

As are shown in Figs. 46 to 48, the stress and strain obviously increase with the decrease of the specimen size, which makes possible to accomplish high strain rates of tested specimens. Unlike applying the increase of the initial velocity of the projectile as in Section 2.6.3, in the current case the difference of the period taken by the impact process is apparent. For a small size of the specimen, the impact process takes a longer time, but the decrease of the velocity of the particles is slower (Fig. 49). The final deformation of the specimen rises distinctly (Fig. 50). The increase of the strain rate is also meaningful (Figs. 51 to 53), and the effect of temperature rise should be considered (Fig. 54).

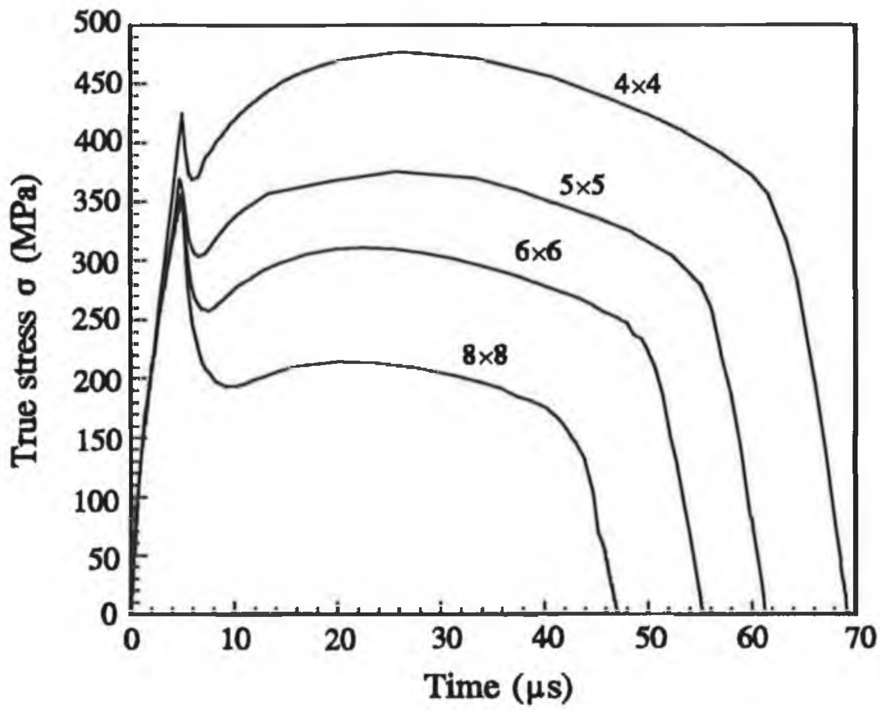

Fig. 46 *Variation of stresses with times at x=0 at various dimensions [D (mm) × L (mm)] of specimens.*

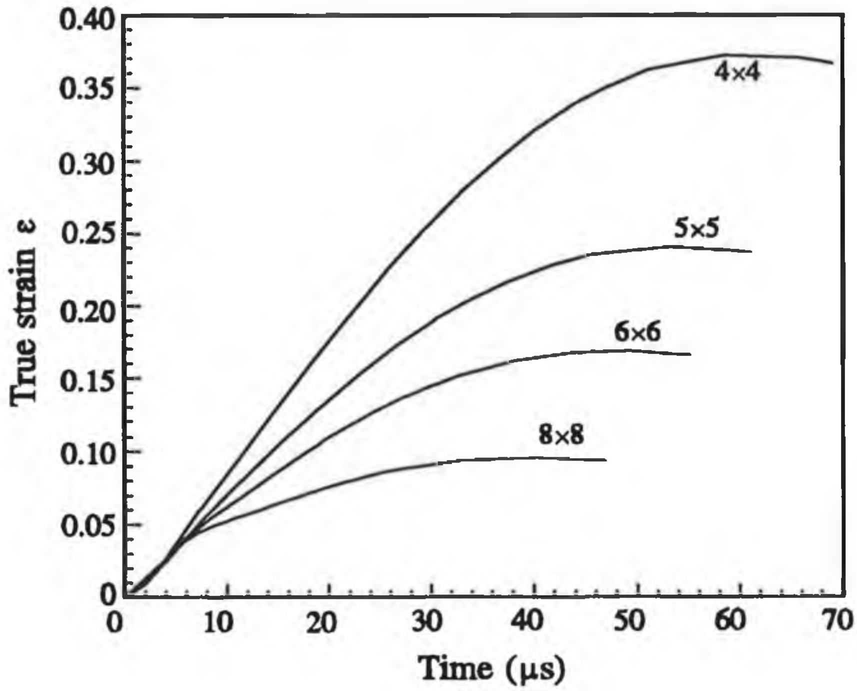

Fig. 47 *Variation of strains with times at x=0 at various dimensions [D (mm) × L (mm)] of specimens.*

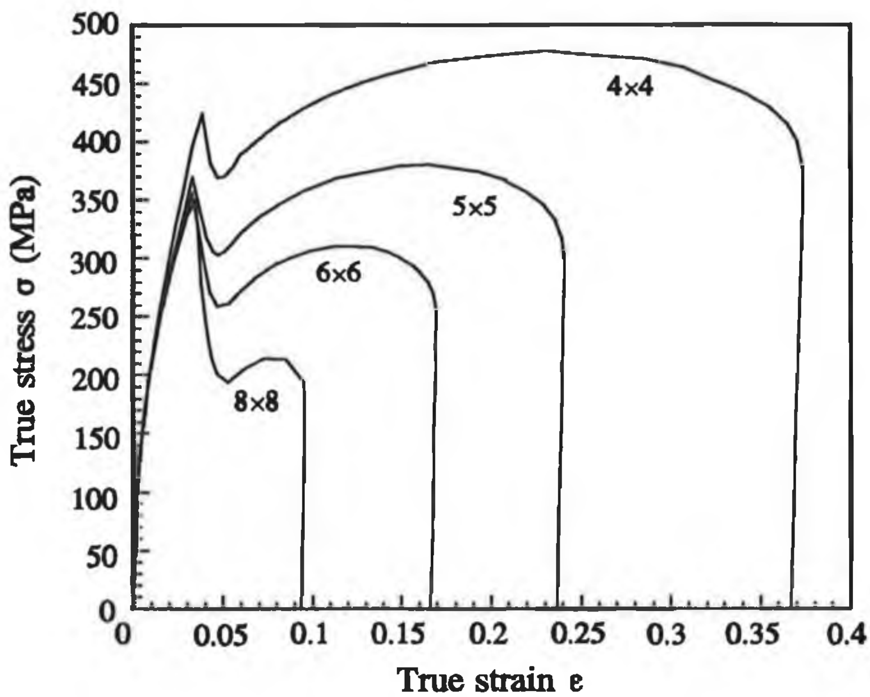

Fig. 48 *Variation of stresses with strains at x=0 at various dimensions [D (mm) × L (mm)] of specimens.*

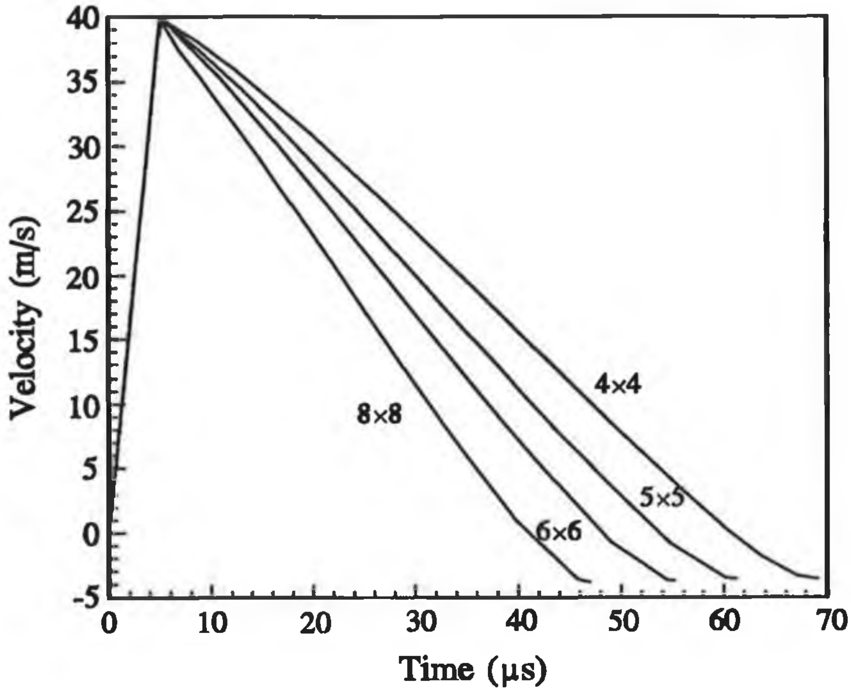

Fig. 49 *Variation of velocities with times at x=0 at various dimensions [D (mm) × L (mm)] of specimens.*

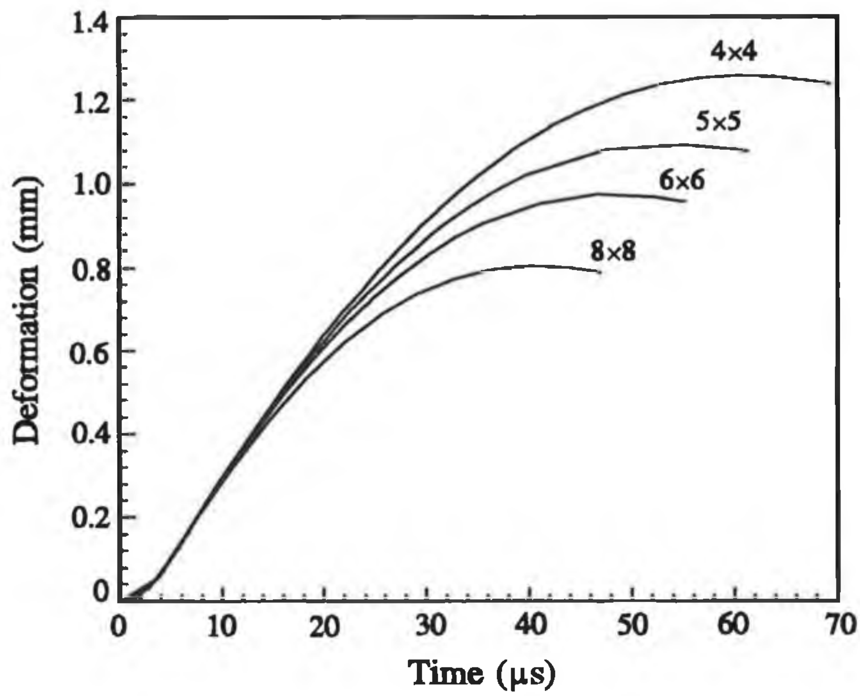

Fig. 50 *Variation of deformation with times at x=0 at various dimensions [D (mm) × L (mm)] of specimens.*

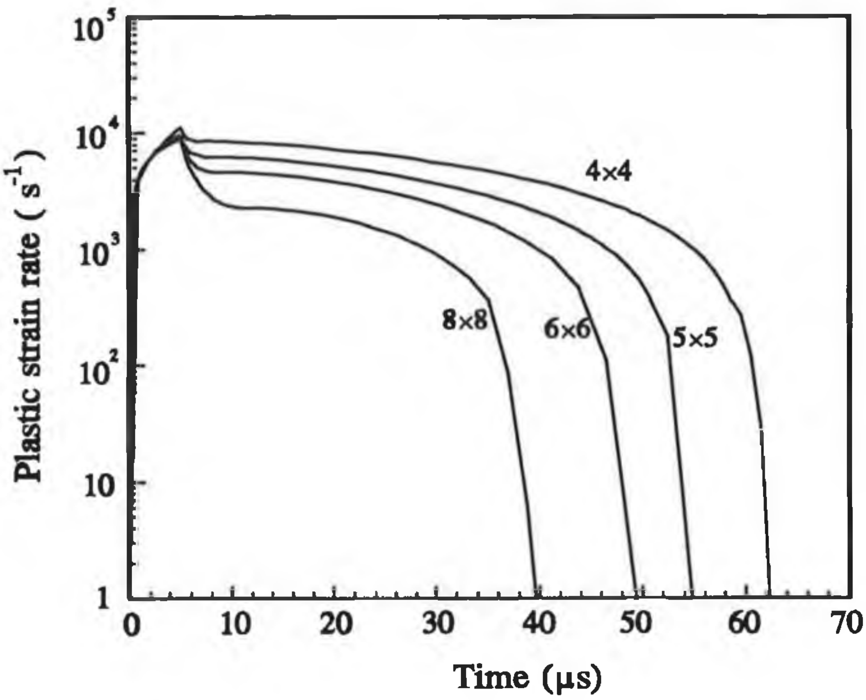

Fig. 51 *Variation of plastic strain rates with times at x=0 at various dimensions [D (mm) × L (mm)]of specimens.*

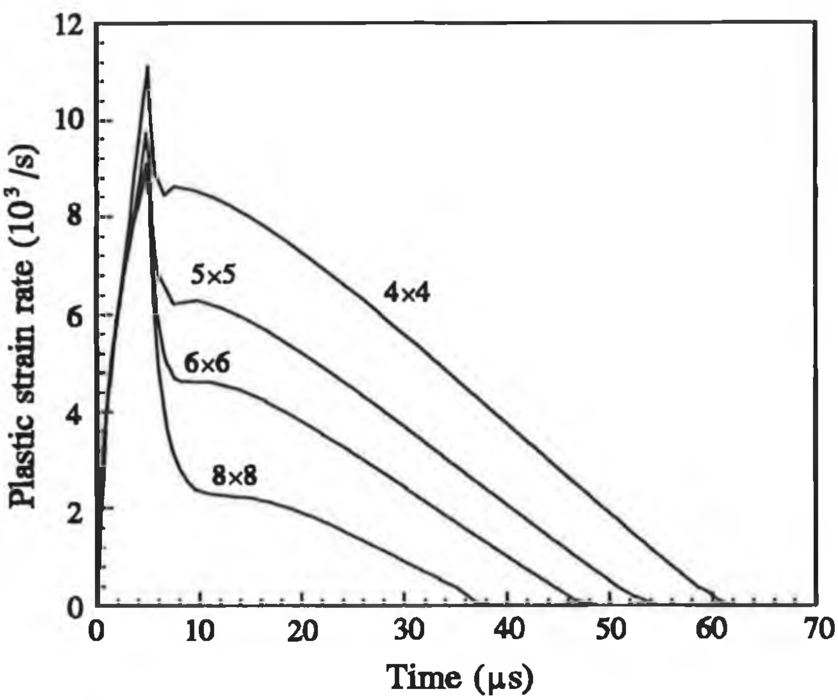

Fig. 52 *Variation of plastic strain rates with times at x=0 at various dimensions [D (mm) × L (mm)]of specimens.*

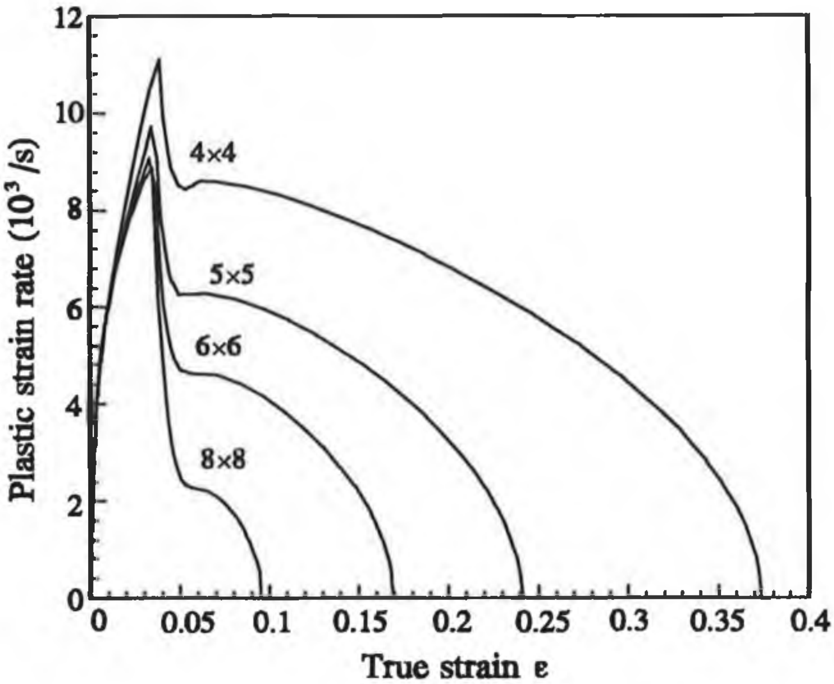

Fig. 53 *Variation of plastic strain rates with strains at x=0 at various dimensions [D (mm) × L (mm)] of specimens.*

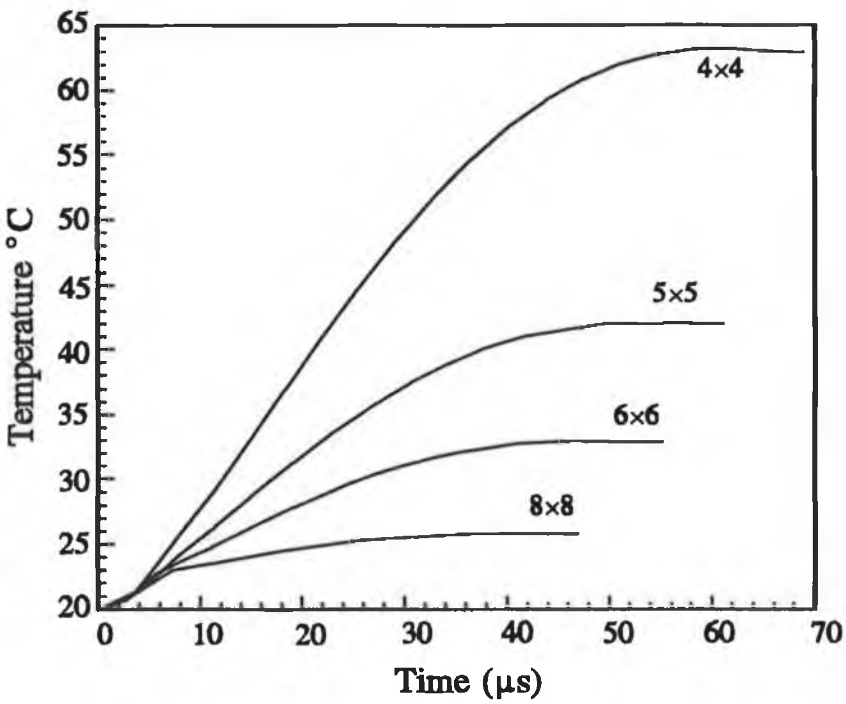

Fig. 54 *Variation of the temperature with the strain at x=0 at various dimensions [D (mm) × L (mm)] of specimens.*

2.7 The Elastic-plastic Boundary Conditions at the Fixed End

Generally, a different kind of boundary condition occurs when the specimen in which a wave is travelling terminates at an interface with the anvil in which the wave will also travel. This type of boundary condition is essentially different because whilst it produces a reflected wave in the specimen it also gives rise to a transmitted wave in the anvil.

There are two boundary conditions at the junction $x=h$. The first is the geometrical condition that the velocity must be continuous:

$$v(-h,t)=v(+h,t) \tag{64}$$

where

$$v(-h,t)=\lim_{x\to h} v(x,t) \quad (x<h) \tag{65}$$

and

$$v(+h,t)=\lim_{x\to h} v(x,t) \quad (x>h). \tag{66}$$

The second is the dynamical condition that the transverse force must be continuous:

$$\sigma(-h,t)=\sigma(+h,t) \tag{67}$$

This condition is necessary because a non-zero resultant force acting on the infinitesimally small mass at $x=h$ would produce an infinite acceleration. It can be seen that on the interface of the specimen with the anvil the stresses and velocities are continuous, but the strains are discontinuous.

In the present experimental system, the length of the anvil is so long that no reflective wave is transmitted back into the specimen from it and the yield stress of the anvil is considerably higher than that of the specimen, the deformation of which is controlled under the range of elasticity.

The equations of propagation of longitudinal waves in the anvil $(x>h)$ are comprised by the following:

$$\left.\begin{aligned} &E_2\frac{\partial \varepsilon}{\partial t}=\frac{\partial \sigma}{\partial t},\\ &\frac{\partial v}{\partial t}=\frac{1}{\rho_2}\frac{\partial \sigma}{\partial x},\\ &\frac{\partial v}{\partial x}=\frac{\partial \varepsilon}{\partial t}.\end{aligned}\right\} \tag{68}$$

where E_2 and ρ_2 are the Young's modulus and density of the anvil respectively. Along the characteristic lines of equations (68)

$$\frac{dx}{dt}=\pm\sqrt{\frac{E_2}{\rho_2}}=\pm c_2 \tag{69}$$

the differential relations are written as

$$d\sigma\mp\rho_2 c_2 dv=0 \tag{70}$$

Along the characteristic line

$$dx=0, \tag{71}$$

the entire differential form is

$$\begin{aligned} &E_2 d\varepsilon=d\sigma && (x\to h^+)\\ &Ed\varepsilon=d\sigma+g(\sigma,\varepsilon)dt && (x\to h^-)\end{aligned} \tag{72}$$

As shown in Fig. 55, having known the solution at nodes M_k, N_k *and* L_1, the values at the interface N_{k+1} between the specimen and the anvil can be solved using following steps. The differential relation from Eq. (42) written in the form

$$\sigma-\sigma_{N_k}=\rho c(v-v_{N_k})-g(\sigma_{N_k},\varepsilon_{N_k})(t-t_{N_k}) \tag{73}$$

is integrated along N_kN_{k+1}, and the relation from the characteristic line of negative slope in Eq. (69) written in the form

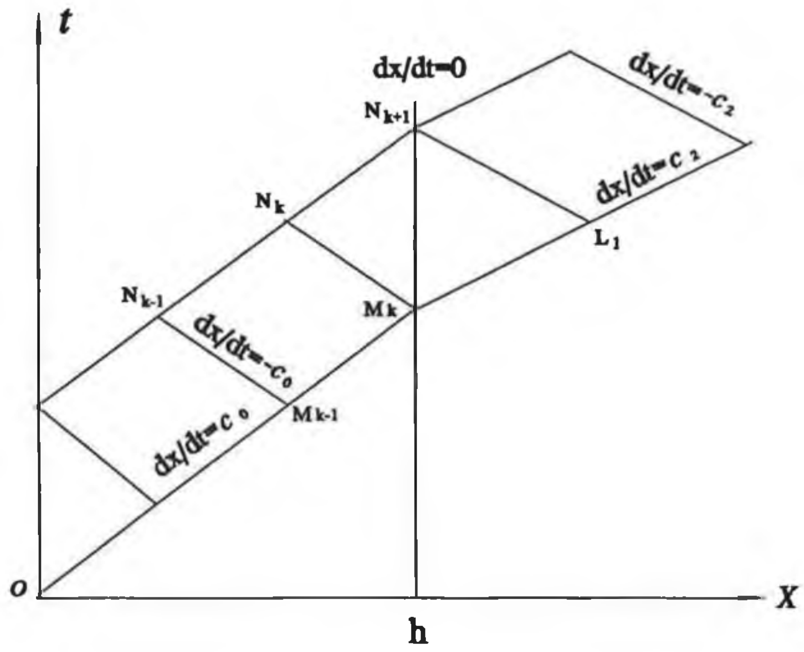

Fig. 55 *The characteristic field at the interface between the specimen and the anvil.*

$$\sigma-\sigma_{L_1}=-\rho_2 c_2(v-v_{L_1}) \tag{74}$$

is integrated along L_1N_{k+1}. Thus, σ_{k+1} and v_{k+1} can be obtained.

At the specimen, the relation (72) is transformed into a finite difference equation

$$E_2(\varepsilon-\varepsilon_{M_k})=\sigma-\sigma_{M_k}+g(\sigma_{M_k},\varepsilon_{M_k})(t-t_{M_k}) \tag{75}$$

and is integrated. Thus, ε_{k+1} at the specimen is obtained. In the same way, ε_{k+1} at the anvil may be attained by the first relation in Eq. (72).

The problem discussed in this Section will be carried out in the subject of further research work [197].

Chapter 3 Experiments and Results

3.1 The Quasi-static Compression Tests

Commercially pure copper (99.99%) and mild steel (C:0.2%) were chosen as the materials of the test specimens, which are machined into cylinders with several dimensions for the requirements of both the static and dynamic tests. The ratio of the diameter to the height (aspect ratio) of a specimen is approximately equal to 1. Both static and dynamic compressive experiments were performed in the conditions of room and high temperatures.

3.1.1 Tests under the ambient temperature

(1) Preparation of the test

Before the test starts, the end surfaces of the specimen are finely ground using sandpaper, the identification number is given to the specimen to be tested, its diameter and height are measured by a micrometer, and the results are noted on a test work sheet.

A 50 kN Instron Universal Material Testing Machine shown in Fig. 56 is used for the static test. To assure load cell stability, about 15 minutes after the machine is turned on, the pre-adjustment of the system is performed:

(a) The load cell is calibrated by means of Electrical Calibration of Self Identifying Load Cells. In this case, the balance operation is performed automatically.

(b) Set the crosshead travel stops and the crosshead speed. In the case of static tests at room-temperature, the crosshead speed is set at 3 mm/s, while in the high temperature static case, it is set at 20 mm/s.

Fig. 56 *The view of 50 kN Instron Universal Material Testing Machine.*

(c) Install test specimen.

(d) Set pen scaling on the X-Y Recorder for load signal, and set x-axis position drive mode. Determine the x-axis at a zero position by moving the crosshead and adjusting x position of the recorder. Set the gage length.

In order to eliminate the gaps between the surfaces of the specimen and of the crossheads, pre-compression tests are performed in the range of elasticity of the specimen which are repeated twice for each specimen.

(2) Performing a test

The nominal heights and diameters of specimens are equal to 8.00 *mm* for copper or 5.0 *mm* for steel, the maximum compressive loads are determined as 50 *kN* for copper specimen or 25 *kN* for steel specimen and the compressive velocity is set as 3 *mm/min* for both materials. In order to reduce the friction between the pressure head and the specimen, polythene sheet 0.5 mm thick has been used as lubricant which is put on the top and bottom ends of the specimen before a test is made. The tests are performed for 4 to 5 times for each material.

(3) The stress-strain curves

According to the calibration of the X-Y recorder, the deformations of the specimen and the loads are obtained, from which the true stress-strain curve for a tested material can be estimated. The conversions of the stress σ from the load and the strain ε from the deformation are made by

$$\begin{aligned} \sigma &= \frac{P}{A} = \frac{P}{V_0/H} = \frac{P \times H}{V_0} \\ \varepsilon &= \ln\frac{H_0}{H} \end{aligned} \tag{76}$$

where P is the compressive load, A and H are variables, the current area of the cross section and height of the specimen corresponding to load P, and V_0 is the volume of the specimen which is considered as constant in the process of the deformation of the specimen.

A simple computer program has been written to calculate the true stresses and strains which are used to draw the stress-strain curve (see Appendix II). Then a mathematical process is applied by means of the graphic software to make the drawn curve smoother.

3.1.2 Tests at high temperatures

In order to reduce the heat loss of the specimen in the process of the compression to largest extent, a large anvil unit with respect to the mass of the specimen has been designed and used. Considering that it is also used for the dynamic tests, the unit is designed as shown in Fig. 57 that it can be easily moved out from the hot furnace using a clamp, and a changeable high hardening alloy anvil is fixed inside the unit by means of a flange and three sunk screws.

Before being heated, the ends of the specimen and the inside of the chamber of the unit are carefully cleaned, the specimen is placed upon the central position of the chamber, and a hardened cylindrical pressure head, whose design diameter approaches but is smaller than the inner diameter of the chamber, is located upon the specimen. Then, they are together put into the furnace to be heated. Generally, after the temperature indicator of the furnace reaches the preselected scale, all the heated components still need to be kept inside the furnace for at least half an hour depending on the level of the preselected temperature to ensure that they attain a stable temperature. The preselected temperature of the furnace is always set at a temperature higher than the test temperature. To save the test time, two sets of chamber units are heated in the same time and they are used alteratively.

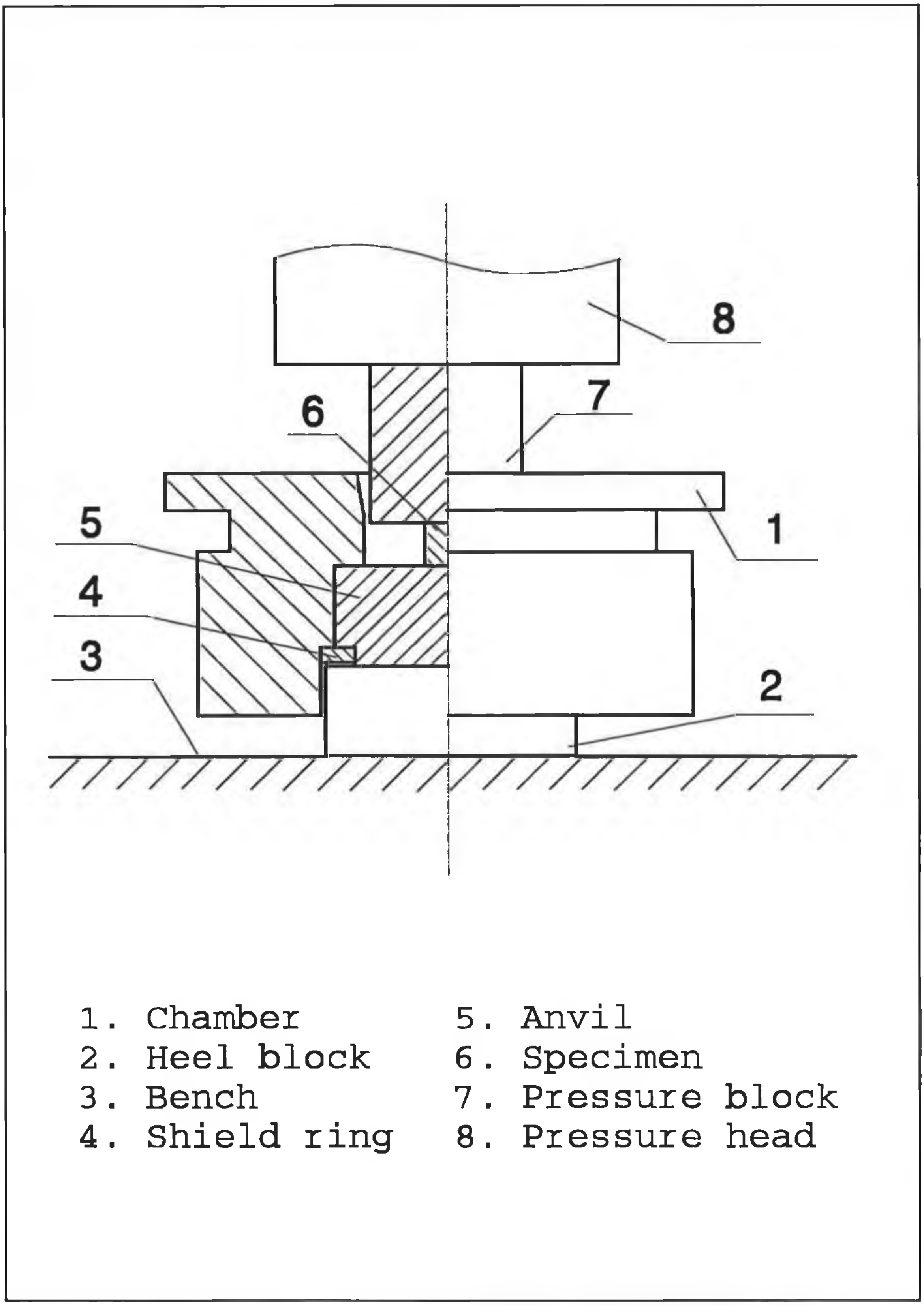

Fig. 57 *The diagram of chamber used for quasi-static compressive test at high temperature.*

A K-type thermocouple with a welded tip insulated by glass fibre and a panel mounting digital temperature indicator are used to monitor the variation of temperature of the specimen in the process of the compression. The measuring range of temperature for this type of thermocouple is from -200°C to +1100°C and the range of error is assured to be within ±3°C for the range 0°C to +400°C and within ±0.75% for the range 400°C to 1100°C. The measuring range of the temperature indicator is -50°C to +1000°C, its resolution is 1°C and the accuracy at 25°C is given as ±0.3%.

The heated anvil unit including the specimen and the pressure head is removed to the static test machine (a heated cylindrical heel block has been placed on the bottom pressure head or the bench of the test machine). Then, the tip of the thermocouple is inserted into the cavity of the chamber from the gap between the heated pressure head and the inner wall of the unit, and the temperature inside the cavity is displayed on the panel mounted digital temperature indicator. When the temperature drops to the required test value, the compression test is started. The time taken by the process of compression and final temperature are recorded to be used later for the calculation of the error of temperature of the test. The test at a definite nominal temperature is preformed 2 or 3 times. Hence, by choosing the various temperatures, a group of stress-strain curves at corresponding temperatures can be obtained.

The quasi-static stress-strain curves for commercially pure copper and mild steel at various temperatures that have been processed mathematically are shown in Figs. 58 and 59 respectively.

3.2 The Static Stress-Strain Equations

The application of computer software makes it possible to attempt various forms of mathematic models to deal with the experimental data. In the current research, the quasi-static stress-strain curves at various temperatures obtained by experiments have been smoothed and regressed in several forms for commercial purity copper and mild steel.

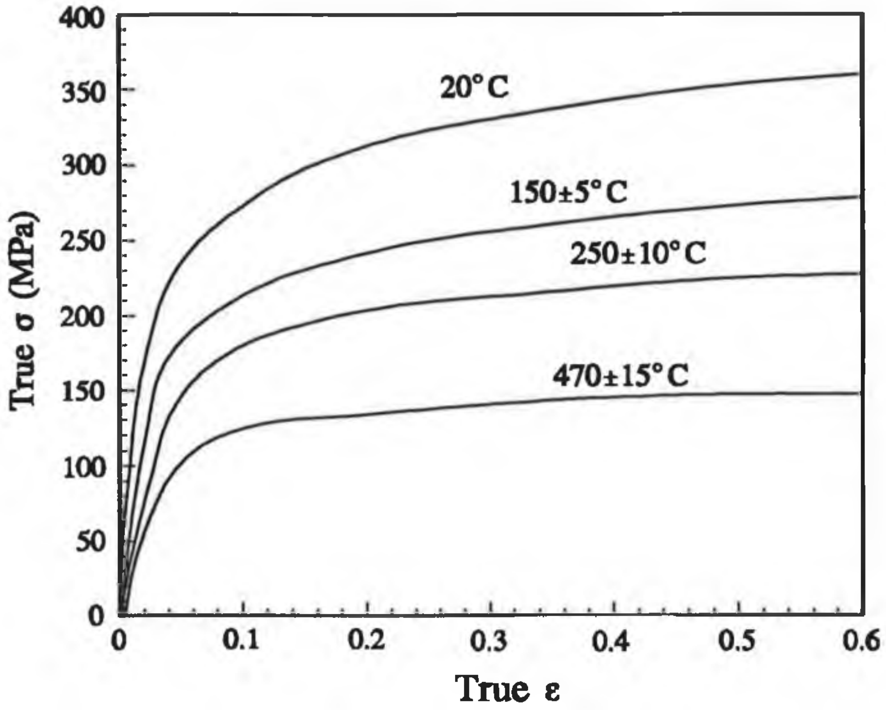

Fig. 58 *Quasi-static stress-strain curves of commercially pure copper at various temperatures.*

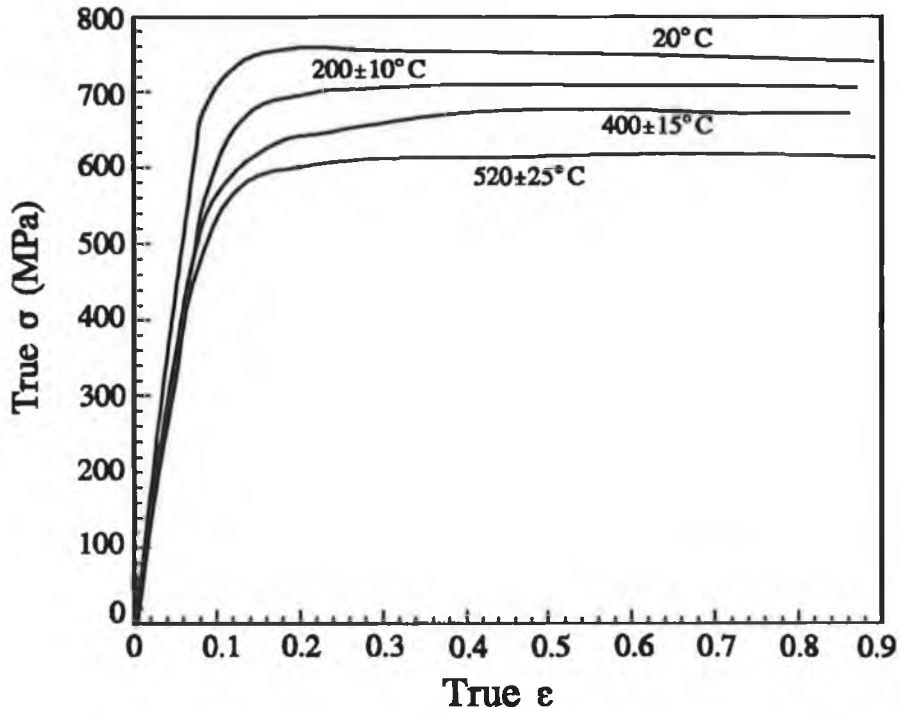

Fig. 59 *Quasi-static stress-strain curves of mild steel at various temperatures.*

3.2.1 Commercially pure copper

As shown in Fig. 60, the quasi-static stress at various temperatures from *20°C* to *470°C* for commercially pure copper is regressed as a 5x2 order polynomial explicit function of strain and temperature, which is expressed as

$$\begin{aligned}\sigma =& 3.98236-0.0370176T+6.07912\times10^{-5}T^2+4734.68\varepsilon-20.082\varepsilon T+0.027065\varepsilon T^2\\ &-26197.3\varepsilon^2+146.847\varepsilon^2T-0.213977\varepsilon^2T^2+70237.6\varepsilon^3-443.625\varepsilon^3T+0.660459\varepsilon^3T^2\\ &-89109.4\varepsilon^4+598.519\varepsilon^4T-0.897697\varepsilon^4T^2+42785.1\varepsilon^5-298.171\varepsilon^5T+0.448959\varepsilon^5T^2\end{aligned} \tag{77}$$

The comparison of the regressed curves with the experimental data is shown in Fig. 61. This type of regression expression can reasonably describe the experimental results, and also be applied in the computation.

With reference to the form proposed by Vinh *et al.* [198], the type of constitutive relation for working-hardening materials is suggested as

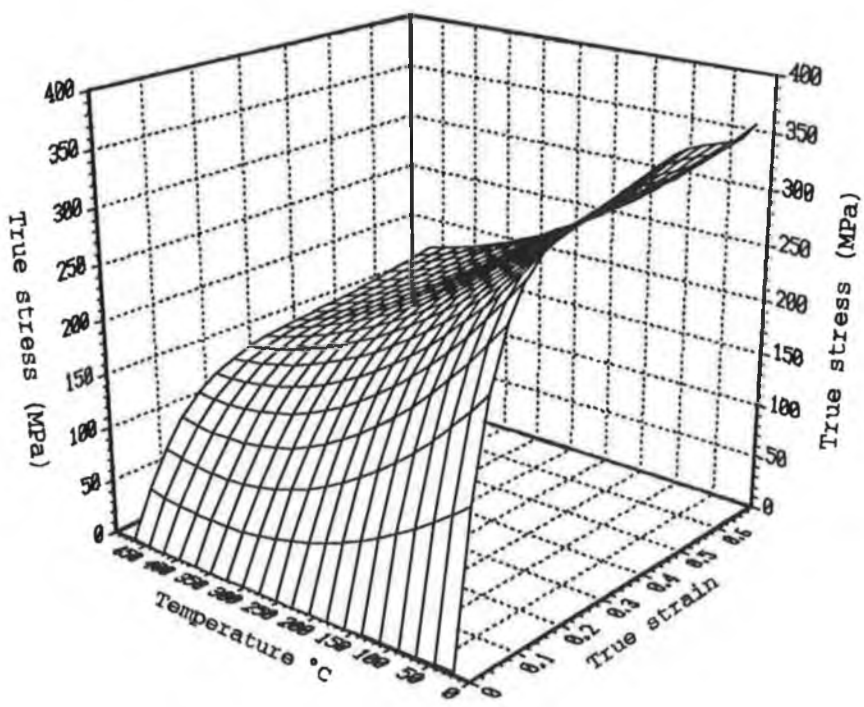

Fig. 60 *The regression surface of the quasi-static stress-strain relation at various temperatures for commercially pure copper based on Eq. (77).*

$$\sigma = a e^{b/T} f_0(\varepsilon) \tag{78}$$

where $f_0(\varepsilon)$ is the quasi-static stress-strain curve at room temperature, T is the temperature(°C), and a and b are constants independent of temperature. Based on the quasi-static stress-strain curve at room temperature, the constitutive relation for commercially pure copper shown in Fig. 62 is regressed as

$$\sigma = 0.4152\varepsilon^{0.196} e^{123.526/T} f_0(\varepsilon) \quad (MPa) \tag{79}$$

where

$$f_0(\varepsilon) = -41329\varepsilon^6 + 139301\varepsilon^5 - 139301\varepsilon^4 + 81550\varepsilon^3 - 25801\varepsilon^2 + 4367\varepsilon + 9.72 \quad (MPa) \tag{80}$$

Comparing with Eq. (77), this type of constitutive relation has further been simplified, but it needs the corresponding experimental stress-strain curve at the room temperature. The accuracy of the curve affects directly those at higher temperatures.

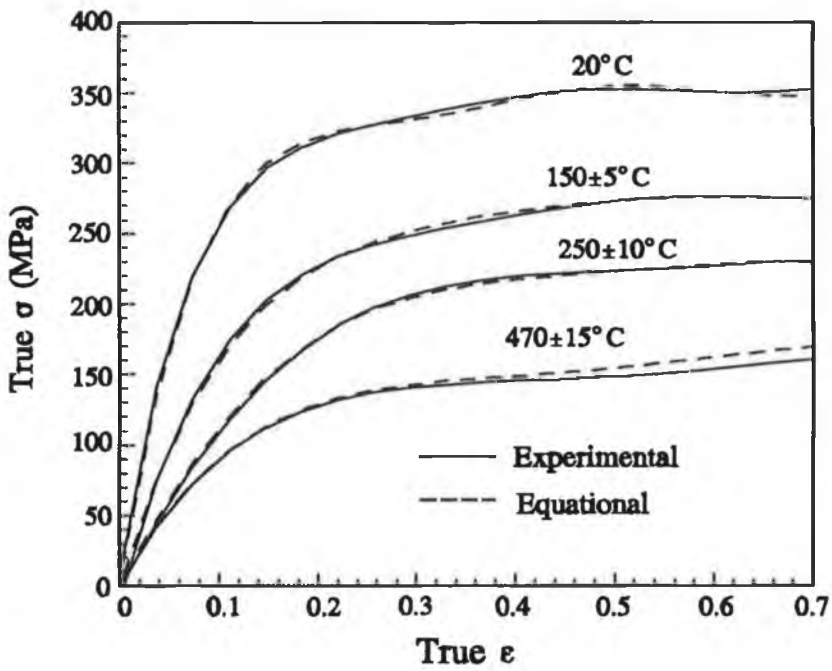

Fig. 61 *Comparison of quasi-static stress-strain curves between the experimental results and the regressed expression based on Eq. (77) at various temperatures.*

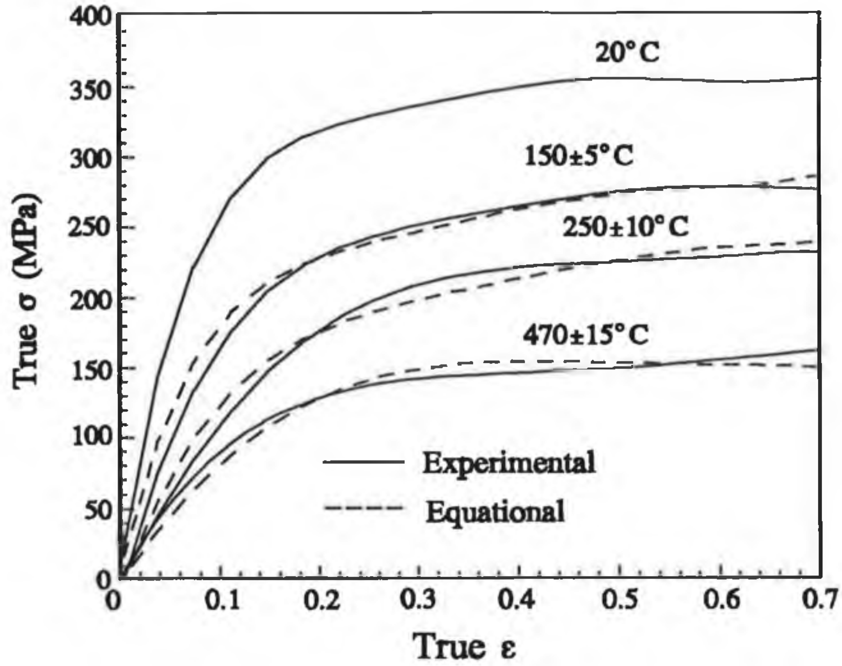

Fig. 62 *The regression of the quasi-static stress-strain curves at various temperatures for commercially pure copper based on Eq. (79).*

For the purpose of the analysis and discussion, it is necessary to propose a simpler form to characterise the mechanical properties of the tested material. Therefore, the following geometrical form of the quasi-static constitutive relation for work-hardening type materials such as copper is suggested

$$\sigma = A(T)\varepsilon^{n(T)} \tag{81}$$

For pure copper, *A(T)* and *n(T)* have been determined as shown in Table 2, and the corresponding curves is demonstrated in Fig. 63.

Table 2 *A(T) and n(T) determined in Eq. (81) for commercially pure copper.*

Temperature (°C)	A(T)	n(T)
20	398	0.150
150±5	305	0.142
250±10	244	0.130
470±15	160	0.120

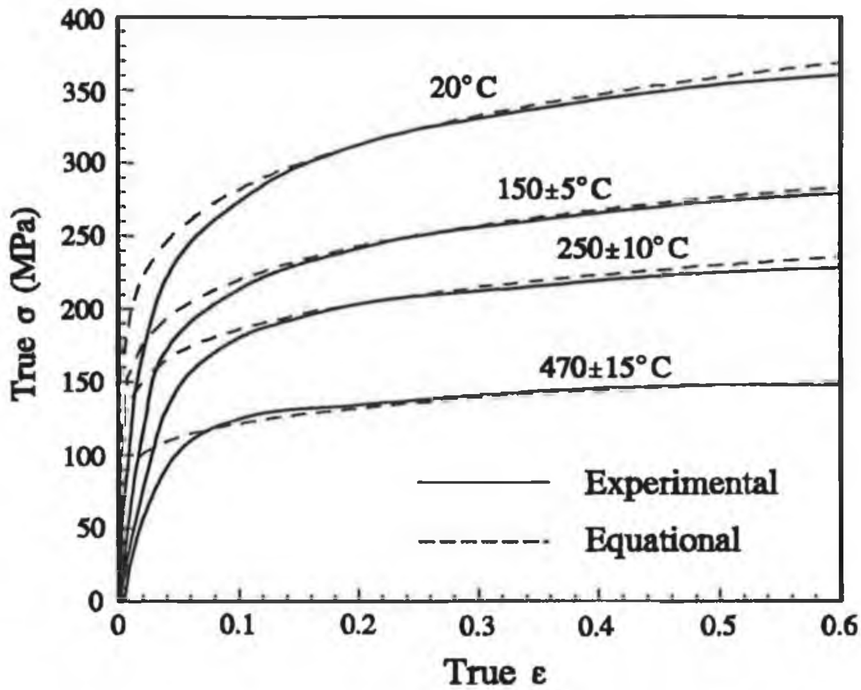

Fig. 63 *The regressive curves of the quasi-static stress-strain relation at various temperatures for commercially pure copper based on Eq. (81) and Table 2.*

Further, both $A(T)$ and $n(T)$ are respectively expressed in the linear regressive forms

$$A(T)=393.5-0.524\,T \quad (MPa),$$
$$n(T)=0.151-6.83\times10^{-5}\,T. \tag{82}$$

where T is the ambient temperature of the tested specimen (°C). The curves based on Eq. (82) in the form of Eq. (81) are shown in Fig. 64.

3.2.2 Mild steel

For elastic/perfectly plastic type materials such as the mild steel used in this study, the corresponding form of stress-strain curve is suggested as

$$\sigma=\varphi(T)(1-e^{-k\varepsilon}) \tag{83}$$

where $\varphi(T)$ is a function of temperature, which is the yield stress at temperature T; k is a material constant. The static compression experiments

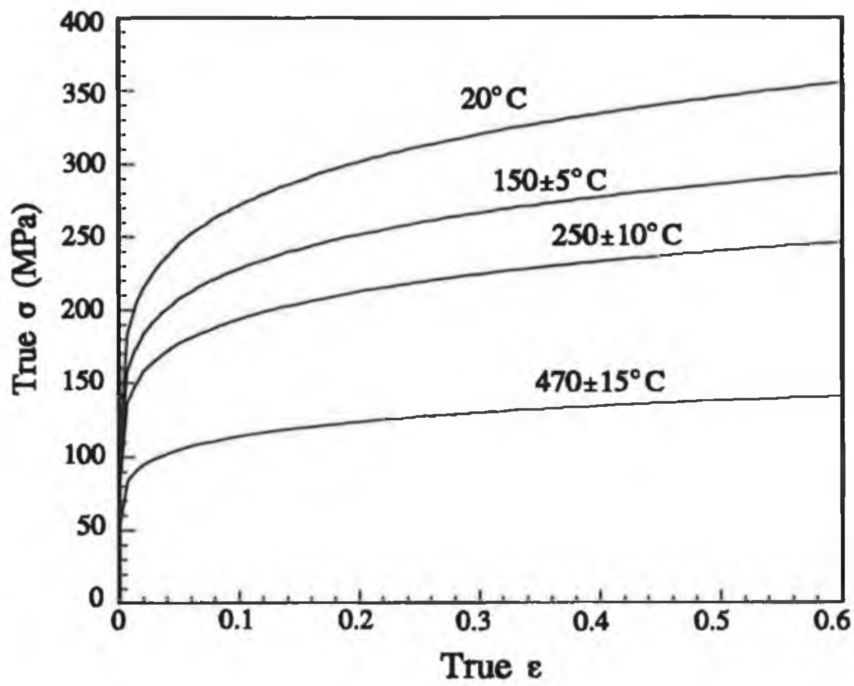

Fig. 64 *The regressive curves of the quasi-static stress-strain relation at various temperatures for commercially pure copper based on Eqs. (81) and (82).*

from the room temperature up to the high temperature of 520°C for mild steel have been made, and for the corresponding static stress-strain curves, $\varphi(T)$ and k have also been determined as shown in Table 3.

Table 3 *φ(T) and k determined in Eq. (83) for mild steel.*

Temperature (°C)	φ(T) (MPa)	k
20	767	28
200±10	730	28
360±15	689	27
520±20	620	28

Actually, $\varphi(T)$ can be considered as the yield stress at the temperature T, while k is a constant related to the Young's modulus. The comparisons of the experimental curves with the analytical expressions based on Eq. (83) and Table 3 are exhibited in Figs. 65 to 68.

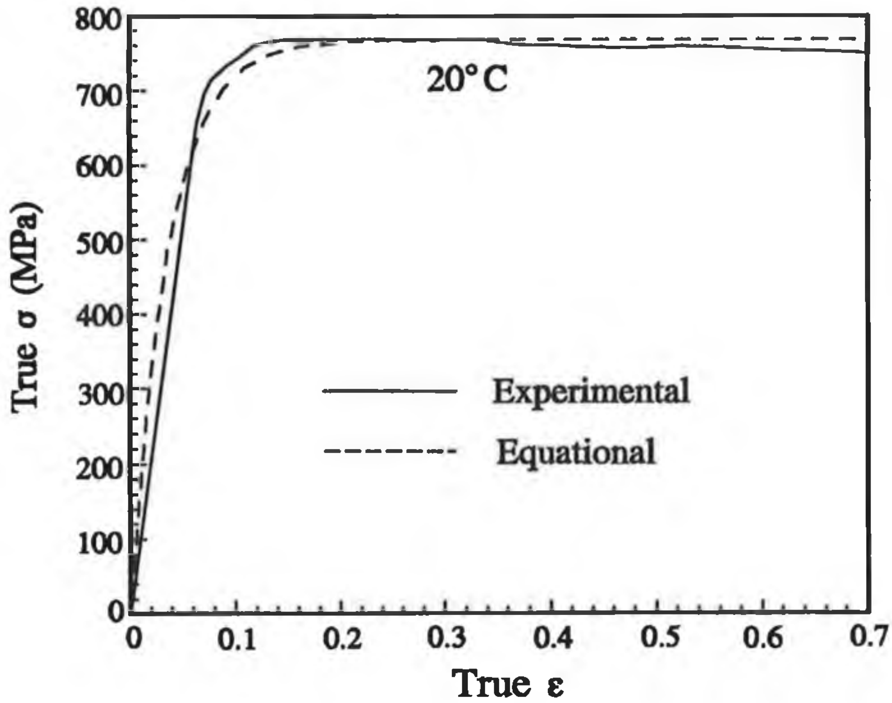

Fig. 65 *Comparison of the quasi-static stress-strain relations obtained by the experiment with based on Eq. (83) and Table 3 at 20 °C for mild steel.*

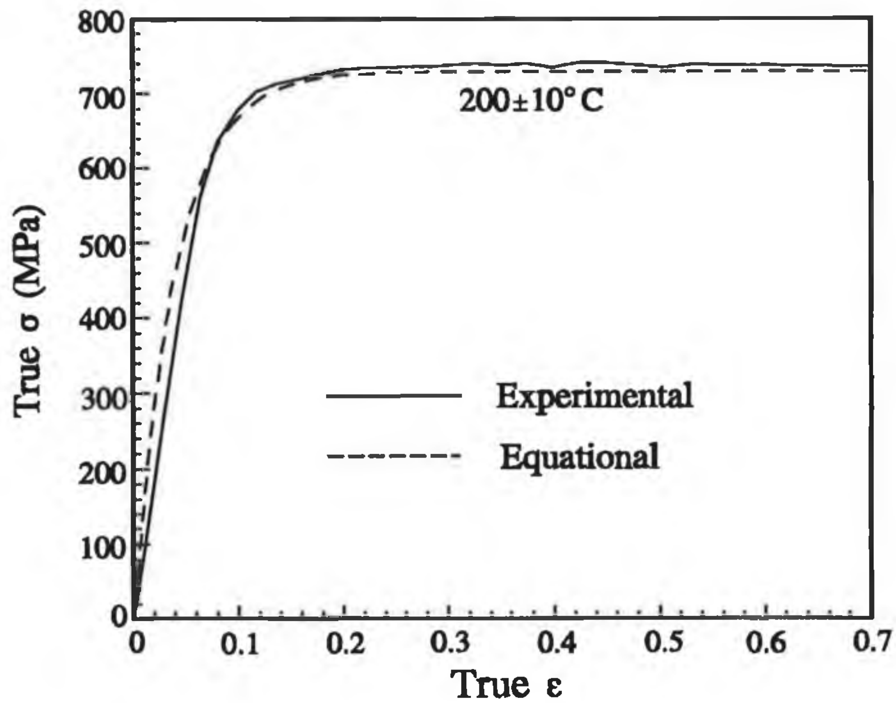

Fig. 66 *Comparison of the quasi-static stress-strain relations obtained by the experiment with based on Eq. (83) and Table 3 at 200 °C for mild steel.*

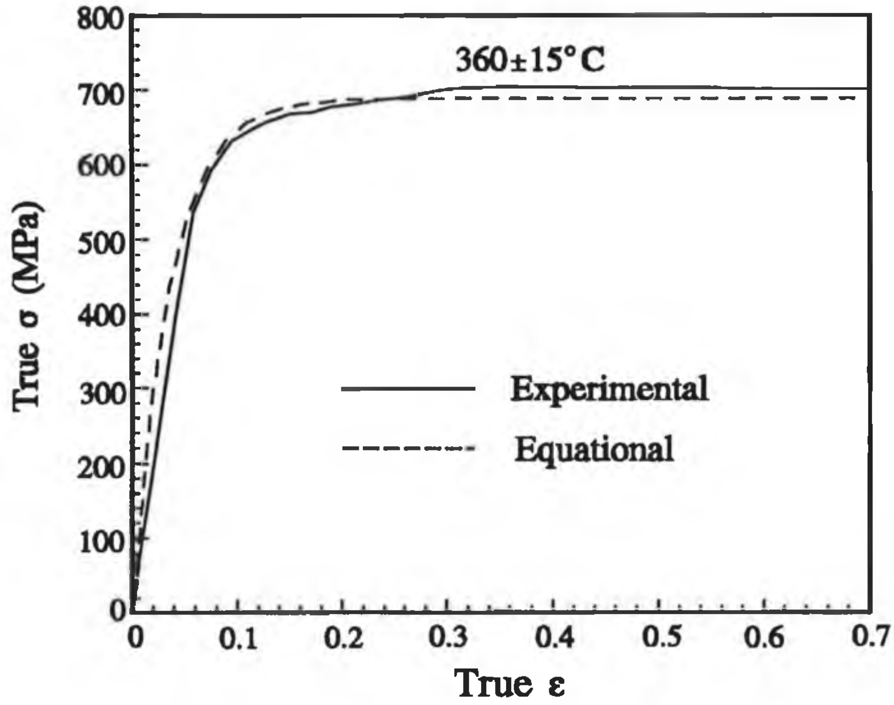

Fig. 67 *Comparison of the quasi-static stress-strain relations obtained by the experiment with based on Eq. (83) and Table 3 at 360 °C for mild steel.*

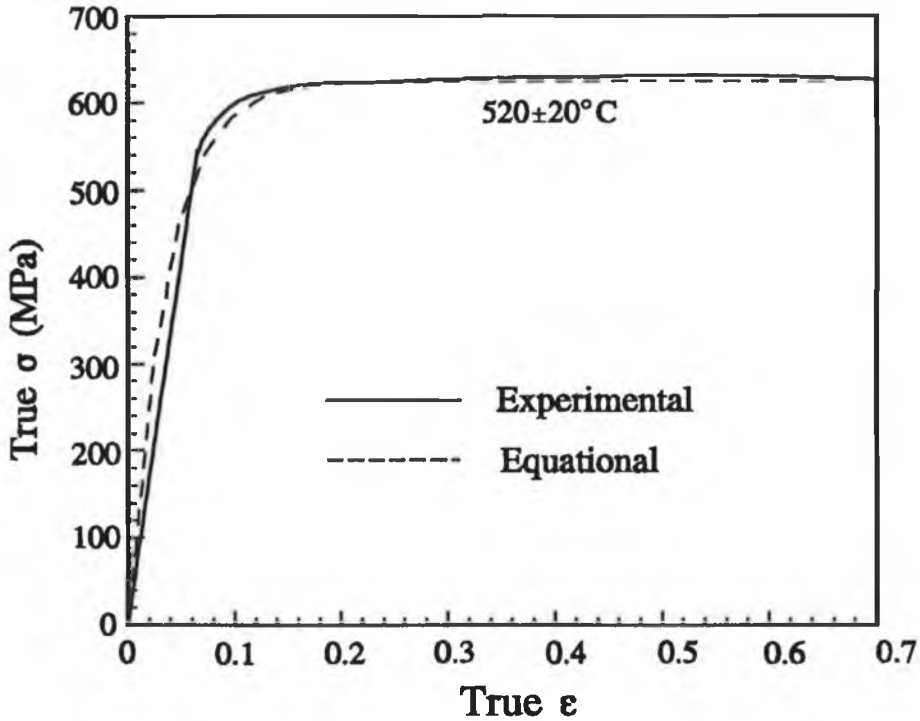

Fig. 68 *Comparison of the quasi-static stress-strain relations obtained by the experiment with based on Eq. (83) and Table 3 at 520 °C for mild steel.*

3.3 Dynamic Impact Tests

3.3.1 Apparatus and principle

The impact experiments were performed with an existing apparatus shown in Fig. 69. This set of experimental system mainly consists of a movable rig, the high pressure power system, the barrel parts, the anvil unit and the projectile velocity measuring system (see Fig. 70).

The main part of frame of the ballistic test machine is composed of a welded construction with steel angle bar. The remaining auxiliary parts are fixed by screws for the purpose of the assembly and disassembly.

In the gas propelled system, a high pressure nitrogen gas cylinder controlled by a 40 *bar* adjusting pressure value supplies the compressive gas to a reservoir unit which is fixed on the rig. At the outlet of the reservoir, a two-way solenoid-controlled valve is attached, which makes the outlet on or off. As shown in Fig. 71, a primary barrel is connected to the solenoid-controlled valve at one end and to extension barrel at the other end. A cut-out segment is machined on the primary barrel through which the projectile can be loaded and pushed upwards inside the projectile gripper mechanism. A close fitting split cover is used to close the cut-out segment, and a sliding collar and a nut are used to hold the assembly firmly to prevent the high pressure gas from escaping. The projectile gripper mechanism consists of three grab screws and spring operated smooth pins incorporated at the upper end of the loading throat. A extension barrel is connected to the primary barrel by means of a threaded and knurled coupling sleeve at one end and is attached a surge suppressor cap at the other end [199].

In order to meet the testing requirement at high temperatures, a new set of anvil units to avoid the loss of the heat was designed and used instead of the original one. This set of units is movable and fitted with the former cylindrical steel bar(see Fig. 72). The relationship of the loss of heat with time for the unit has been measured as is shown Fig. 73.

Fig. 69 *The view of the ballistic test machine.*

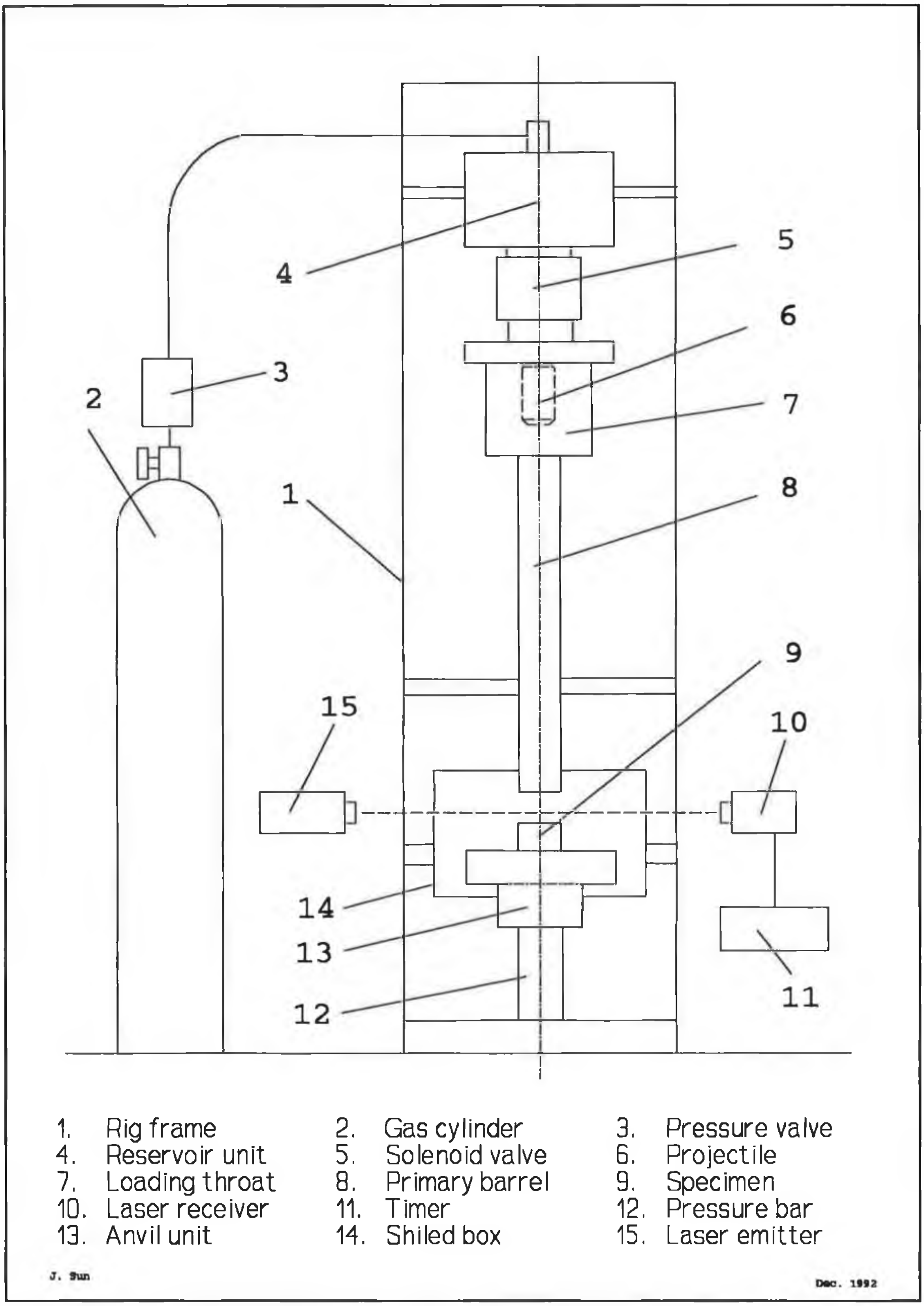

Fig. 70 *Schematic diagram of the ballistic test machine.*

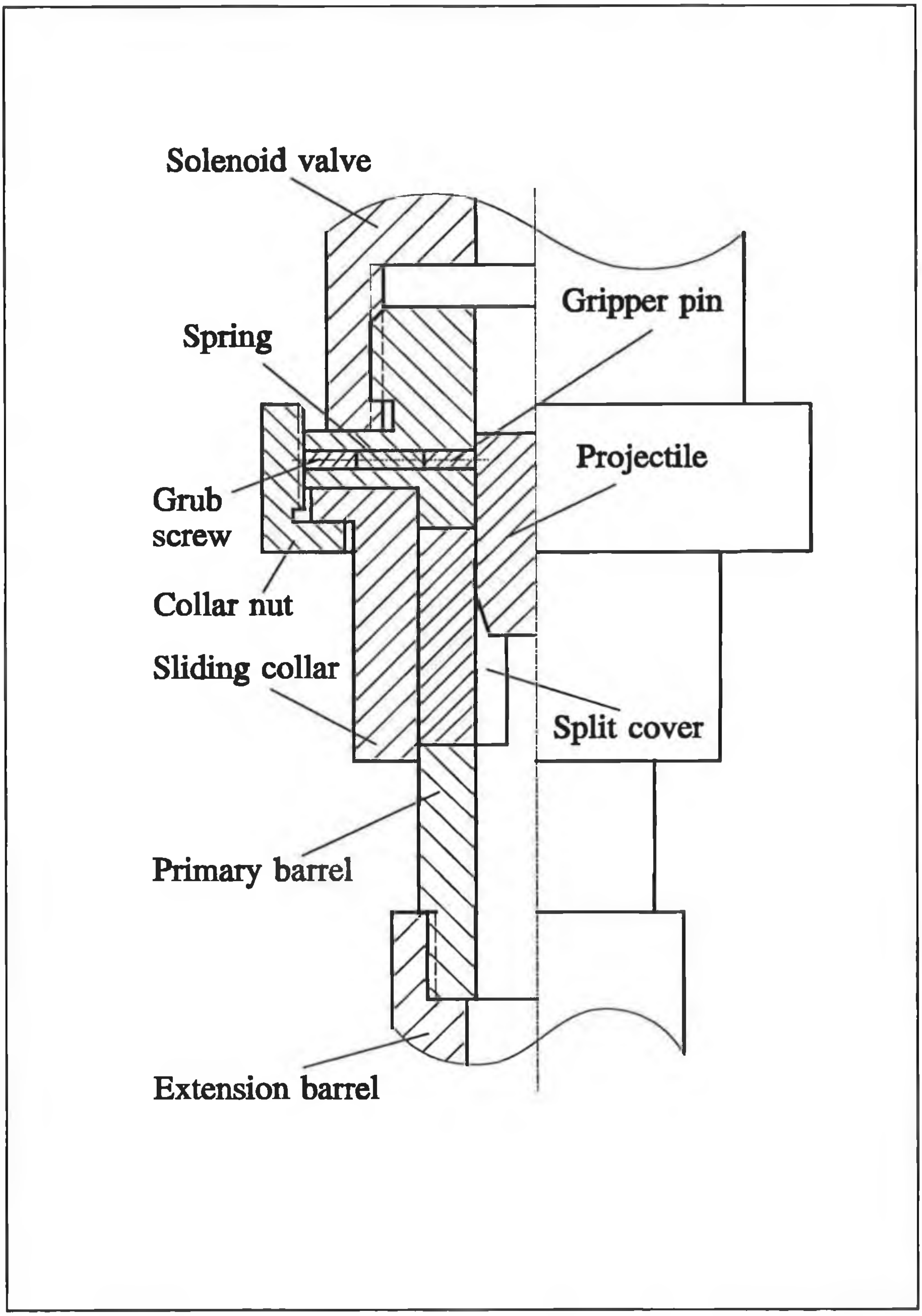

Fig. 71 *Schematic diagram of the loading unit of the ballistic test machine.*

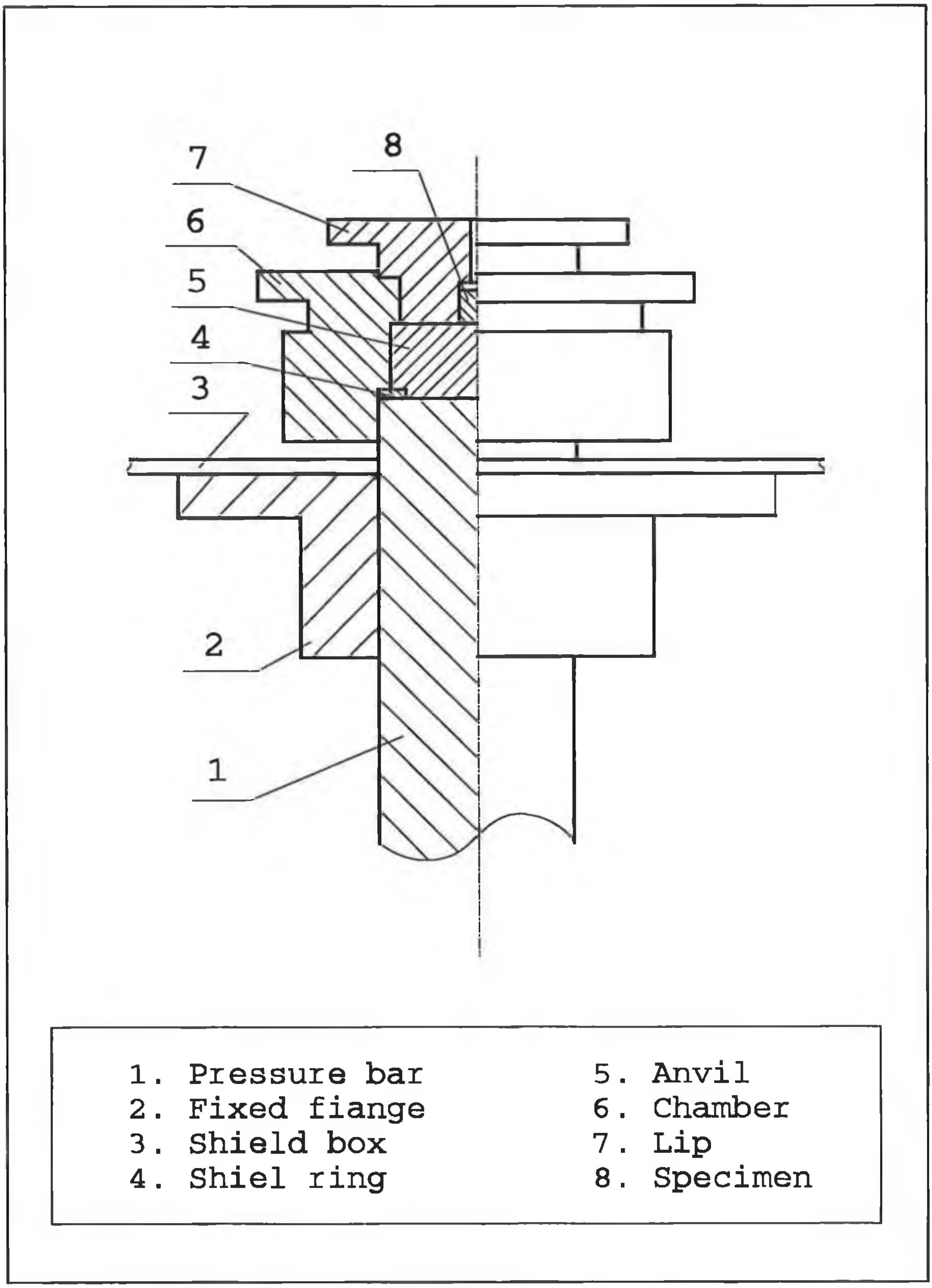

Fig. 72 *The chamber unit used for impact compressive test at high temperatures.*

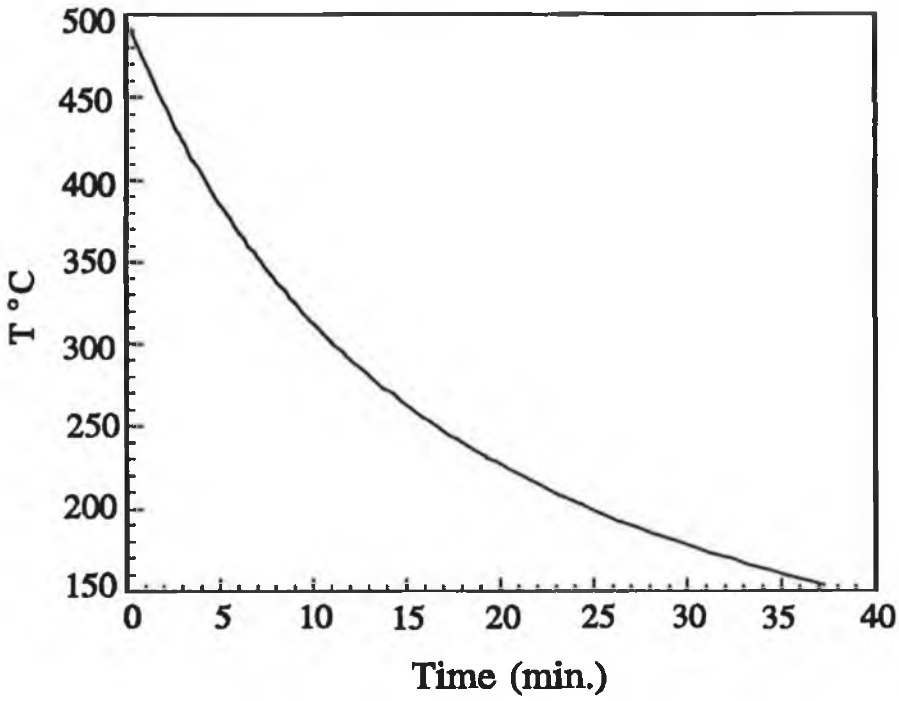

Fig. 73 *The relationship of heat loss with time for the impact chamber.*

The velocity measuring system consists of a laser beam emitter, a laser beam receiver and a universal counter-timer. The velocity of the projectile is obtained by means of measuring the time interval for the two ends of the projectile to pass through some reference point. Then, the velocity is calculated by means of the known length of the projectile and the measured time interval. Before measuring, the laser beam receiver is triggered by the emissive device and the function of counter-timer is keyed at the *Single Time Interval*. The steps to perform this are as follows:

(a) Check the connections of the emitter, receiver and counter-timer, and assure them at the proper positions.

(b) Switch them on and adjust the positions of the emitter and receiver to assure the beam emitted by the emitter both to pass through the centre extending line of the anvil and to trigger the receiver.

(c) On the panel of the counter-timer, select Time INT function, depress single measure and select 1 cycle measure with Gate push-button. Set Coupling at 50Ω. Ensure the signal edge of the slope as ┘ at input A and └ at input B. Set Attenuation to ×10 position and adjust Trigger Level at the near middle position.

(d) Press Start/Stop button of the counter timer. The gate LED (Light Emitting Diode) will illuminate to indicate that the counter is primed and ready to make a measurement.

As the front end of the projectile reaches and begins to pass the laser beam, the upper gate LED of the receiver gets off. The signal edge of the selected slope appears at input *A* and the timing cycle begins. When the rear end of the projectile begins to pass the laser beam, the upper gate LED of the receiver comes on. The signal of the selected edge appears at input *B*, the timing cycle ceases and the result is displayed. The displayed result is held until a *Reset* occurs.

3.3.2 Modification of the test machine

(1) Chamber unit

The impact tests are performed on the original equipment, while some of its parts can not meet the requirement of the current tests. Therefore, in order to accommodate the requirement of high temperature tests, the improvement and renovation for the machine have been made.

In order to reduce the number of renewed parts and utilise as many original parts as possible in the condition that the test requirement is assured, two sets of chamber units shown in Fig. 72 for the dynamic test were designed and machined. This unit can also be used for the static test with an extra pressure head and a heel block (Fig. 57). In order to reduce the heat loss of specimen in the process of the test to restrict the variation of the temperature of the specimen as shown Fig. 74, the chamber with respect to the specimen was designed with a large mass. During the tests, two sets of the chamber units are used alternatively. They can be easily moved in and out from the hot furnace by a clamp. Considering the life of the working surface of the anvil, a changeable alloy anvil (Fig. 75) is fixed on the chamber by means of a shield ring (Fig. 76) and three sunk screws. Various sizes of lips with respects to the dimensions of specimen shown in Fig. 77 have been employed to prevent the heat in the cavity from escaping and to keep the specimen at the central line position of the unit. The thin hole on the lip is used for the measurement of temperature using a thermocouple.

(2) Projectile

In order to avoid the projectile from being blocked, especially after it has been used for several times, the originally designed projectile has been modified according to the configuration as shown in Fig. 79. A 3° angle guide cone is made in the front of the projectile. Further, to guarantee the high pressure air pushing on the rear end of the projectile, a very small clearance fitting between its lateral surface and the inside face of the primary barrel of the machine is chosen. After the thermal treatment, the hardness of its front end is controlled in the range of 62-65 *HRC*.

(3) Shield box

For the purpose of safety and the convenient collection of the specimens after each test, a close shield box was designed and manufactured as shown in Fig. 80. It consists of a welded square steel frame on which aluminium plates are fixed by screws. To allow the laser beam for the measurement of the velocity of the projectile to pass through the box, the corresponding holes on its two sides are made. The angle steel sections and a flange attached on the box are linked to the rig and the pressure bar of the test machine by screws respectively.

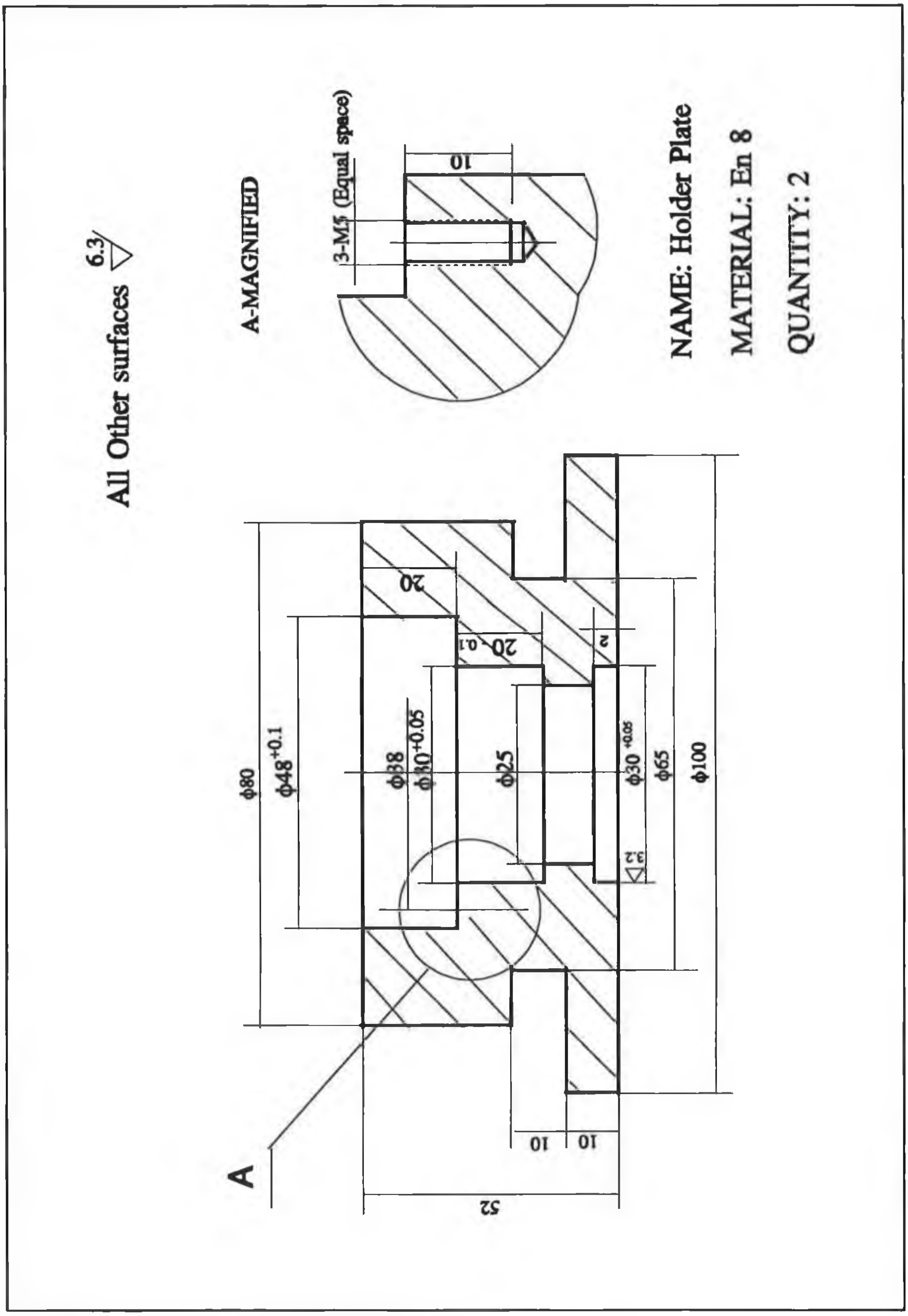

Fig. 74 *The chamber used for static and dynamic tests at high temperatures.*

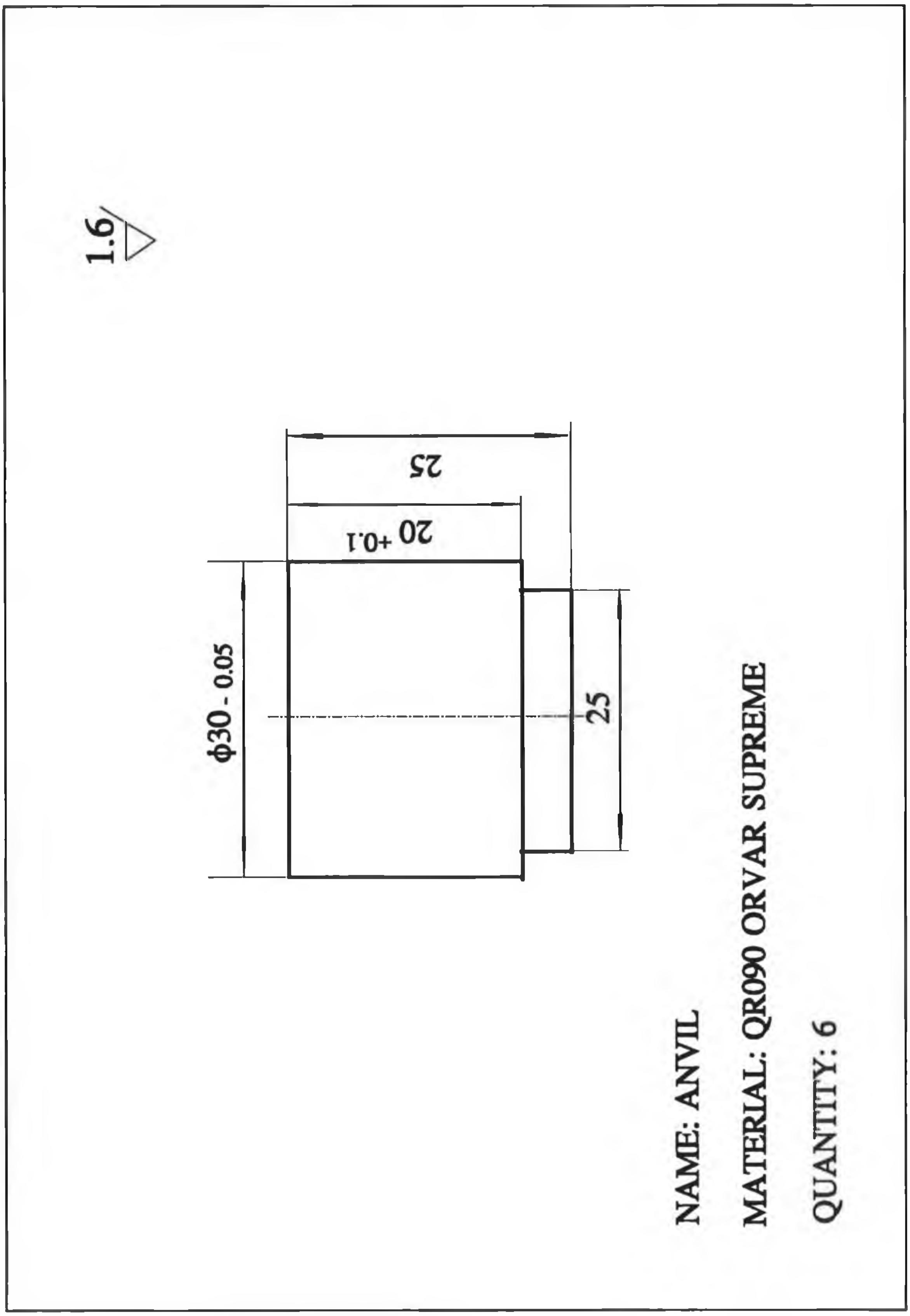

Fig. 75 *The anvil used for impact and static tests at high temperatures.*

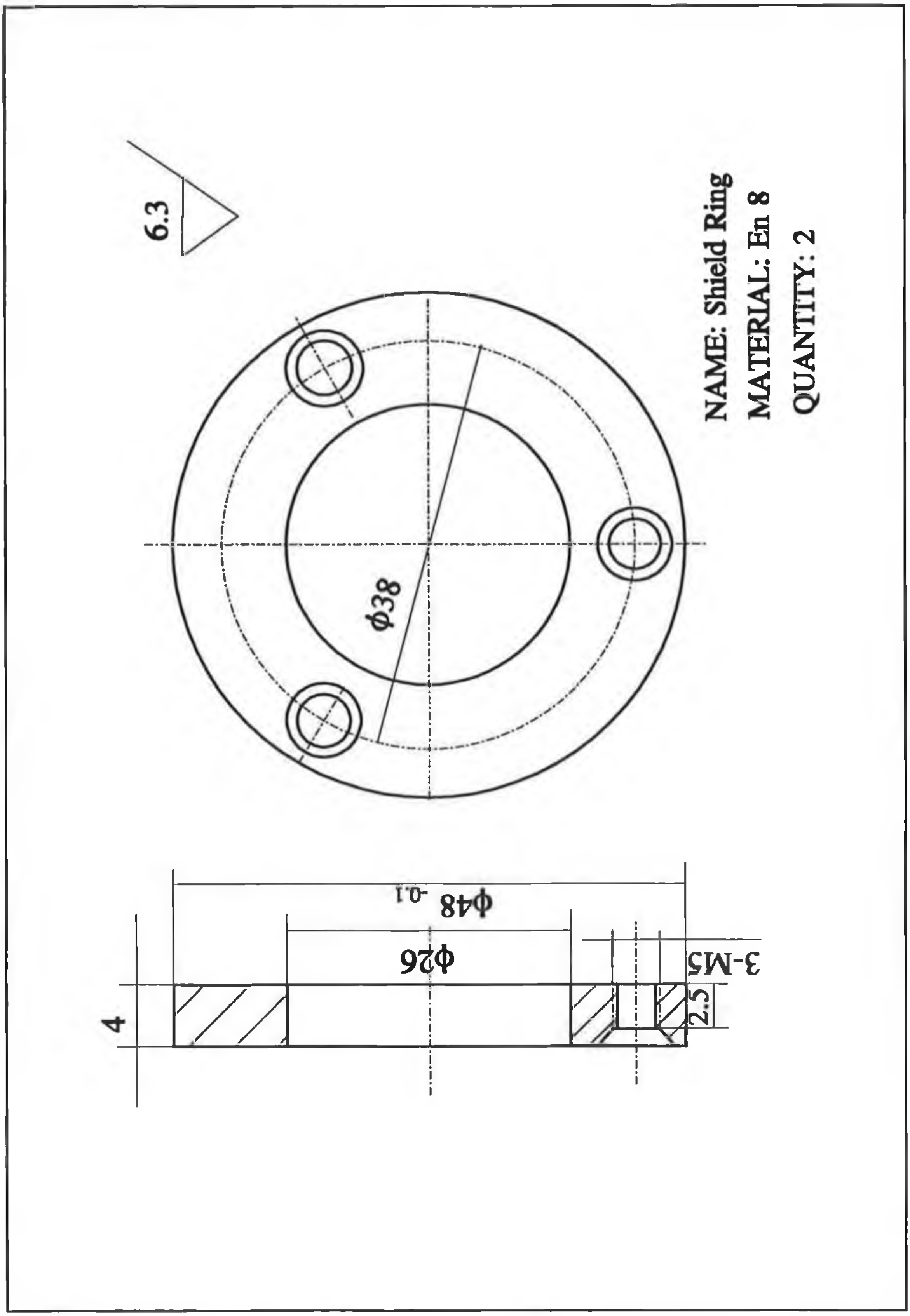

Fig. 76 *The shield ring used to fix the anvil.*

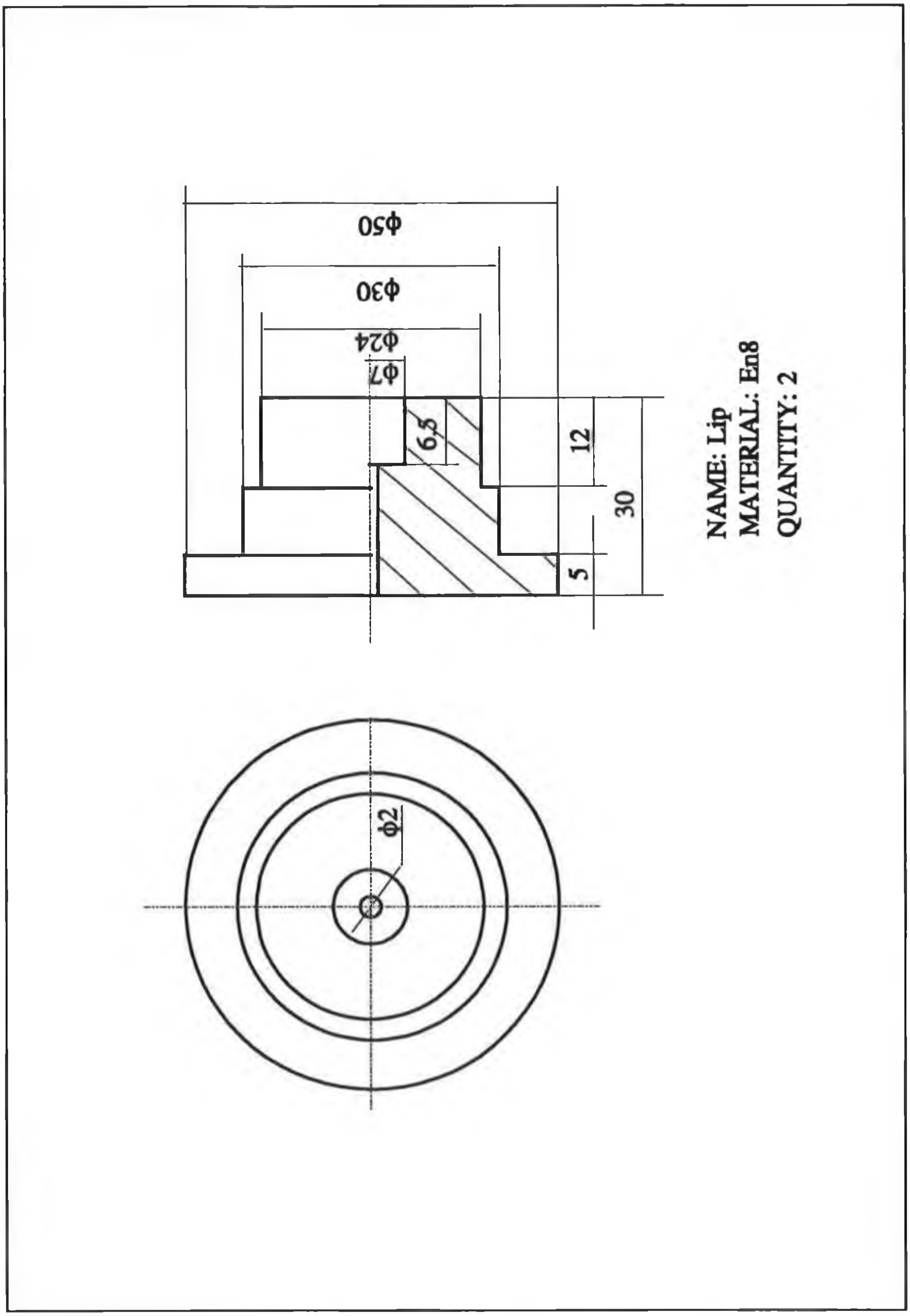

Fig. 77 *The lip used for the impact test of φ6×6 specimen.*

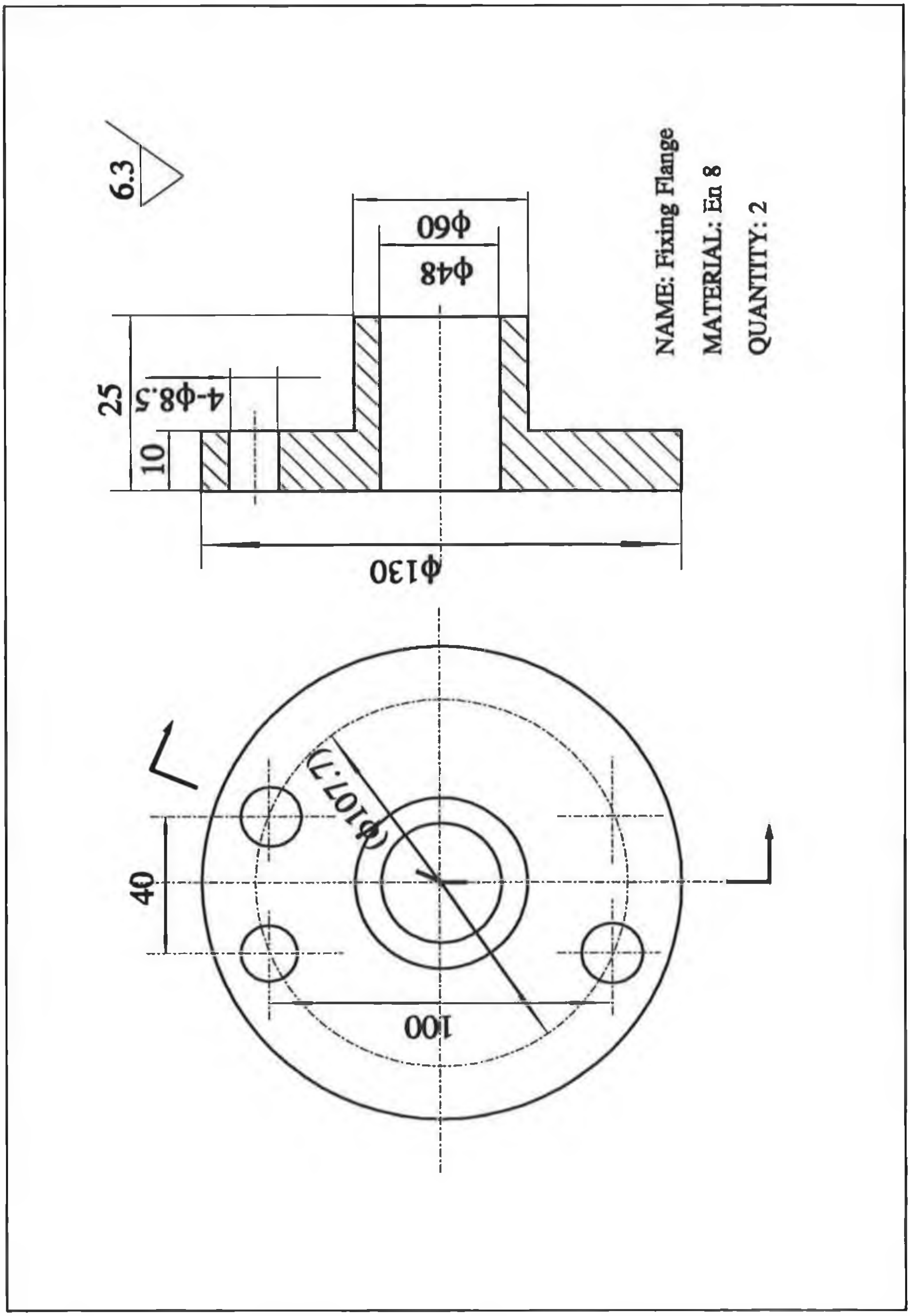

Fig. 78 *The flange used to fix the shield box with the rig.*

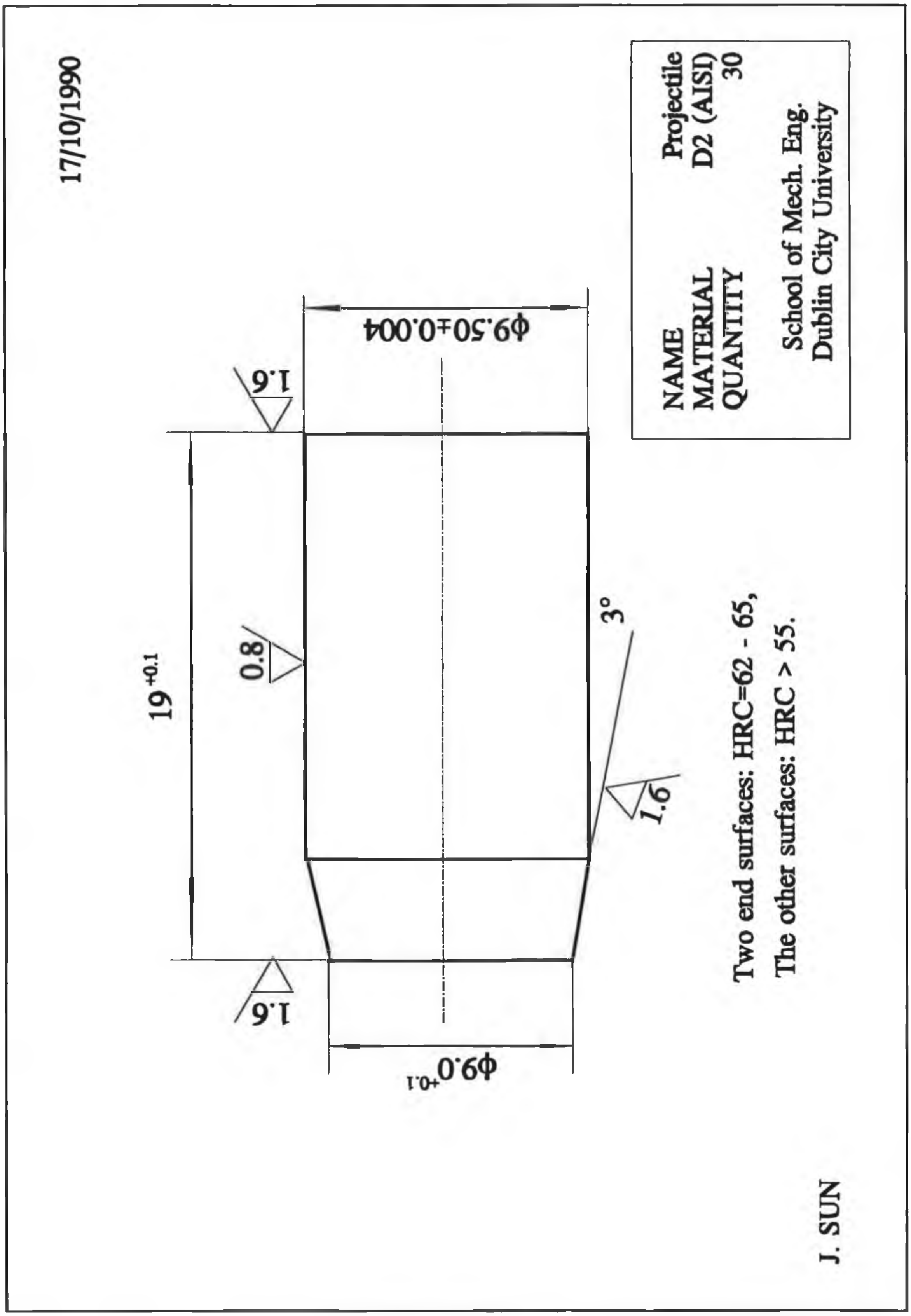

Fig. 79 *The projectile used for high velocity impact tests.*

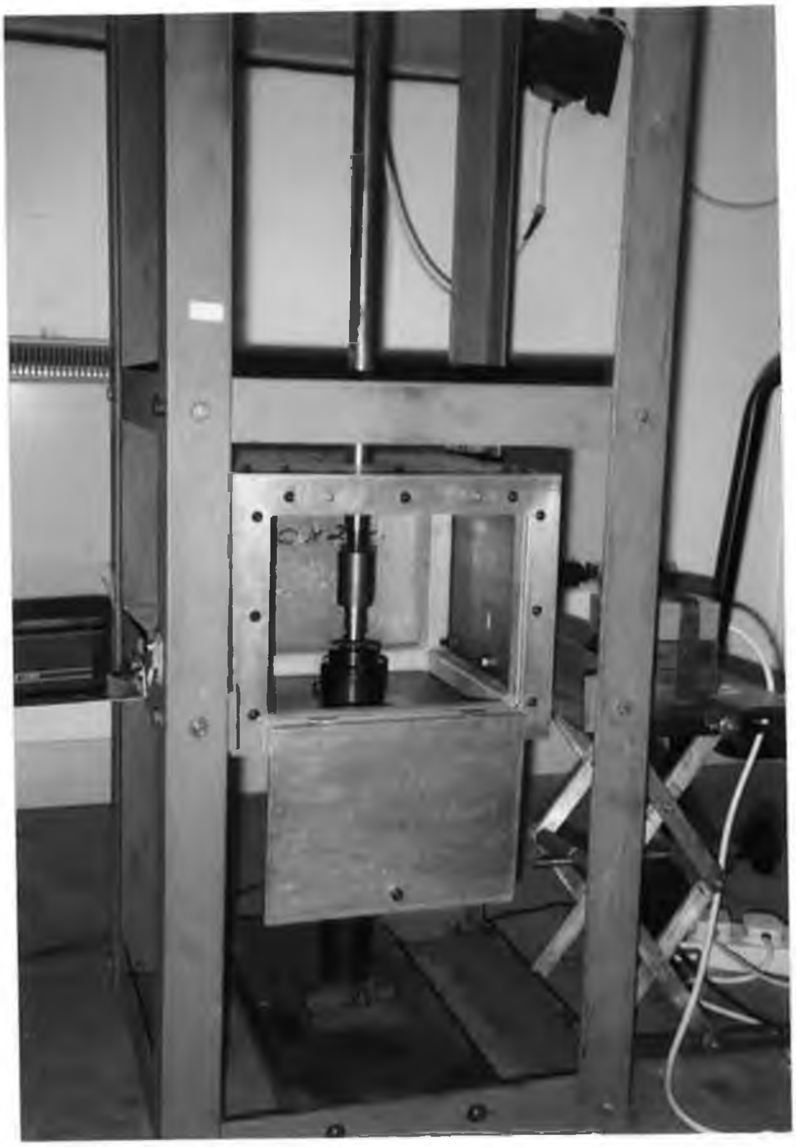

Fig. 80 *The view of shield box.*

(4) Solenoid valve

In order to obtain the experimental results of the specimen at high strain rates, a high pressure solenoid valve was purchased and used. The maximum working pressure of the chosen solenoid valve with 2 ports-2 position is 25 *bar*, the basic technical parameters are as follows:

(a) Fluid: nitrogen gas;
(b) Maximum allowable pressure: 40 *bar*;
(c) Maximum differential pressure: 25 *bar*;
(d) Temperature range of fluid: : -10 - 180 °C;
(e) Ambient: -10 to 60 °C;
(f) Ports BSP: G1.

The maximum working pressure 25 *bar* (363 *psi*) means that at the present experimental condition, the velocity of a projectile weighing 10 *g* can reach 200 m/s. The practical measured relation of the pressure in the solenoid valve with the velocity of the projectile is shown in Fig. 81.

In order to meet the requirement of high pressure test, a 40 *bar* pressure gage and a pressure regulator were also chosen and used.

3.3.3 Performance of impact tests under the ambient temperature

(1) Preparation of the test

The test specimens are chosen as mild steel and pure copper. The specimens in the present experimental work are made as the identical length and diameter, which is 5 *mm* for both pure copper and mild steel. The performing steps are as follows,

(a) Before the test starts, as the same as performing a static test, the end surfaces of a specimen are finely ground using sandpaper, the identification number is given to the specimen to be tested, its diameter

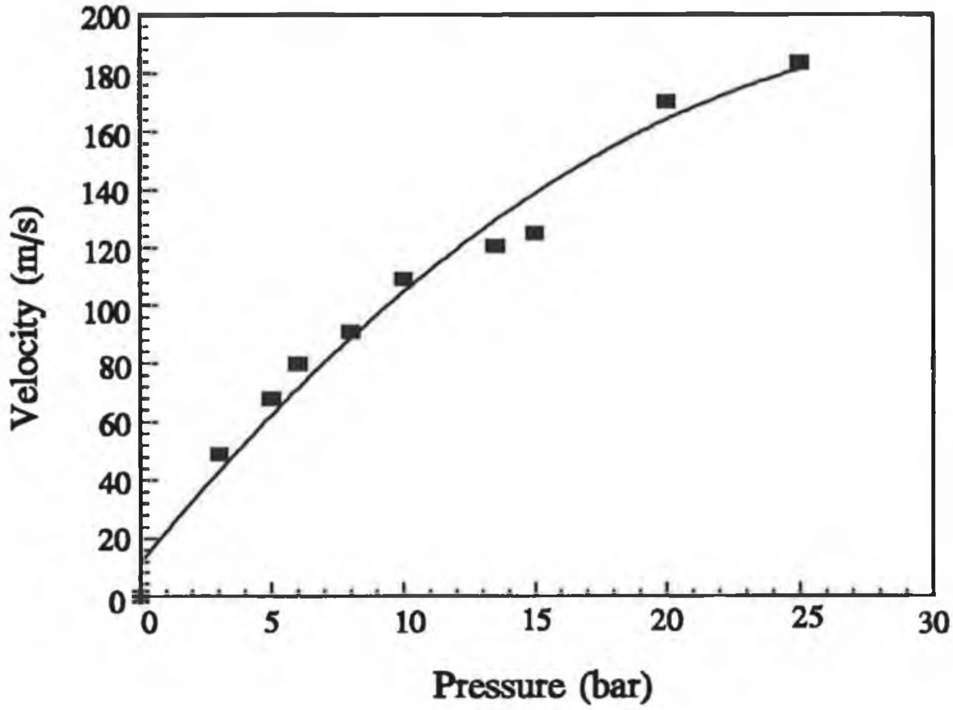

Fig. 81 *The calibrating curve of the velocity of the projectile with the pressure in the solenoid valve.*

and height are measured by a micrometer, and the results are noted on a testing work sheet. The end surfaces of a specimen are daubed with a layer of pure petroleum jelly about 0.5 mm thick to reduce the friction, then it is carefully put on the central position of the anvil.

(b) The projectile is installed inside the loading throat through the entrance slot, then pushed up into the gripper mechanism, and kept in suspension. The slot opening is then closed with the split cover and the sliding collar is slid over and clamped using the collar-nut.

(c) As mentioned in Section 3.3.1, the measuring system of the velocity of the projectile is adjusted and ready for measurement.

(d) The valve of the compressed air cylinder is opened slowly and kept open until the reservoir air pressure reaches the predetermined level as indicated by the pressure gage attached to it.

(e) Turn on the solenoid valve to perform the impact test.

(f) The reading on the display of the universal counter-timer is taken, the deformed specimen is collected and its average diameter and height are measured and written down.

3.3.4 Experimental results

The dynamic impact tests have been made at various temperatures for pure copper and mild steel, and the typical specimens before and after the tests are shown in Figs. 82 and 83. The height reductions and the diameter increments with respect to the initial velocity of the projectile and their corresponding regressed relations have been obtained as shown in Figs. 84 to 87. These results will be used to determine the constitutive relations of these materials at the corresponding conditions in the following chapter.

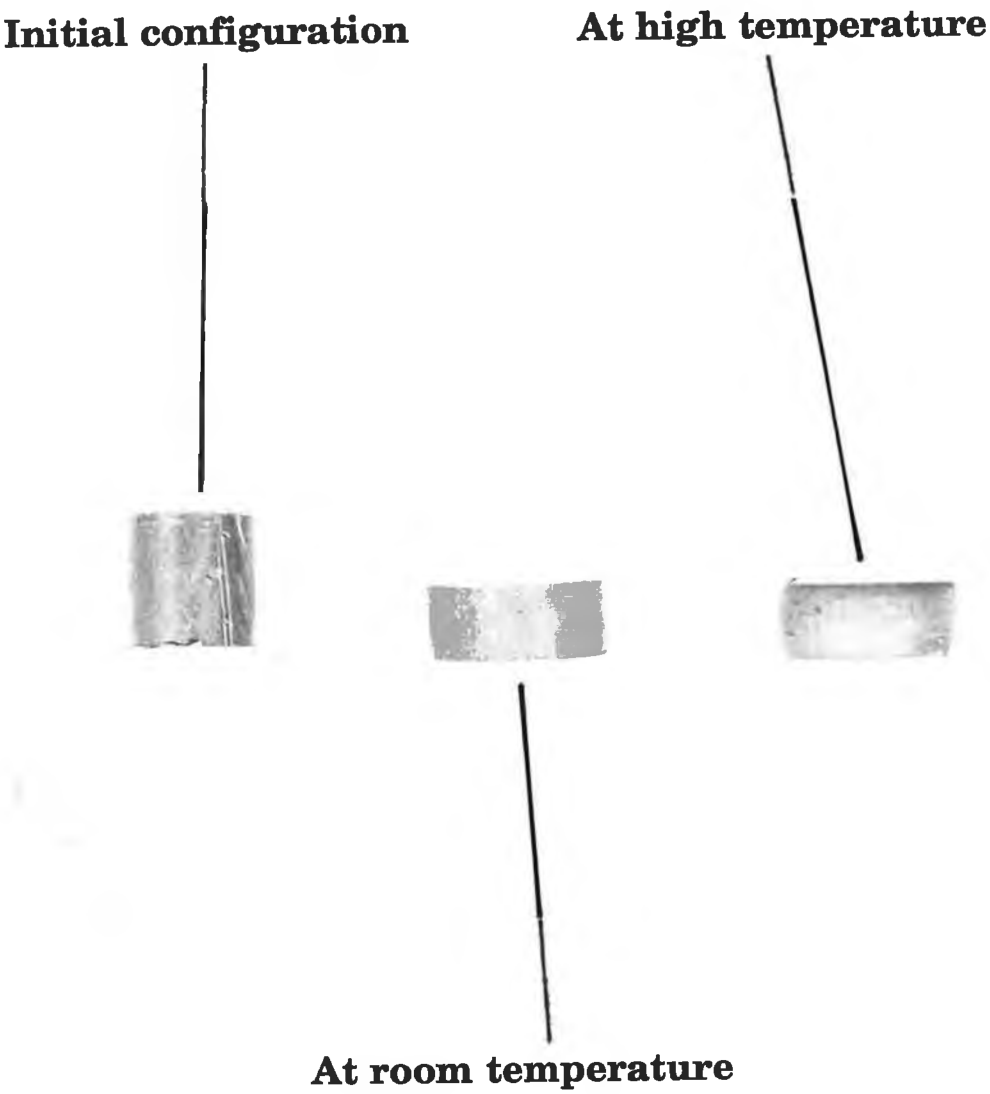

Fig. 82 *Typical pure copper specimen, before and after dynamic test.*

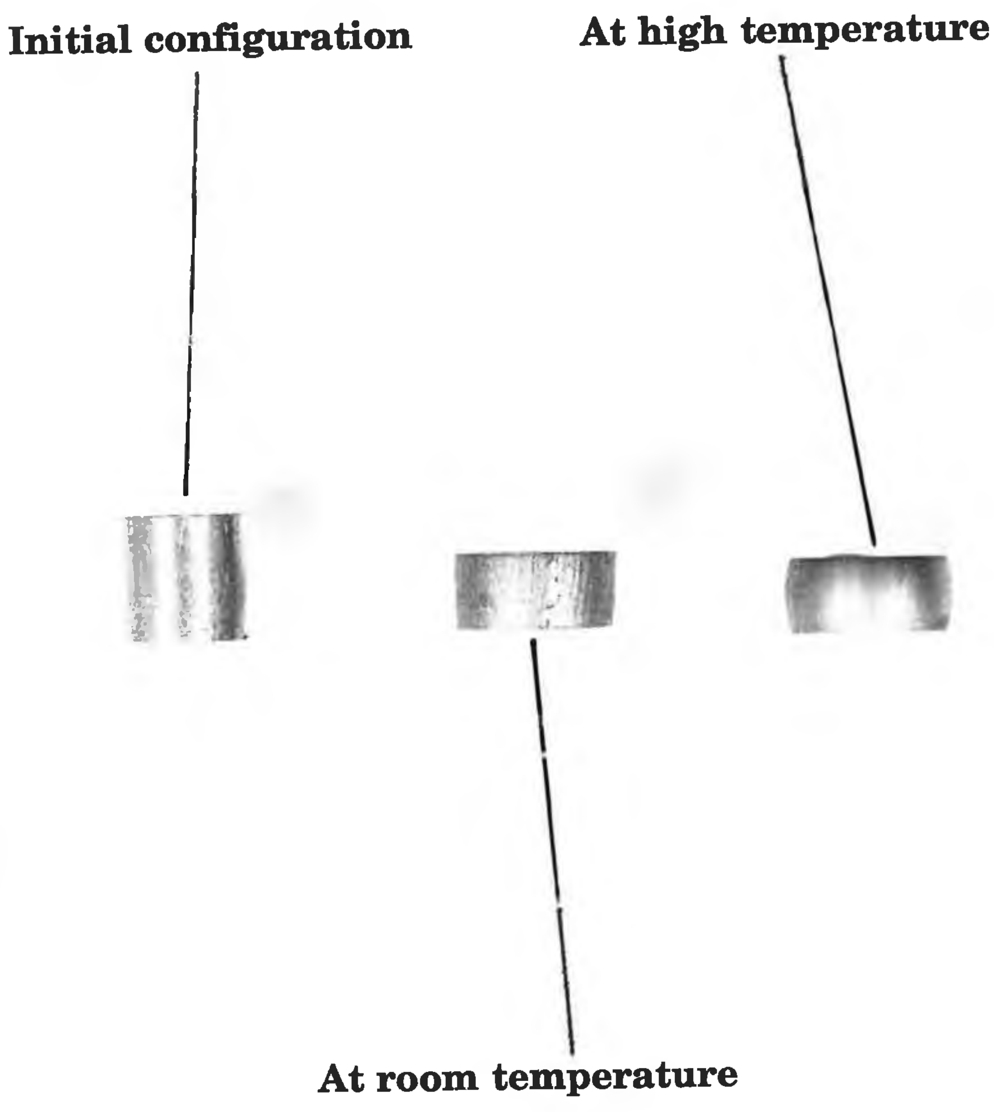

Fig. 83 *Typical mild steel specimen, before and after dynamic test.*

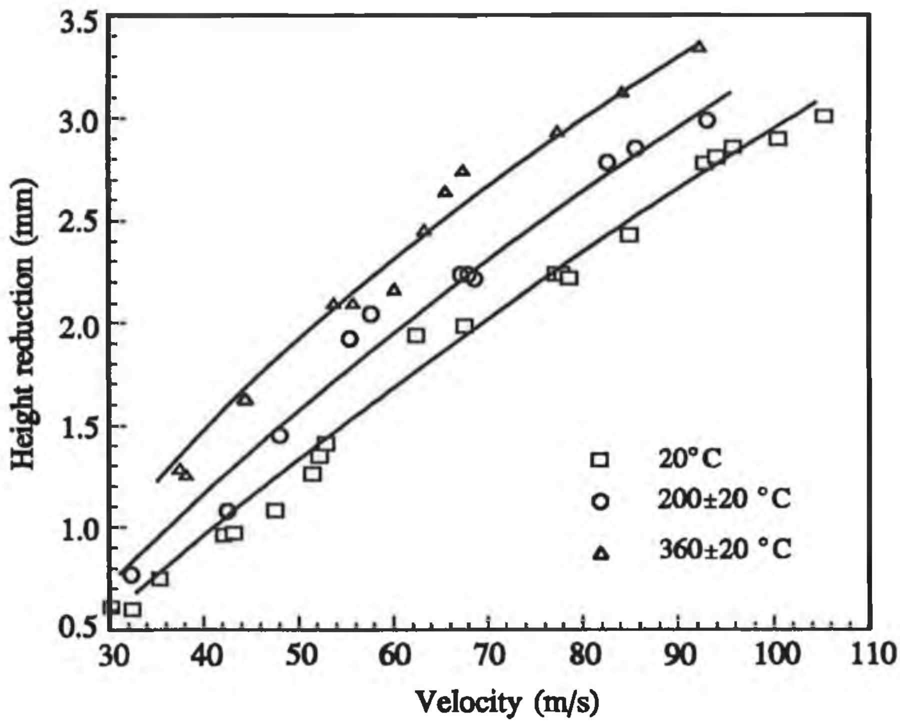

Fig. 84 *The height reduction of the specimen impacted by a projectile at various velocities for commercially pure copper.*

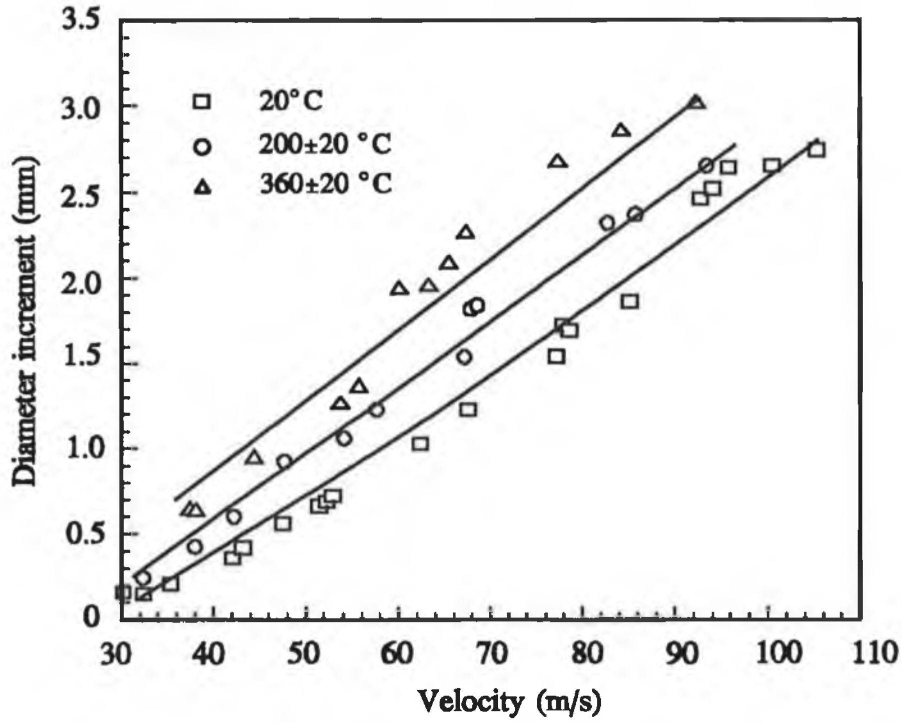

Fig. 85 *The diameter increment of the specimen impacted by a projectile at various velocities for commercially pure copper.*

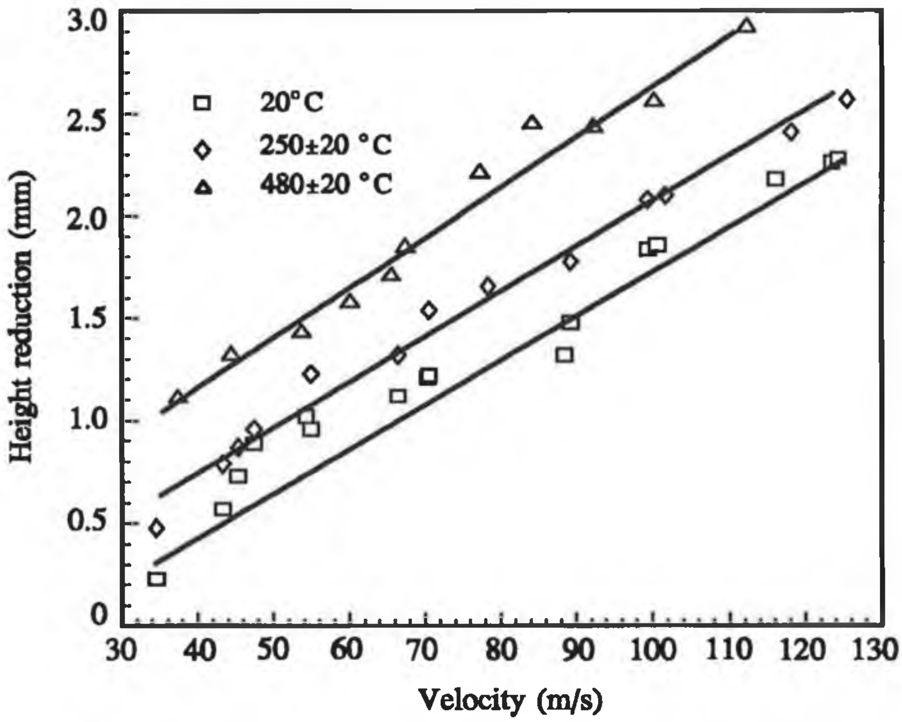

Fig. 86 *The height reduction of the specimen impacted by a projectile at various velocities for mild steel.*

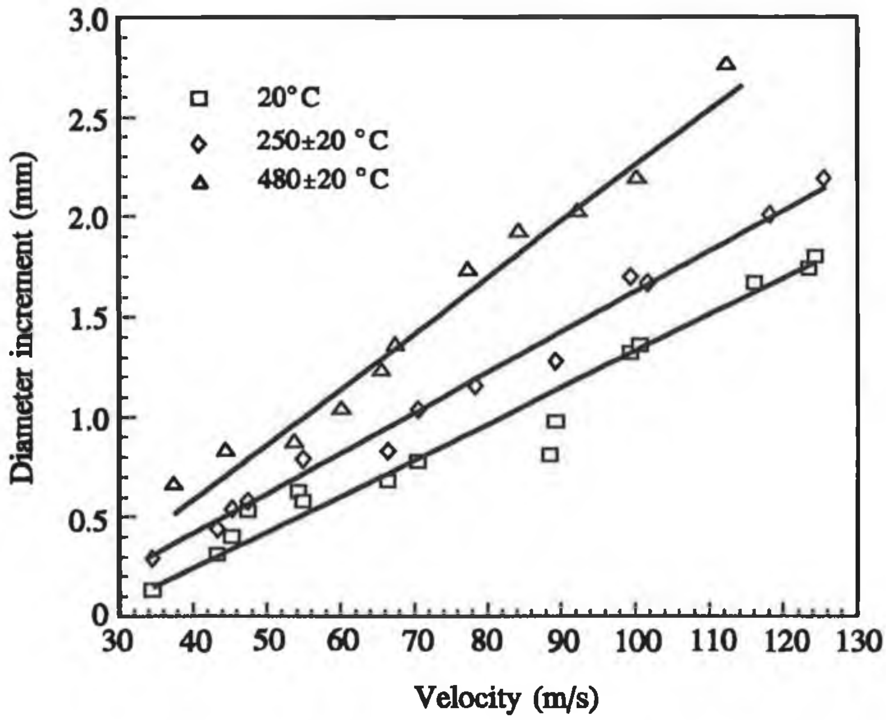

Fig. 87 *The diameter increment of the specimen impacted by a projectile at various velocities for mild steel.*

Chapter 4 Constitutive Equations

4.1 Introduction

A lot of experiments have shown that for nearly all technological materials and under a wide range of conditions, an increase of the rate of strain produces an increase of the dynamic yield stress and of the work-hardening modulus [200]. The dynamic yield stress is certainly not a characteristic constant of the material. For a given material with various loading histories, one obtains various dynamic yield stresses. Thus, the dynamic yield stress is a consequence of the constitutive equation used for the considered material and of the loading rate. The mechanism of wave propagation produces a non-homogeneous distribution of the rate of strain in the body. As a result, during a single experiment, a different stress-strain relation - and consequently a different dynamic yield stress - will be obtained in each particle of the body.

Experiments involving the observation of the transient wave propagation phenomena provide indirect methods to determine the dynamic mechanical properties of materials. In experiments involving the properties of uniaxial stress waves in rods, the procedure applied is to assume that the material submits to a certain constitutive law and then through calculations based on the law to predict the propagation characteristics. The predicted results are then compared with the experiment results. Agreement between the two usually leads to the conclusion that the equation assumed is the constitutive law for the material.

The primary view to determine a new constitutive equation is that a material with its intrinsic mechanical property behaves in a singular process of deformation corresponding to a certain external loading condition. The uniqueness of relationship between the external condition and the process of deformation makes possible to determine the strain rate dependent constitutive equation of the material by means of the record of the deformation.

In this chapter, various constitutive equations proposed by many earlier researchers are first reviewed. Secondly, the micro explanation for the behaviour of those materials under high strain-rates is given and adiabatic shear phenomena and the effect of shock wave front in the process of the impact are also discussed. Following this review, the constitutive relations for FCC metal copper and BCC metal steel at various temperatures are suggested, and the parameters in the proposed equations are determined according to the current experiments for commercially pure copper and mild steel. Finally, these results are discussed and compared with those reported earlier.

4.2 The Constitutive Equation Review

Many authors have proposed various constitutive equations in order to describe the mechanical properties of materials that exhibit the rate effect. All have started from the assumption, suggested by experimental evidence, that, even while the stress is being continuously increased, there is no longer a one-to-one correspondence between stress and strain as prescribed by a finite stress-strain relation. It is meaningless to speak of a single finite stress-strain relation able to describe various dynamic mechanical properties of different materials. It is better to speak of classes of constitutive equations, each class being characterized by certain predominant mechanical properties of the materials considered.

Ludwik [201] and then Prandtl [202] observed that for a fixed plastic strain the corresponding stress is the higher, the greater the rate of strain at which the experiment is performed. The rate of strain referred to is the average rate of strain, such as has been used in nearly all the experiments. Ludwik postulated the following logarithmic equation

$$\sigma=\sigma_1+\sigma_0\ln(\dot{\varepsilon}^p/\dot{\varepsilon}_0^p), \tag{84}$$

where σ_1, σ_0 and $\dot{\varepsilon}_0^p$ are material constants. Here σ_1 is the yield stress corresponding to a strain rate $\dot{\varepsilon}_0^p$. If the strain rate is greater than $\dot{\varepsilon}_0^p$, the stress corresponding to a certain plastic strain is greater; σ_0 is the measure of this increment.

Many of the authors who have proposed various constitutive equations to describe the rate effect have started from Eq. (84). This relation or variants of it have been verified experimentally or discussed by many authors [156].

If the material is work-harkening and if the conventional quasi-static stress-strain relation is $\sigma=f(\varepsilon)$, then Malvern [167,203] proposed the use of the expression:

$$\sigma=f(\varepsilon)+a\ln(1+b\dot{\varepsilon}^p) \tag{85}$$

instead of Eq. (84). In Eq. (85), a and b are characteristic constants for the material considered. Solving Eq. (85) with respect to the rate of strain, the following form of this relation can be obtained:

$$\dot{\varepsilon}^p=\frac{1}{b}\left\{\exp\left(\frac{\sigma-f(\varepsilon)}{a}\right)-1\right\} \tag{86}$$

Eq. (86) suggests a generalization in the sense that the plastic rate of strain must be a function of the over-stress σ-$f(\varepsilon)$, that is, of the difference between the dynamic and the actual static yield stress (corresponding to a certain plastic strain). Thus,

$$E\dot{\varepsilon}^p=F(\sigma-f(\varepsilon)) \tag{87}$$

Since in most cases the elastic part of the strain is connected with the stress by Hooke's law

$$E\varepsilon^e=\sigma \tag{88}$$

the full constitutive equation can be written in the form

$$E\dot{\varepsilon}=\dot{\sigma}+F(\sigma-f(\varepsilon)) \tag{89}$$

The function *F(z)* from Eqs. (87) and (89), must possess the following properties

$$\begin{aligned} &F(z)>0 \quad \text{if } z>0 \\ &F(z)=0 \quad \text{if } z\leq 0 \end{aligned} \tag{90}$$

More generally, instead of Eq. (87) the plastic rate of strain can be considered a function of stress and strain

$$E\dot{\varepsilon}^{p}=g(\sigma,\varepsilon). \tag{91}$$

In place of Eq. (89), this yields the constitutive equation

$$E\dot{\varepsilon}=\dot{\sigma}+g(\sigma,\varepsilon) \tag{92}$$

This form of the constitutive equation has been used by Malvern [167,203] who, in connection with a numerical application, used the following linear expression for the function g

$$g(\sigma,\varepsilon)=k[\sigma-f(\varepsilon)] \tag{93}$$

A constitutive equation of the form (92) was previously used by Sokolovskii [204,205] for perfectly plastic materials with the function g written in the form

$$g(\sigma,\varepsilon)=kF(|\sigma|-\sigma_y) \tag{94}$$

where σ_y is the static yield stress. A similar constitutive equation

$$\mu\dot{\varepsilon}^{p}=\sigma-\sigma_y \operatorname{sign}\sigma \tag{95}$$

was used by Richter [206] in order to study the propagation of longitudinal waves in bars. A different linear equation

$$g(\sigma,\varepsilon)=2k(\sigma-E_1\varepsilon) \tag{96}$$

was used by Rubin [207].

Many other expressions for the function $g(\sigma, \varepsilon)$ have been considered in the literature. Ting and Symonds [208] used the expression

$$g(\sigma,\varepsilon)=D\left(\frac{\sigma}{\sigma_y}-1\right)^q \tag{97}$$

where D and q are constants, specific for the material considered. On the basis of observations on the motion of dislocations Johnston and Gilman [209] suggested

$$g(\sigma)=\dot{\varepsilon}_0\exp(-A/\sigma) \tag{98}$$

where $\dot{\varepsilon}_0$ and A are material constants.

Fan [210] proposed a function of the form

$$g(\sigma,\varepsilon)=A\{1-\exp[-b(1-\varepsilon)(\sigma-f(\varepsilon))]\} \tag{99}$$

while Lindholm [211], considering the average rate of strain as a parameter, has verified experimentally a relation of the form

$$\sigma=\sigma_0(\varepsilon)+\sigma_1(\varepsilon)\ln\dot{\varepsilon}, \tag{100}$$

for strain rates in the range 10^{-4} to 10^3, where $\sigma_0(\varepsilon)$ is the stress-strain relation for unit strain rate.

Plass and Wang [212] extended the work of Malvern, studying both a linear and an exponential law for dynamic over-stress based on results obtained experimentally for copper and perlitic steel. They found that the exponential law gave better prediction for larger plastic strain, while for small strains the two laws were not discernible.

Kotliarevskii [213,214] starting from the concept of delayed yield, proposed a constitutive equation of the type

$$\sigma=\sigma_y+\nu(\dot{\varepsilon})\dot{\varepsilon}, \tag{101}$$

where $\nu(\dot{\varepsilon})$ is a variable coefficient of plastic viscosity; this coefficient is considered constant within certain ranges of variation of the rate of strain, but changes its value when passing from one range to another. To describe delayed yield phenomena, Lenskii and Fomina [215] used a constitutive equation of the form $\sigma=\sigma(\varepsilon,t)$; in the plastic domain this relation is particularized to

$$\sigma=E_1\varepsilon+(E-E_1)\varepsilon_y(t-x/c_0), \tag{102}$$

where ε_y is a function of the argument $t\text{-}x/c_0$.

Table 4 *Constants in equations (103) and (104)*

Temp (°C)	k (MPa)	Logarithmic σ (MPa)	k/σ	n	Power law σ (kg/mm)
30	2.85	86.87	0.034	0.017	216.79
150	3.43	68.33	0.05	0.022	178.93
250	5.48	57.18	0.096	0.028	152.68
350	7.65	41.30	0.185	0.04	116.43
450	9.03	28.06	0.322	0.073	86.07
550	14.45	0.90	....	0.141	44.82

For aluminium at various temperatures Chiddester and Malvern [92] used a stress-strain relation of the form

$$\frac{\sigma}{\sigma_0}=1+\left(\frac{k}{\sigma_0}\right)\ln\dot{\varepsilon} \tag{103}$$

or

$$\frac{\sigma}{\sigma_0}=\dot{\varepsilon}^n, \tag{104}$$

where σ_0 is the stress at unit strain rate. Such formulas have been discussed by various authors. The rate sensitivity parameters k/σ_0 and n are found to depend to a small extent on strain within the range of strains considered from 0.05 to 0.10. They are however, highly temperature dependent (see Table 4).

A constitutive equation of the form

$$\ln(\sigma/\sigma_0)=N\ln(\dot{\varepsilon}/\dot{\varepsilon}_0) \tag{105}$$

was discussed by Sokolov [216] for moderate rates of strain. Here σ_0 is a conventional constant stress corresponding to a strain rate $\dot{\varepsilon}_0$, which is considered to represent the limit of the quasi-static domain ($\dot{\varepsilon}_0=6\times10^{-4}$ s^{-1}); N is a constant which depends on the temperature and certainly on the material tested, and which may be determined experimentally. Various numerical values for these coefficients are given for steel, copper and lead.

The form

$$\sigma=\sigma_s[1+(\dot{\varepsilon}/D)^{1/p}] \tag{106}$$

was used by Hashmi [58] for mild steel up to strain rate of 10^5 s^{-1}, where σ_s is the static flow stress, respectively, and D and p are the constants dependent on the material considered.

In torsional tests on copper at strain rates of 0.001 and 900/s, Campbell *et al.* [217] found that the equation

$$\tau=A(\gamma)^n[1+m\ln(1+\dot{\gamma}/B)] \tag{107}$$

can describe very closely the room-temperature stress-strain response, using the same values for the experimentally determined constants, *a, m, n* and *B*, at both rates of strain.

The constitutive form

$$\sigma_D=A\varepsilon^{n\alpha}[1+Bf^3] \tag{108}$$

was used by Haque and Hashmi [60] for structural steel at strain rates of up to 10^5 s^{-1} at various temperatures and gave closer results with those obtained experimentally,

where $\alpha = exp(-f^{0.25})$,
$f = ln(\dot{\varepsilon} / \dot{\varepsilon}_0)$,
$\dot{\varepsilon}$=prevailing strain,
ε=natural strain,
$\dot{\varepsilon}_0$, B, A and n are constants of material.

The same form applying to an aluminium alloy and high purity copper at room temperatures has been also given by Hashmi and Haque [218]. All the acquired constants are shown in Table 5.

Table 5 *Values of the constants for equation (108) for aluminium, copper and steel.*

Material	Constants		
	A (MPa)	n	B
Aluminium	500	0.20	6.5×10^{-4}
Copper	450	0.22	7.0×10^{-4}
Steel (En 8)	1000	0.18	5.85×10^{-4}

Various other ways of expressing the function $g(\sigma, \varepsilon)$, which depend only on the over-stress but contain a larger number of material constants, were proposed by Perzyna [219] in order to describe more accurately the mechanical properties of the materials considered. These take the forms:

$$g(\sigma)=\sum_{\alpha=1}^{N}\left[\exp\left(\frac{\sigma}{\sigma_0}-1\right)^{\alpha}-1\right],$$

$$g(\sigma)=\sum_{\alpha=1}^{N}B_{\alpha}\left(\frac{\sigma}{\sigma_y}-1\right)^{\alpha}, \qquad (109)$$

etc.

All the functions and constants which occur in various expressions of the function g are, more or less, time and temperature dependent. There is certainly no longer any question of averaging out the rate of strain, which must on the contrary be computed locally since, during wave propagation phenomena and generally, in dynamic problems, the rate of strain, as well as the stress and strain themselves, are to a great extent non-uniformly distributed along the body.

The basic idea of constitutive equations such as those mentioned above and typified by Eq. (89) which have been widely used, is that the elastic constants are independent of the rate of strain and the plastic strains, and that the plastic rate of strain is a function only of the dynamic over-stresses which leads to the conclusion that in the plastic range the stress-strain curves for various constant rates of plastic straining are parallel curves.

The experimental results in refs. [17] and [220] indicated that the stress-strain curves for various constant rates of plastic straining are not parallel. Thus, instead of constitutive equations of the form (89), Cristescu suggested the general quasi-linear constitutive equations of the form [221]

$$\frac{\partial \varepsilon}{\partial t}=\phi(\sigma,\varepsilon)\frac{\partial \sigma}{\partial t}+\Psi(\sigma,\varepsilon) \tag{110}$$

where the function Φ and Ψ govern the instantaneous and non-instantaneous response, respectively.

Variants of this quasi-linear constitutive relation were also used by Béda [222], Lubliner [223] and Larina [224]. The latter author wrote this relation in form

$$\varphi'[\varepsilon-(s-1)\varepsilon_y]\frac{\partial \varepsilon}{\partial t}=\frac{\partial \sigma}{\partial t}+k[\sigma-\varphi(\varepsilon)] \tag{111}$$

where $\sigma=\psi(\varepsilon)$ is the static stress-strain curve, ε_y is the strain at the static yield point, k is a material constant and s a parameter characterizing the dynamical properties of the material: in static tests $s<1$, while in dynamic tests $s=s0$. Thus, this parameter may be discontinuous due to a shock wave front.

Considering the effects of strain, strain rate and temperature, the stress of a material can be expressed by a relationship $\sigma=\sigma(\varepsilon,\dot{\varepsilon},T)$ (ε=strain, $\dot{\varepsilon}$=strain rate, T=absolute temperature), the distribution of the stress is given by

$$d\sigma=\left(\frac{\partial\sigma}{\partial\varepsilon}\right)_{\dot{\varepsilon},T}d\varepsilon+\left(\frac{\partial\sigma}{\partial\dot{\varepsilon}}\right)_{\varepsilon,T}d\dot{\varepsilon}+\left(\frac{\partial\sigma}{\partial T}\right)_{\varepsilon,\dot{\varepsilon}}dT \quad (112)$$

where $(\partial\sigma/\partial\varepsilon)$, $(\partial\sigma/\partial\dot{\varepsilon})$ and $(\partial\sigma/\partial T)$ represent the strain hardening, strain-rate hardening and temperature softening.

Early attempts at developing such an equation concentrated on the equivalence between temperature and strain rate, leading to such formulations as that of Zener and Holloman [225]

$$Z=\dot{\varepsilon}_p\exp(U/kT) \quad (113)$$

where $\dot{\varepsilon}$ is the plastic strain rate, T the absolute temperature, U is an activation energy and Z is constant at a given stress and strain.

A relation was proposed by Vinh *et al.* [198] using results obtained in high-speed torsion tests. They found reasonable agreement between the predictions of the expression

$$\tau=F(\gamma)^n(\dot{\gamma}/\dot{\gamma}_0)^m\exp(W/T) \quad (114)$$

and their experimental results for duralumin, copper and mild steel, F, n, m and W being parameters which had to be determined experimentally for each material. However, for mild steel F, n, and W were also required to be functions of strain rate, so the process essentially became a curve fitting exercise.

a modified expression of Eq. (114) was also applied to polyethylene oxide (semicrystalline), highly crystalline polyamide and amorphous polycarbonate. The proposed equation [226] is of the form

$$\tau = F(\gamma)^n(\dot{\gamma})^m \exp[W(T-T_0)^a] \tag{115}$$

where T_0 and T are the ambient and specimen temperature, τ is the shear stress and γ and $\dot{\gamma}$ are the shear strain and strain rate respectively.

A simple expression with an allowance for thermal softening was proposed by Johnson and Cook [227], which has the form

$$\sigma = (A + B\varepsilon^n)(1 + C\ln\dot{\varepsilon})(1 - \bar{T}^m) \tag{116}$$

in which there are five material constants, A, B, C, n and m, and $\bar{T}$ is the thermal softening term

$$\bar{T} = (T - T_r)/(T_m - T_r) \tag{117}$$

where T is the absolute temperature and suffixes r and m indicate room temperature and the melting temperature respectively. Assuming adiabatic deformation at high strain rates, this term allows for the reduction in strength corresponding to the increase in temperature due to plastic work. At a given strain and temperature equation (116) shows the semi-logarithmic dependence of stress on strain rate often observed experimentally. At a given temperature and strain rate it follows an empirical power-law work-hardening curve where the exponent n is assumed to be a constant so that the shape of the stress-strain curve will be independent of temperature and strain rate. There is considerable experimental evidence, however, that this is not the case for BCC materials.

Starting more explicitly from an understanding of the dislocation processes controlling plastic flow, Zerilli and Armstrong [228] derived two forms of constitutive relation, one for FCC materials

$$\sigma = \Delta\sigma_G' + C_2\sqrt{\varepsilon}\exp[-C_3T + C_4T\ln\dot{\varepsilon}] + k/\sqrt{l} \tag{118}$$

and one for BCC materials

$$\sigma=\Delta\sigma_G^{\prime}+C_1\exp[-C_3T+C_4T\ln\dot{\varepsilon}]+C_5\varepsilon^n+k/\sqrt{l} \tag{119}$$

where C_1 to C_5, k and n are material constants, l is the average grain diameter and $\Delta\sigma'_G$ is a non-thermal stress component related to the original microstructure of the material. These differ from the Johnson and Cook relation in that they divide the non-thermal stress into two components and relate each to a specific process resisting deformation. They differ from each other in that for FCC materials a parabolic work-hardening law coupled with the temperature and rate-dependent term is assumed while for materials of BCC structure work-hardening is assumed to be temperature and strain rate independent, as in the Johnson and Cook relation but in conflict with much experimental data.

Once the separate effects of temperature and strain rate on the stress-strain response for a given material are known, the usual approach to developing a constitutive relationship or mechanical equation of state is to determine a unique function relating the four parameters stress, strain, strain rate and temperature which describes these effects with a reasonable degree of accuracy. This implies that the four parameters are all state functions, *i.e.* that at a given applied strain rate and external temperature the material will support a uniquely defined stress at any given value of strain. In practice, it is untrue for a much wider range of materials as may be seen from the many tests which have been performed in which the applied strain rate has been varied in a controlled manner [229].

The strain-rate sensitivity, evaluated at constant strain, which is defined as $\lambda=\partial\sigma/\partial(log\dot{\varepsilon}^p)$, is found to increase when the strain rate is raised above roughly 10^3 s^{-1}. When the maximum strain rate investigated is limited to 10^3 s^{-1}, such an increase is virtually not seen [19,135,139]. The experiments also show that for small rates of strain (10^{-4} - 10^{-2} s^{-1}), the stress-strain curve does not change significantly; this stress-strain curve will be considered as the "quasi-static" curve [33].

4.3 General Physical Description of Mechanical Response

When the flow stress corresponding to a given plastic strain is determined at different applied strain rates and external temperatures three distinct types of response are frequently found. The results presented in Fig. 88 were obtained over a wide range of both temperature and strain rate [30]. They allow, therefore, a general description of the types of response shown by many metals and alloys at different strain rates and temperatures.

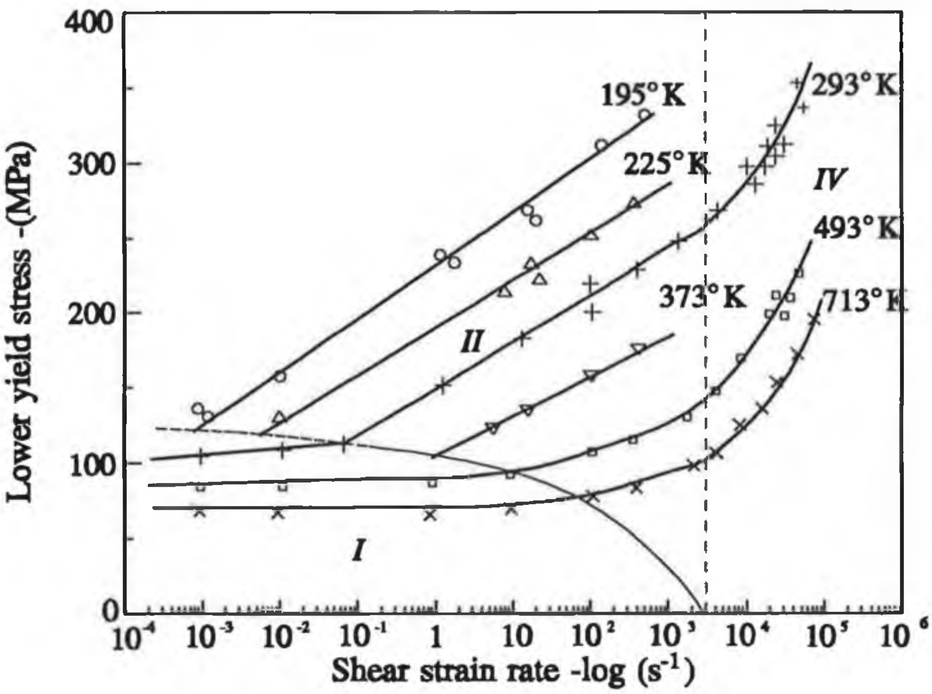

Fig. 88 *Strain-rate dependence of flow stress at very high strain rates for annealed mild steel [30].*

Region I corresponds to low strain rates and high temperatures, where the flow stress is essentially constant and independent of temperature and strain rate. The controlling mechanism of flow is the long-range friction stress due, for example, to the presence of large precipitates. Thermal vibrations in the lattice are unable to assist in overcoming these barriers. This 'athermal' friction stress increases with increasing alloy content and predominates in highly-alloyed materials which, in consequence, appear less sensitive to strain rate.

At lower temperatures and higher strain rates the short range barriers to flow, such as dislocation interaction, become relatively more important. Here thermal vibrations can assist in overcoming the barriers, and flow becomes sensitive to temperature and strain rate. The rates of straining will be related to the absolute temperature according to an Arrhenius type of exponential low, of the form

$$\dot{\varepsilon}_p=\dot{\varepsilon}_0\exp[-\Delta G_{(\sigma^*,T)}/kT] \quad (120)$$

where ΔG, the free energy of activation, is a function of the local (thermal) stress σ^* and the absolute temperature T, and $\dot{\varepsilon}_0$ is a frequency factor (or nominal limiting strain rate) which depends on the mobile dislocation density, *i.e.* on the structural state of the material. A dependence on stress is implicit, both through the $\Delta G(\sigma^*,T)$ and also, possibly, through a stress dependence of $\dot{\varepsilon}_0$. It is usual, however, to assume that $\dot{\varepsilon}_0$ is independent of strain rate and temperature (and hence of stress) and to take ΔG to be a unique function of stress. Assuming that a single thermally activated mechanism controls flow and that the corresponding force-displacement relationship is rectangular, ΔG may be expressed as a linear function of stress, of the form

$$\Delta G=\Delta G_0-V(\sigma-\sigma_A) \quad (121)$$

where ΔG_0 is the free energy of activation in the absence of stress, V is the activation volume, σ the total applied stress and σ_a the athermal component of stress, *i.e.* that associated with region I. At high rates of strain Eqs. (120) and (121) may be combined to give

$$\sigma=\sigma_a+\Delta G_0/V+(kT/V)\ln(\dot{\varepsilon}_p/\dot{\varepsilon}_0) \quad (122)$$

In practice, Eq. (122) gives a reasonably good description of the behaviour of FCC metals and alloys, for those of BCC structure the semi-logarithmic dependence of the flow stress on strain rate is generally non-linear and the stress dependence of the activation energy is more complex.

Despite the variety of mechanical response described above, there is general agreement that in region II, *i.e.* for strain rates up to ~5000 s^{-1}, thermal activation is the rate-controlling mechanism. At strain rates above this, however, a change in the rate-controlling mechanism is generally thought to occur. In region IV of Fig. 88, an approximately linear dependence of flow stress directly on strain rate, rather than on the logarithm of strain rate, is observed, implying that flow at these strain rates is viscous in nature. It is usual, therefore, to associate the change in mechanical response at strain rates above ~5000 s^{-1} with a change from thermal activation to phonon drag as the rate-controlling mechanism [136]. However, not all investigators agree. Lindholm [230], for example, has suggested that in aluminium there is a transition to a second thermally activated mechanism while for copper his results could be represented, despite some experimental scatter, by a constant value of λ without any dramatic increase in strain-rate sensitivity up to a strain rate approaching 10^5 s^{-1}. In contrast, Follansbee *et al.* [146], also working on copper and using miniaturised versions of the Split Hopkinson Pressure Bar (SHPB) at the highest strain rates, found clear evidence for a dramatic increase in strain-rate sensitivity of the flow stress at 15% strain, over the strain rate range from 10^3 to $3x10^4$ s^{-1}. From an analysis of their results in terms of dislocation dynamics they conclude that only at the upper end of this strain rate range does the dislocation velocity approach the drag-controlled limit. Below this the results correspond to a transition zone between the regions where thermal activation and dislocation drag are rate controlling. At even higher strain rates, approaching 10^7 s^{-1}, Huang and Clifton [231], using an inclined-plate pressure-shear test, have found almost an order of magnitude increase in the shear flow stress over that at 10^3 s^{-1}, from which they also concluded that above ~10^4 s^{-1} dislocation motion is governed by the intrinsic resistance of the clear lattice.

4.4 Adiabatic Shear Phenomena

4.4.1 Phenomenon mechanism

In metals and alloys, it has been determined that at room temperature about 90% of the work of deformation energy goes into heat. Adiabatic shearing is a particular situation in which the heat generated in localized bands cannot be dissipated because of the strain rate and the thermal properties of the material. In fact, a truly adiabatic deformation does not exist, some part of the heat being always lost to the surrounding metal, but the term adiabatic is taken here to show that a large part of the heat is retained in the band.

Shear bands form as a result of a thermo-mechanical instability due to the presence of a local inhomogeneity, inducing local deformation and heating. If the thermal properties of the material are not sufficient to conduct the generated heat away, the deformation becomes unstable.

When metals and alloys are deformed at very large strains and at very high strain rates such as in ballistic impact and penetration, forging and machining, localized shearing can occur, leading to localized deformation and a localization of heat generation. Generally, the flow stress increases with strain and strain-rate increase. However, in localized shearing, the increased temperature reduces the flow stress.

4.4.2 The temperature rise in a struck specimen

As mentioned above, the temperature of the metal rises during plastic deformation because of the heat generated by plastic work. The deformation energy per volume, w, is equal to the area under the stress-strain curve

$$w=\int_0^{\varepsilon}\sigma(\varepsilon,\dot{\varepsilon},T)d\varepsilon. \qquad (123)$$

Only a small fraction of this energy is stored (principally as dislocations and vacancies). The rest is released as heat. If the deformation is adiabatic, *i.e.*, no heat transfers to the surroundings, and the stress is considered as a function of strain, strain rate and temperature, when the strain increases from ε to $\varepsilon+\Delta\varepsilon$, the temperature rise is given by

$$\Delta T = \frac{\alpha}{\rho C_p}\int_{\varepsilon}^{\varepsilon+\Delta\varepsilon}\sigma(\varepsilon,\dot{\varepsilon},T)d\varepsilon = \frac{\alpha\bar{\sigma}\Delta\varepsilon}{\rho C_p} \tag{124}$$

where $\bar{\sigma}$ is the average value of σ over the strain interval ε to $\varepsilon+\Delta\varepsilon$, ρ is the density, C_p is the mass heat capacity, and α is the fraction of work converted into heat. For copper, C_p=383 $J/kg{\cdot}K$ and α=0.92; for steel, C_p=465 $J/kg{\cdot}K$ and α=0.865.

Any temperature increase causes the flow stress to drop, but there are two cases in which the effect of temperature can be ignored, *i.e.* deformation can be considered isothermal. One effect is the case at low strain rates, where heat can be transferred to surroundings, and the other is that at small strain, where very little heat is generated. Therefore, when testing over the wide range of strain rates or strains, there is a transition from isothermal to adiabatic test conditions.

Combining Eq. (63) with Eq. (79), which have been proposed in this study, the following temperature dependent constitutive relation has been used to compare with temperature independent ones

$$\begin{aligned}
&\sigma = 0.4\varepsilon^{0.2}e^{124/T}f_0(\varepsilon) + (0.64+43.1\varepsilon)(\log\dot{\varepsilon}_p+4)\ (MPa) && \dot{\varepsilon}_p \le 10^3 s^{-1} \\
&\sigma = 0.4\varepsilon^{0.2}e^{124/T}f_0(\varepsilon) + (4.5+302\varepsilon) + 2.9\times(10^{-3}\dot{\varepsilon}_p-1)\ (MPa) && \dot{\varepsilon}_p > 10^3 s^{-1}
\end{aligned} \tag{125}$$

where

$$f_0(\varepsilon) = 255.1\times\log(34.1315\varepsilon+1) \quad (MPa) \tag{126}$$

A comparison of results for a ϕ5×5 (mm) pure copper specimen at room temperature based on Eq. (63) and Eq. (125) has been done. The former is independent upon temperature, while the latter is dependent upon temperature. The calculated results at various initial velocities of the projectile are shown in Figs. 89 to 95.

The temperature rise at the impact end with respect to time and initial velocity of the projectile at room temperature is shown in Figs. 89 and 90. It can be seen that the temperature in the specimen rapidly increases with the initial impact velocity of the projectile. When this velocity reaches 100 m/s, the temperature rise may arrive at 150 °C.

From these results, it can also be seen that with the increase of impact velocity, the differences between the corresponding curves are all raised. As is shown in Fig. 95. the deformation considering the effect of temperature is smaller than that when this effect is disregarded. Under a high initial impact velocity of the projectile, the effect of temperature on the final deformation of the impacted specimen becomes quite important. Therefore, in the process of analysis of high speed impact tests, adiabatic shear phenomena can not be disregarded.

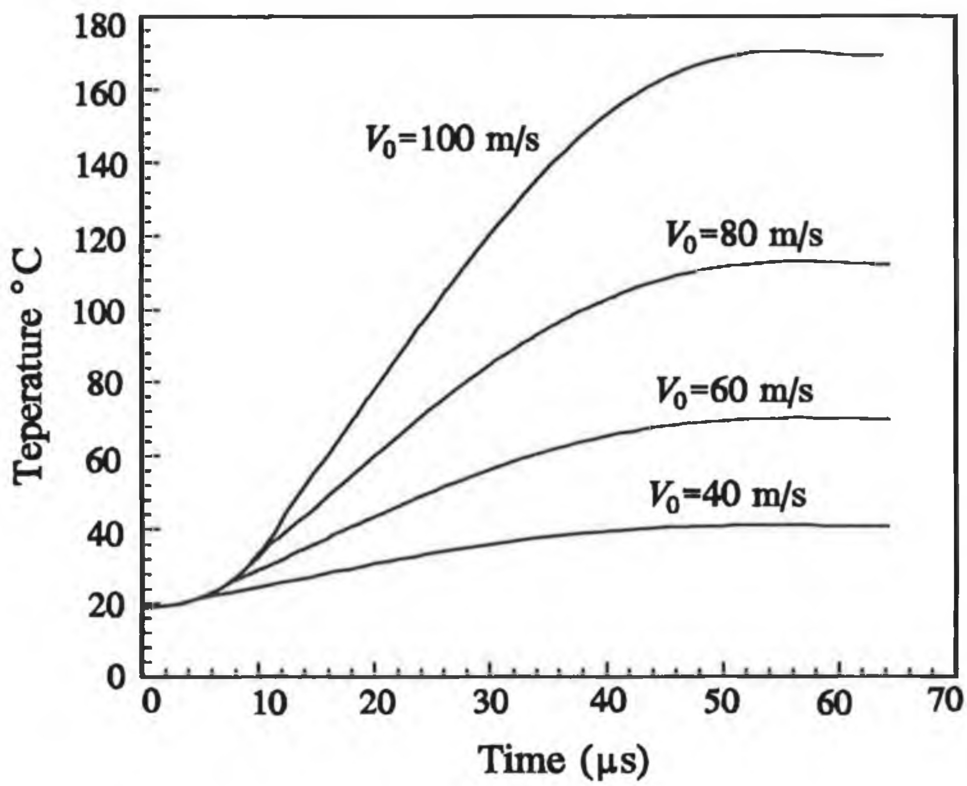

Fig. 89 *The temperature rise with respect to time at the impact end of the for pure copper specimen at room temperature at various initial velocities of the projectile.*

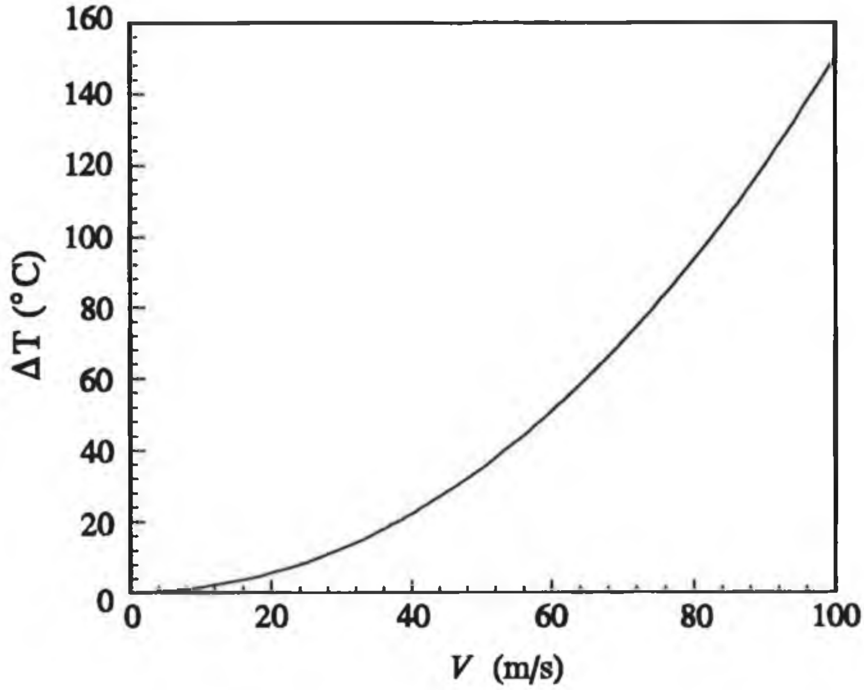

Fig. 90 *The temperature rise with respect to the initial velocity of the projectile at the impact end of a ϕ5×5 (mm) pure copper specimen at room temperature.*

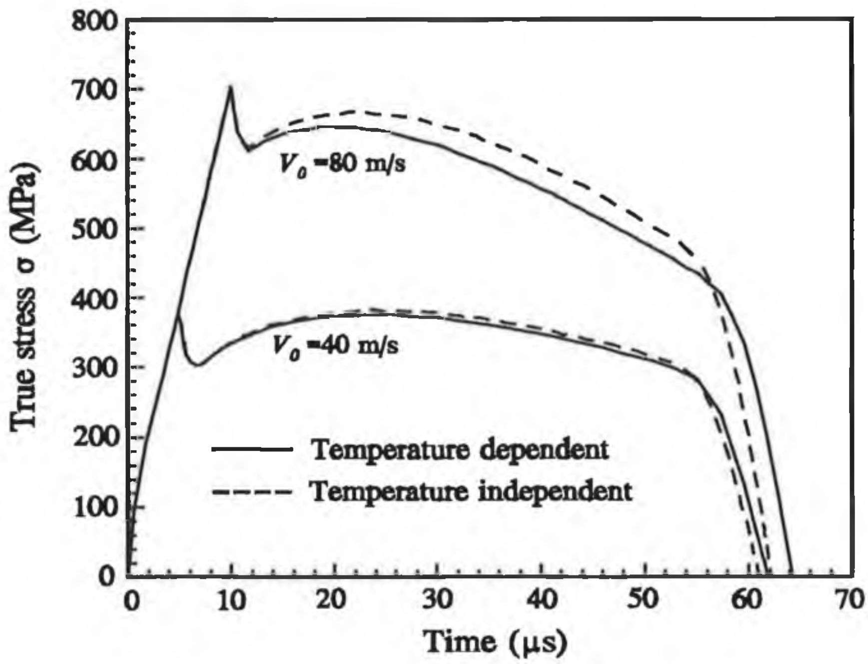

Fig. 91 *Comparison of the stresses to time at the impact end of the specimen based on temperature dependent and independent constitutive relations at the initial speeds of the projectile of 40 m/s and 80 m/s.*

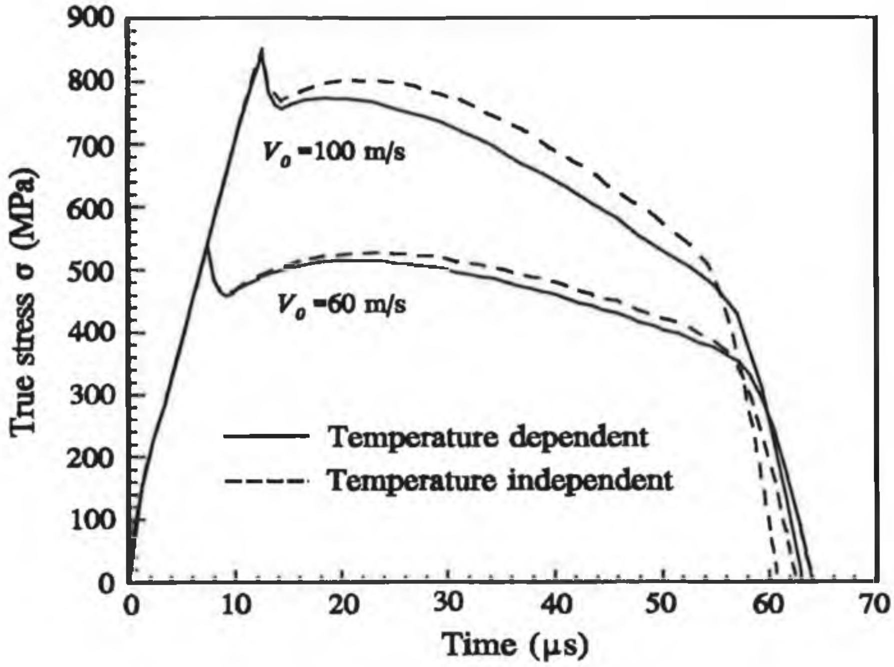

Fig. 92 *Comparison of the stresses at the impact end of the specimen with time based on temperature dependent and independent constitutive relations at the initial speeds of the projectile of 60 m/s and 100 m/s.*

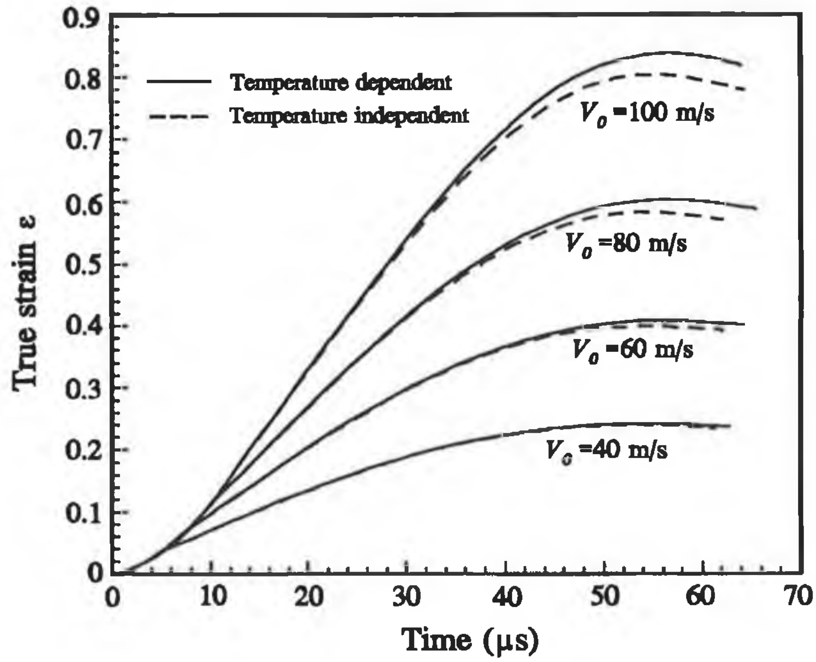

Fig. 93 *Comparison of the dynamic strain at the impact end of the specimen with regard to time based on temperature dependent and independent constitutive relations at various initial speeds of the projectile.*

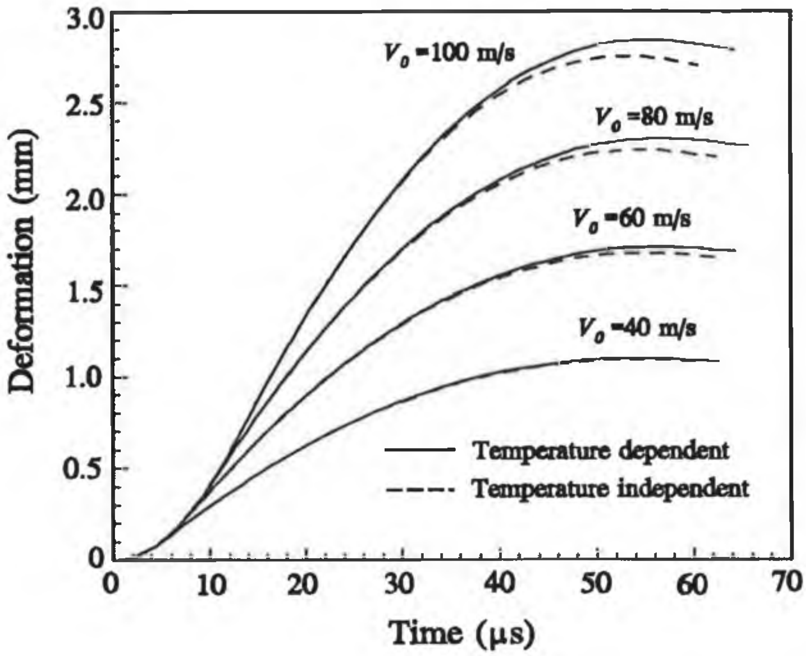

Fig. 94 *Comparison of deformation of the specimen at the impact end with regard to time based on temperature dependent and independent constitutive relations at various initial impact velocities of the projectile.*

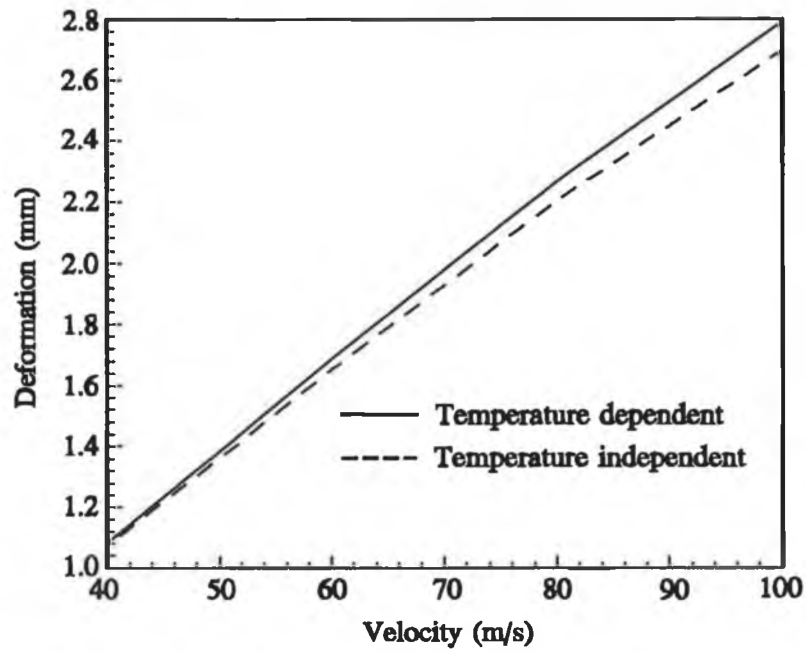

Fig. 95 *Comparison of the deformation of the specimen at the impact end with regard to initial impact velocities of the projectile based on temperature dependent and independent constitutive relations.*

4.5 The Effect of Shock Loading

In the process of the impact, the specimen is subjected to shock waves. It is expected that both the velocity of the projectile and the shock pulse duration within which the stress is increased to its peak value can have some effect on the shock dynamic behaviour and the residual properties simply because the disturbance created within the shock front and the dynamic response of the material will be altered by these two parameters.

In the prevailing experiment the initial velocity of the projectile is dependent upon the firing pressure which can be controlled by adjusting the solenoid valve on the impact test machine and be measured by the laser velocity-measuring system. A shock loading is a complicated process. The time involved is indeed very short, usually never exceeding 10 μs [232]. In order to simplify the calculation, the sudden impact is handled by a fast, but smooth variation of the impact within T_0 which is the time during which the shock wavefront increases up to the peak stress.

At first, it is assumed that the velocity at the impact end of the specimen increases from the static state to the initial velocity of the projectile, v_0, with a certain acceleration, a_v, which can be expressed as

$$a_v = \frac{v_0}{T_0} \tag{127}$$

At various accelerations, the relationship of the final deformation of the specimen with respect to the initial velocity of the projectile is shown in Fig. 96. It can be seen that the calculated final deformations of the specimen increase with the reduction of the acceleration. At the lower initial velocity of the projectile, the difference of deformations is not obvious. With the increase of the acceleration, its effect on the calculated deformations of the impacted specimen is decreased. As has been mentioned above, the time taken by shock waves is smaller than 10 μs, *i.e.* the acceleration of shock waves is not less than $8\times10^6\ m/s^2$.

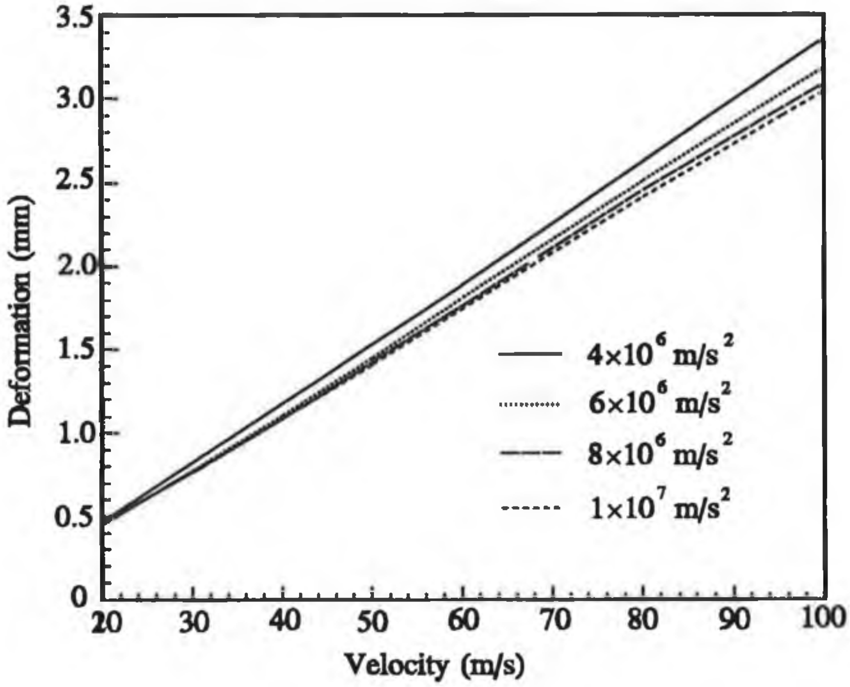

Fig. 96 *Variation of the deformation of the impacted copper specimen with respect to the initial velocity of the projectile at various shock accelerations at room temperature.*

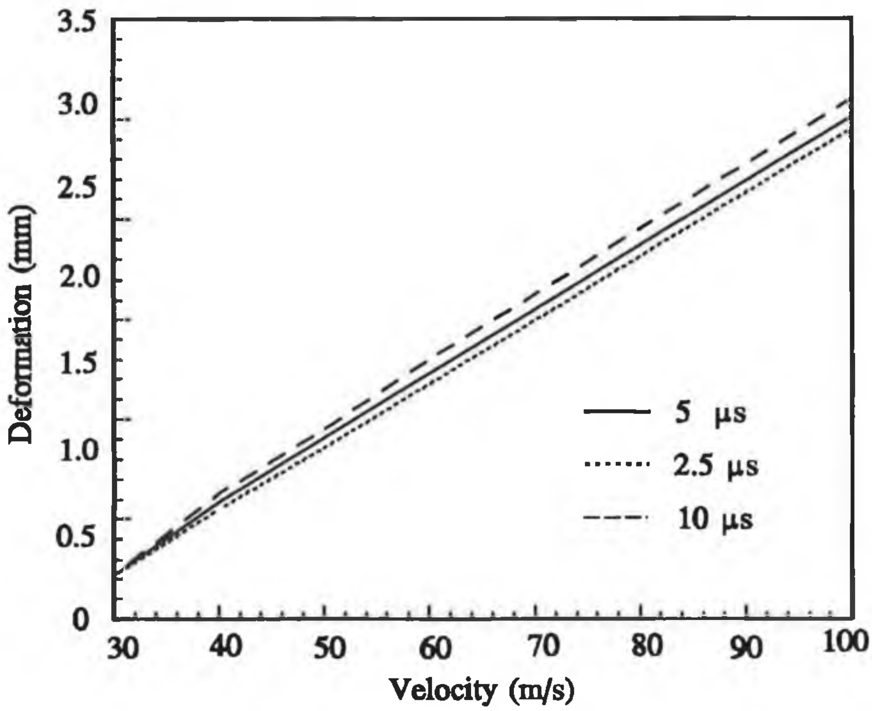

Fig. 97 *Variation of the final deformation of the impacted copper specimen with respect to the initial velocity of the projectile at various shock durations at room temperature.*

On the other hand, the stronger shock waves will occur in the process of higher striking velocity. The acceleration of the shock wave cannot remain constant, which will become greater with the increase of the impact velocity. Considering these reasons and a smooth variation of the shock load, the duration of shock wave is assumed as constant, *i.e.* it is independent of the initial velocity of the projectile. The variation of the final deformation with respect to the initial velocity of the projectile at various shock durations for a 5×5 *mm* pure copper specimen at room temperature is shown in Fig. 97, from which it can be found that although the shock duration may cause the variation of the final deformation of the impacted specimen, it is not apparent. Therefore, in the present study, the shock duration is chosen to be 5 μs.

4.6 The Dynamic Constitutive Equations

4.6.1 Commercially pure copper

Due to different controlling mechanisms [233], for many FCC metals and alloys the logarithmic strain rate sensitivity $\lambda=\partial\sigma/\partial(\log\dot{\varepsilon}^p)$, evaluated at constant strain and temperature, is basically constant over the range of rates from 10^{-5} to 10^3 s^{-1}, but is found to increase when the strain rate is raised above 10^3 s^{-1}. At the strain rates exceeding 10^3 s^{-1}, there exists a linear relationship between the stress σ and plastic strain rate $\dot{\varepsilon}^p$, *i.e.* the linear strain rate sensitivity $\lambda=\partial\sigma/\partial\dot{\varepsilon}^p$ keeps constant [33]. Following these evidences, the constitutive equations for pure copper can be suggested as

$$\begin{aligned} \sigma(\varepsilon,\dot{\varepsilon},T) &= f_0(\varepsilon,T)+\lambda_1(\varepsilon,T)(\log\dot{\varepsilon}^p-\log\dot{\varepsilon}_0^p) \qquad \dot{\varepsilon}^p\le\dot{\varepsilon}_1^p \\ \sigma(\varepsilon,\dot{\varepsilon},T) &= f_1(\varepsilon,T)+\lambda_2(\varepsilon,T)(\dot{\varepsilon}^p-\dot{\varepsilon}_1^p) \qquad \dot{\varepsilon}^p>\dot{\varepsilon}_1^p \end{aligned} \tag{128}$$

where $\dot{\varepsilon}_0^p$, taken as 10^{-4} s^{-1}, is the strain rate corresponding to the quasi-static stress-strain curve $f_0(\varepsilon,T)$ at temperature T; $f_1(\varepsilon,T)$ is the stress-strain curve at constant strain rate $\dot{\varepsilon}_1^p$ at temperature T, which is equal to 10^3 s^{-1} for pure copper, and λ_1 and λ_2 are the logarithmic and linear strain rate sensitivities respectively. The effect of adiabatic shear has been considered by means of the quasi-static stress strain curve $f_0(\varepsilon,T)$ and the stress-strain curve at constant strain rate $\dot{\varepsilon}_1^p$, $f_1(\varepsilon,T)$, which is expected to allow for the temperature softening of stress to some extent. On the other hand, strain rate sensitivities λ_1 and λ_2 are considered the function of both strain and temperature.

This suggested form can not only effectively reflect the practical properties of the material in a wide range of strain rates and but also represents continuous properties at the connection of two different analytical expressions. It should be noted that having an exact expression to reflect the constitutive relation in the range of low and moderate strain rates is absolutely necessary, since due to the impact, the specimen experiences such a process that at the first the strain rate increases from static state to its highest point within the shock duration, then through moderate region to the low region (see Fig. 14). The deformation of the specimen itself is an accumulating process, which is related with its deformation track. Therefore, the final deformation of the specimen obtained by a calculation relies on the constitutive relation both in the range of high strain rate and in the low and moderate ranges.

The determination of Eq. (128) requires similar procedures as the other proposed forms. Having known the quasi-static strain curve of a material, the unknown function λ_1 in the constitutive equation may be first determined from the experimental results in the range of strain rate less than 10^3 s^{-1}, then, $f_1(\varepsilon)$ may be estimated from the expression thus obtained. Finally, based on the known $f_1(\varepsilon)$, the unknown function λ_2 can be determined.

The simplest consideration is that the parameters λ_1 and λ_2 are assumed as constants for pure copper. It was found that the agreement of the finial deformation of the specimen between the program calculations and experimental results are acceptable for $\lambda_1 \approx 8\sim10$ (*MPa*) and $\lambda_2 = 2.0\sim2.5$ *(kPa)* at room temperature. It is noticed that sensitivities λ_1 and λ_2 are inversely depend on each other, *i.e.* a higher λ_1 is with regard to a lower λ_2. It can also be observed that the sensitivity in the range of lower strain rates will directly affect the determination of that in the range of higher strain rates. However, the conclusion from this assumed values of λ_1 and λ_2 is that the theoretical sensitivities are far higher than the experimental results obtained by others, especially in the range of lower strain rates.

Although λ_1 and λ_2 can be considered as constants at a certain strain, a number of experimental results reported have shown that at various strains, the strain rate sensitivity does not remain as constant. Therefore, the assumption of the linear forms of λ_1 and λ_2 is made

$$\begin{aligned} &\frac{\sigma(\varepsilon)-\sigma_0(\varepsilon)}{\log \dot{\varepsilon}^p - \log \dot{\varepsilon}_0^p} = \alpha_1 + \beta_1 \varepsilon \qquad \dot{\varepsilon}^p \le 10^3\, s^{-1} \\ &\frac{\sigma(\varepsilon)-\sigma_1(\varepsilon)}{\dot{\varepsilon}^p - \dot{\varepsilon}_1^p} = \alpha_2 + \beta_2 \varepsilon \qquad \dot{\varepsilon}^p > 10^3\, s^{-1} \end{aligned} \tag{129}$$

The calculations based on this form of constitutive equations have been carried out, and the predicted final deformation of the specimen are then compared with the experimental results as shown in Fig. 98. The optimised parameters determined in Eq. (129) are listed in Table 6.

The stress-strain curves at various temperatures for pure copper based on the form (129) and the values in Table 6 are shown in Figs. 99 to 101, and the stress at a constant strain versus strain rate at various temperatures are shown in Figs. 102 to 104.

Table 6 *The strain rate sensitivities of pure copper determined based on Eq. (129).*

Temperature (°C)	λ_1 (MPa)		λ_2 (kPa sec)	
	α_1	β_1	α_2	β_2
20	12	20	9	5
200	8	20	7	5
360	5	18	4	5

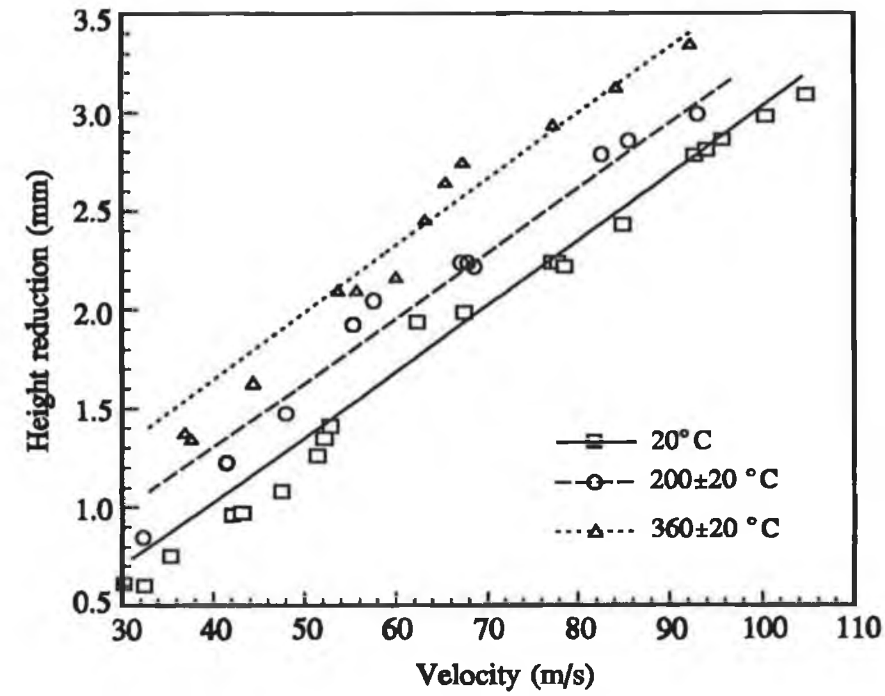

Fig. 98 *Comparison of deformation of the specimen based on the form (129) and the values in Table 6 with the experiment at various temperatures.*

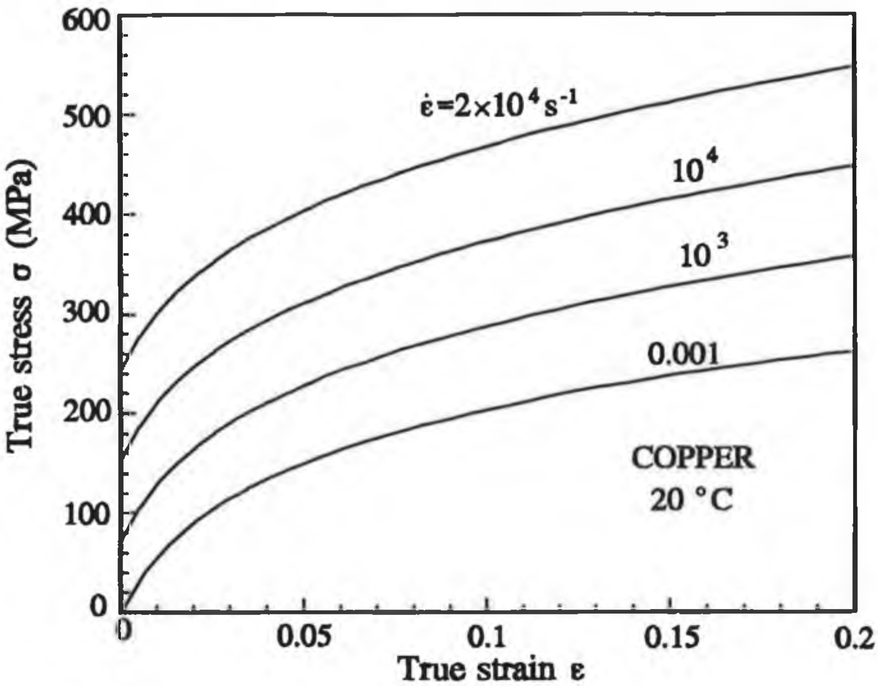

Fig. 99 *Stress-strain curves for pure copper based on the form (129) and the values in Table 6 at 20 °C.*

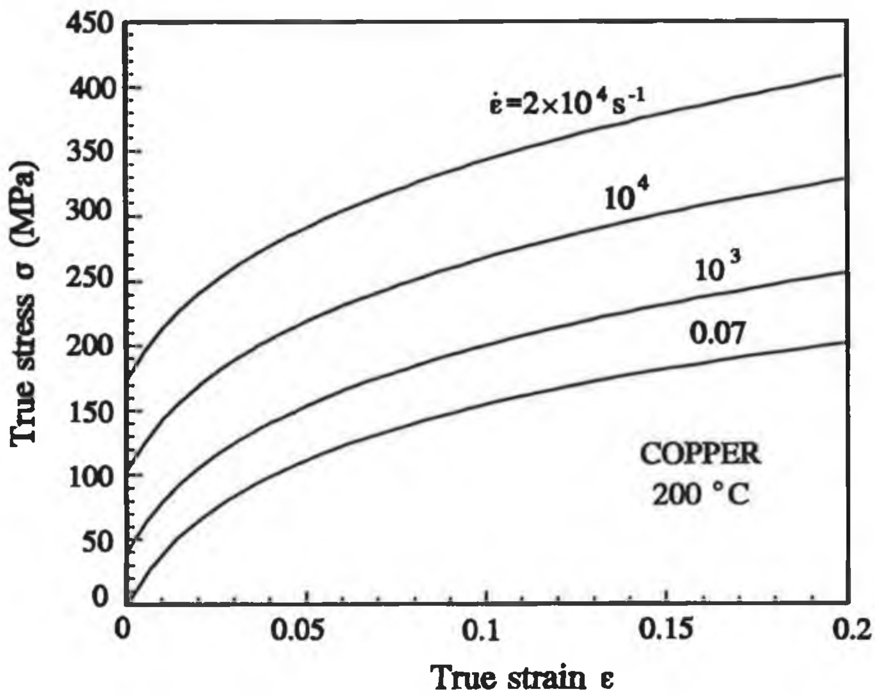

Fig. 100 *Stress-strain curves for pure copper based on the form (129) and the values in Table 6 at 200 °C.*

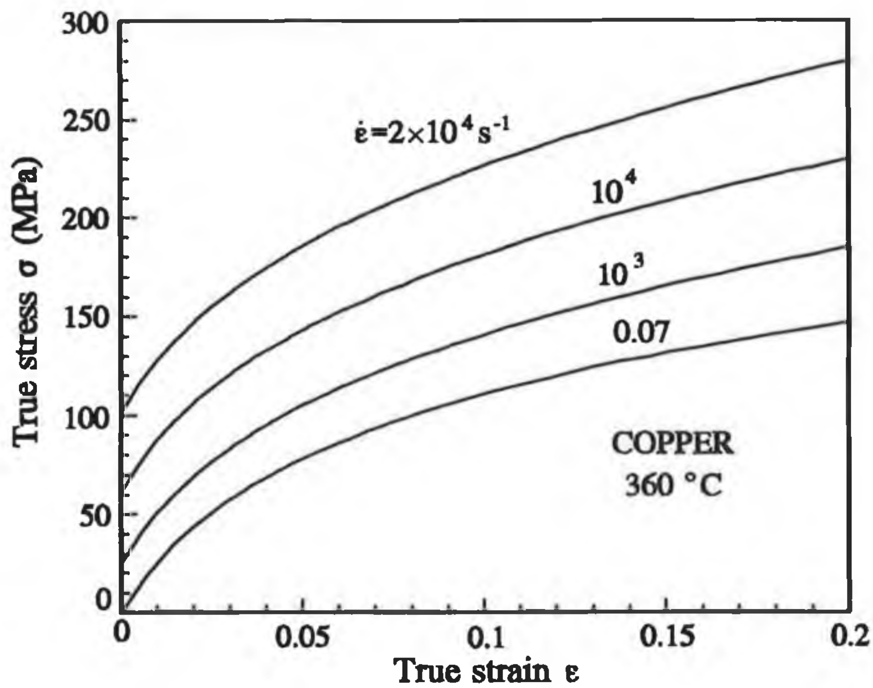

Fig. 101 *Stress-strain curves for pure copper based on the form (129) and the values in Table 6 at 360 °C.*

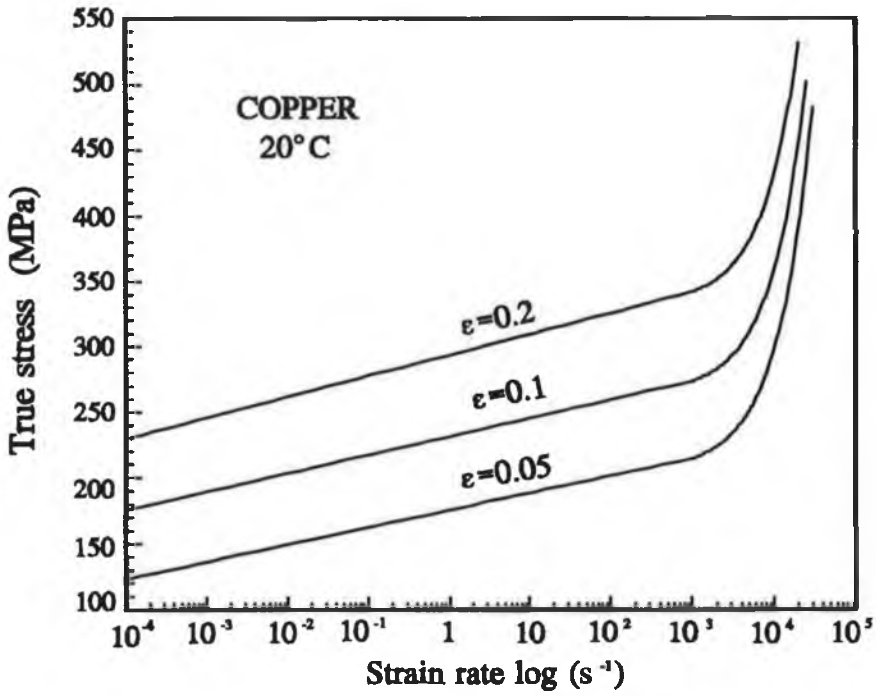

Fig. 102 *Stress at a constant strain versus strain rate for pure copper based on the form (129) and the values in Table 6 at 20 °C.*

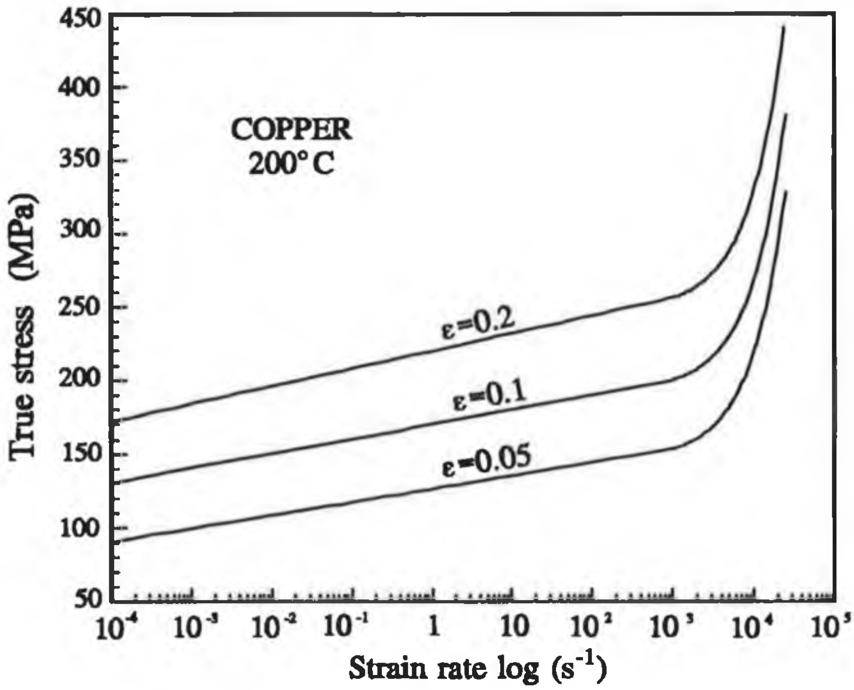

Fig. 103 *Stress at a constant strain versus strain rate for pure copper based on the form (129) and the values in Table 6 at 200 °C.*

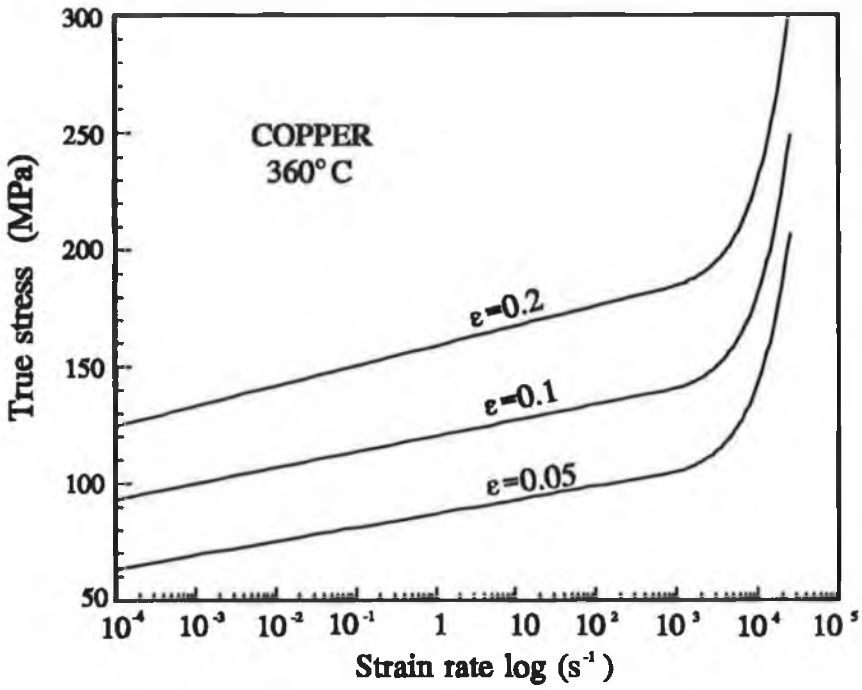

Fig. 104 *Stress at a constant strain versus strain rate for pure copper based on the form (129) and the values in Table 6 at 360 °C.*

It was found that the form (129) can validly describe the dynamic properties of this material at the strain rate $\dot{\varepsilon} \leq 10^4\ s^{-1}$, but beyond this range, its use becomes inappropriate. In order to obtain a better expression used for wider strain rates, an index constant is appended. Therefore, the following modified form was suggested,

$$\begin{aligned} &\frac{\sigma(\varepsilon)-\sigma_0(\varepsilon)}{\log \dot{\varepsilon}^p - \log \dot{\varepsilon}_0^p} = \alpha_1 + \beta_1 \varepsilon \qquad \dot{\varepsilon}^p \leq 10^3\, s^{-1} \\ &\frac{\sigma(\varepsilon)-\sigma_1(\varepsilon)}{(\dot{\varepsilon}^p)^n - (\dot{\varepsilon}_1^p)^n} = \alpha_2 + \beta_2 \varepsilon \qquad \dot{\varepsilon}^p > 10^3\, s^{-1} \end{aligned} \tag{130}$$

where $0<n\leq 1$ is an unknown constant, and the others have the same meanings as above. It may be seen that the constant n is a strain rate hardening index. The calculations based on Eq. (130) were made, and the predicted final deformation for the pure copper specimen were then compared with the experimental results as shown in Fig. 105. The optimised parameters based

on the form (130) at various temperatures have been determined, and the corresponding coefficients are listed in Table 7.

Table 7 *The strain rate sensitivities of pure copper determined based on Eq. (130).*

Temperature (°C)	λ_1 (MPa)		λ_2 (kPa)		n
	α_1	β_1	α_2	β_2	
20	12	20	30	20	0.88
200	8	20	26	18	0.86
360	5	18	21	17	0.80

Based on the form (130) and the values in Table 7, the stress-strain curves at various temperatures for pure copper are shown in Figs. 106 to 108, the stress at a constant strain versus strain rate at various temperatures for pure copper are shown in Figs. 109 to 111, and the temperature and strain-rate dependence of the stress at various strain of pure copper are shown in Figs. 112 to 114.

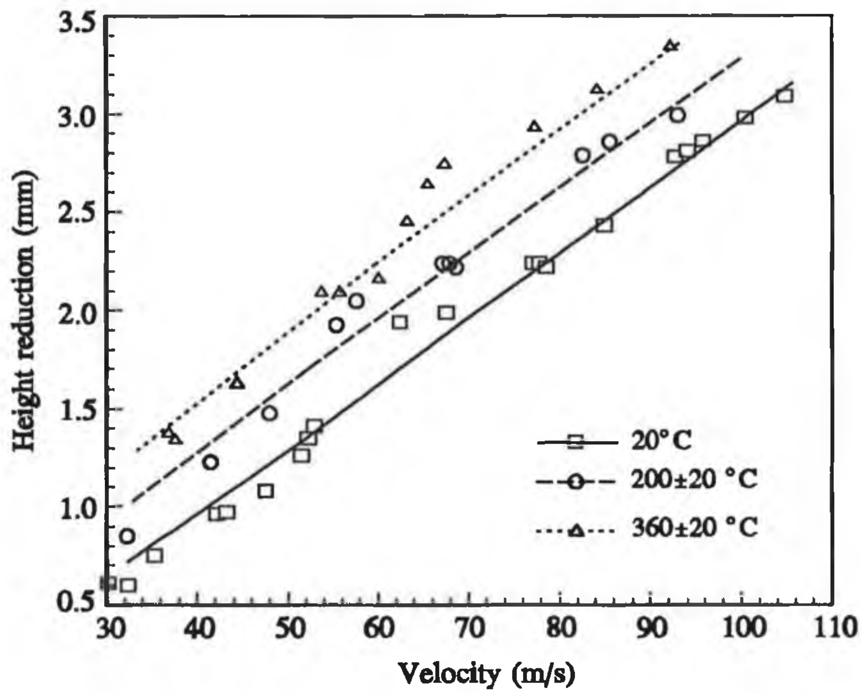

Fig. 105 *Comparison of deformation of the specimen based on the form (130) and the values in Table 7 with the experiment at various temperatures.*

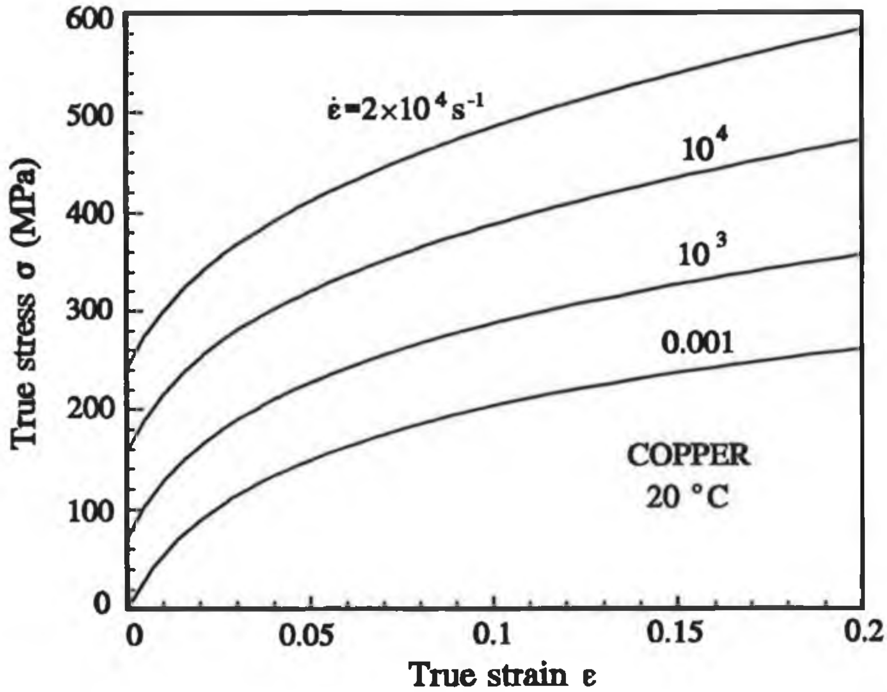

Fig. 106 *Stress-strain curves for pure copper based on the form (130) and the values in Table 7 at 20 °C.*

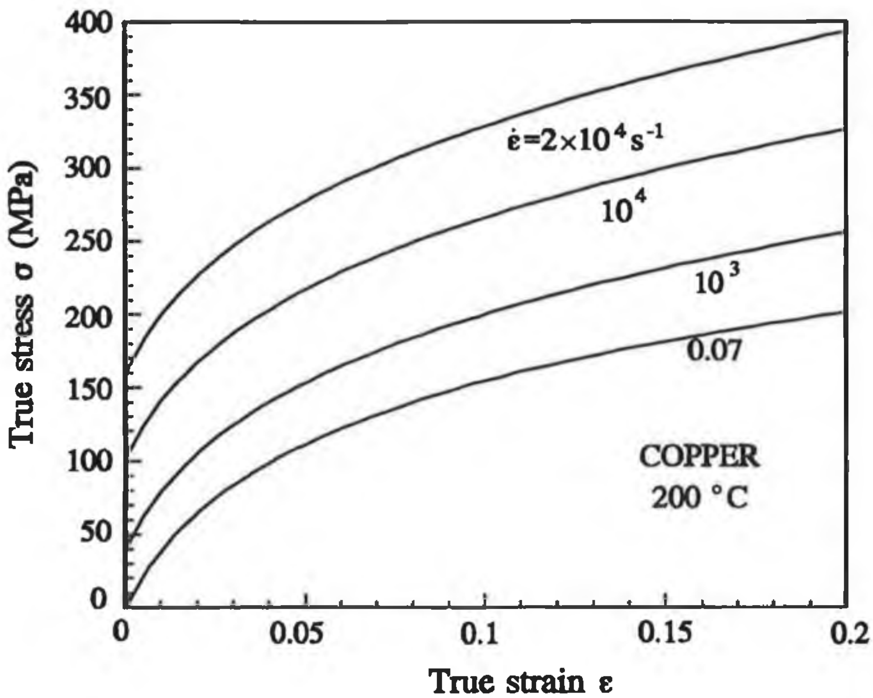

Fig. 107 *Stress-strain curves for pure copper based on the form (130) and the values in Table 7 at 200 °C.*

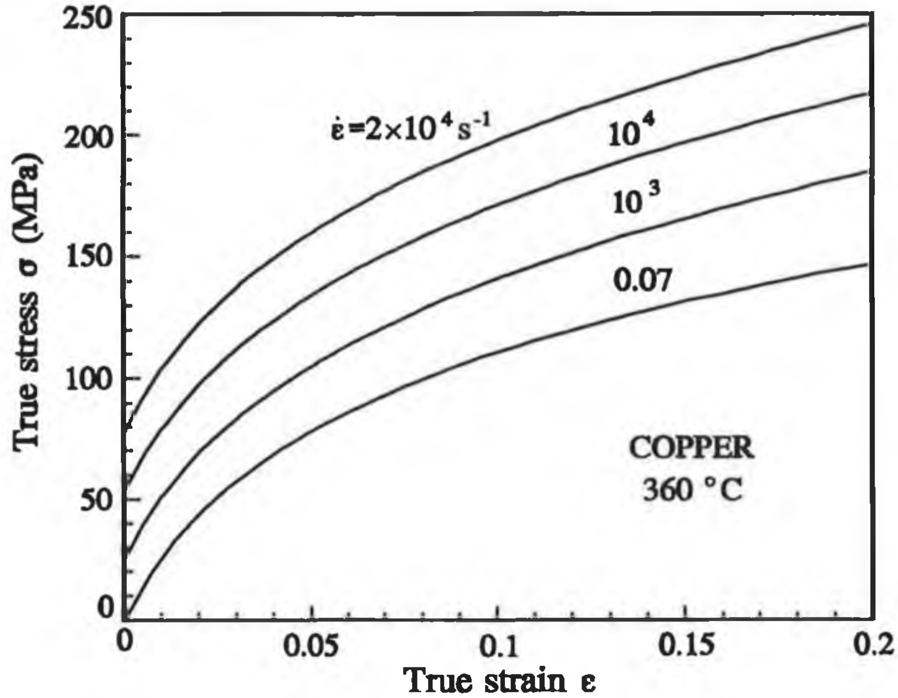

Fig. 108 *Stress-strain curves for pure copper based on the form (130) and the values in Table 7 at 360 °C.*

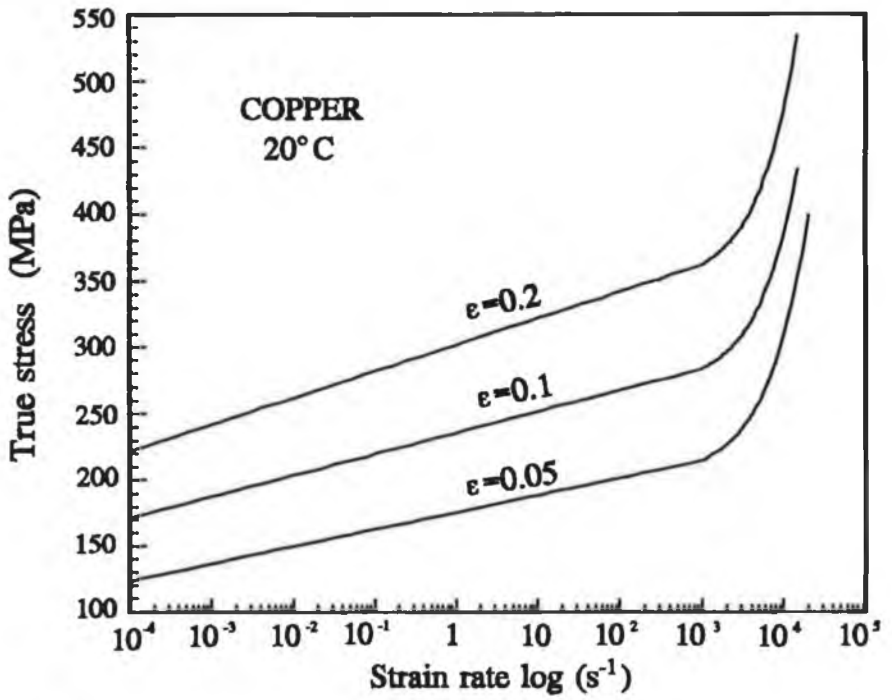

Fig. 109 *Stress at a constant strain versus strain rate for pure copper based on the form (130) and the values in Table 7 at 20 °C.*

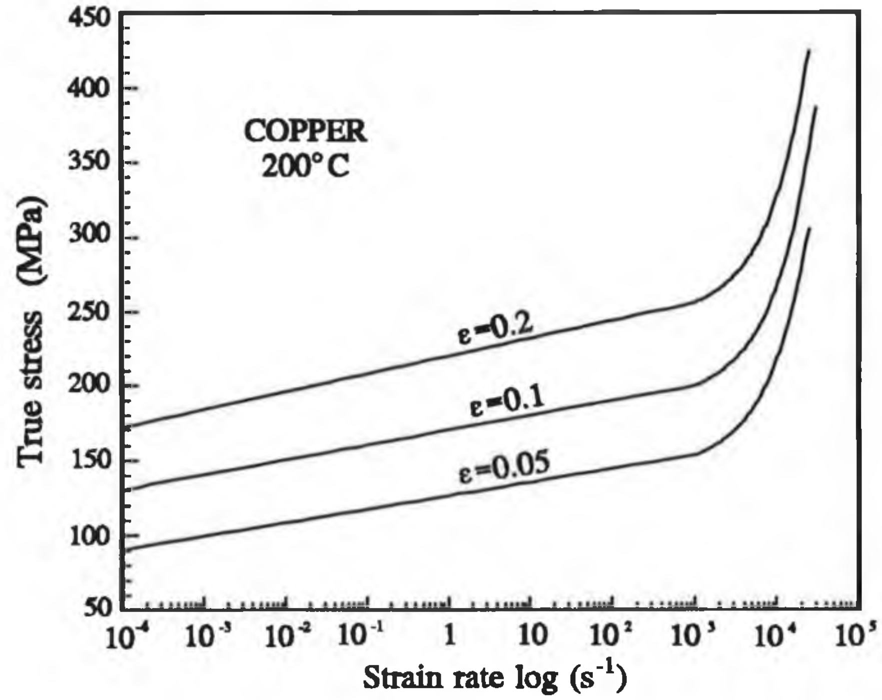

Fig. 110 *Stress at a constant strain versus strain rate for pure copper based on the form (130) and the values in Table 7 at 200 °C.*

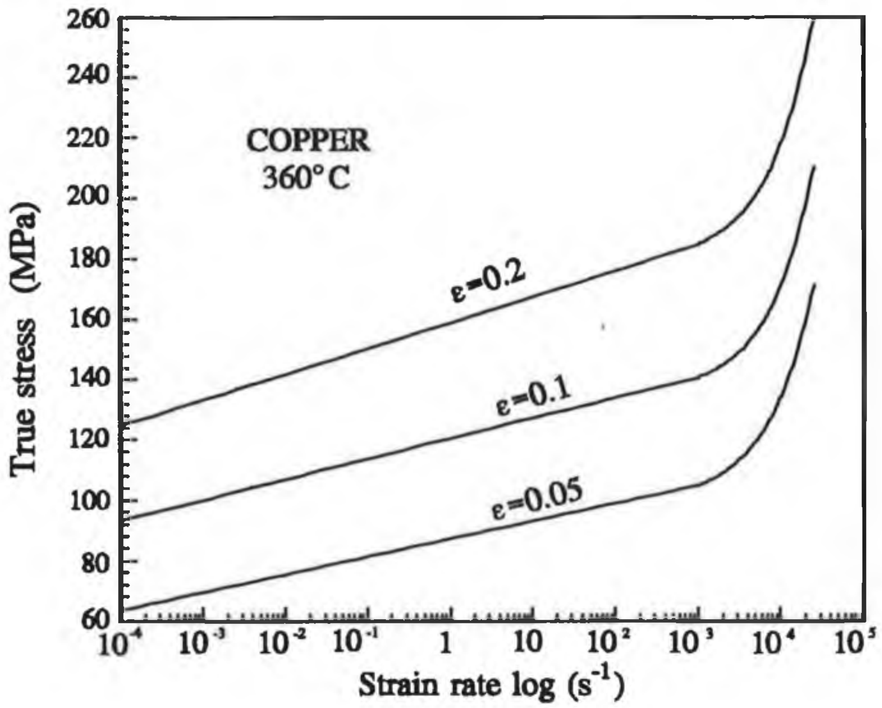

Fig. 111 *Stress at a constant strain versus strain rate for pure copper based on the form (130) and the values in Table 7 at 360 °C.*

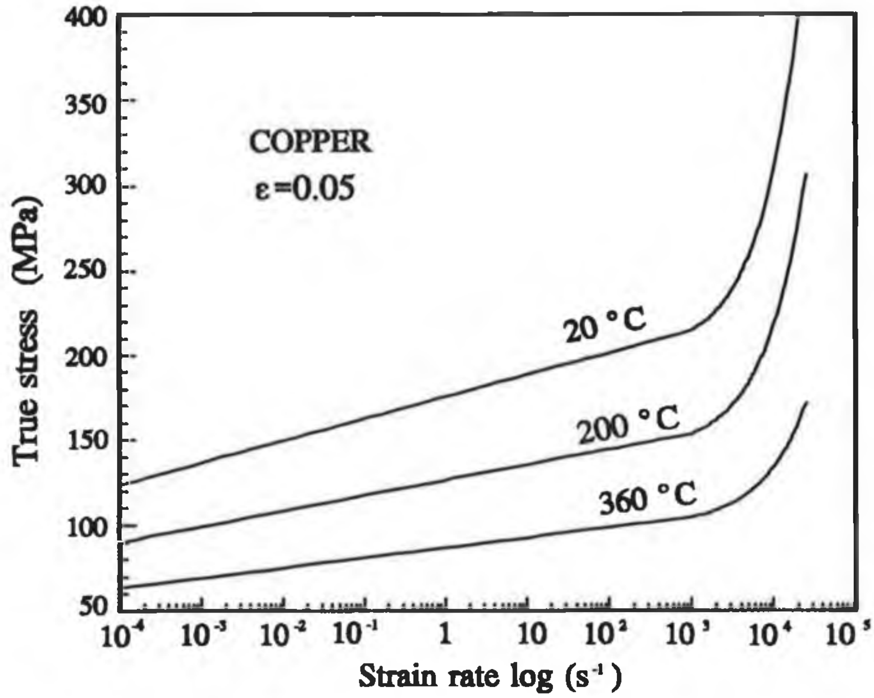

Fig. 112 *Temperature and strain-rate dependence of the stress at $\varepsilon=0.05$ of pure copper based on the form (130) and the values in Table 7.*

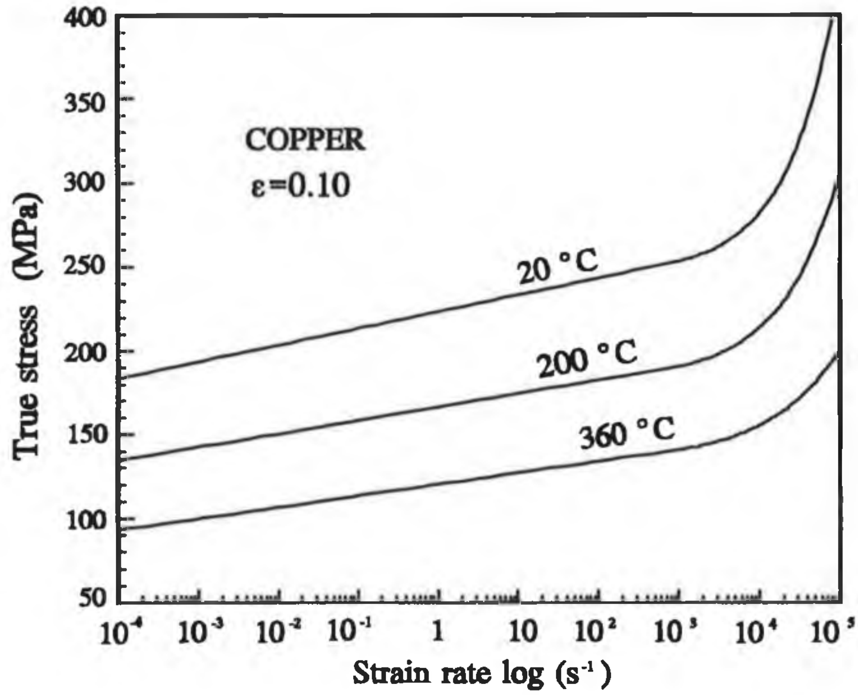

Fig. 113 *Temperature and strain-rate dependence of the stress at $\varepsilon=0.10$ of pure copper based on the form (130) and the values in Table 7.*

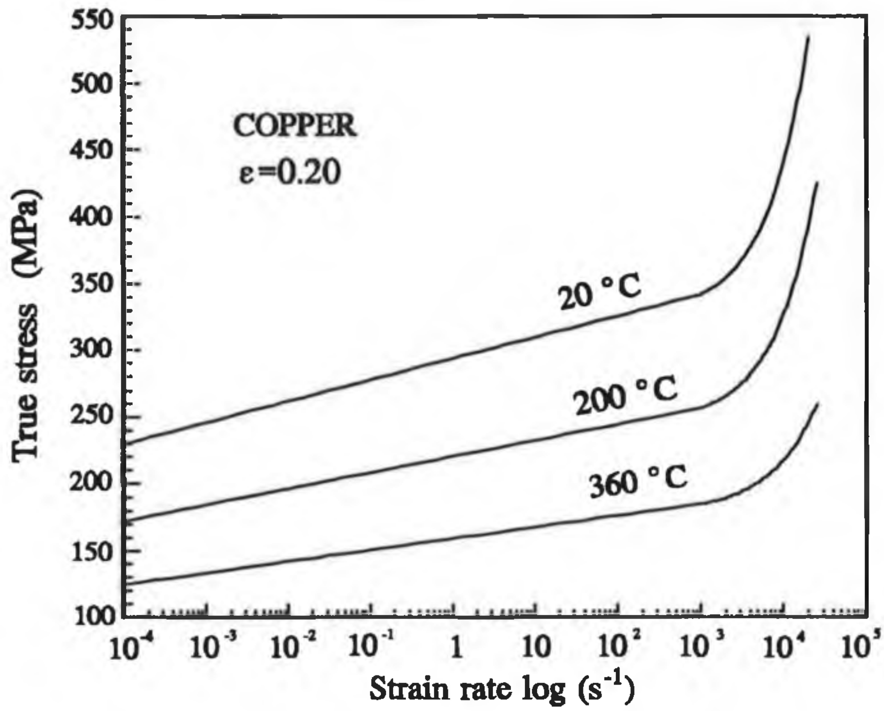

Fig. 114 *Temperature and strain-rate dependence of the stress at ε=0.20 of pure copper based on the form (130) and the values in Table 7.*

In practice, it was found that the Eq. (130) is an ideal form of constitutive relations, in which the interpretation of the corresponding constants are clear. $\alpha_1+\beta_1\varepsilon$ and $\alpha_2+\beta_2\varepsilon$ represent strain-rate hardening in the corresponding strain rate ranges; β_1 and β_2 reflect the effect of strain on the strain rates. For $\beta_1=\beta_2=0$, the stress-strain relations are a group of parallel curves in the individual coordinate systems (semi-logarithmic and rectangular). The contribution of the constant n to the constitutive equations is that it can flexibly and validly relax the strain-rate hardening in the range of high strain rates, because the assumption of linear strain rate sensitivity in this region often causes very strong strain-rate hardening, particularly at very high strain rates.

4.6.2 Mild steel

BCC metals and alloys, especially steels, show even greater rate sensitivity, which varies in a complex manner with stress, strain and temperature. The strain rate sensitivity increases with increasing strain rate and decreases with increasing strain. Generally, it is concluded that for BCC metals such as mild steel at low strain rates and high temperatures, the flow stress shows only small temperature and strain-rate sensitivity, the latter decreasing with increasing temperature; at lower temperatures and higher strain rates the flow becomes sensitive to temperature and strain rate; at much higher strain rates a rapid increase in the logarithmic rate sensitivity ($\partial\sigma/\partial\log\dot{\varepsilon}$) with increasing strain rate is obtained, this parameter being approximately independent of temperature [30]. Hence, the form of the constitutive equation proposed for mild steel is as follows

$$\frac{\sigma(\varepsilon)-\sigma_0(\varepsilon)}{\log\dot{\varepsilon}^p-\log\dot{\varepsilon}_0^p}=\alpha_1(1+e^{-\beta_1\varepsilon}) \qquad \dot{\varepsilon}^p\leq 10^3\,s^{-1}$$

$$\frac{\sigma(\varepsilon)-\sigma_1(\varepsilon)}{(\dot{\varepsilon}^p)^n-(\dot{\varepsilon}_1^p)^n}=\alpha_2(1+e^{-\beta_2\varepsilon}) \qquad \dot{\varepsilon}^p>10^3\,s^{-1} \tag{131}$$

The static stress-strain relation considering the effect of temperature for mild steel is expressed as

$$\sigma=(781.0-0.289T)(1-e^{-28\varepsilon}) \tag{132}$$

The calculations based on Eq. (131) have been made, and the corresponding optimised parameters at various temperatures have been determined, which are listed in Table 8. The predicted final deformation are compared with the experimental results as shown in Fig. 115. At various temperatures, the stress-strain curves are shown in Figs. 116 to 118 and the stress at a constant strain versus strain rate are shown in Figs. 119 to 121. The temperature and strain-rate dependence of the stress at various strain are shown in Figs. 122 to 124.

Table 8 *The strain rate sensitivities of mild steel determined based on Eq. (131).*

Temperature (°C)	λ_1		λ_2		n
	α_1(MPa)	β_1	α_2(kPa)	β_2	
20	45	12	40	1	0.87
220	35	12	32	1	0.85
440	20	12	30	1	0.84

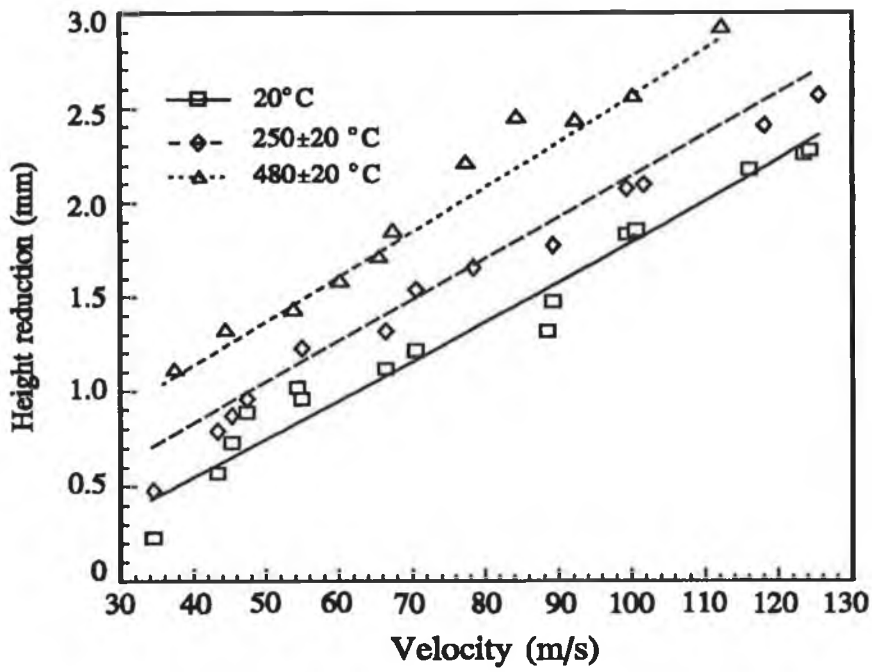

Fig. 115 *The comparison of deformation of mild steel specimens based on the Eq. (131) and Table 8 with the experiment at various temperatures.*

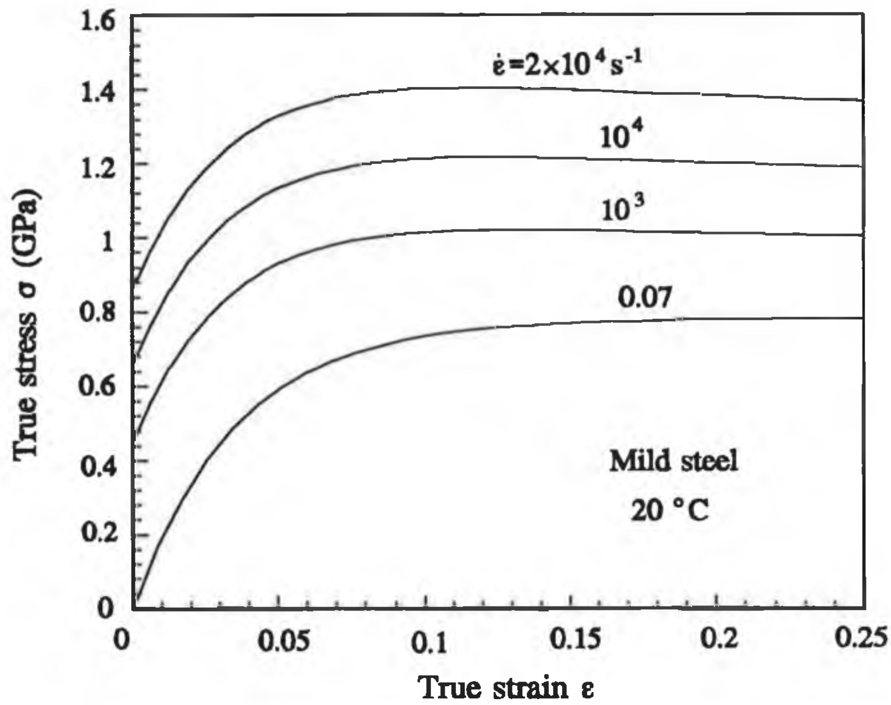

Fig. 116 *Stress-strain curves for mild steel based on Eq. (131) and the values in Table 8 at 20 °C.*

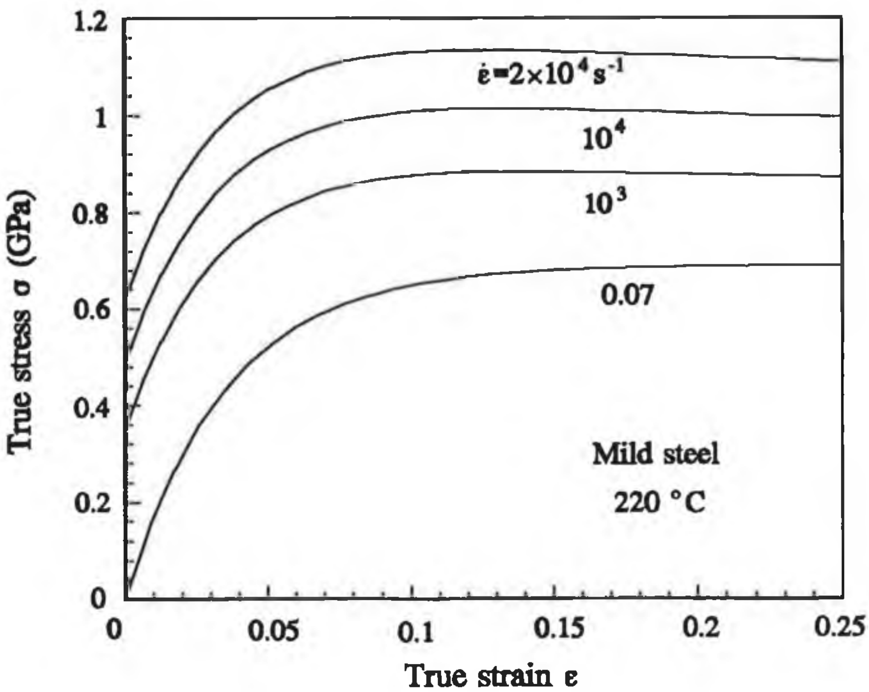

Fig. 117 *Stress-strain curves for mild steel based on Eq. (131) and the values in Table 8 at 220 °C.*

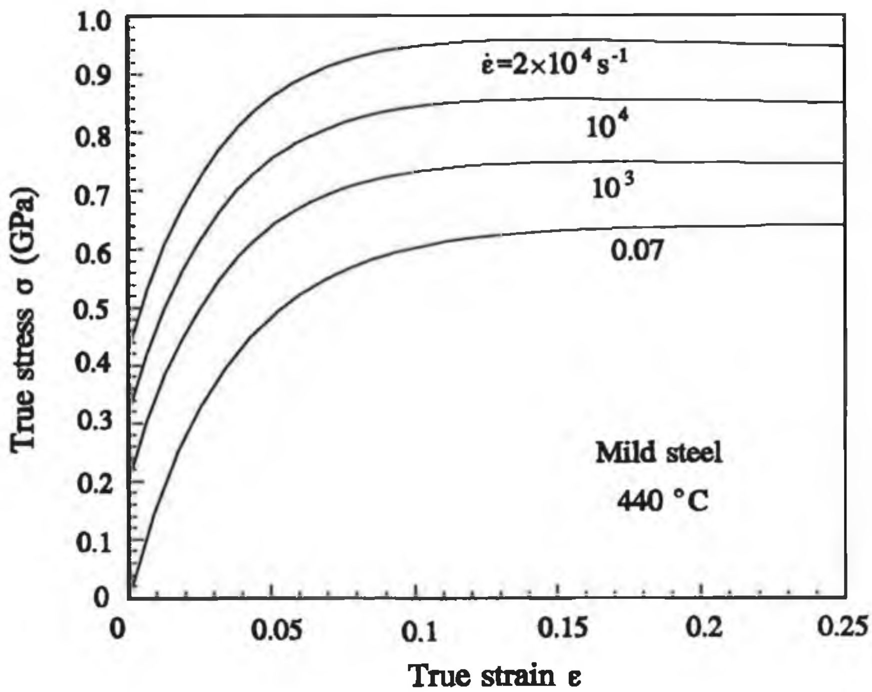

Fig. 118 *Stress-strain curves for mild steel based on Eq. (131) and the values in Table 8 at 440 °C.*

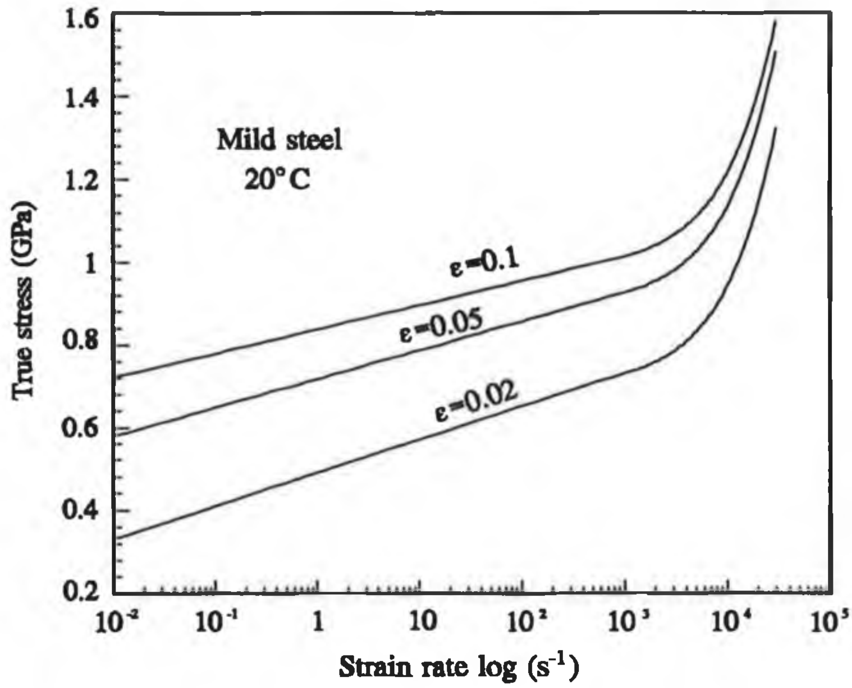

Fig. 119 *Stress at a constant strain versus strain rate for mild steel based on Eq. (131) and the values in Table 8 at 20 °C.*

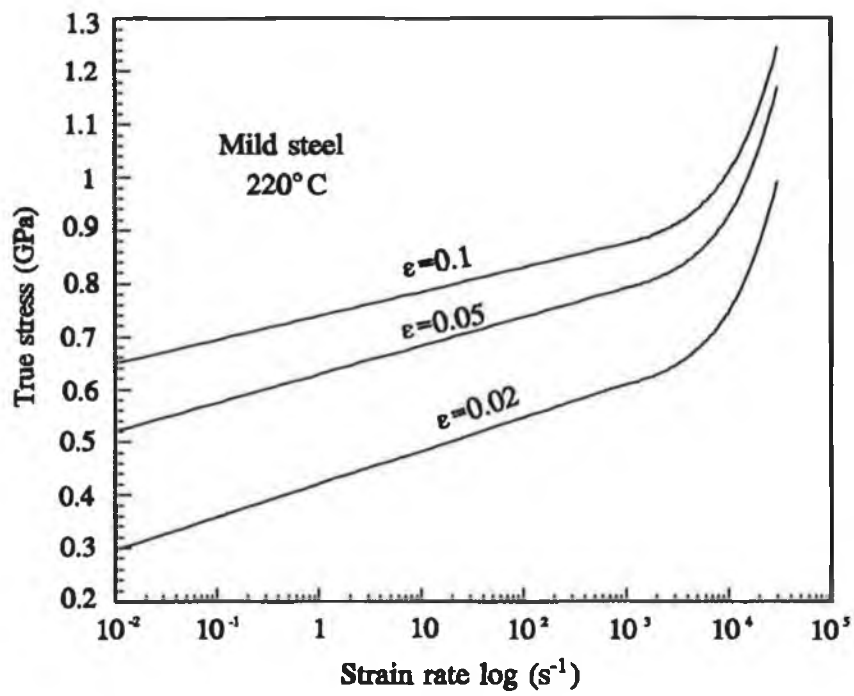

Fig. 120 *Stress at a constant strain versus strain rate for mild steel based on Eq. (131) and the values in Table 8 at 220 °C.*

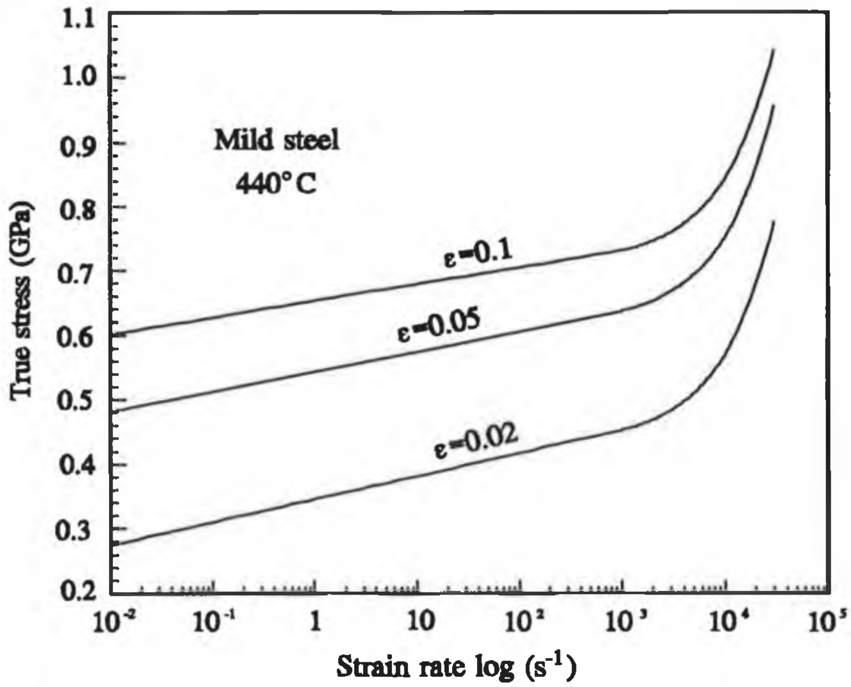

Fig. 121 *Stress at a constant strain versus strain rate for mild steel based on Eq. (131) and the values in Table 8 at 440 °C.*

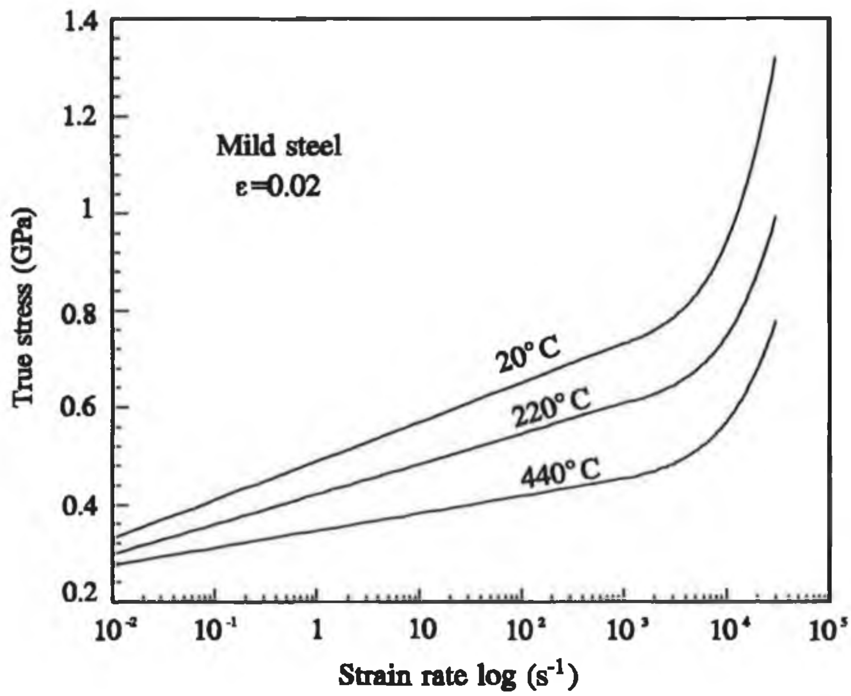

Fig. 122 *Temperature and strain-rate dependence of the stress at ε=0.02 of mild steel based on Eq. (131) and the values in Table 8.*

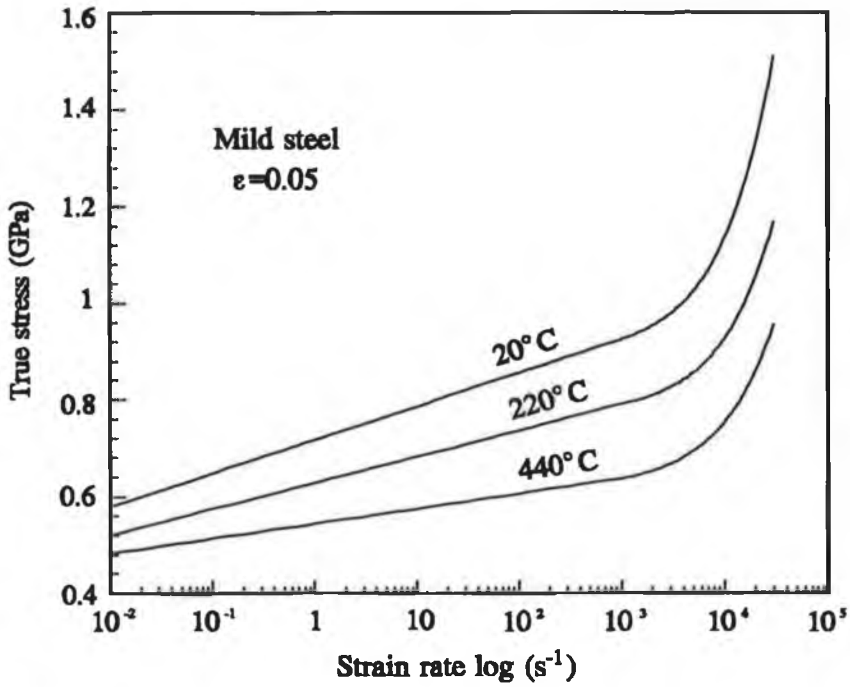

Fig. 123 *Temperature and strain-rate dependence of the stress at ε=0.05 of mild steel based on Eq. (131) and the values in Table 8.*

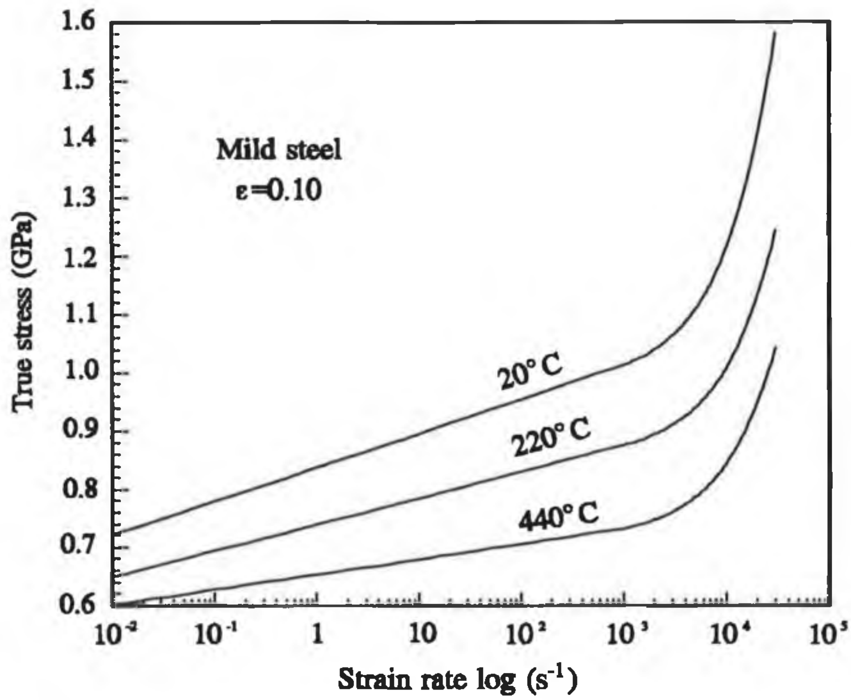

Fig. 124 *Temperature and strain-rate dependence of the stress at ε=0.10 of mild steel based on Eq. (131) and the values in Table 8.*

4.7 The Effect of Radial Expansion

One of the limitations of compression tests in high speed impact is radial expansion of the specimen during its deformation. This expansion affects the stress in the specimen in two ways: firstly by causing frictional shear stresses which act at the interfaces of the specimen with the anvil and the projectile, and secondly by introducing inertial body forces within the specimen.

The first of these effects can be minimized by lubrication of the projectile-specimen and anvil-specimen interfaces. In the current research, polythene sheet was used in the static tests and pure petroleum jelly in the dynamic tests to reduce the friction on the interfaces. In the experiments, the barrelling of the impacted specimen at room temperature is not distinct, but it can be observed at the high temperatures.

The second constitutes a limitation in obtaining accurate constitutive relations. Because of radial inertia, in a test at constant strain rate the measured axial stress exceeds the true uniaxial flow stress by an amount which increases as the increase of the strain rate.

The explicit solutions for the estimation of inertial effects in high-velocity plane strain and axisymmetric compression of rigid-perfectly plastic materials for a variety of frictional conditions have been derived by Sturgess and Jones [38], which predicts that increased impact velocity increases inertial effects, but increased interface friction tends to suppress these effects. However, the effects of strain rates and plastic wave propagation were not taken into account.

An approximate expression calculating the effect of inertia from energy considerations is derived by Samanta [23], which can be written as

$$\sigma_d=\sigma_m+\rho\left(\frac{h^2}{12}+\frac{d^2}{8}\right)\ddot{\varepsilon}+\rho\left(\frac{h^2}{12}-\frac{d^2}{16}\right)\dot{\varepsilon}^2 \tag{133}$$

where σ_d is a spatial stress value, σ_m is the mean measured contact pressure at the impact end, ρ is the density of the specimen, h and d are the initial height and diameter of the specimen respectively, $\dot{\varepsilon}$ is the mean strain rate, $\ddot{\varepsilon}$ is the derivative of strain rate with respect to time.

In the experiments performed, strain rate was nearly time-independent for a large part of the deformation. Therefore, Eq. (133) can be simplified as

$$\sigma_d=\sigma_m+\rho(\frac{h^2}{12}-\frac{d^2}{16})\dot{\varepsilon}^2 \tag{134}$$

In the current research, typically, for pure copper specimen of initial dimensions *d=5 mm* and *h=5 mm* the inertia correction is 0.13% of the flow stress 360 *MPa* at 0.05 strain and 0.09% of the flow stress 440 *MPa* at 0.2 strain, at a strain rate of 10^4 s^{-1} at room temperature.

It can be seen that because of the choice of small dimensions of test specimens, the effect of radial inertia in the current experimental condition may be ignored.

4.8 Discussion of the Constitutive Relations

As is predicted, it can be seen that the strain rate sensitivity λ, evaluated at constant strain and temperature, for commercially pure copper increases appreciably when the strain rate is raised above roughly 10^3 s^{-1}. When the maximum strain rate investigated is limited to 10^3 s^{-1}, such an increase is not found. As are shown in Figs. 109 to 111, although stresses increases with increasing strain rates, the strain-rate sensitivity does not vary until strain rate exceeds 10^3 s^{-1}.

A number of constitutive relations for pure copper specimens have been suggested by means of different tests and calculating methods. Although the materials used in these results are all commercially pure copper, it is impossible to require that such primary mechanical properties as the static stress-strain relations in the individual research are identical because of testing conditions, the type of the chosen material, and especially, the extent of work-harkening of tested materials. In order to ensure that the present results are comparable with those used by other researchers, a concept of so-called stress sensitivity is used, which is defined as the ratio of dynamic stress, σ_1, to quasi-static stress, σ_0.

Comparing with earlier results at room temperatures attained by various methods, the relations of stress sensitivities versus strain rates at constant strains and room temperatures are shown in Fig. 125 for pure copper materials. Using the split Hopkinson pressure bar (SHPB) technology, Lindholm [19] determined the rate sensitivity for annealed pure copper in the range of strain rate from 3.3×10^{-4} to 1.75×10^{3} s^{-1} (curve 1 in Fig. 125). Follansbee [33] determined the stress strain behaviour of oxygen-free electronic copper in the range of strain rate up to 1.5×10^{4} s^{-1} applying a developed SHPB experimental technology (curve 2 in Fig. 125). Hashmi obtained the stress-strain performance in a higher range of strain rate up to 10^{6} s^{-1} by applying a bullet fired at a target (curve 3 in Fig. 125). Curves 4 and 5 in Fig. 125 is respectively the stress-strain relations based on Eq. (129) and Table 6, and Eq. (130) and Table 7 in the current research. Dowling *et al* [31] investigated the shear strain rate sensitivity of the yield and flow stresses of copper over a range of strain rates from 10^{-3} to 4×10^{4} s^{-1} by means of high velocity punching technology (curve 6 in Fig. 125). Using a ballistic test and a high speed photography method, Hashmi and Haque [218] obtained the stress-strain characteristics of high pure copper at strain rates between 10^{3} to 4×10^{4} s^{-1} (curve 7 in Fig. 125).

It can be seen from Fig. 125 that in the present research (curves 4 and 5), the stresses increase linearly with logarithmic strain rates at low and moderate strain rates ($\leq3\times10^{3}$ s^{-1}). Stress sensitivities, *i. e.* λ/σ_0 (the tangent of the curves), keep unchanged in this range. This is consistent with previous results (curves 1, 2 and 6), in which no distinct change for λ occurs, however, stress sensitivities according to the present research are higher than previous results.

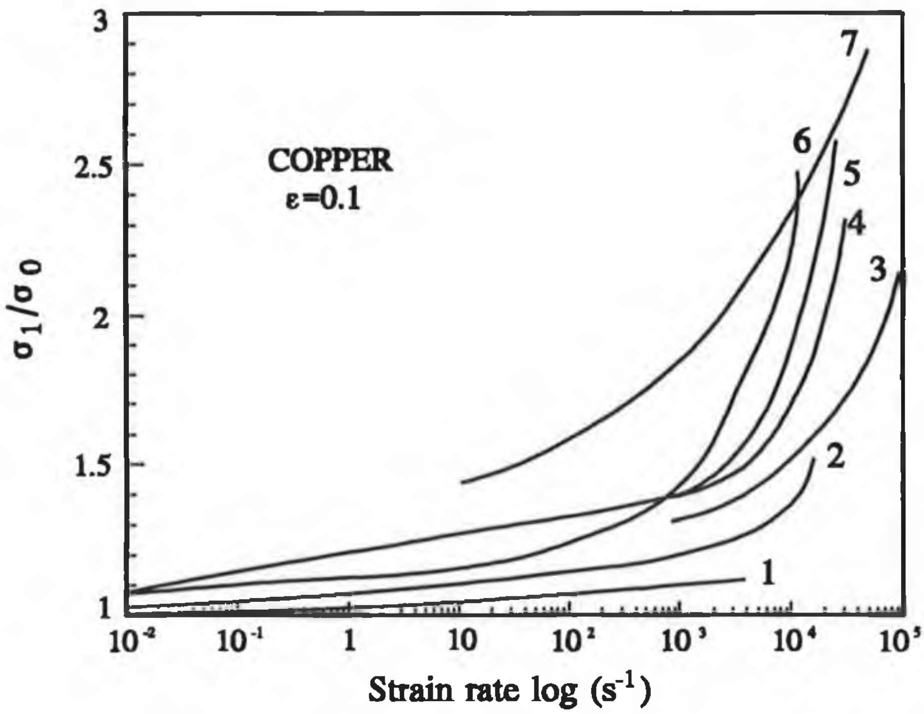

Fig. 125 *Comparison of the dynamic stress sensitivities at ε=0.1 for pure copper material at room temperatures, 1. ref. [19]; 2. ref. [33]; 3. ref. [234]; 4. Based on Eq. (129) and Table 6; 5. Based on Eq. (130) and Table 7; 6. ref. [31]; 7. ref. [218].*

At high strain rates (>10^3 s^{-1}), the increase of strain rate sensitivity becomes rapid and complicated. The increase of λ for curves 6 and 7 occurs earlier, while that for curve 5 is fastest. On the other hand, the stress sensitivity of curve 7 is the greatest.

As is shown in Fig. 126, the stress sensitivity for mild steel at the lower yield stress point at room temperatures in the prevailing research is also compared with those earlier results. Curve 1 is derived from the shear tests of Campbell and Ferguson [30], which ranges from 10^{-3} to 4×10^4 s^{-1}; curve 2 is from the tension tests of Campbell and Cooper [235]; curve 3 is from punching tests of Dowling and Harding [183]; curve 4 is obtained from the ballistic tests of Haque and Hashmi; curve 5 is based on Eq. (134) and Table 8; curve 6 is acquired from the punching shear tests of Dowling, Harding and Campbell [31]; and curve 7 comes from the result of Symonds [236].

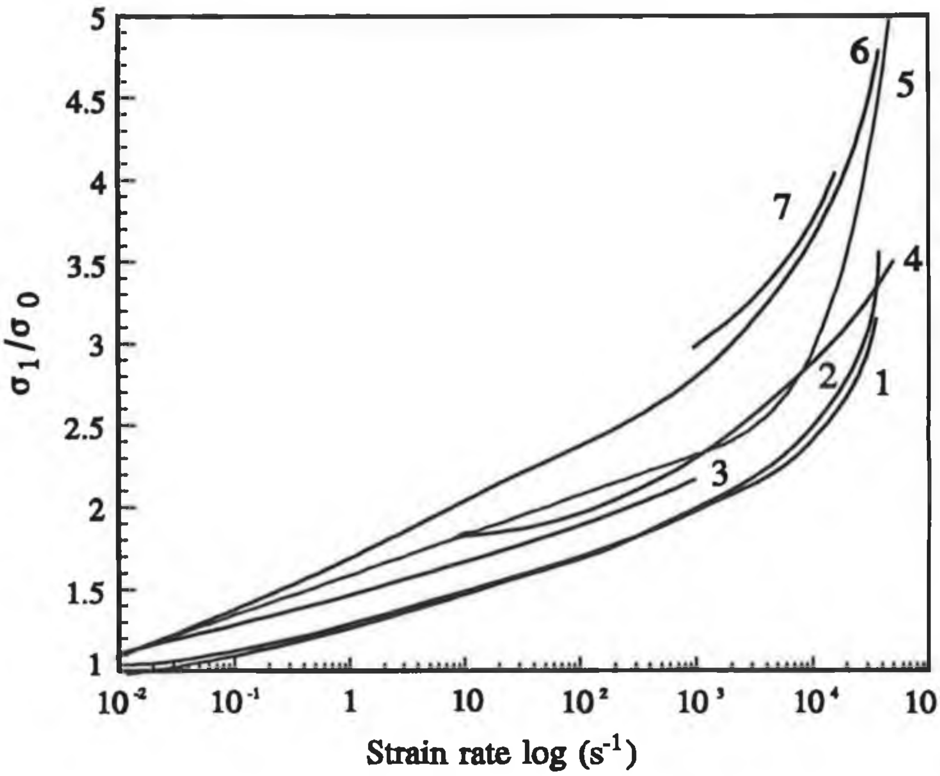

Fig. 126 *Comparison of the dynamic stress sensitivities for mild steel at lower yield stress point, 1. ref. [30]; 2. ref. [235]; 3. ref. [183]; 4. ref. [60] (ε=0.01); 5. Based on Eq. (134) and Table 8 (ε=0.02); 6. ref. [31]; 7. ref. [236].*

Unlike copper, the stress sensitivity for mild steel keeps a distinct trend of increase at lower strain rates. The curves from experiments show that even at low and moderate rates the strain rate sensitivity exhibits an increasing trend, while at high strain rate it become more apparent. Comparably, the assumption of linear dependence of the flow stress on the logarithm of the strain rate in the range of low strain rates is more suitable for copper.

The comparison at higher temperatures between the present research and the results obtained by Campbell and Ferguson [31] is shown in Fig. 127. Comparing with Fig. 126, it can be found that strain rate sensitivity for mild steel decreases with increasing temperature (see Figs. 122 to 124), while it is not so obvious for copper as shown in Figs. 112 to 114.

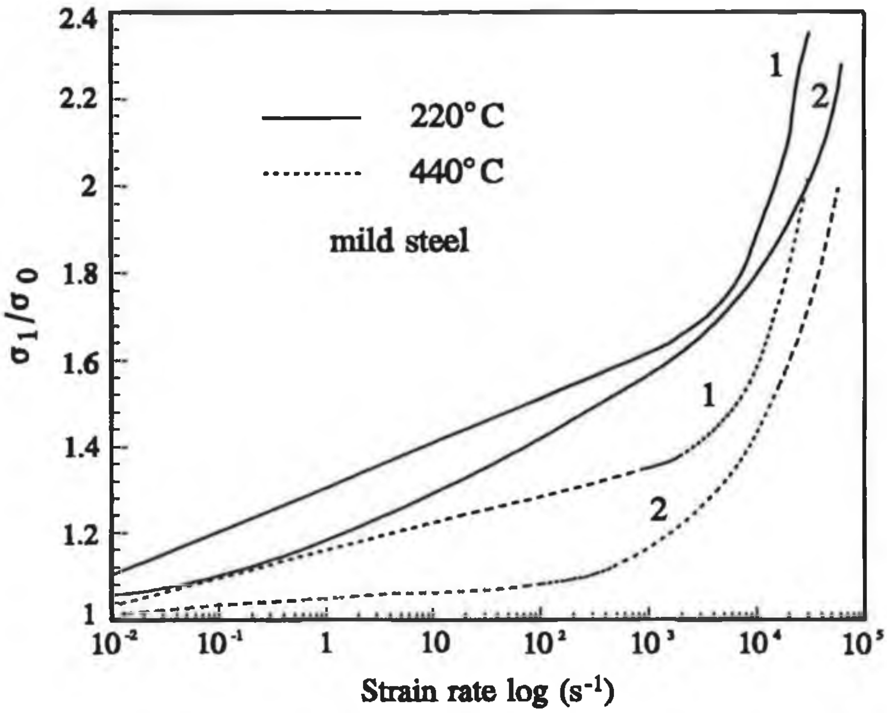

Fig. 127 *Comparison of dynamic stress sensitivities for mild steel at 220 °C and 440 °C, 1. Based on Eq. (134) and Table 8 at ε=0.05; 2. ref. [31] at lower yield stress point.*

The effect of the strain on strain rate sensitivity for the two materials are different. For mild steel, the strain rate sensitivity decreases with increasing strain as shown in Figs. 119 to 121, while for pure copper the increase of λ is not so evident as shown in Figs. 109 to 111.

It should be pointed out that the principal difficulty in the determination of constitutive equations by predicting the agreement of the final deformation of the impacted specimen with theoretical calculations is the lack of a unique solution even if the experimental results are predicted by the proposed constitutive law. For instant, for the same experimental data, it can be assumed that there is a higher strain rate sensitivity in the range of high strain rates, while a lower strain rate sensitivity in the low one. To overcome this problem, the previously reported experimental results in the range of low strain rates have been referred to.

It should be also noted that due to the effect of friction, the assumption of the uniaxial stress in the specimen can give rise to error in the calculated deformation. The existence of friction may make the sensitivities of strain rates determined by the prevailing method higher than the practical ones.

The validity of the determined constitutive relations is also noteworthy. The strain rate can really reach a quite high level of up to 10^5 s^{-1} under a high impact velocity of the projectile, however, this usually takes place in the region of small strain. With the increase of strain, the strain rate decreases rapidly. Therefore, at high strain rates the region involved by these constitutive equations is under a condition of small strain. With the reduction of strain rates, this region will gradually extend to larger strains. Nevertheless, this does not obstruct the application of these constitutive relations. In fact, the hardening of materials will be increased with increasing strain rates, *i. e.* the failure of materials will occur at a smaller strain.

Chapter 5 Conclusions and Suggestions

5.1 Concluding Remarks

(1) The investigations of the rate effects of metals deformed plastically have been extensively carried out during the last four decades and significant progress in studying high-speed deformation has been achieved. Therefore, a review of earlier work on aspects of experimental methods, experimental results, the development of wave propagation theory and their applications has been made, in which over 200 scientific sources are included.

(2) Impact testing is a very important technique in the study of dynamic behaviour of materials. When a specimen is subjected to impact, inertial stresses must be taken into account, that is, wave propagation in the material must be allowed for in interpreting the results. In general, plastic wave propagation requires the use of a rate-dependent constitutive relation for its proper description. The constitutive relation proposed by Malvern has been widely used, in which the plastic strain rate is a function of stress and strain. This relation implies that an incremental wave propagates at the elastic wave speed.

Experiments involving the observation of the transient wave propagation phenomena provide indirect methods to determine the dynamic mechanical properties of materials. In experiments involving the properties of uniaxial stress waves in rods, the procedure applied is to assume that the material submits to a certain constitutive law and then through calculations based on the law to predict the propagation characteristics. The predicted results are then compared with the experiment results. Agreement between the two usually leads to the conclusion that the equation assumed is the constitutive law for the material.

The broad uses of computers have brought about the rapid development of various numerical solutions. Computer codes have been developed to treat problems where loading and response times are in the submillisecond regime.

The experimental results in the present study have been obtained using a ballistic test rig to fire a hardened tool steel projectile onto a small cylindrical specimen placed upon a hardened anvil. Compressed nitrogen gas is used to propel the projectile and the final deformation of the struck specimen is recorded.

For the purpose of studying the dynamic respond of the struck specimen and the determination of its constitutive equation, a mechanical model of the above experimental configurations which may be used to determine such laws has been set up. The elastic solution is given in which some basic concepts of the propagation of longitudinal wave are exhibited. Further, the theory of propagation of longitudinal waves of plastic deformation is applied to the model, the quasi-linear elastic-plastic system equilibrium equations with a mixed boundary condition are established, along with their characteristic lines, the program of the numerical solutions of the forward integration procedure is given. The solutions of the equations conforming to the constitutive equation reported elsewhere under the typical parameters in the form of graphics are given and discussed. Some geometrical and physical parameters affecting the dynamic procedure of the specimen are also examined.

(3) Commercially pure copper and mild steel are chosen as the test materials of the specimens. Both the static and dynamic compressive experiments are performed in the conditions of room and high temperatures of up to 500 °C and 440 °C respectively.

Using an existing ballistic test machine, small cylindrical specimens of commercially pure copper and mild steel were placed upon a rigid anvil and were impacted by a hardened tool steel projectile. The initial velocity of the projectile up to 120 m/s was recorded by a laser velocity-measuring device, and the deformation of the impacted specimen was measured after each test. For the propose of high temperature tests, modification of the machine was necessary and a movable anvil unit to reduce the loss of heat has been designed and used.

(4) Various constitutive equations both considering and ignoring the effect of temperature proposed by many earlier researchers have been reviewed. The form of all these constitutive equations suggested, started from experimental evidence. It is pointed out that the general relation proposed by Malvern that plastic rate of strain is a function of the over-stress σ-$f(\varepsilon)$ is widely applied.

The micro explanation for the behaviour of those materials under high strain-rates is given. At low strain rates and high temperatures, where the flow stress is essentially constant and independent of temperature and strain rate, the controlling mechanism of flow is the long-range friction stress. At lower temperatures and higher strain rates, where greater rate and temperature sensitivities of the flow stress has been noted, the short range barriers to flow become relatively more important. At very high strain rates, for which the temperature dependence is unaffected, a rapid increase in the sensitivity with increasing strain rate is observed, which is believed to be due to viscous resistance to dislocation motion which becomes rate-controlling under these conditions.

Although the flow stress generally increases with strain and strain-rate, adiabatic deformation causes the increase of temperature so that flow stress is reduced. Adiabatic shear phenomena should be considered when the struck specimen is deformed to very large strains and at very high strain rates. There are two cases that the effect of temperature may be ignored, *i.e.* deformation can be considered isothermal. One is the case at low strain rates, where heat can be transferred to the surroundings, and the other is at small strain, where little heat is generated.

Shock loading is a complex process. In the current research, the sudden impact is handled by a fast, but smooth variation of the impact within a very short time of period, during which the shock wave-front linearly increases up to the peak stress.

It is generally accepted that for many FCC metals and alloys the logarithmic strain rate sensitivity $\lambda = \partial\sigma/\partial(\log\dot{\varepsilon}^p)$, evaluated at constant strain and temperature, is basically constant over the range of rates from 10^{-5} to 10^3 s^{-1}, but is found to increase when the strain rate is raised above 10^3 s^{-1}. At the strain rates exceeding 10^3 s^{-1}, there exists a linear relationship between the stress σ and plastic strain rate $\dot{\varepsilon}^p$, *i.e.* the linear strain rate sensitivity $\lambda=\partial\sigma/\partial\dot{\varepsilon}^p$ keeps constant.

Following various experimental evidence, a constitutive form considering the effect of temperature shown in Eq. (131) for pure copper is suggested. This form can not only effectively and flexibly reflect the practical properties of the material in a wide range of strain rates and also behaves a continuous properties at the connection of two different analytical expressions. The determination of this form is also as simple as other proposed forms. Further, the constitutive form suggested is extended to apply to mild steel.

The experimental results obtained on the impact test machine are compared with those from the program calculation based on the assumed constitutive equations. The agreement in terms of the final deformations of the struck specimen between the experimental and theoretical results confirms that the assumed constitutive law for the material is acceptable.

Finally, the constitutive relations obtained is compared with those reported elsewhere.

5.2 The Existing Problems and Further Suggestions

(1) In the experiments, since a new chamber unit was designed and used, the loss of temperature in the tests has been controlled. However, due to the current temperature measuring devices, there are still difficulties when the specimen is tested at higher temperatures. On the other hand, because the projectile passes through a long path before it impacts the specimen, it is not

so easy to assure a good contact of the surfaces between the projectile and the struck specimen, which can affect the uniformity of the deformation of the specimen.

Theoretically, main difficulty is in the determination of constitutive equations by predicting the agreement of the final deformation of the impacted specimen with theoretical calculations. There is a lack of a unique solution even if the experimental results are accurately predicted by the proposed constitutive law.

(2) It is expected that tests can be performed in a wider range of temperatures, so that the effect of temperature on the dynamic properties of the tested material can be used for this wider range. In order to compare with the previous results, the specimens should have an annealing treatment so that the residual stress existing in the specimens can be relieved. If the entire deformation process of the struck specimen could be recorded by a more modern measuring device, this would make it easier to determine the parameters in the proposed constitutive equations by the comparison of the deformation process of the specimen struck instead of its final deformation.

REFERENCES

1 Clark, G. S. and G. Datwyler, Proc. ASTM, 38, 1938, pp. 98.

2 Manjoine, M. and A. Nadai, Proc. ASTM, 40, 1940, pp. 822.

3 Orowan, E., Brit. Iron Steel Res. Assoc. Rept. No. MW/F/22/50, 1950.

4 Alder, J. F. and V. A. Phillips, J. Inst. Metals, 83, 1954-1955, pp. 80.

5 Cook, P. M., In: *Proc. Conf. on the Properties of Materials at High Rates of Strain*, Inst. Mech. Engrs., London, 1957, pp. 86.

6 Hockett, J. E., Trans. Am. Inst. Min. Engrs., 239, 1967, pp. 969.

7 Clark, D. S. and D. S. Wood, Proc. ASTM, 49, 1949, pp. 717.

8 Campbell, J. D. and K. J. Marsh, Phil. Mag., 7, 1962, pp. 933.

9 Maiden, K. J. and J. D. Campbell, J. Mech. Phys. Solids, 11, 1963, pp. 49.

10 Maiden, C. J. and S. J. Green, *Compressive Strain-rate Tests on Six Selected Materials at Strain Rates from 10^{-3} to 10^{4} in/in/sec.*, J. Appl. Mech., 33, 1966, pp. 496.

11 Lindholm, U. S. and L. M. Yeakley, Exp. Mech., 7, 1967, pp. 1.

12 Hopkinson, B., *A Method of Measuring the Pressure Produced in the Detonation of High Explosives or by the Impact of Bullets*, Phil. Trans. Roy. Soc. London, A213, 1914, pp. 437-456.

13 Kolsky, H., *An Investigation of the Mechanical Properties of Materials at Very High Rates of Loading*, Proc. Phys. Soc. (London), B 62, 1949, pp. 676-700.

14 Edington, J. W., in U. S. Lindholm (ed.), *Advances in Materials Research*, Vol. 2, Interscience, New York, 1968, pp.17.

15 Krafft, J. M., A. M. Sullivan and C. F. Tipper, Proc. Roy. Soc. (London), A221, 1954, pp. 114-127.

16 Campbell, J. D. and J. Duby, Proc. Roy. Soc. (London), A236, 1956, pp. 24.

17 Hauser, F. E., J. A. Simmons and J. E. Dorn, in P. G. Shewmon and V. F. Zackay (eds.), *Response of Metals to High Velocity Deformation*, Interscience, New York, 1961, pp. 93.

18 Davies, E. D. H. and S. C. Hunter, *The Dynamic Compression Testing of Solids by the Method of the Split Hopkinson Pressure Bar*, J. Mech. Phys. Solids, 11, 1963, pp. 155-179.

19 Lindholm, U. S., *Some Experiments with the Split Hopkinson Pressure Bar*, J. Mech. Phys. Solids, 12, 1964, pp. 317.

20 Yoshida S. and N. Nagata, Trans. Japan Inst. Metals, 7, 1966, pp. 273.

21 Efron L. and L. E. Malvern, *Electromagnetic Velocity-transducer Studies of Plastic Waves in Aluminum Bars*, Exp. Mech., 9, 1969, pp. 255-262.

22 Dusěk, F., Czech. J. Phys., B20, 1970, pp. 776.

23 Samanta, S. K., *Dynamic Deformation of Aluminium and Copper at Elevated Temperatures*, J. Mech. Phys. Solids, 19, 1971, pp. 117-135.

24 Harding, J., E. O. Wood and J. D. Campbell, *Tensile Testing of Materials at Impact Rates of Strain*, J. Mech. Eng. Sci., 2, 1960, pp. 88-96.

25 Campbell, J. D. and J. Harding, *The Effect of Grain Size, Rate of Strain, and Neutron Irradiation on the Tensile Strength of α-iron,* in: P. G. Shewmon and V. F. Zackay (eds.), *Response of Metals to High Velocity Deformation*, Proc. Conf. Colorado, Interscience, New York, 1961, pp. 51-75.

26 Harding, J., J. Mech. Eng. Sci., 7, 1965, pp. 163.

27 Lindholm U. S. and L. M. Yeakley, *High Strain-rate Testing: Tension and Compression,* Exp. Mech., 8, 1968, pp. 1.

28 Larsen, T. L., S. L. Rajnak, F. E. Hauser and J. E. Dorn, *Plastic Stress / strain-rate / temperature Relation in H. C. P. Ag-Al under Impact Loading*, J. Mech. Phys. Solids, 12, 1964, pp. 361-376.

29 Ferguson, W. G., F. E. Harser and J. E. Dorn, Brit. J. Appl. Phys., 18, 1967, pp. 411.

30 Campbell, J. D. and W. G. Ferguson, *The Temperature and Strain-rate Dependence of the Shear Strength of Mild Steel,* Phil. Mag., 21, 1970, pp. 63.

31 Dowling, A. R., J. Harding and J. D. Campbell, *The Dynamic Punching of Metals,* J. Inst. Metals, 98, 1970, pp. 215.

32 Baker W. E. and C. H. Yew. J. Appl. Mech., 33, 1966, pp. 917.

33 Follansbee, P. S., *High-strain-rate Deformation of FCC Metals and Alloys,* In: L. E. Murr, K. A. Staudhammer and M. A. Myers (eds.), *Metallurgical Applications of Shock-wave and High Strain-rate Phenomena*, Marcel Dekker, New York, 1986.

34 Davies, R. M., *A Critical Study of the Hopkinson Pressure Bar*, Phil. Trans. Roy. Soc. London, A240, pp. 375, 1948.

35 Klepaczko, J., Rept. 17/1969, Inst. Fundamental Tech. Res., Polish Academy of Sciences, 1969.

36 Hillier, M. J., Trans. ASME B88, 1966, pp. 369.

37 Lippmann, H., Proc. 7th Int. MTDR Conf., Birmingham, 1966.

38 Sturgess C. E. N. and M. G. Jones, *Estimation of Dynamic Forces in High-speed Compression Using a Free-flight Impact Forging Device*, Int. J. Mech. Sci., Vol. 13, 1971, pp. 309-322.

39 Duffy, J., J. D. Campbell and R. H. Hawley, J. Appl. Mech., Trans. ASME, 38, 1971, pp. 83.

40 Nicholas, T. and J. E. Lawson, J. Mech. Phys. Solids, 20, 1972, pp. 57.

41 Campbell, J. D., and A. R. Dowling, J. Mech. Phys. Solids, 18, 1970, pp. 43.

42 Lewis, J. L., and J. D. Campbell, Exp. Mech., 12, 1972, pp. 520.

43 Niordson, F., Exp. Mech., 5, 1965, pp. 29.

44 Hoggatt, C. R., W. T. Orr and R. F. Recht, In: *1st Intern. Conf. of the Center for High Energy Forming*, Denver, 1967, Vol. 2, pp.741.

45 Madsen, P., and F. I. Niordson, Tech. Rept. AFML-TR-71-79, AFML, Wright-Patterson Air Force Base, Ohio, 1971.

46 Christopherson, D. G. and B. Parsons, *Proc. Conf. on the Properties of Materials at High Rates of Strain*, Inst. Mech. Engrs., London, 1957, pp.115.

47 Kececioglu, D., Trans. Am. Soc. Mech. Engrs., 80, 1958, pp. 158.

48 Oxley, P. L. B. and M. G. Stevenson, *Measuring Stress-strain Properties at Very High Strain Rates Using a Machining Test*, J. Inst. Metals, 95, 1967, pp. 308.

49 Stevenson, M. G. and P. L. B. Oxley, Proc. Inst. Mech. Engrs., 185, 1970/1971, pp. 741.

50 Edington, J. W., *The Influence of Strain Rate on the Mechanical Properties and Dislocation Substructure in Deformed Copper Single Crystals*, Phil. Mag., 19, 1969, pp. 1189.

51 Lindholm, U. S., *Deformation Maps in the Region of High Dislocation Velocity*, In: K. Kawata and J. Shioiri (eds.), *High Velocity Deformation of Solids*, Springer-Verlag, New York, 1978.

52 Wulf, G. L. and G. T. Richardson, J. Phys. E. (Sci. Inst.) 7, 1974, pp. 167.

53 Wingrove, A. L. J., Phys. E. (Sci. Inst.), 7, 1974, pp. 873.

54 Gorham, D. A., *Measurement of Stress-strain Properties of Strong Metals at Very High Rates of Strain*, In: J. Harding (ed.), *Mechanical Properties at High Rates of Strain*, Institute of Physics, London, 1980, pp. 16.

55 Taylor, G. L., *The Use of Flat-ended Projectiles for Determining Dynamic Yield Stress*, Part I, *Theoretical Considerations*, Proc. Roy. Soc., A194, 1948, pp.289-299.

56 Whiffin, A. C., *The Use of Flat-ended Projectiles for Determining Dynamic Yield Stress*, Part II, *Tests on Various Metallic Materials*, Proc. Roy. Soc., A194, 1948, pp. 300.

57 Hawkyard, J. B., D. E. Eaton and W. Johnson, *The Mean Dynamic Yield Strength of Copper and Low Carbon Steel at Elevated Temperatures from Measurements of the 'Mushrooming' of Flat-ended Projectiles*, Int. J. Mech. Sci., 10, 1968, pp. 929-948.

58 Hashmi, M. S. J., *Strain Rate Sensitivity of a Mild Steel at Room Temperature and Strain Rate of up to 10^5 s^{-1}*, J. Strain Analysis, 15, 1980, pp. 201-207.

59 Hashmi M. S. J. and P. J. Thompson, *A Numerical Method of Analysis for the Mushrooming of Flat-ended Projectiles Impinging on a Flat Rigid Anvil*, Int. J. Mech. Sci, 19, 1977, pp. 273-281.

60 Haque M. M. and M. S. J. Hashmi, *Stress-strain Properties of Structural Steel at Strain Rates of up to 10^5 Per Second at Sub-zero, Room and High Temperatures*, Mechanics of Materials, 3, 1984, pp. 245-256.

61 Ripperger, E. A. and H. Watson, *The Relationship between the Constitutive Equation and One-dimensional Wave Propagation*, In: U. S. Lindholm (ed.), *Mechanical Behaviour of Materials under Dynamic Loads*, Springer-Verlag, New York, 1968, pp. 294.

62 Percy, J. H., In: *Proc. of Symp. on Structural Dynamics under High Impulse Loading*, ASD-TDR-63-140, Wright-Patterson, AFB, Ohio, 5, 1963, pp. 123-143.

63 Hopkinson, J., *On the Rupture of Iron Wire by a Blow*, Collected scientific papers, Vol.II, 1872, pp. 316-320.

64 Hopkinson, B., *The Effects of Momentary Stresses in Metals*, Proc. Roy, Soc. A 74, 1905, pp. 498-506.

65 Brown, A. F. C. and N. D. G. Vincent, Proc. Inst. Mech. Engrs. 141, 1941, pp. 126.

66 Taylor, G. L., *The Testing of Materials at High Rates of Loading,* J. Inst. Civil Engrs. 2, 1946, pp. 486-519.

67 Davies, R. M., *The Determination of Static and Dynamic Yield Stresses Using a Steel Ball*, Proc. Roy. Soc. A 197, 1949, pp. 416-432.

68 Duwez P. E. and D.S. Clark, Proc. Am. Doc. Test. Mat. 47, 1947, pp 502.

69 Hillier, K. W. and H. Kolsky, *An Investigation of the Dynamic Elastic Properties of Some High Polymers*, Proc. Phys. Soc. B, 62, 1949, pp. 111-121.

70 Write. M. P., J. Appl. Mech. 16, 1949, pp. 300-322.

71 Smith, R. C., T. E. Pardue and I. Vigness, Proc. Soc. Exptl. Stress Anal. 13, 1956, pp. 183-197.

72 Campbell, W. R., J. Wash. Acad. Sci. 43, 1953, pp. 102-103.

73 De Costello, E., *Yield Strength of Steel at an Extremely High Rate of Strain*, In: *Proc. Conf. Properties of Materials at Hight Rates of Strain*, London, 1957, pp. 13-21.

74 Davis, C. D. and S. C. Hunter, Sheet Metal Ind. 39, 1962, pp. 261-263.

75 Vincent, B. J., R. Gee and S. C. Hunter, *A Study of Rapid Micro-Yielding in Mild Steel by Scleroscopic Methods*, In: *Proc. Conf. Properties of Materials at High Rates of Strain*, London, pp. 51-65.

76 Lifschitz, J. M. and H. Kolsky, J. Mech. Phys. Solids 12, 1964, pp. 35-43.

77 Durelli, A. J. and W. F. Riley, J. Appl. Mech. 24, 1957, pp. 69-76.

78 Feder, J. C., R. A. Gibbons, J. T. Gilbert and E. L. Offenbacher, Proc. Soc. Exp. Stress Anal, 14, 1956, pp. 109-118.

79 Clark, A. B. J., Proc. Soc. Exptl. Stress Anal. 14, 1956, pp. 195-204.

80 Goldsmith, W. and L. Dabaghian, Proc. Soc. Exp. Stress Anal.,18, 1961, pp 121-128.

81 Clark, A. B. J. and R. J. Sanford, Proc. Soc. Exptl. Stress Anal. 20, 1963, pp. 148-151.

82 Perkins, H. C., J. Appl. Mech. 20, 1953, pp. 140-141.

83 Ely, R. E., *Review of a High Speed Tensile Testing Program for Thermoplastics*, In: A. G. H. Dietz and F. K. Eirich (eds.), *High Speed Testing*, Proc. Symp. Boston, Massachusetts, 1958, pp. 3-24.

84 Strella, S., *High Strain Rate Tension Testing of Plastics*, In: A. G. H. Dietz and F. R. Eirich (eds.), *High Speed Testing*, Proc. Symp. Boston, Mass., 1958, Vol. I, pp 27-40.

85 Bills, Jr. K. W., K. H. Sweeny and F. S. Salcedo, *The Tensile Properties of Highly Filled Polymers; Effects of Filler Concentrations*, in: A. G. H. Dietz and F. R. Eirich (eds.), *High Speed Testing*, Proc. Symp. Boston, Mass., 1960, Vol. II, pp 3-12.

86 Jones, J. W., *The Tensile Testing of Elastomers at Ultra-High Strain Rates*, In: A. G. H. Dietz and F. R. Eirich (eds.), *High Speed Testing*, Proc. Symp. Boston, Mass., Vol. II, 1960, pp 29-35.

87 Ivanov, N. P., V. A. Lagunov and V. A. Stepanov, Plasticheskie Massy, 8, 1963, pp. 49-53.

88 Back, P. A. A. and J. D. Campbell, *The Behaviour of a Reinforced Plastic Material under Dynamic Compression*, In: *Proc. Conf. Properties of Materials at High Rates of Strain*, London, 1957, pp. 221-228.

89 Pilsworth Jr. M. N. , and H. J. Hoge, Textile Res. J. 35, 1965, pp. 129-144.

90 Ivanov, N. P. and V. A. Stepanov, Mehanika Polimerov, Riga 5, 1965, pp. 34-48.

91 Bodner, S. R., and H. Kolsky, *Stress Wave Propagation in Lead*, In: Proc. 3rd U. S. Nat. Congr. Appl. Mech. 1958, pp. 495-501.

92 Chiddester, J. L. and L. E. Malvern, *Compression Impact Testing of Aluminum at Elevated Temperatures*, Proc. Soc. Exptl. Stress Anal. 20, 1963, pp. 81-89.

93 Ainbinders, S. B., Izv. Akad. Nauk Latv. SSR 1, 1951, pp. 137-148.

94 Ainbinders, S. B., Izv. Akad. Nauk Latv. SSR 8, 1952, pp. 127-136.

95 Campbell, J. D., J. Mech. Phys. Solids 1, 1953, pp. 113-123.

96 Johnson, J. E., D. S. Wood and D. S. Clark, J. Appl. Mech. 20, 1953, pp. 523-529.

97 Campbell, J. D., J. Mech. Phys. Solids 3, 1954, pp. 54-62.

98 Taylor, D. B. C., J. Mech. Phys. Solids 3, 1954, pp. 38-46.

99 Taylor, D. B. C., *Non-uniform Yield in a Mild Steel under Dynamic Straining*, In: *Proc. Conf. Properties of Materials at High Rates of Strain*, London, pp. 229-238.

100 Harris, D. B. and M. P. White, J. Appl. Mech. 21, 1954, pp. 194-195.

101 Maiden, C. J. and J. D. Campbell, Phil, Mag. 3, 1958, pp. 872-885.

102 Koshelev, F. P. and G. V. Uzhik, Izv. Akad. Nauk SSSR, Otd, Tekhn. Nauk, Mekhan. I Mashinostr. 1, 1959, pp. 111-118.

103 Uzhik, G. V. and Yu. Ya. Voloshenko-Klimovitskii, *On the Elastic-Plastic Strain of Steels under Longitudinal Impact*, In: *Proc. Conf. Properties of Materials at High Rates of Strain*, London, 1957, pp. 239-243.

104 Uzhik, G. V. and Yu. Ya. Voloshenko-Klimovitskii, *The Resistance of the Initial Plastic Deformation to the Shock Tension for Low Temperatures*, In: *Some Problems about the Strength of the Solid Body*, Moscow, 1959, pp. 238-245.

105 Voloshenko-Klimovitskii, Yu. Ya., Izv. Akad. Nauk SSSR, Otd. Tekhn. Nauk, Mekhn. Mashinostr. No. 1, 1962, pp. 152-156.

106 Vitman, F. F. and N. A. Zlatin, J. Techn. Phys. 19, 1949, pp. 315.

107 Vitman, F. F., N. A. Zlatin and B. S. Ioffe, J. Tech,. Phys. 19, 1949, pp. 300.

108 Vitman, F. F., N. A. Zlatin, Izv. Akad. Nauk SSSR, Otd. Tekhn. Nauk, Mekhn. Mashinostr. No. 6. 1962. pp. 175.

109 Taylor, D. B. C. and L. E. Malvern, *Dynamic Stress and Deformation in a Mild Steel at Normal and Low Temperatures*, In: P. G. Shewmon and V. F. Zackay (eds.), *Response of Metals to High Velocity Deformation*, Proc. Conf. Colorado, Interscience Publ., New York-London, 1960, pp. 77-91.

110 Perzyna, P. and T. Wierzbicki, Arch. Mech. Stos. 16, 1964, pp. 135-143.

111 Jones, O. E. and J. R. Holland, J. Appl. Phys. 35, 1964, pp. 1771-1773.

112 MacDonald, R. J., R. L. Carlson and W. T. Lankford, Proc. Soc. Exp. Stress Anal. 14, 1956, pp. 163-170.

113 Riparbelli, C., *On the Relation among Stress, Strain and Strain Rate in Copper Wires, Submitted to Longitudinal Impact*, Proc. Soc. Exptl. Stress Anal. 14, 1956, pp. 55-70.

114 Smith, R. C., Proc. Soc. Exptl. Stress Anal. 18, 1961. pp. 153-159.

115 Hawkyard, J. B., and P. Freeman, British J. Appl. Phys. 7. 1956, pp. 3-4.

116 Voloshenko-Klimovitskii, Yu. Ya., Izv. Akad. Nauk SSSR, Otd. Tekhn. Nauk No. 4, 1956, pp. 147-150.

117 Voloshenko-Klimovitskii, Yu. Ya., *On the Measuring of the Yield Stress for the Dynamic Loading*, In: *Problems of Strength in Construction of Machines*, Moscow, 1959, pp. 89-95.

118 Moldovan, V., Bull. Stiint. Inst. Politec. Cluj 8, 1965, pp. 355-371.

119 Chang, Tso-Mei and Chao, Shih-To, Scientia Sinica 13, 1964, pp. 823-836.

120 Konstantinov, V. N. and E. I. Timofeev, *The Influence of High Rate of Strain on the Mechanical Properties of the Alloy of Type V-95 after Different Stages of Ageing*, In: *Some Problems about the Strength of the Solid Body*, Moscow, 1959, pp. 230-237.

121 Nicholas T. and J. D. Campbell, Exp. Mech., 12, 1972, pp. 441.

122 Klepaczko, J., In: A. Sawczuk (ed.), *Symposium on Foundations of Plasticity*, Noordhoff, Amsterdam, pp. 451.

123 Hughes, D. S. and C. Maurette, J. Appl. Phys. 27, 1956, pp. 1184-1186.

124 Jukov, A. M., Inzh. Sb. 30, 1960, pp. 3-16.

125 Jukov, A. M., *Some Particularities of the Metal Response to Elastic-Plastic Deformation*, In: *The Problems of the Theory of Plasticity*, Moscow, 1961, pp. 30-57.

126 Hrazdil, F. and M. Krejči, Kovové Materialy 2, Bratislava, 1964, pp. 245-253.

127 Hrazdil, F. and M. Krejči, Kovové Materialy 3, Bratislava, 1965, pp. 52-59.

128 Klepaczko, J., Arch. Mech. Stosowanej, 19, 1967, 211.

129 Klepaczko, J., J. Mech. Phys. Solids, 16, 1968, pp. 255.

130 Tsao, M. C. C. and J. D. Campbell, Oxford Univ. Engng. Lab., Report No. 1055/73, 1973.

131 Eleiche A. M. and J. D. Campbell, Ibid, Report No. 1106/74, 1974.

132 Lindholm U. S. and R. L. Bessey, Tech. Rept. AFML-TR-69-119, Air Force Materials Laboratory, Wright-Patterson Air Force Base, Ohio, 1969.

133 Jiang, C. W., and Chen, M. M., Report No. AMMRC CTR 74-23, Watertown, MA. 1974.

134 Karnes, C. H. and E. A. Ripperger, J. Mech. Phys. Solids, 14, 1966, pp.75.

135 Holt, D. L., S. G. Babcock, S. J. Green and C. J. Maiden, Trans. ASM, 60, 1967, pp. 152.

136 Ferguson, W. G., A. Kumar and J. E. Dorn, J. Appl, Phys. 30, 1967, pp. 1863.

137 Kumar, A., F. E. Hauser and J. E. Dorn, Acta Meta. 16, 1968, pp. 1189.

138 Dharan C. K. H., and F. E. Hauser, Exp. Mech. 10, 1970, pp. 370.

139 Green, S. J., C. J. Maiden, S. G. Babcock and F. L. Schierloh, *The High Strain-rate Behaviour of Face-centred Cubic Metals*, In: M. Kanninen, W. Adler, A. Rosenfield and R. Jaffee (eds.), *Inelastic Behaviour of Solids*, McGraw-Hill Co., New York, 1970.

140 Chiem, C. Y. and J. Duffy, *Strain Rate History Effects and Observations of Dislocating Substructure in Aluminum Single Crystals Following Dynamic Deformation*, Materials Research Laboratory, Brown University, MRL E-137, 1981.

141 Ripperger, E. A., *Dynamic Plastic Behaviour of Aluminum, Copper and Iron*, In: N. J. Huffington (ed.), *Behaviour of Materials under Dynamic Loading*, Am. Soc. Mech. Engr., Chicago, 1965.

142 Kumar A. and R. G. Kumble, J. Appl. Phys. 40, 1969, pp. 3475.

143 Dusek, F., Z. Jasinski, J. Buchar, A. Litwora and A. Piatkowski, Czech. J. Phys. B26, 1976, pp. 538.

144 Stelly M. and R. Dormeval, *Some Results on the Dynamic Deformation of Copper*, In: K. Kawata and J. Shioiri (eds.), *High Velocity Deformation of Solids*, Springer-Verlag, New York, 1968.

145 Shioiri, J., K. Satoh and K. Nishimura, *Experimental Studies on the Behaviour of Dislocations in Copper at High Rates of Strain*, In: K. Kawata and J. Shioiri (eds.), *High Velocity Deformation of Solids*, Sprinter-Verlag, New York, 1978.

146 Follansbee, P. S., G. Regazzoni and U. F. Kocks, In: J. Harding (ed.), *3rd Conf. on Mechanical Properties at High Rates of Strain*, Inst. Physics Conf. Series No. 70, Bristol & London, 1984, pp. 71.

147 Malatynski M. and J. Klepaczko, Int. J. Mech. Sci. 22, 1980, pp. 173.

148 Muller, T., J. Mech. Engr. Sci. 14, 1972, pp. 3.

149 Donnell, L. H. Trans. ASME, 52, 1930, pp. 153.

150 Kármàn Th., and P. Duwez, *The Propagation of Plastic Defamation in Solids*, J. Appl. Phys., 21, 1950, pp. 987.

151 Rakhmatulin, H. A., *On the Propagation of the Unloading Wave*, Prikl. Mat. Mekh., 9, 1945, pp. 91-100.

152 Bell, J. F., *Study of Initial Conditions in Constat Velocity Impact*, J. Appl. Phys., 31, 1960, pp. 2188.

153 Rakhmatulin, Kh, and Yu. A. Demyanov, *Strength under High Transient Loads*, Israel Program Of Scientific Translations, Jerusalem, 1966.

154 Malvern, L. E., In: N. J. Huffington, Jr. (ed.), *Behaviour of Materials under Dynamic Loading*, ASME, New York, 1955.

155 Hopkins, H. G., *Dynamic Expansion of Spherical Cavities in Metals*, In: I. N. Sneddon and R. Hill (eds.), *Progress in Solid Mechanics*, North-Holland Publ. Co., Amsterdam, 1960, pp. 85.

156 Cristescu, N., *Dynamic Plasticity*, North-Holland Publ. Co., Amsterdam, 1967.

157 Bell. J. F., Rept. No. 5, Dept. Mech. Eng., The Johns Hopkins University, Baltimore, 1951.

158 Sternglass, E. J. and D. A. Stuart, *An Experimental Study of the Propagation of Transient Longitudinal Deformation in Elasto-plastic Media*, J. Appl. Mech., 20, 1953, pp. 427-434.

159 Malyshev, B. M., J. Prikl. Mech. Tech. Fiz., 2, 1961, pp. 104.

160 Bianchi, G., *Some Experimental and Theoretical Studies on the Propagation of Longitudinal Plastic Waves in a Strain-rate-dependent Material,* In: H. Kolsky and W. Prager (eds.), *Stress Waves in Anelastic Solids*, Springer, Berlin, 1964, pp. 101.

161 Craggs, J. W., *The Propagation of Infinitesimal Plane Waves in Elastic-plastic Materials*, J. Mech. Phys. Solids, 5, 1957, pp. 115-124.

162 De Vault, G. P., J. Mech. Phys. Solids, 13, 1965, pp. 51.

163 Convery, E. and H. Ll. D. Pugh, *The Velocity of Torsional Waves in Metals Stressed Statically into the Plastic Range*, J. Mech. Eng. Sci., 10, 1968, pp. 153.

164 Yew, C. H. and H. A. Richardson, Jr., *The Strain Rate Effect and the Incremental Plastic Wave in Copper*, Exp. Mech., 9, 1969, pp. 366-373.

165 Duvall, G. E., In: P. G. Shewmon and V. F. Zackay (eds.), *Response of Metals to High Velocity Deformation*, Interscience, New York, 1961, pp. 165.

166 Taylor J. W., and M. H. Rice, *Elastic-plastic Properties of Iron*, J. Appl. Phys., 34, 1963, pp. 364-371.

167 Malvern, L. E., *The Propagation of Longitudinal Waves of Plastic Deformation in a Bar of Material Exhibiting a Strain Rate Effect*, J. Appl. Mech., 18, 1951, pp. 203-208.

168 Lubliner, J., *A Generalized Theory of Strain-rate Dependent Plastic Wave Propagation in Bars*, J. Mech. Phys. Solids, 12, 1964, pp. 59.

169 Nowacki, W. K., *Stress Waves in Non-elastic Solids*, Pergamon, Oxford, 1978.

170 Clifton, R. J., In: S. Nemat-Nasser (ed.), *Mechanics Today*, Vol. 1, Pergamon, New York, pp.102, 1974.

171 Craggs, J. W., *Plastic Waves*, In: I. N. Sneddon and R. Hill (eds.), *Progress in Solid Mechanics*, Vol. II, North Holland, Amsterdam, 1961, pp. 141-197.

172 Hunter, S. C., *Viscoelastic Waves*, In: I. N. Sneddon and R. Hill (eds.), *Progress in Solid Mechanics*, Vol. I, North Holland, Amsterdam, pp. 3, 1960.

173 Hopkins, H. G., *Progress in Applied Mechanics*, Macmillan, New York, 1963, pp. 55.

174 Campbell, J. D., *Dynamic Plasticity: Macroscopic and Microscopic Aspedts,* Mater. Sci. Eng., 12, 1973, pp. 3.

175 Chou, P. C. and A. K. Hopkins, *Dynamic response of materials to intense impulsive loading*, Air Force Materials Laboratory, Wright-Patterson AFB, Ohio.

176 Kolsky, H. and W. Prager, (ed.), *Stress Waves in Anelastic Solids*, Springer-Verlag, Berlin, 1964.

177 Atkins, A. G., J. Inst. Metals, 97, 1969, pp. 289.

178 Atkins A. G. and D. P. Porter, U. S. Steel Corp. Appl. Res. Lab. Rept., 1967.

179 Stevenson, M. G. and P. L. B. Oxley, Proc. Inst. Mech Engrs., 184, 1969-70, pp. 561.

180 Johnson, W. and R. A. C. Slater, *A Comparison of the Energy Required for Slow Speed and Dynamic Blanking Using an Improved Linear Motor, High-rate Forming,* Proc. Inst. Mech. Engrs., 179, 1964, pp. 257-263.

181 Davies, R. and S. M. Dhawan, *A Preliminary Investigation of High-speed Blanking and Piercing of Metals*, Proc. Inst. Mech. Engrs., 180, 1966, pp. 197.

182 Johnson, W. and F. W. Travis, Proc. Inst. Mech. Engrs., 180, 1966, pp. 197.

183 Dowling, A. R. and J. Harding, *1st Intern. Conf. of the Center for High Energy Forming*, Denver, 1967, Vol. 2, pp.731.

184 Rawlings, B., Proc. Roy. Soc. (London), A275, 1963, pp. 528.

185 Aspden, R. J. and J. D. Campbell, Proc. Roy. Soc. (London), A290, 1966, pp.266.

186 Parkes, E. W., Proc. Roy. Soc. (London), A228, 1955, pp. 462.

187 Bodner, S. R. and P. S. Symonds, *Plastic deformations in impact and impulsive loading of beams,* In: E. H. Lee and P. S. Symonds (eds.),

Plasticity, Proc. Second Symp. on Naval Structural Mechanics, Providence, Pergamon, Oxford, 1960, pp. 488-500.

188 Bodner, S. R. and P. S. Symonds, *Experimental and Theoretical Investigation of the Plastic Deformation of Canti-lever Beams Subjected to Impulsive Loading*, J. Appl. Mech., 29, 1962, pp. 719.

189 Rawlings, B., Intern. J. Mech. Sci., 9, 1967, pp. 633.

190 Kelly, J. M. and T. R. Wilshaw, Proc. Roy. Soc. (London), A306, 1968, pp. 435.

191 Griffith, A. A., Phil. Trans. Roy. Soc. London, A221, 1920, pp. 163.

192 Irwin, G. R., Encyclopedia of Physics, Springer, Berlin, 1958, Vol. 6, pp. 551.

193 Kenny, P. and J. D. Campbell, *Progress in Materials Science*, Pergamon, Oxford, 1968, pp. 135.

194 Kanninen, M. F., A. K. Mukherjee, A. R. Rosenfield and G. T. hahn, In: U. S. Lindholm (ed.), *Mechanical Behaviour of Materials under Dynamic Loads*, Sprinter, New York, 1968, pp. 96.

195 Cristescu, N., *A Procedure for Determining the Constitutive Equations for Materials Exhibiting Both Time-dependent and Time-independent Plasticity*, Int. J. Solids Structures, 8, 1972, pp. 511.

196 Nicholas, T., Air Force Materials Laboratory Report, AFML-TR-73-73, Wright-Patterson AFB, Ohio, 1973.

197 Sun, J. and M. S. J. Hashmi, *A Numerical Solution for Longitudinal Waves of Plastic Deformation in a Bar Struck by a High Speed Projectile*, 4th Int. Conf. on the Technology of Plasticity, Beijing, Sept. 1993.

198 Vinh, T., Afzali, M. and Roche, A. In: K. J. Miller and R. F. Smith (eds), *Mechanical Behaviour of Materials*, Proc. ICM 3, Pergamon Press, Oxford & New York, 1979, pp. 633.

199 Haque, M. M., *Stress-strain properties and micro-structural change in metal deformed at strain rates of up to 10^5 per second,* Ph. D thesis, Sheffield City Polytechnic, 1983.

200 Harding, J., *The Effect of High Strain Rate on Material Properties,* In: T. Z. Blazynski (ed.), *Materials at High Strain Rates*, Elsevier Applied Science, London & New York, 1987, pp. 133-186.

201 Ludwik, P., *Über den Einfluss der Deformations-geschwindigkeit bei bleibenden Deformationen mit besonderer berücksichtigung der Nachwirkungserscheinungen*, Physik. Z. 10, 1909, pp. 411-417.

202 Prandtl, L., *Ein Gedankenmodell zur kinetischen Theorie der festen Körper*, Z. Angew. Math. Mech. 8, 1928, pp. 85-106.

203 Malvern, L. E., *Plastic Wave Propagation in a Bar of Material Exhibiting a Strain Rate Effect*, Quart. Appl. Math. 8, 1951, pp. 405-411.

204 Sokolovskii, V. V., *Propagation of Elastic-viscoplastic Waves in Bars*, Dokl. Akad. Nauk SSSR 60, pp. 775-778.

205 Sokolovskii, V. V., *The Propagation of Elastic-visco-plastic Waves in Bars*, Prikl. Mat. Meh. 12. 1948, pp. 261-280.

206 Richter, H., Z. Angew. Math. Phys. 33, 1953, pp. 237-244.

207 Rubin, R. J., *Propagation of Longitudinal Deformation Waves in a Prestressed Rod of Material Exhibiting a Strain Rate Effect*, J. Appl. Phys. 25, 1954, pp. 528-531.

208 Ting T. C. T. and P. S. Symonds, *The Plastic Deformation of a Cantilever Beam with Strain-rate Sensitivity under Impulsive Loading*, J. Appl. Mech. 31. Ser. E, 1964, pp. 38-42.

209 Gilman, J. J., *Physical Nature of Plastic Flow and Fracture*, In: E. H. Lee and P. S. Symonds (eds.), *Plasticity*, Proc. Second Symp. on Naval Structural Mechanics, Providence, 1960, pp. 44-99.

210 Fan, L., Acta Mech. Sinica, 7, 1964, pp. 63-80.

211 Lindholm, U. S., *Some Experiments with the Split Hopkinson Pressure Bar*, J. Mech. Phys. Solids 12, 1964, pp. 317-335.

212 Plass, J. J. Jr. and N. M. Wang, Proc. 4th Midwest Conf. on Solid Mech., pp. 33

213 Kotliarevskii, V. A., J. Prikl. Mech. Tech. Fiz. 6, 1961, pp. 145-152.

214 Kotliarevskii, V. A., J. Prikl. Mech. Tech. Fiz. 3, 1962, pp. 81-87.

215 Lenskii V. S. and M. A. Tarasova, Vestn. Mosk. Univ., 12, 1959, pp. 133-136.

216 Sokolov, L. D., Dokl, Akad. Nauk SSSR 67, 1949, pp. 459-462.

217 Campbell, J. D., A. M. Eleiche and M. M. C. Tsao, In: *Fundamental Aspects of Structural Alloy Design*, Plenum Publishing Corp. New York, 1977, pp. 545-563.

218 Hashmi, M. S. J. and M. M. Haque, *High Strain Rate Properties of an Aluminium Alloy and High Purity Copper at Room Temperature, Int. Conf. of Metal under Dynamics Loading*, 1986, pp. 637-649.

219 Perzyna, P., Arch. Mech. Stos. 15, 1963, pp. 113-130.

220 Béta, G., Acta Tech. Acad. Sci. Hung. 38, 1962, pp. 161-187.

221 Cristescu, N., *On the Propagation of Elastic-plastic Waves in Metallic Rods*, Bull. Acad. Pol. Sci., 11, 1963, pp. 129.

222 Béta, G., *Differentialgleichungen der möglichen Stoffgesetze des dynamischen plastischen Zuges*, Publ. of the Techn. University for Heavy Industry, Miskolc, Hungary, Vol. 25, 1965, pp. 197-204.

223 Lubliner, J., *The Strain-rate Effect in Plastic Wave Propagation*, J. Mécan. 4, 1965, pp. 111-120.

224 Larina, T. B., Izv. Akad. Nauk SSSR, Mehanika, No. 4, 1965, pp. 200.

225 Zener, C. and J. H. Holloman, J. Appl. Phys., 15, 1944, pp. 22.

226 Vinh, T. and Khalil, T. In: J. Harding (ed.), *Mechanical Properties at High Rates of Strain*, Institute of Physics, Bristol and London, 1984, pp. 39.

227 Johnson, G. R. and Cook, W. H., In: Proc. 7th Int. Symp. on Ballistics, The Hague, The Netherlands, 1983, pp. 541.

228 Zerilli, F. J. and Armstrong, R. W., J. Appl. Phys. 61, No. 5, 1987, pp. 1816-1825.

229 Harding, J., *The Development of Constitutive Relationships for Material Behaviour at High Rates of Strain*, Inst. Conf. Mech. Prop. Materials at High Strain Rates of Strain, Oxford, 1989, pp. 189-203.

230 Lindholm, U. S., In: *High Velocity Deformation of Solids*, IUTAM Symp., University of Tokyo, 1977, pp. 26.

231 Huang, S. and R. J. Clifton, In: *Macro and Micro-mechanics of High Velocity Deformation and Fracture*, IUAAM Symp., Science Council of Japan, Tokyo, 1985.

232 Murr, L. E., *Metallurgical Effects of Shock and High-strain Rate Loading*, In: Blazynski, T. Z. (ed.), *Materials at High Strain Rates*, Elsevier Applied Science, London, 1987, pp. 1-46.

233 Ashby, M. F. and Frost, H. J. In: *Frontiers in Materials Science: Distinguished Lectures*, L. E. Murr and C. Stein, (ed.), Marcel Dekker, New York, 1976, Chap. 11, pp. 391.

234 Hashmi, M. S. J., Sheffield City Polytechnic, Report No. SCP/MPE/R-106, Oct. 1978.

235 Campbell, J. D. and R. H. Cooper, *Physical Basis of Yield and Fracture*, Institute of Physics and Physical Society, London, 1966, pp. 77.

236 Symonds, P. S., *Survey of Methods of Analyzing for Plastic Deformation of Structures under Dynamic Loadings*, Brown University, Report BU/NSRDC/1-67, 1967.

Appendix I. List of Figures

Fig. 1 Arrangement of projectile, specimen and anvil. 27

Fig. 2 Diagram for governing equilibrium equation. 28

Fig. 3 A bar with a fixed end struck by a moving mass at the other end. 31

Fig. 4 Idealized schematic view of a shock pulse travelling through a solid material. 35

Fig. 5 Characteristic field for floating boundaries. 38

Fig. 6 Characteristic line showing leading wave front and interior mesh points. 39

Fig. 7 Characteristic field for fixed boundary. 45

Fig. 8 The regressed stress, strain and plastic strain-rate surface for copper at the room temperature based on data in [33]. 47

Fig. 9 The initial variations of stress with respect to the time and positions. 50

Fig. 10 The process of the variation of stress at fixed cross sections of the specimen. 51

Fig. 11 Dynamic stress-strain at fixed cross sections of the specimen. 51

Fig. 12 Variations of velocity with respect to the time and positions within the specimen. 52

Fig. 13 Variation of particle velocity at the fixed cross-sections. 52

Fig. 14 Variation of true strain rate at fixed cross sections of the specimen. 53

Fig. 15 Variation of strain with respect to the time and positions within the specimen. 53

Fig. 16 Variation of strain at the fixed cross-sections. 54

Fig. 17 Variation of displacement at fixed cross sections of the specimen. 54

Fig. 18 Variation of the stress with the time at x=0 at various T_0. 57

Fig. 19 Variation of the stress with the strain at x=0 at various T_0. 58

Fig. 20 Variation of the velocity with the time at x=0 at various T_0. 58

Fig. 21 Variation of the peak stress with T_0 at x=0. 59

Fig. 22 Variation of the strain with the time at x=0 at various T_0. 59

Fig. 23 Variation of the temperature with the time at x=0 at various T_0. 60

Fig. 24 Variation of the deformation with the time at x=0 at various T_0. 60

Fig. 25 Variation of the plastic strain rate with times at x=0 at various T_0. 61

Fig. 26 Variation of the plastic strain rate with times at x=0 around the peak at various T_0. 61

Fig. 27 Variation of the plastic strain rate with the strain at x=0 around the peak at various T_0. 62

Fig. 28 Variation of stresses with times at x=0 at various initial lengths of specimens. 63

Fig. 29 Variation of strains with times at x=0 at various initial lengths of specimens. 64

Fig. 30 Variation of stresses with strains at x=0 at various initial lengths of specimens. 64

Fig. 31 Variation of plastic strain rates with times at x=0 at various initial lengths of specimens. 65

Fig. 32 Variation of plastic strain rates with times at x=0 around the peak at various initial lengths of specimens. 65

Fig. 33 Variation of plastic strain rates with strains at x=0 at various initial lengths of specimens. 66

Fig. 34 Variation of deformation with times at x=0 at various initial lengths of specimens. 66

Fig. 35 Variation of velocities with times at x=0 at various initial lengths of specimens. 67

Fig. 36 Variation of the temperature with the strain at x=0 at various initial lengths of specimens. 67

Fig. 37 Variation of stresses with times at x=0 at various initial velocities of the projectile. 69

Fig. 38 Variation of strains with times at x=0 at various initial velocities of the projectile. 69

Fig. 39 Variation of stresses with strains at x=0 at various initial velocities of the projectile. 70

Fig. 40 Variation of velocities with times at x=0 at various initial velocities of the projectile. 70

Fig. 41 Variation of deformation with times at x=0 at various initial velocities of the projectile. 71

Fig. 42 Variation of plastic strain rates with times at x=0 at various initial velocities of the projectile. 71

Fig. 43 Variation of plastic strain rates with times at x=0 around the peak at various initial velocities of the projectile. 72

Fig. 44 Variation of plastic strain rates with strains at x=0 at various initial velocities of the projectile. 72

Fig. 45 Variation of temperatures with strains at x=0 at various initial velocities of the projectile. 73

Fig. 46 Variation of stresses with times at x=0 at various dimensions [D (mm) × L (mm)] of specimens. 74

Fig. 47 Variation of strains with times at x=0 at various dimensions [D (mm) × L (mm)] of specimens. 75

Fig. 48 Variation of stresses with strains at x=0 at various dimensions [D (mm) × L (mm)] of specimens. 75

Fig. 49 Variation of velocities with times at x=0 at various dimensions [D (mm) × L (mm)] of specimens. 76

Fig. 50 Variation of deformation with times at x=0 at various dimensions [D (mm) × L (mm)] of specimens. 76

Fig. 51 Variation of plastic strain rates with times at x=0 at various dimensions [D (mm) × L (mm)]of specimens. 77

Fig. 52 Variation of plastic strain rates with times at x=0 at various dimensions [D (mm) × L (mm)]of specimens. 77

Fig. 53 Variation of plastic strain rates with strains at x=0 at various dimensions [D (mm) × L (mm)] of specimens. 78

Fig. 54 Variation of the temperature with the strain at x=0 at various dimensions [D (mm) × L (mm)] of specimens. 78

Fig. 55 The characteristic field at the interface between the specimen and the anvil. 81

Fig. 56 The view of 50 kN Instron Universal Material Testing Machine. 83

Fig. 57 The diagram of chamber used for quasi-static compressive test at high temperature. 86

Fig. 58 Quasi-static stress-strain curves of commercially pure copper at various temperatures. 88

Fig. 59 Quasi-static stress-strain curves of mild steel at various temperatures. 88

Fig. 60 The regression surface of the quasi-static stress-strain relation at various temperatures for commercially pure copper based on Eq. (77). 89

Fig. 61 Comparison of quasi-static stress-strain curves between the experimental results and the regressed expression based on Eq. (77) at various temperatures. 90

Fig. 62 The regression of the quasi-static stress-strain curves at various temperatures for commercially pure copper based on Eq. (79). 91

Fig. 63 The regressive curves of the quasi-static stress-strain relation at various temperatures for commercially pure copper based on Eq. (81) and Table 2. 92

Fig. 64 The regressive curves of the quasi-static stress-strain relation at various temperatures for commercially pure copper based on Eqs. (81) and (82). 93

Fig. 65 Comparison of the quasi-static stress-strain relations obtained by the experiment with based on Eq. (83) and Table 3 at 20 °C for mild steel. 94

Fig. 66 Comparison of the quasi-static stress-strain relations obtained by the experiment with based on Eq. (83) and Table 3 at 200 °C for mild steel. 94

Fig. 67 Comparison of the quasi-static stress-strain relations obtained by the experiment with based on Eq. (83) and Table 3 at 360 °C for mild steel. 95

Fig. 68 Comparison of the quasi-static stress-strain relations obtained by the experiment with based on Eq. (83) and Table 3 at 520 °C for mild steel. 95

Fig. 69 The view of the ballistic test machine. 97

Fig. 70 Schematic diagram of the ballistic test machine. 98

Fig. 71 Schematic diagram of the loading unit of the ballistic test machine. 99

Fig. 72 The chamber unit used for impact compressive test at high temperatures. 100

Fig. 73 The relationship of heat loss with time for the impact chamber. 101

Fig. 74 The chamber used for static and dynamic tests at high temperatures. 104

Fig. 75 The anvil used for impact and static tests at high temperatures. 105

Fig. 76 The shield ring used to fix the anvil. 106

Fig. 77 The lip used for the impact test of $\phi 6\times 6$ specimen. 107

Fig. 78 The flange used to fix the shield box with the rig. 108

Fig. 79 The projectile used for high velocity impact tests. 109

Fig. 80 The view of shield box. 110

Fig. 81 The calibrating curve of the velocity of the projectile with the pressure in the solenoid valve. 112

Fig. 82 Typical pure copper specimen, before and after dynamic test. 114

Fig. 83 Typical mild steel specimen, before and after dynamic test. 115

Fig. 84 The height reduction of the specimen impacted by a projectile at various velocities for commercially pure copper. 116

Fig. 85 The diameter increment of the specimen impacted by a projectile at various velocities for commercially pure copper. 116

Fig. 86 The height reduction of the specimen impacted by a projectile at various velocities for mild steel. 117

Fig. 87 The diameter increment of the specimen impacted by a projectile at various velocities for mild steel. 117

Fig. 88 Strain-rate dependence of flow stress at very high strain rates for annealed mild steel. 130

Fig. 89 The temperature rise with respect to time at the impact end of the for pure copper specimen at room temperature at various initial velocities of the projectile. 135

Fig. 90 The temperature rise with respect to the initial velocity of the projectile at the impact end of a $\phi 5 \times 5$ (mm) pure copper specimen at room temperature. 136

Fig. 91 Comparison of the stresses to time at the impact end of the specimen based on temperature dependent and independent constitutive relations at the initial speeds of the projectile of 40 m/s and 80 m/s. 136

Fig. 92 Comparison of the stresses at the impact end of the specimen with time based on temperature dependent and independent constitutive relations at the initial speeds of the projectile of 60 m/s and 100 m/s. 137

Fig. 93 Comparison of the dynamic strain at the impact end of the specimen with regard to time based on temperature dependent and independent constitutive relations at various initial speeds of the projectile. 137

Fig. 94 Comparison of deformation of the specimen at the impact end with regard to time based on temperature dependent and independent constitutive relations at various initial impact velocities of the projectile. 138

Fig. 95 Comparison of the deformation of the specimen at the impact end with regard to initial impact velocities of the projectile based on temperature dependent and independent constitutive relations. 138

Fig. 96 Variation of the deformation of the impacted copper specimen with respect to the initial velocity of the projectile at various shock accelerations at room temperature. 140

Fig. 97 Variation of the final deformation of the impacted copper specimen with respect to the initial velocity of the projectile at various shock durations at room temperature. 140

Fig. 98 Comparison of deformation of the specimen based on the form (129) and the values in Table 6 with the experiment at various temperatures. 144

Fig. 99 Stress-strain curves for pure copper based on the form (129) and the values in Table 6 at 20 °C. 144

Fig. 100 Stress-strain curves for pure copper based on the form (129) and the values in Table 6 at 200 °C. 145

Fig. 101 Stress-strain curves for pure copper based on the form (129) and the values in Table 6 at 360 °C. 145

Fig. 102 Stress at a constant strain versus strain rate for pure copper based on the form (129) and the values in Table 6 at 20 °C. 146

Fig. 103 Stress at a constant strain versus strain rate for pure copper based on the form (129) and the values in Table 6 at 200 °C. 146

Fig. 104 Stress at a constant strain versus strain rate for pure copper based on the form (129) and the values in Table 6 at 360 °C. 147

Fig. 105 Comparison of deformation of the specimen based on the form (130) and the values in Table 7 with the experiment at various temperatures. 148

Fig. 106 Stress-strain curves for pure copper based on the form (130) and the values in Table 7 at 20 °C. 149

Fig. 107 Stress-strain curves for pure copper based on the form (130) and the values in Table 7 at 200 °C. 149

Fig. 108 Stress-strain curves for pure copper based on the form (130) and the values in Table 7 at 360 °C. 150

Fig. 109 Stress at a constant strain versus strain rate for pure copper based on the form (130) and the values in Table 7 at 20 °C. 150

Fig. 110 Stress at a constant strain versus strain rate for pure copper based on the form (130) and the values in Table 7 at 200 °C. 151

Fig. 111 Stress at a constant strain versus strain rate for pure copper based on the form (130) and the values in Table 7 at 360 °C. 151

Fig. 112 Temperature and strain-rate dependence of the stress at $\varepsilon=0.05$ of pure copper based on the form (130) and the values in Table 7. 152

Fig. 113 Temperature and strain-rate dependence of the stress at $\varepsilon=0.10$ of pure copper based on the form (130) and the values in Table 7. 152

Fig. 114 Temperature and strain-rate dependence of the stress at $\varepsilon=0.20$ of pure copper based on the form (130) and the values in Table 7. 153

Fig. 115 The comparison of deformation of mild steel specimens based on the Eq. (131) and Table 8 with the experiment at various temperatures. 155

Fig. 116 Stress-strain curves for mild steel based on Eq. (131) and the values in Table 8 at 20 °C. 155

Fig. 117 Stress-strain curves for mild steel based on Eq. (131) and the values in Table 8 at 220 °C. 156

Fig. 118 Stress-strain curves for mild steel based on Eq. (131) and the values in Table 8 at 440 °C. 156

Fig. 119 Stress at a constant strain versus strain rate for mild steel based on Eq. (131) and the values in Table 8 at 20 °C. 157

Fig. 120 Stress at a constant strain versus strain rate for mild steel based on Eq. (131) and the values in Table 8 at 220 °C. 157

Fig. 121 Stress at a constant strain versus strain rate for mild steel based on Eq. (131) and the values in Table 8 at 440 °C. 158

Fig. 122 Temperature and strain-rate dependence of the stress at ε=0.02 of mild steel based on Eq. (131) and the values in Table 8. 158

Fig. 123 Temperature and strain-rate dependence of the stress at ε=0.05 of mild steel based on Eq. (131) and the values in Table 8. 159

Fig. 124 Temperature and strain-rate dependence of the stress at ε=0.10 of mild steel based on Eq. (131) and the values in Table 8. 159

Fig. 125 Comparison of the dynamic stress sensitivities at ε=0.1 for pure copper material at room temperatures, 1. ref. [19]; 2. ref. [33]; 3. ref. [234]; 4. Based on Eq. (129) and Table 6; 5. Based on Eq. (130) and Table 7; 6. ref. [31]; 7. ref. [218]. 163

Fig. 126 Comparison of the dynamic stress sensitivities for mild steel at lower yield stress point, 1. ref. [30]; 2. ref. [235]; 3. ref. [183]; 4. ref. [60] (ε=0.01); 5. Based on Eq. (134) and Table 8 (ε=0.02); 6. ref. [31]; 7. ref. [236]. 164

Fig. 127 Comparison of dynamic stress sensitivities for mild steel at 220 °C and 440 °C, 1. Based on Eq. (134) and Table 8 at ε=0.05; 2. ref. [31] at lower yield stress point. 165

Appendix II. Program of Conversion of Data

By Jian Sun, 10 October 1990

```
C       D0,H0,X(I),(mm); Y(I),(kN); STRESS(I),(MPa).
        DIMENSION X(40),Y(40),STRESS(40),STRAIN(40)
        CHARACTER FILE_N*8,FILE_D*20,FILE_R*20
        WRITE(6,10)
        READ(*,'(A8)') FILE_N
 10     FORMAT(' The Name of File =')
        FILE_D(1:8)=FILE_N
        FILE_D(9:12)='.DAT'
        FILE_R=FILE_N
        FILE_R(9:12)='.RES'
        OPEN (5,FILE=FILE_D,STATUS='OLD')
        OPEN (6,FILE=FILE_R,STATUS='NEW')
        READ (5,*) N, D0,H0
        V0=3.1415926*D0*D0/4*H0
        DO 50 I=1, N
        READ (5,*) X(I),Y(I)
 35     FORMAT (2F8.3)
 50     CONTINUE
        STRESS(1)=0.
        STRAIN(1)=0.
        DO 60 I=2,N
        STRESS(I)=(H0-X(I))*Y(I)/V0*1000
 60     STRAIN(I)=LOG(H0/(H0-X(I)))
 45     FORMAT (I4)
        DO 70 I=1,N
        WRITE (6,55) STRAIN(I),STRESS(I)
 55     FORMAT (2E10.3)
 70     CONTINUE
        CLOSE (5)
        CLOSE (6)
        END
```

Appendix III.
Program for the Drawing of Curves

By Jian Sun, 7 May 1990

```
#include <graphic.h>
#if TCQ
extern unsigned _stklen=6144;
#endif
float x[150], y[150], xn[600], yn[600], x1[2], y1[2], sfact, xw0,
      xw1, yw0, yw1;
float lheight, cheight, wleft, d0, h0, ingin1, ingin2, inheight1,
      inheight2;
float xleg, yleg, wspeed;
char  title[90], xaxisn[30], yaxisn[30], tkf[20], datf[10][20], diti[50];
char  typ, tkfsert[20], str1[20];
int   i, j, k, nxdiv, nydiv, isgrid, n1, n2, n[20], m[20], iscross,
      frameon, ftick, load;
int   fisgrid, fnxdiv, fnydiv, wkind;
static char *symbstyle[]={"", "6", "0", "1", "5", "7", "2", "3", "4"};
static char *linstyle[]={"", "solid", "ldot", "finedot", "dash", "dot",
       "chndsh", "solid", "ldot", "finedot", "dash", "dot"};
static int colour[]={0,1,4,3,2,6,5,7,8,9,10,11,12,13,14,15};
main()
{
  style();
  input();
  curtyp();
  txyname();
  bgnplot(1,'g',tkf);
  startplot(8);
  font(4,"complex.fnt",'\310',"triplex.fnt",'\311',"block1.fnt",
  '\312',"compgrma.fnt",'\313');
  page(9.0,6.855);
  area2d(6.2,4.0);
  cross(iscross);
    if(k==1)
    window(xw0,yw0,xw1,yw1);
    else
    linestyle();
  frame(frameon,ftick);
  fgrid(fisgrid,fnxdiv,fnydiv);
  grid(isgrid);
  upright(1);
  color(2);
  xymax(x1,y1);
  scales(nxdiv,nydiv,x1,y1,2);
  color(5);
  xname(xaxisn);
  yname(yaxisn);
  if(typ=='P'||typ=='E')
    {
      for(i=0;i<k;i++)
```

```
        {
        curve(&x[n[i]],&y[n[i]],(n[i+1]-n[i]),-1);
        }
      }
    for (i=0;i<k;i++)
    {
    color(colour[i]);
    curve(&xn[m[i]],&yn[m[i]],(m[i+1]-m[i]),0);
    }
    intest();
    endplot();
    if(k==1) windows();
    stopplot();
}

style()
{
 FILE *style;
 style=fopen("stylem.typ","r");
 fscanf(style,"%d %d %f",&load,&wkind,&wspeed);
 fscanf(style,"%d %d %f\n",&n1,&n2,&sfact);
 fscanf(style,"%d %d\n",&nxdiv,&nydiv);
 fscanf(style,"%d\n",&isgrid);
 fscanf(style,"%d %d %d",&fisgrid,&fnxdiv,&fnydiv);
 fscanf(style,"%d\n",&iscross);
 fscanf(style,"%d %d\n",&frameon,&ftick);
 fscanf(style,"%f %f %f %f\n",&xw0,&yw0,&xw1,&yw1);
 fscanf(style,"%f %f %f\n",&cheight,&lheight,&wleft);
 fscanf(style,"%f %f",&xleg,&yleg);
 fscanf(style,"%f %f %f %f\n",&ingin1,&inheight1,&ingin2,&inheight2);
 fclose(style);
}

input()
{
 char ext[20],ch,noo[1];
 FILE *in,*out;
 float v0,x0,x1,a0;
 float pi=3.1415926;
 n[0]=0 ; k=0;
 out=fopen("exam.chk","w");
 do {
        k+=1;
        puts("\nThe name of data file ? ");
        scanf("%s",datf[k]);
        if (datf[k]!=NULL)
        {
           strcpy(ext,datf[k]);
           strcat(ext,".dat");
           in=fopen(ext,"r");
           fscanf(in,"%d\n",&n[k]);
           if (n[k]==NULL)
             {
              k-=1;
              printf ("No this file in default directory,type again.\n");
```

```
            }
         else
            {
            strcpy(tkf,datf[k]);
            fscanf(in,"%f %f %f\n",&d0,&h0,&x0);
            v0=pi*d0*d0/4*h0;
            a0=pi*d0*d0/4;
            n[k]+=n[k-1];
            fprintf(out,"n[%d]=%d n[%d]=%d\n",k-1,n[k-1],k,n[k]);
            for (i=n[k-1];i<n[k];i++)
            {  fscanf(in,"%f %f\n",&x[i],&y[i]);
            if (load==0)              /*deformation*/
             x[i]=x[i]-x0;
            if (load<0)               /*engineering stress*/
            {
            x[i]=(x[i]-x0)/h0;
            y[i]=y[i]/a0;
            }
            if(load>0)                /*true stress*/
            {
               x1=h0-x[i]+x0;
               y[i]=y[i]*x1/v0*1000;
               x[i]=log(h0/x1);
             }
               fprintf(out,"%d %f %f\n",i,x[i],y[i]); }
             }
         fclose(in);
        }
        printf("Press 'Q' to END data input,any other key to continue:");
 } while ((ch=getch())!='Q');
      fclose(out);
 if(k>1)
   {
   gets(noo);
   puts("\nThe number of figure?");
   gets(tkf);
   }
}

xymax(float x1[],float y1[])
{
 float xm,ym;
 int ix,iy;
 xm=0.;
 ym=0.;
  for (i=0;i<(k*n1);i++)
    {
     if (xm<xn[i])
        xm=xn[i];
     if (ym<yn[i])
        ym=yn[i];
     }
  x1[0]=0;y1[0]=0;
  y1[1]=ym;x1[1]=xm;
}
```

```
curtyp()
{
 FILE *chk;
 printf("\n\nChoose the type of your curves:");
 printf("\n\n'S'  Using cubic spline to smooth the curve(s);");
 printf("\n'E'  Using cubic spline and their specimen points;");
 printf("\n'R'   Using the weighted linear regression;");
 printf("\n'P'     Drawing the regressive curves and their specimen
points;");
 printf("\n Any other key for normal curves:");
      typ=getch();
      switch(typ)
      {
   case'R':
   case'P':
      chk=fopen("chk.chk","w");
      m[0]=0;
      for (i=0;i<k;i++)
       {
      rfit(&x[n[i]],&y[n[i]],(n[i+1]-n[i]),n2,
      sfact,n1,&xn[i*n1],&yn[i*n1]);
      m[i+1]=(i+1)*n1;
      fprintf(chk,"%d\n",(i+1)*n1);
      for (j=i*n1;j<(i+1)*n1;j++)
      fprintf(chk,"%f %f\n",xn[j],yn[j]);
       }
      fclose(chk);
      break;
   case'S':
   case'E':
      chk=fopen("chk.chk","w");
      m[0]=0;
      for(i=0;i<k;i++)
      {
      spline (&x[n[i]], &y[n[i]], (n[i+1]-n[i]), n1,
      1.0e30, 1.0e30, &xn[i*n1], &yn[i*n1]);
      m[i+1]=(i+1)*n1;
      fprintf(chk,"%d\n",(i+1)*n1);
      for (j=i*n1;j<(i+1)*n1;j++)
      fprintf(chk,"%f %f\n",xn[j],yn[j]);
       }
      fclose(chk);
       break;
  default:
      m[0]=0;
      for (i=0;i<k;i++)
      {
         m[i+1]=n[i+1];
         for (j=n[i];j<n[i+1];j++)
          {
          xn[j]=x[j];
          yn[j]=y[j];
          }
      }
      break;
```

```
     }
}

txyname()
{
 char tfnt[25],xfnt[25],yfnt[25],ch;
 if(load==0)
       {

       strcpy(diti,"\311Fig.");
       strcat(diti,tkf);
       strcat(diti,"  Quasi-static compression test");
       strcpy(xaxisn,"\311Deformation \313D\312h (mm)");
       strcpy(yaxisn,"\311Load P (KN)");
       if(k==1)
       strcpy(title,"\312|15|Load |3|- |12|Deformation |4|Curve");
       else
       strcpy(title,"\312|15|Load |12|- |9|Deformation |4|Curves");
       }
 if(load>0)
       {

       strcpy(diti,"\311Fig.");
       strcat(diti,tkf);
       strcat(diti,"  Quasi-static compression test");
       strcpy(xaxisn,"\313e\311 Ln(Ho/H)");
       strcpy(yaxisn,"\313s\311 (MN/M[2])");
       if(k==1)
       strcpy(title,"\312|4|True |12|Stress|9|-|3|Strain |15|Curve");
       else
       strcpy(title,"\312|4|True |12|Stress|9|-|3|Strain |15|Curves");
       }
 if(load<0)
       {
      strcpy (diti,"\311Fig.");
      strcat (diti,tkf);
      strcat (diti,"  Quasi-static compression test");
      strcpy (xaxisn,"\313e");
      strcpy (yaxisn,"\313s\311 (MN/M[2])");
      if(k==1)
      strcpy  (title,"\311|12|Engineering  |9|Stress|3|-|4|Strain  |15|
      Curve" );
      else
      strcpy   (title,   "\311|12|Engineering   |9|Stress|4|-|3|Strain
      |15|Curves");
       }
}
 windows()
 {
      char specimen[30], diameter[30], height[30], bufd[10], bufh[10],
      bufv[10], speed[30];
      strcpy(specimen,"\311Test No: ");
      strcat(specimen,tkf);
      strcpy(diameter,"\311Diameter: \311");
      gcvt(d0,5,bufd);
```

```
      strcat(diameter,bufd);
      strcat(diameter," \311(mm)");

      strcpy(height,"\310Height: \310");
      gcvt(h0,5,bufh);
      strcat(height,bufh);
      strcat(height," \310(mm)");
      strcpy(speed,"\310Test speed:");
      gcvt(wspeed,3,bufv);
      strcat(speed,bufv);
      strcat(speed,"(mm/min)");
      startplot(1);
      color(0);
      box();
      tfont(1);
      color(1);
      setscale(1);
      tmargin(0.5);
      if (wkind==0) ctline("\311  MILD STEEL ",cheight);
      else
      {
      if (wkind>0)   ctline("\311  PURE COPPER ",cheight);
      else
      ctline("\311  STAINLESS STEEL",cheight);
      }
      linesp(2.5);
      lmargin(wleft);
      ltline(specimen,lheight);
      linesp(2.2);
      ltline(speed,lheight);
      linesp(2.2);
      ltline(diameter,lheight);
      linesp(2.2);
      ltline(height,lheight);
      setscale(0);
  endplot();
 }

intest()
{
  tfont(1.5);
  color(2);
  tmargin(ingin1);
  color(15);
  ctline(title, inheight1);
  tmargin(ingin2);
  color(14);
  ctline(diti, inheight2);
}

linestyle()
{
  legpos(k,xleg,yleg);
  for(i=1;i<=k;i++)
{
```

```
  if(typ=='E'||typ=='P')
  legend(0,datf[i],symbstyle[i],.2,colour[i-1]);
  else
  legend(1,datf[i],linstyle[i],.2,colour[i-1]);
}
}
```

Appendix IV.
Program for Numerical Solution of Plastic Wave

By Jian Sun, 29 March 1992

```
C*********************************************************************
C            PROGRAM OF FINITE DIFFERENCE OF EXPLICIT IMPACT
C*********************************************************************
      COMMON NELEM,NCONT(0:500),PLETH,PMODL,PPEXP,PCOFB,PYILD,PBROK,
     . TLIMIT,SWITCH,PDESY,PVELO,XLETH(0:20000),TIME(0:20000),
     . STRAN(0:20000),STRES(0:20000),VELOY(0:20000),DEFOM(0:20000)
C** INPUT THE INITIAL DATE
      CALL DINPUT (PDAMT,PPMAS,NUMBR,JSTEP,NTP)
C** SOLVE THE EQUATION OF STRAIN
      CALL EQUATN(NUMBR,NTP,N0I,PDAMT,PPMAS)
C** OUTPUT THE RESULTS
      CALL OUTPUT(N0I,NUMBR,JSTEP)
      STOP
      END


      SUBROUTINE DINPUT (PDAMT,PPMAS,NUMBR,JSTEP,NTP)
C*********************************************************************
C              INIATIAL INPUT AND CALCULATION OF PARAMETERS
C*********************************************************************
      COMMON NELEM,NCONT(0:500),PLETH,PMODL,PPEXP,PCOFB,PYILD,PBROK,
     . TLIMIT,SWITCH,PDESY,PVELO,XLETH(0:20000),TIME(0:20000),
     . STRAN(0:20000),STRES(0:20000),VELOY(0:20000),DEFOM(0:20000)
      CHARACTER TITLE*20
      OPEN (5,FILE='BOND.DAT',STATUS='OLD')
      OPEN (10,FILE='BOND.RES',STATUS='NEW')
      READ(5,330) TITLE
  330 FORMAT(A40)
      WRITE(10,340) TITLE
  340 FORMAT(//,5X,10A4)
      READ (5,*) NELEM,NUMBR,JSTEP,NTP
      WRITE(10,301) NELEM,NUMBR,JSTEP,NTP
  301 FORMAT (/'NELEM =',I4/
     . 'THE PARAMETER OF OUTPUT STEP LENGTH NUMBR=',I4/
     . 'THE PARAMETER OF OUTPUT STEP LENGTH JSTEP =',I4/
     . 'THE NUMBER OF TIME PERIOD =',I4)
C *** READ THE SPECIMEN DIMENSIONS AND THE PROPERTY PARAMETERS.
      READ (5,*) SWITCH,PDAMT,PLETH,PMODL,PYILD,PBROK,TLIMIT,PPEXP,
     . PCOFB,PDESY
      WRITE (10,303)
      WRITE (10,305) PDAMT,PLETH,PMODL,PYILD,PBROK,TLIMIT,PPEXP,
     .PCOFB,PDESY
  304 FORMAT(3F12.2)
  303 FORMAT(/5X,'INITIAL AND PROPERTY PARAMETERS'/)
  305 FORMAT('THE INITIAL DIAMETER= ',F12.4,'(m)'/
     .'THE INITIAL LENGTH  L=    ',F14.4,'(m)'/
     .'THE YOUNG'S MODULUS E=    ',E14.4,'(N/m²)'/
     .'STATIC YIELD STRESS σ0=   ',E14.4,'(N/m²)'/
```

```
     .'STATIC BREAKING STRESS σ1= ',E14.4,'(N/m²)'/
     .'TIME CONSTANAT OF SHOCK T=',E14.4,'(Sec)'/
     .'CONST.   EXPONENT P =',E14.4/
     .'CONST. COEFFICIENT B=',E14.4/
     .'DENCITY OF SPECIMEN =',E14.4,'(Kg/m³)'/)
C *** READ THE PROJECTILE PARAMETERS.
      READ(5,*) PVELO,PPMAS
      WRITE(10,311)PVELO,PPMAS
  311 FORMAT('INITIAL VELOCITY OF PROJECTILE=',F12.4,'(m/s)'/
     .'THE MASS OF PROJECTILE       =',F12.4,'(Kg)')
      CLOSE(5)
      RETURN
      END

      SUBROUTINE INITIAL(DVEC0,DTIME)
C*********************************************************************
C                         THE INITIAL CONDITIONS
C*********************************************************************
      COMMON NELEM,NCONT(0:500),PLETH,PMODL,PPEXP,PCOFB,PYILD,PBROK,
     . TLIMIT,SWITCH,PDESY,PVELO,XLETH(0:20000),TIME(0:20000),
     . STRAN(0:20000),STRES(0:20000),VELOY(0:20000),DEFOM(0:20000)
      IF (TLIMIT .NE. 0.) THEN
      DO 100 J=0,NELEM
      STRES(J)=0.
      STRAN(J)=0.
      VELOY(J)=0.
      TIME(J)=J*DTIME
      XLETH(J)=DVEC0*TIME(J)
      DEFOM(J)=0.
 100  CONTINUE
      ELSE
      DO 200 J=0,NELEM
      VELOY(J)=PVELO
      STRES(J)=-PVELO*SQRT(PMODL*PDESY)
      STRAN(J)=STRES(J)/PMODL
      TIME(J)=J*DTIME
      XLETH(J)=DVEC0*TIME(J)
 200  CONTINUE
      END IF
      RETURN
      END

      SUBROUTINE EQUATN(NUMBR,NTP,N0I,PDAMT,PPMAS)
C*********************************************************************
C                      THE SOLUTION OF THE EQUATION
C*********************************************************************
      COMMON NELEM,NCONT(0:500),PLETH,PMODL,PPEXP,PCOFB,PYILD,PBROK,
     . TLIMIT,SWITCH,PDESY,PVELO,XLETH(0:20000),TIME(0:20000),
     . STRAN(0:20000),STRES(0:20000),VELOY(0:20000),DEFOM(0:20000)
      DVEC0=SQRT(PMODL/PDESY)
      DLOC0=PDESY*DVEC0
      DLETH=PLETH/NELEM
      DTIME=DLETH/DVEC0
      DPMAS=PPMAS*4./3.1415926/PDAMT/PDAMT
      NPEAK=0
```

```
      OPEN (10,FILE='BOBO.RES',STATUS='NEW')
      CALL INITIAL(DVEC0,DTIME)
      I=0
      NCONT(0)=0
      WRITE(10,205)
 205  FORMAT(//'   I   J      TIME(µs) XLETH(mm) VELOY(m/s)',
     +'     σ            ε        DEFORM(mm)')
      DO 210 J=0,NELEM,NUMBR
      WRITE(10,215) I,J,TIME(J)*1E6,XLETH(J)*1E3,VELOY(J),
     . STRES(J)/PYILD,STRAN(J),DEFOM(J)*1E3
 210  CONTINUE
 215  FORMAT(2I4,2F10.4,2F12.3,2F10.4)
      WRITE(10,225)
 225  FORMAT(/)
 200  NCONT(I+1)=NCONT(I)+NELEM+1
      I=I+1
      IF (INT(I/NUMBR)*NUMBR .EQ. I) WRITE(10,255)
 255  FORMAT(//'   I   J      TIME(µs) XLETH(mm) VELOY(m/s)',
     +'     σ*           ε*       DEFORM(mm)')
      IF (I. GT. NTP*NELEM/2) GOTO 400
C      IF (VELOY(NCONT(I)) .GT. 0.) GOTO 400
      CALL BOUND1(DPMAS,DLOC0,I)
      DO 300 J=1,NELEM-1
      CALL INNER(DVEC0,DLOC0,I,J)
      IF (INT(I/NUMBR)*NUMBR .EQ. I) THEN
      IF (INT((J-1)/NUMBR)*NUMBR .EQ.(J-1)) THEN
      WRITE(10,215) I,J-1,TIME(NCONT(I)+J-1)*1E6,XLETH(NCONT(I)
     . +J-1)*1E3,VELOY(NCONT(I)+J-1),STRES(NCONT(I)+J-1)/PYILD,
     . STRAN(NCONT(I)+J-1),DEFOM(NCONT(I)+J-1)*1E3
      END IF
      END IF
 300  CONTINUE
      CALL BOUND2(NUMBR,DVEC0,DLOC0,I)
      IF (INT(I/NUMBR)*NUMBR .EQ. I) THEN
      WRITE(10,215) I,NELEM,TIME(NCONT(I)+NELEM)*1E6,XLETH(NCONT(I)
     .+NELEM)*1E3,VELOY(NCONT(I)+NELEM),STRES(NCONT(I)+NELEM)/PYILD,
     . STRAN(NCONT(I)+NELEM),DEFOM(NCONT(I)+NELEM)*1E3
      END IF
      GOTO 200
 400  N0I=I
      WRITE(10,235) NCONT(I)
 235  FORMAT(I6)
      CLOSE (10)
      RETURN
      END

      SUBROUTINE BOUND1(DPMAS,DLOC0,I)
C*********************************************************************
C           CALCULATING THE BOUNDARY VALUES AT THE STRUCK END
C*********************************************************************
      COMMON NELEM,NCONT(0:500),PLETH,PMODL,PPEXP,PCOFB,PYILD,PBROK,
     . TLIMIT,SWITCH,PDESY,PVELO,XLETH(0:20000),TIME(0:20000),
     . STRAN(0:20000),STRES(0:20000),VELOY(0:20000),DEFOM(0:20000)
      TIME(NCONT(I))=TIME(NCONT(I-1)+1)-(XLETH(NCONT(I-1))
     . -XLETH(NCONT(I-1)+1))/DLOC0*PDESY
```

```
      IF (((TIME(NCONT(I))+TIME(NCONT(I-1)))/2) .LE. TLIMIT) THEN
      VELOY(NCONT(I))=PVELO*TIME(NCONT(I))/TLIMIT
      ELSE
      VELOY(NCONT(I))=VELOY(NCONT(I-1))+(TIME(NCONT(I))
     . -TIME(NCONT(I-1)))/DPMAS*STRES(NCONT(I-1))
      END IF
      STRES(NCONT(I))=STRES(NCONT(I-1)+1)-DLOC0*(VELOY(NCONT(I))
     . -VELOY(NCONT(I-1)+1))-(TIME(NCONT(I))-TIME(NCONT(I-1)+1))
     .  *FUNSTA(STRES(NCONT(I-1)+1),STRAN(NCONT(I-1)+1))
      STRAN(NCONT(I))=STRAN(NCONT(I-1))+(STRES(NCONT(I))
     . -STRES(NCONT(I-1))+(TIME(NCONT(I))-TIME(NCONT(I-1)))
     . *FUNSTA(STRES(NCONT(I-1)),STRAN(NCONT(I-1))))/PMODL
      ATRES1=(STRES(NCONT(I-1)+1)+STRES(NCONT(I)))/2.
      ATRAN1=(STRAN(NCONT(I-1)+1)+STRAN(NCONT(I)))/2.
      ATRES2=(STRES(NCONT(I-1))+STRES(NCONT(I)))/2.
      ATRAN2=(STRAN(NCONT(I-1))+STRAN(NCONT(I)))/2.
      IF (((TIME(NCONT(I))+TIME(NCONT(I-1)))/2) .GT. TLIMIT) THEN
      VELOY(NCONT(I))=VELOY(NCONT(I-1))+(TIME(NCONT(I))
     . -TIME(NCONT(I-1)))/DPMAS*ATRES2
      END IF
      STRES(NCONT(I))=STRES(NCONT(I-1)+1)-DLOC0*(VELOY(NCONT(I))
     . -VELOY(NCONT(I-1)+1))-(TIME(NCONT(I))
     . -TIME(NCONT(I-1)+1))*FUNSTA(ATRES1,ATRAN1)
      STRAN(NCONT(I))=STRAN(NCONT(I-1))+(STRES(NCONT(I))
     . -STRES(NCONT(I-1))+(TIME(NCONT(I))-TIME(NCONT(I-1)))
     . *FUNSTA(ATRES2,ATRAN2))/PMODL
 100  RETURN
      END

      SUBROUTINE BOUND2(NUMBR,DVEC0,DLOC0,I)
C*********************************************************************
C           CALCULATING THE BOUNDARY VALUES AT THE ANVIL END
C*********************************************************************
      COMMON NELEM,NCONT(0:500),PLETH,PMODL,PPEXP,PCOFB,PYILD,PBROK,
     . TLIMIT,SWITCH,PDESY,PVELO,XLETH(0:20000),TIME(0:20000),
     . STRAN(0:20000),STRES(0:20000),VELOY(0:20000),DEFOM(0:20000)
      XLETH(NCONT(I)+NELEM)=PLETH
      VELOY(NCONT(I)+NELEM)=0.
      TIME(NCONT(I)+NELEM)=TIME(NCONT(I)+NELEM-1)
     . +(XLETH(NCONT(I-1)+NELEM)-XLETH(NCONT(I)+NELEM-1))/DVEC0
      STRES(NCONT(I)+NELEM)=STRES(NCONT(I)+NELEM-1)+DLOC0*
     .  (VELOY(NCONT(I)+NELEM)-VELOY(NCONT(I)+NELEM-1))
     . -(TIME(NCONT(I)+NELEM)-TIME(NCONT(I)+NELEM-1))
     . *FUNSTA(STRES(NCONT(I)+NELEM-1),STRAN(NCONT(I)+NELEM-1))
      STRAN(NCONT(I)+NELEM)=STRAN(NCONT(I-1)+NELEM)+(STRES(NCONT(I)
     . +NELEM)-STRES(NCONT(I-1)+NELEM)+(TIME(NCONT(I)+NELEM)
     . -TIME(NCONT(I-1)+NELEM))*FUNSTA(STRES(NCONT(I-1)+NELEM),
     . STRAN(NCONT(I-1)+NELEM)))/PMODL
      ATRES1=(STRES(NCONT(I)+NELEM-1)+STRES(NCONT(I)+NELEM))/2.
      ATRAN1=(STRAN(NCONT(I)+NELEM-1)+STRAN(NCONT(I)+NELEM))/2.
      ATRES2=(STRES(NCONT(I-1)+NELEM)+STRES(NCONT(I)+NELEM))/2.
      ATRAN2=(STRAN(NCONT(I-1)+NELEM)+STRAN(NCONT(I)+NELEM))/2.
      STRES(NCONT(I)+NELEM)=STRES(NCONT(I)+NELEM-1)+DLOC0
     . *(VELOY(NCONT(I)+NELEM)-VELOY(NCONT(I)+NELEM-1))
     . -(TIME(NCONT(I)+NELEM)-TIME(NCONT(I)+NELEM-1))
```

```
     . *FUNSTA(ATRES1,ATRAN1)
      STRAN(NCONT(I)+NELEM)=STRAN(NCONT(I-1)+NELEM)+(STRES(NCONT(I)
     . +NELEM)-STRES(NCONT(I-1)+NELEM)+(TIME(NCONT(I)+NELEM)
     . -TIME(NCONT(I-1)+NELEM))*FUNSTA(ATRES2,ATRAN2))/PMODL
      DXLETH=(STRAN(NCONT(I)+NELEM-1)+STRAN(NCONT(I)-2))/2.
     . *(XLETH(NCONT(I)-2)-XLETH(NCONT(I)+NELEM-1))
      DEFOM(NCONT(I)+NELEM-1)=DEFOM(NCONT(I)-2)+DXLETH
      DEFOM(NCONT(I)+NELEM)=0.
      IF (INT(I/NUMBR)*NUMBR .EQ. I) THEN
      IF (INT((NELEM-1)/NUMBR)*NUMBR .EQ.(NELEM-1)) THEN
      WRITE(10,215) I,NELEM-1,TIME(NCONT(I)+NELEM-1)*1E6,
     . XLETH(NCONT(I)+NELEM-1)*1E3,VELOY(NCONT(I)+NELEM-1),
     . STRES(NCONT(I)+NELEM-1)/PYILD,STRAN(NCONT(I)
     . +NELEM-1)*PMODL/PYILD,DEFOM(NCONT(I)+NELEM-1)*1E3
      END IF
      END IF
 215  FORMAT(2I4,2F10.4,2F12.3,2F10.4)
 100  RETURN
      END

      SUBROUTINE INNER(DVEC0,DLOC0,I,J)
C*********************************************************************
C                    THE SOLUTION OF THE INNER FIELD
C*********************************************************************
      COMMON NELEM,NCONT(0:500),PLETH,PMODL,PPEXP,PCOFB,PYILD,PBROK,
     . TLIMIT,SWITCH,PDESY,PVELO,XLETH(0:20000),TIME(0:20000),
     . STRAN(0:20000),STRES(0:20000),VELOY(0:20000),DEFOM(0:20000)
      XLETH(NCONT(I)+J)=((TIME(NCONT(I-1)+J+1)-TIME(NCONT(I)+
     . J-1))*DVEC0+XLETH(NCONT(I-1)+J+1)+XLETH(NCONT(I)+J-1))/2.
      TIME(NCONT(I)+J)=(TIME(NCONT(I-1)+J+1)+TIME(NCONT(I)+J-1)+
     . (XLETH(NCONT(I-1)+J+1)-XLETH(NCONT(I)+J-1))/DVEC0)/2.
      STRES(NCONT(I)+J)=((VELOY(NCONT(I-1)+J+1)-VELOY(NCONT(I)
     . +J-1))*DLOC0+STRES(NCONT(I-1)+J+1)+STRES(NCONT(I)+J-1)
     . -(TIME(NCONT(I)+J)-TIME(NCONT(I-1)+J+1))*FUNSTA(STRES(
     . NCONT(I-1)+J+1),STRAN(NCONT(I-1)+J+1))-(TIME(NCONT(I)+J)
     . -TIME(NCONT(I)+J-1))*FUNSTA(STRES(NCONT(I)+J-1),
     . STRAN(NCONT(I)+J-1)))/2.
      STRESP=((XLETH(NCONT(I)+J)-XLETH(NCONT(I)+J-1))
     . *STRES(NCONT(I-1)+J+1)+(XLETH(NCONT(I-1)+J+1)
     . -XLETH(NCONT(I)+J))*STRES(NCONT(I)+J-1))
     . /(XLETH(NCONT(I-1)+J+1)-XLETH(NCONT(I)+J-1))
      STRANP=((XLETH(NCONT(I)+J)-XLETH(NCONT(I)+J-1))
     . *STRAN(NCONT(I-1)+J+1)+(XLETH(NCONT(I-1)+J+1)
     . -XLETH(NCONT(I)+J))*STRAN(NCONT(I)+J-1)
     . )/(XLETH(NCONT(I-1)+J+1)-XLETH(NCONT(I)+J-1))
      TIMEP=((XLETH(NCONT(I)+J)-XLETH(NCONT(I)+J-1))
     . *TIME(NCONT(I-1)+J+1)+(XLETH(NCONT(I-1)+J+1)-XLETH(NCONT(I)
     . +J))*TIME(NCONT(I)+J-1))
     . /(XLETH(NCONT(I-1)+J+1)-XLETH(NCONT(I)+J-1))
      STRAN(NCONT(I)+J)=STRANP+(STRES(NCONT(I)+J)-STRESP+(TIME(
     . NCONT(I)+J)-TIMEP)*FUNSTA(STRESP,STRANP))/PMODL
      ATRES1=(STRES(NCONT(I-1)+J+1)+STRES(NCONT(I)+J))/2.
      ATRAN1=(STRAN(NCONT(I-1)+J+1)+STRAN(NCONT(I)+J))/2.
      ATRES2=(STRESP+STRES(NCONT(I)+J))/2.
      ATRAN2=(STRANP+STRAN(NCONT(I)+J))/2.
```

```
      ATRES3=(STRES(NCONT(I)+J-1)+STRES(NCONT(I)+J))/2.
      ATRAN3=(STRAN(NCONT(I)+J-1)+STRAN(NCONT(I)+J))/2.
      STRES(NCONT(I)+J)=((VELOY(NCONT(I-1)+J+1)-VELOY(NCONT(I)+
     . J-1))*DLOC0+STRES(NCONT(I-1)+J+1)+STRES(NCONT(I)+J-1)
     . -(TIME(NCONT(I)+J)-TIME(NCONT(I-1)+J+1))
     . *FUNSTA(ATRES1,ATRAN1)-(TIME(NCONT(I)+J)
     . -TIME(NCONT(I)+J-1))*FUNSTA(ATRES3,ATRAN3))/2.
      VELOY(NCONT(I)+J)=(VELOY(NCONT(I-1)+J+1)+VELOY(NCONT(I)
     . +J-1))/2.+(STRES(NCONT(I-1)+J+1)-STRES(NCONT(I)+J-1)
     . +(TIME(NCONT(I)+J)-TIME(NCONT(I-1)+J+1))
     . *FUNSTA(ATRES1,ATRAN1) -(TIME(NCONT(I)+J)
     . -TIME(NCONT(I)+J-1))*FUNSTA(ATRES3,ATRAN3))/2./DLOC0
      STRAN(NCONT(I)+J)=STRANP+(STRES(NCONT(I)+J)-STRESP+
     . (TIME(NCONT(I)+J)-TIMEP)*FUNSTA(ATRES2,ATRAN2))/PMODL
      DXLETH=(STRAN(NCONT(I)+J-1)+STRAN(NCONT(I-1)+J+1))/2.
     . *(XLETH(NCONT(I-1)+J+1)-XLETH(NCONT(I)+J-1))
      DEFOM(NCONT(I)+J-1)=DEFOM(NCONT(I-1)+J+1)+DXLETH
      RETURN
      END

      FUNCTION FUNSTA(STRESF,STRANF)
C*******************************************************************
C              THE FUNCTION OF STATIC CONSTITUTIVE EQUATION
C*******************************************************************
      COMMON NELEM,NCONT(0:500),PLETH,PMODL,PPEXP,PCOFB,PYILD,PBROK,
     . TLIMIT,SWITCH,PDESY,PVELO,XLETH(0:20000),TIME(0:20000),
     . STRAN(0:20000),STRES(0:20000),VELOY(0:20000),DEFOM(0:20000)
      AX0=(0.694+43.1*STRANF)*1.E6
      AX1=2.9331E+3
      AXS=(0.694+43.1*PYILD/PMODL)*1.E6
      PYILD3=PYILD+AXS
      IF (STRESF .LE. PYILD) THEN
      STRES0=PMODL*STRANF
      ELSE
      STRES0=(200.*LOG10(34.1315*(-LOG(1-STRANF)
     . -PYILD/PMODL)+1)+55.)/(1-STRANF)*1.E6
      END IF
      IF (STRESF .LE. PYILD3) THEN
      STRES1=PMODL*STRANF
      ELSE
      STRES1=STRES0+AX0*7.
      END IF
      IF (STRESF .LE. STRES0) THEN
      FUNSTA=0.
      ELSE
      IF (STRESF .LE. STRES1) THEN
      FUNSTA=PMODL*EXP(LOG(10.)*((STRESF-STRES0)/AX0-4.))
      ELSE
      FUNSTA=PMODL*((STRESF-STRES1)/AX1+3.E3)/10.
      END IF
      END IF
      RETURN
      END

      SUBROUTINE OUTPUT(N0I,NUMBR,JSTEP)
```

```
C**********************************************************************
C                              THE OUTPUT OF RESULTS
C**********************************************************************
      COMMON NELEM,NCONT(0:500),PLETH,PMODL,PPEXP,PCOFB,PYILD,PBROK,
     . TLIMIT,SWITCH,PDESY,PVELO,XLETH(0:20000),TIME(0:20000),
     . STRAN(0:20000),STRES(0:20000),VELOY(0:20000),DEFOM(0:20000)
      OPEN (6,FILE='XBOND.RES',STATUS='NEW')
      OPEN (7,FILE='TBOND.RES',STATUS='NEW')
      OPEN (1,FILE='VBOND.RES',STATUS='NEW')
      OPEN (2,FILE='SBOND.RES',STATUS='NEW')
      OPEN (3,FILE='EBOND.RES',STATUS='NEW')
      OPEN (4,FILE='VBONDC.RES',STATUS='NEW')
      OPEN (8,FILE='SBONDC.RES',STATUS='NEW')
      OPEN (9,FILE='EBONDC.RES',STATUS='NEW')
      JHALF=INT(JSTEP/2)
      NHALF=INT(NELEM/2)
      NQUAT=INT(NELEM/4)
      IF (NQUAT .NE. JHALF*INT(NQUAT/JHALF)) THEN
      NQUAT=NQUAT+1
      NHALF=2*NQUAT
      END IF
      IHALF=INT(NUMBR/2)
      DO 100 J=0, NELEM,JSTEP
      WRITE(6,110)
 110  FORMAT(//'   I   J      TIME(μs) XLETH(mm) VELOY(m/s)',
     +'      σ(MPa)         ε      DEFORM(mm)')
      DO 100 I=0,NOI-1,IHALF
      WRITE(6,220) I,J,TIME(NCONT(I)+J)*1E6,XLETH(NCONT(I)+J)*1E3,
     . VELOY(NCONT(I)+J),STRES(NCONT(I)+J)/1.E6*(1-STRAN(NCONT(I)
     . +J)),-LOG(1-STRAN(NCONT(I)+J)),DEFOM(NCONT(I)+J)*1000
 100  CONTINUE
      WRITE(7,210)
 210  FORMAT(//'   I   J      TIME(μs) XLETH(mm) VELOY(m/s)',
     +'      σ(MPa)         ε     DEFORM(mm)')
 215  DO 240 I=NUMBR,NOI,NUMBR
      DO 200 J=0,I,JSTEP
      IF ((2*J) .GT. NELEM) GOTO 240
      WRITE(7,220) I,J,TIME(NCONT(I-J)+2*J)*1E6,XLETH(NCONT(I-J)+2*J)
     + *1000,VELOY(NCONT(I-J)+2*J),STRES(NCONT(I-J)+2*J)/1.E6*(1
     . -STRAN(NCONT(I-J)+2*J)), -LOG(1-STRAN(NCONT(I-J)+2*J)),
     . DEFOM(NCONT(I-J)+2*J)*1000
 200  CONTINUE
 240  CONTINUE
 220  FORMAT(2I4,2F10.4,2F12.3,2F10.4)
      WRITE(1,310) (XLETH(J)*1000,J=0,NHALF,2*JHALF)
      WRITE(2,310) (XLETH(J)*1000,J=0,NHALF,2*JHALF)
      WRITE(3,310) (XLETH(J)*1000,J=0,NHALF,2*JHALF)
      WRITE(4,310) (XLETH(J)*1000,J=2*(NQUAT+JHALF),NELEM,2*JHALF)
      WRITE(8,310) (XLETH(J)*1000,J=2*(NQUAT+JHALF),NELEM,2*JHALF)
      WRITE(9,310) (XLETH(J)*1000,J=2*(NQUAT+JHALF),NELEM,2*JHALF)
      DO 300 I=0,NOI-1,IHALF
      IF (2*I .LE. NELEM) THEN
      IF (2*I .LE. NHALF) THEN
      WRITE(1,330) TIME(NCONT(I))*1.E6,(-VELOY(NCONT(I-J)+2*J),
     . J=0,I,JHALF)
```

```
      WRITE(2,320) TIME(NCONT(I))*1.E6,(STRES(NCONT(I-J)+2*J)/1.E6
     . *(1-STRAN(NCONT(I-J)+2*J)),J=0,I,JHALF)
      WRITE(3,340) TIME(NCONT(I))*1.E6,
     . (-LOG(1-STRAN(NCONT(I-J)+2*J)),J=0,I,JHALF)
      ELSE
      WRITE(1,330) TIME(NCONT(I))*1.E6,(-VELOY(NCONT(I-J)+2*J),
     . J=0,NQUAT,JHALF)
      WRITE(2,320) TIME(NCONT(I))*1.E6,(STRES(NCONT(I-J)+2*J)/1.E6
     . *(1-STRAN(NCONT(I-J)+2*J)),J=0,NQUAT,JHALF)
      WRITE(3,340) TIME(NCONT(I))*1.E6,
     . (-LOG(1-STRAN(NCONT(I-J)+2*J)),J=0,NQUAT,JHALF)
      WRITE(4,330) TIME(NCONT(I))*1.E6,(-VELOY(NCONT(I-J)+2*J),
     . J=NQUAT+JHALF,I,JHALF)
      WRITE(8,320) TIME(NCONT(I))*1.E6,(STRES(NCONT(I-J)+2*J)/1.E6
     . *(1-STRAN(NCONT(I-J)+2*J)),J=NQUAT+JHALF,I,JHALF)
      WRITE(9,340) TIME(NCONT(I))*1.E6,
     . (-LOG(1-STRAN(NCONT(I-J)+2*J)),J=NQUAT+JHALF,I,JHALF)
       END IF
      ELSE
      WRITE(1,330) TIME(NCONT(I))*1.E6,(-VELOY(NCONT(I-J)+2*J),
     . J=0,NQUAT,JHALF)
      WRITE(2,320) TIME(NCONT(I))*1.E6,(STRES(NCONT(I-J)+2*J)/1.E6
     . *(1-STRAN(NCONT(I-J)+2*J)),J=0,NQUAT,JHALF)
      WRITE(3,340) TIME(NCONT(I))*1.E6,
     . (-LOG(1-STRAN(NCONT(I-J)+2*J)),J=0,NQUAT,JHALF)
      WRITE(4,330) TIME(NCONT(I))*1.E6,(-VELOY(NCONT(I-J)+2*J),
     . J=NQUAT+JHALF,NHALF,JHALF)
      WRITE(8,320) TIME(NCONT(I))*1.E6,(STRES(NCONT(I-J)+2*J)/1.E6
     . *(1-STRAN(NCONT(I-J)+2*J)),J=NQUAT+JHALF,NHALF,JHALF)
      WRITE(9,340) TIME(NCONT(I))*1.E6,
     . (-LOG(1-STRAN(NCONT(I-J)+2*J)),J=NQUAT+JHALF,NHALF,JHALF)
      END IF
300   CONTINUE
310   FORMAT(6X,15F6.1)
320   FORMAT(F6.3,15F6.1)
330   FORMAT(F6.3,15F6.2)
340   FORMAT(F6.3,15F6.3)
      CLOSE (1,STATUS='KEEP')
      CLOSE (2,STATUS='KEEP')
      CLOSE (3,STATUS='KEEP')
      CLOSE (6,STATUS='KEEP')
      CLOSE (7,STATUS='KEEP')
      CLOSE (4,STATUS='KEEP')
      CLOSE (8,STATUS='KEEP')
      CLOSE (9,STATUS='KEEP')
      RETURN
      END
```